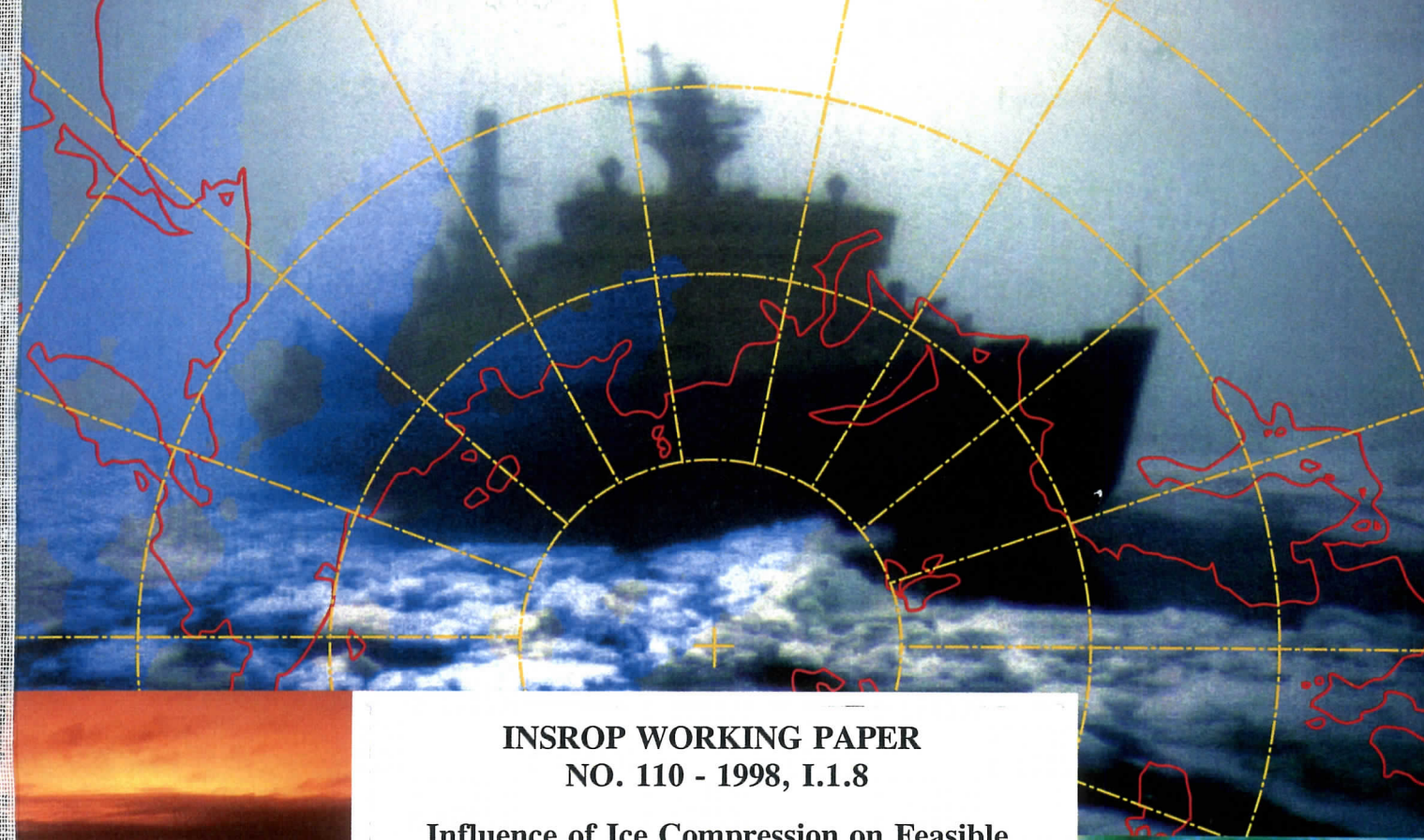

INSROP WORKING PAPER NO. 110 - 1998, I.1.8

Influence of Ice Compression on Feasible Navigation on the Northern Sea Route Part II

By Kimmo Juurmaa, Torsten Heideman, Arto Uuskallio, Matthew Patey, and Lauri Kosomaa

INSROP International Northern Sea Route Programme

Central Marine Research & Design Institute, Russia

The Fridtjof Nansen Institute, Norway

Ship and Ocean Foundation, Japan

International Northern Sea Route Programme (INSROP)

Central Marine Research & Design Institute, Russia

The Fridtjof Nansen Institute, Norway

Ship & Ocean Foundation, Japan

INSROP WORKING PAPER NO. 110-1998

Sub-programme I:	Natural Conditions and Ice Navigation
Project I.1.8:	Influence of Ice Compression on Feasible Navigation on the Northern Sea Route
Supervisor:	Kimmo Juurmaa, Kværner Masa-Yards Arctic Research Centre, Finland
Title:	**Influence of Ice Compression on Feasible Navigation on the Northern Sea Route**
Authors:	**Kimmo Juurmaa(1), Torsten Heideman(1), Arto Uuskallio(1), Matthew Patey(2), Lauri Kosomaa(2).**
Addresses:	(1) Kvaerner Masa-Yards Arctic Research Centre, Kaanaatie 3A, 00560 Helsinki, Finland (2) Helsinki University of Technology, Ship Laboratory, Arctic Offshore Research Centre, Tietotie 1, 02150 Espoo, Finland
Date:	25th August 1998
Reviewed by:	Ken Croasdale, K.R. Croasdale & Associates Ltd, Calgary, Alberta, Canada

What is an INSROP Working Paper and how to handle it:

This publication forms part of a Working Paper series from the **International Northern Sea Route Programme - INSROP**. This Working Paper has been evaluated by a reviewer and can be circulated for comments both within and outside the INSROP team, as well as be published in parallel by the researching institution. A Working Paper will in some cases be the final documentation of a technical part of a project, and it can also sometimes be published as part of a more comprehensive INSROP Report. For any comments, please contact the authors of this Working Paper.

FOREWORD - INSROP WORKING PAPER

INSROP is a five-year multidisciplinary and multilateral research programme, the main phase of which commenced in June 1993. The three principal cooperating partners are **Central Marine Research & Design Institute (CNIIMF)**, St. Petersburg, Russia; **Ship and Ocean Foundation (SOF)**, Tokyo, Japan; and **Fridtjof Nansen Institute (FNI)**, Lysaker, Norway. The INSROP Secretariat is shared between CNIIMF and FNI and is located at FNI.

INSROP is split into four main projects: 1) Natural Conditions and Ice Navigation; 2) Environmental Factors; 3) Trade and Commercial Shipping Aspects of the NSR; and 4) Political, Legal and Strategic Factors. The aim of INSROP is to build up a knowledge base adequate to provide a foundation for long-term planning and decision-making by state agencies as well as private companies etc., for purposes of promoting rational decisionmaking concerning the use of the Northern Sea Route for transit and regional development.

INSROP is a direct result of the normalization of the international situation and the Murmansk initiatives of the former Soviet Union in 1987, when the readiness of the USSR to open the NSR for international shipping was officially declared. The Murmansk Initiatives enabled the continuation, expansion and intensification of traditional collaboration between the states in the Arctic, including safety and efficiency of shipping. Russia, being the successor state to the USSR, supports the Murmansk Initiatives. The initiatives stimulated contact and cooperation between CNIIMF and FNI in 1988 and resulted in a pilot study of the NSR in 1991. In 1992 SOF entered INSROP as a third partner on an equal basis with CNIIMF and FNI.

The complete series of publications may be obtained from the Fridtjof Nansen Institute.

SPONSORS FOR INSROP

- Nippon Foundation/Ship & Ocean Foundation, Japan
- The Government of the Russian Federation
- The Norwegian Research Council
- The Norwegian Ministry of Foreign Affairs
- The Norwegian Ministry of Industry and Trade
- The Norwegian Ministry of the Environment
- The Central and Eastern Europe programme
- State Industry and Regional Development Fund, Norway
- Norsk Hydro
- Norwegian Federation of Shipowners
- Fridtjof Nansen Institute
- Kværner a.s.
- Phillips Petroleum Company Norway

PROFESSIONAL ORGANISATIONS PERMANENTLY ATTACHED TO INSROP

- Ship & Ocean Foundation, Japan
- Central Marine Research & Design Institute, Russia
- Fridtjof Nansen Institute, Norway
- National Institute of Polar Research, Japan
- Ship Research Institute, Japan
- Murmansk Shipping Company, Russia
- Northern Sea Route Administration, Russia
- Arctic & Antarctic Research Institute, Russia
- Norwegian Polar Research Institute
- SINTEF (Foundation for Scientific and Industrial Research - Civil and Environmental Engineering), Norway.

PROGRAMME COORDINATORS

- **Yury Ivanov, CNIIMF**
  Kavalergardskaya Str.6
  St. Petersburg 193015, Russia
  Tel: 7 812 271 5633
  Fax: 7 812 274 3864
  E-mail: cniimf@neva.spb.ru
- **Willy Østreng, FNI**
  P.O. Box 326
  N-1324 Lysaker, Norway
  Tel: 47 67 11 19 00
  Fax: 47 67 11 19 10
  E-mail: sentralbord@fni.no
- **Hiroyasu Kawai, SOF**
  Senpaku Shinko Building
  15-16 Toranomon 1-chome
  Minato-ku, Tokyo 105, Japan
  Tel: 81 3 3502 2371
  Fax: 81 3 3502 2033
  E-mail:sofkawa@blue.ocn.ne.jp

TABLE OF CONTENTS

1. SUMMARY 1

2. INTRODUCTION 2

2.1. THE OBJECTIVE OF PROJECT I.1.8 2
2.2. THE RESULTS OF PART I 2

3. FULL SCALE TESTS 4

3.1. MAIN PARTICULARS OF NUCLEAR ICEBREAKER "LENIN" 4
3.2. THE RESULTS OF THE FULL SCALE TESTS 4

4. MODEL SCALE TESTS 7

4.1. THE MODEL 7
4.2. MODEL SCALE TEST CONDITIONS 7
4.3. TEST RESULTS AND CONCLUSION 8

APPENDICES

APPENDIX 1: Ship Resistance in Compressive Pack Ice
Results of Model Scale Tests

TABLES

TABLE 1: SPEED OF NUCLEAR ICEBREAKER "LENIN" 5

FIGURES

FIGURE 1: ICE THICKNESS VS. SHIP SPEED WITH COMPRESSION AS A PARAMETER. 5
FIGURE 2: ICE RESISTANCE OF NIB "LENIN" 6

1. Summary

Part II of the INSROP Project I.1.8 was initiated to find better ways than the subjective ball scale to describe the ice compression and it's influence on the ice resistance. The selected way to proceed was to analyse existing full scale measurements and to try to repeat the corresponding measurements in model scale under controlled conditions.

The only full scale results found were those of the Russian icebreaker Lenin. Based on these the resistance increase under different severity of ice compression was determined.

The model tests were performed in the ice laboratory of the Helsinki University of Technology. Two models were used for the testing. One was a model of an icebreaker similar to the full scale reference vessel icebreaker Lenin and the other was a model of an arctic cargo vessel.

The model test results with the ice breaker model showed that a useful measure to describe the ice compression is Compaction Factor. This is ratio between the areas of an uncompressed ice field and the area of a compressed ice field. It is assumed that the forces within the ice field are transferred through compaction. This is a fact at least in larger scale and in ice fields that are broken due to compression. Based on the comparison between full and model scale results, it seems that Compaction Factors in the range of 1.20 - 1.53 are comparable to ice compression of 2 balls on the 0 - 3 balls scale.

The results with the model of the arctic cargo vessel proved to be somewhat doubtful. Based on these results the Compaction Factor has lower influence on the resistance increase with the cargo vessel than with the icebreaker. The tests were performed with a segmented model and that offers an opportunity for further analysis of the forces acting on the vessel. It is recommended that this analysis and possible further testing will be performed at a later stage.

2. Introduction

Ice compression is a phenomenon that has a drastic influence on the feasibility Arctic operations. Experience has shown that today, even the most powerful icebreakers will become immobilised during events of severe ice compression. This means that the influence of compression must be taken into account when calculations regarding NSR shipping operations are performed.

Despite its big importance there has been published surprisingly little systematic data about ice compression and how to account for it. In calculations ice compression is normally sidelined with the help of an unspecified down-time allowance which in turn is based on various subjective judgements.

From an analytic point of view there is a clear need to develop a procedure to include the effects of ice compression into the performance calculations.

2.1. The Objective of Project I.1.8

The ultimate objective of INSROP Project I. 1. 8 is to develop the first ever tool to assess the influence of ice compression on ship operation, both from a technical and an economic point of view. It was decided that the total project will be covered by two reports.

This first one deals with the present knowledge of ice compression and the second one concentrates on creating the analytical computational tool to account for it.

2.2. The Results of Part I

The Arctic and Antarctic Research Institute in St. Petersburg was contracted to survey their databases and reports and compile a report covering the present status of Russian knowledge of ice compression along the NSR. Part I of the INSROP report is a translated and shortened version of the rather comprehensive AARI report in Russian language. In Part I results of major interest from a navigational point of view have been extracted.

Part I describes the different forms of ice compression, the factors that influence it, means of identifying it and finally it gives a review of existing data on the occurrence of ice compression along the NSR.

Ice compression is normally divided into categories, based on their origins. The Russian practice is to divide the ice compression in dynamic compression due to wind, tide and current and static compression due to thermal expansion.

Wind is by far the most important cause of ice compression. In almost 90 % of the cases of severe ice compression, that is more than 2 balls, the direction of the wind coincides with that of the ice movement.

The most common method to identify ice compression is to study the behaviour of the channel behind the ship and the interaction between the ice and the hull of the ship.

Based on long term Russian statistics the probability of encountering ice compression is claimed to be in the order of 60 %. However, this figure is not undisputed since it is not supported by observations from numerous Arctic voyages undertaken by KMY.

Transit calculations performed by KMY indicate that a down-time figure of about 5% still is acceptable. This means that a vessel is supposed to be able to operate in ice compression up to the intensity of 1-2 balls, which based on fig. 10 in Part I, even considering the uncertainties in the presented figures, by far are the most common ones.

When designing a ship capable of operating in 1-2 balls of ice compression the designer needs information about how this intensity of ice compression translates into terms of physical added ice resistance. Unfortunately the survey of the Russian knowledge did not reveal any conclusions about the correlation between the ice compression in ball units and physically measurable units.

The obvious continuation of the project is to try to find this link, a way to relate the readings of the ball scale to physically defined measures, such as stresses in the ice field or forces exerted on ships and structures.

The Russians have published results from icebreaker tests where the parameters are speed of advance and intensity of ice compression on the ball scale, Reference 1. It is possible to reproduce the results from the full scale tests in an ice model basin where the compressive force can be monitored and controlled. As a result the relationship between the compressive force and the ice compression expressed in balls can be established.

The next step would be to apply the compressive force corresponding to 1-2 balls to a model of a representative Arctic cargo vessel to find out what that ice compression means in the form of added ice resistance.

3. Full Scale Tests

In the paper Voevodin compiles the results from tests over a period of several years. The full scale tests were performed in the Kara Sea in the fall and winter navigation periods during the years of 1971 to 1973. In his paper the author does not say which icebreaker was used for the tests, he merely states that it is an icebreaker having 32000 horsepower utilising 70 % of the maximum output.

A recalculation of these figures yields a maximum output of about 46000 horsepower for the icebreaker. A survey of the status of the Soviet icebreaker fleet in the early 70´s reveals that the only plausible icebreaker is the nuclear powered polar icebreaker "Lenin".

3.1. Main Particulars of Nuclear Icebreaker "Lenin".

This information is from Reference 2 presented by V. V. Ruksha from the Murmansk Shipping Company at the Polar Tech ´96 conference in Sankt Petersburg in September 1996:

- Length overall 134 m
- Maximum breadth 27.6 m
- Draught 11.5 m
- Displacement 16400 tons
- Shaft power 32 MW

The icebreaker was commissioned in December 1959 and decommissioned in December 1989.

The main particulars are not undisputed since the literature is full of numbers that slightly differ from the ones above. It must also be remembered that "Lenin" underwent an extensive overhaul between 1967 and 1970. The reactor compartment was completely rebuilt after what is commonly believed to have been a contamination accident. The three old reactors were replaced by a single new one and it is possible that the power output was changed. This assumption is supported by the fact that before the conversion "Lenin" was referred to as a 44000 shaft horsepower icebreaker while it after the conversion was a 32 MW ship.

3.2. Results of the Full Scale Tests

In his paper Voevodin presents the performance of the icebreaker in table form.
Table 1 is a reproduction of the table in the paper and it presents the speed of "Lenin" in knots in different ice thickness at different levels of ice compression using 70 % of the maximum power output. It should, however, be noted that the ice condition is not level ice but rather drifting ice with a concentration of 9-10 balls. In the Russian system the ice concentration is expressed with the help of a ball scale ranging from 0-10, which directly corresponds to the more familiar tenth-system, for instance 6 balls of concentration is equal to 6/10.

Table 1: Speed of nuclear icebreaker "Lenin"

Balls	Ice Thickness (m), drifting ice, 9-10 balls of concentration						
	0.2	0.4	0.6	0.8	1.0	1.2	1.4
0	19	15	12	10	8.5	7.5	6.5
0-1	17	13.5	11	9.5	8	7	6
1	15	12.5	10.5	8.5	7.5	6.5	5.5
1-2	13.5	11	9.5	7	6	5.5	4.5
2	12	10	8	6	5	4.5	3
2-3	10.5	8.5	6.5	5	4	2	0
3	9.5	7	5	4	3	1	0

The results presented in table form are not so easy to grasp. However, when the results are presented in the form of speed versus ice thickness plots for the different intensities of ice compression they become more perceivable.

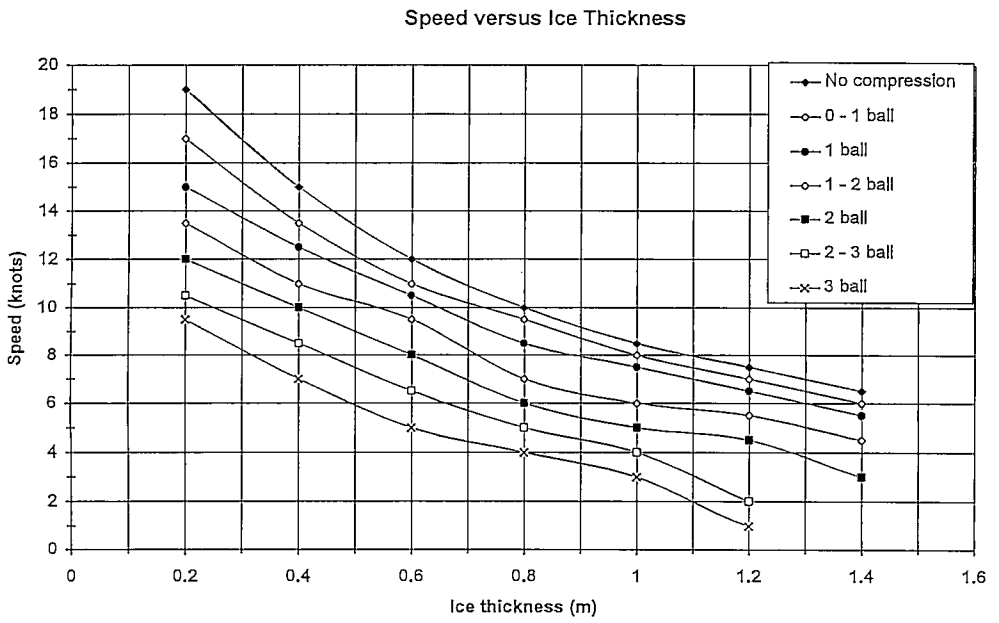

Figure 1: Ice thickness vs. ship speed with compression as a parameter.

Figure 1 is a straight plot of the results in
Table 1 without any mathematical fairing.

A closer look at Figure 1 shows that in thicker ice the influence of ice compression splits into three groups:

- ice compression with an intensity up to 1 ball does not affect the performance of the icebreaker to any significant extent.
- ice compression with an intensity ranging from more than 1 and up to 2 balls clearly affects the performance.
- ice compression of more than 2 balls seriously impairs the performance of the icebreaker.

In thinner ice this grouping tendency seems to have been lost and an almost linear effect of the intensity of the ice compression on the performance of the icebreaker can be detected.

The speed versus ice thickness graph will be converted into an ice resistance versus speed graph using the following assumptions:

- the bollard pull at 70 % of maximum power, or 32000 hp, is 290 ton
- the open water speed at the same power level is 19.5 knots
- the net thrust to overcome the ice resistance is:

$$T_{Net} = T_{Boll} * \left(1 - \frac{1}{3} * \left(\frac{v}{v_{ow}}\right) - \frac{2}{3} * \left(\frac{v}{v_{ow}}\right)^2\right)$$

- the velocity dependency of the ice resistance is assumed to be the same as that for icebreaker "Otso" in 0.8 m thick ice, Reference 3.

Based on these assumptions the ice resistance of NIB "Lenin" can be reconstructed and it is presented in Figure 2.

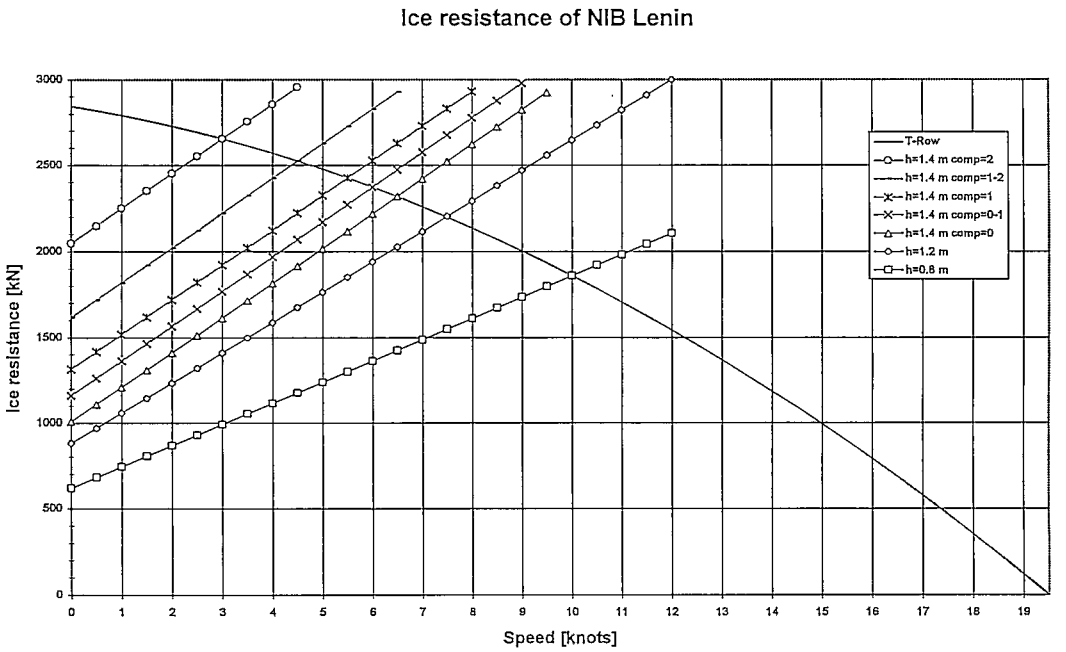

Figure 2: Ice resistance of NIB "Lenin"

4. Model Scale Tests

The idea of the model tests is to model the performance of icebreaker "Lenin" in an icebreaking laboratory. In the laboratory the ice conditions and the ice compression are simulated and the resistance of the icebreaker is measured. This ice resistance is then compared to the one derived from Figure 1 at corresponding ice thickness and speed according to the Froude scaling law.

4.1. The Model

In order to be theoretically correct a model of icebreaker "Lenin" should have been used. However, there is not believed to exist any exact models of that icebreaker outside Russia, partly because the Russians have not published very detailed lines of the icebreaker and partly because there has not been any strong incentive to investigate that icebreaker in the West. To overcome this problem it was decided to use an existing model with a resembling hull form.

During the years 1982-83 Wärtsilä Helsinki Shipyard delivered three icebreakers of the "Mudyug" class, named after the lead vessel, to the Soviet Union. Prior to construction these vessels were thoroughly tested in Wärtsilä's ice model basin and it was decided to use a model of this class for the tests.
The characteristics of the model are:

- Scale factor 1:20.8
- Length (wl) 3.77 m
- Breadth (wl) 0.96 m
- Draught (wl) 0.29 m
- Displacement abt 589 kg

In order to define the appropriate scale factor one must realise that a comparison of length, beam and draught all will yield different scale factors because the model is not a perfect down-scaled "Lenin". A reasonably good compromise is to calculate the scale factor using the displacement ratio. This yields a scale factor of 1:30.

To get more information from the different forces acting in a situation with ice compression, additional testing with a model of an arctic cargo vessel was performed. The characteristics of this other model are:

- Length (wl) 5.88 m
- Breadth (wl) 0.88 m
- Draugth (wl) 0.30 m

4.2. Model Scale Test Conditions

Previous model tests that have been performed in ice under compression have been done using unbroken level ice which was moved against the model with either constant speed or constant force. Observations from full scale have shown that in normal cases of ice compression the ice field is broken, rafted and contains pressure ridges. It was assumed that this was also the case during the full scale testing of

icebreaker "Lenin". To be able to simulate this condition the ice laboratory of the Helsinki University of Technology, having enough space for such simulation, was selected. During the tests the speed of the ice field and the degree of rafting were varied to create similar resistance increase as was observed during the full scale tests.

4.3. Test Results and Conclusion

The complete model test report is presented as Appendix 1 of this report. The actual test program covered tests both with a simple icebreaker model as well as tests with a segmented model of an arctic cargo vessel. The tests with the segmented model were made to get better understanding of the forces acting against the ship hull during operation in ice under compression. The results are discussed more in detail in Appendix 1. For this project the main results are those related to the comparison between resistance increase values in full scale and model scale.

From the full scale results in Figure 2 one can conclude that the 2 ball resistance increase with the ice breaker varies between 66% - 105%. From the model scale results of the icebreaker model presented in figures 4.1.2 and 4.1.3 in Appendix 1 similar results are achieved with Compaction Factor values in the range of 1.20 - 1.53. Considering all the inaccuracies involved in the whole process, the result may be seen as guideline for further research.

The Compaction Factor is a physically determined measure and for any sea area and ice condition it can be determined with satellite images or local observations. It is recommended that full scale observations based on the use of the Compaction Factor will be performed in the future.

The resistance increase with the cargo vessel tests can be found on pages B.3-4, B.3-6 and B.3-8 of the Appendix 1. From these results one can see that for Compaction Factor range 1.20 - 1.53 the ice resistance increase varies between 16% - 83%. This is well below the resistance increase measured for the icebreaker model. It is difficult to find a physical explanation to this, since the cargo vessel has a much longer parallel midbody than the icebreaker. To understand this further analysis and further testing should be carried out with the segmented model.

References

Reference 1, V. A. Voevodin. *To the Problem of Ice Compression Effect on Navigation.* AANII Transactions 384, 1981.

Reference 2, V. V. Ruksha. *The Experience of Atomic Icebreaker's Exploitation in Russia.* Polar Tech`96, Petersburg 1996.

Reference 3, J.-E. Jansson et al. *Operational Experience with the New Type Baltic Icebreaker "Otso".* POAC 1989, Helsinki.

Further reading of pack ice compression

Croasdale, K.R. and Marcelllus, R.W. 1981. *Ice Forces on Large Marine Structures.* Proc. of IAHR Intl. Symposium on Ice, Quebec City, 1981. Vol. 2. pp 755-765

Comfort, G. and Ritch, R. 1990. *Field Measurements of Pack Ice Stresses.* Proc. of OMAE Conference, Houston 1990.

Comfort, G., Ritch, R. and Frederking, R. 1992. *Pack Ice Stress Measurements.* Proc OMAE Conference, Calgary, 1992.

Croasdale and others, 1987. *A Pilot Program to Measure Pack Ice Driving Forces.* Proc. POAC Conference, Fairbanks, Alaska, 1987.

Coon, M.D. and others, 1989. *Observations of Floe Stresses In the Eastern Arctic.* Proc. of POAC Conference, Luleå, Sweden, 1989.

Coon, M.D. and others, 1995. *Sea Ice Deformation and Stress, a comparison across Space Scales.* Proc. of Sea Ice Mechanics and Arctic Modelling Workshop, Anchorage, April 1995.

Sandwell, 1994. *Processing of Pack Ice Stress Data.* Cold Regions Science and Technology, 20, pp 119—139.

Fleet Technology Ltd. 1994. *Limit Force Ice Loads and Their Significance to Offshore Structures in the Beaufort Sea.* Prepared for the National Research Council, Ottawa.

Croasdale, K.R. 1984. *The Limiting Driving Force Approach to Ice Loads.* OTC paper 47, Houston 1984.

Croasdale, K.R., Frederking, R., Wright, B. and Comfort G. 1992. *Size Effect on Pack Ice Driving Forces.* Proceedings of IAHR Ice Symposium 1992, Banff.

APPENDIX 1

HELSINKI UNIVERSITY OF TECHNOLOGY

Ship Laboratory

Arctic Offshore Research Centre

Ship Resistance in Compressive Pack Ice

Results of Model Scale Tests

Appendix 1 for INSROP PROJECT I. 1. 8, Part II

Influence of Ice Compression on Feasible Navigation on the NSR

Matthew Patey

Lauri Kosomaa

Approved :

Kaj Riska

Professor

Otaniemi, October 1997

Contents

1. Introduction 1
1.1. The General Problem 2
1.2. Previous Studies 6
2. Experimental Arrangement 10
3. Tests Conducted 15
3.1. Measurements 15
3.2. Summary of Tests 17
4. Results 21
4.1. Simple Model 23
4.2 Segmented Model 27
4.2.1. Comparison of Force Magnitudes 31
4.2.2. Variations in Average Forces with Compaction Rate 33
4.2.3. Influence of Ice Mechanical Properties 37
4.2.4. Comparison of F_{Bow} and $F_{Compression}$ 40
4.2.5. Comparison of F_{Bow} and $2F_{seg}$ 42
4.2.6. Friction Coefficient Variation 43
5. Conclusions 45
References 48

Tables

Table 2.1: Main Dimensions of Simple Model 12
Table 2.2: Main Dimensions of Segmented Model 14
Table 3.2.1: Test Parameters for Simple Model 18
Table 3.2.2: Ice Properties for Simple Model Tests 19
Table 3.2.3: Test Parameters for Segmented Model 19
Table 3.2.4: Ice Properties for Segmented Model Tests 20
Table 4.1.1: Average Forces for Simple Model Tests 23
Table 4.1.2: Ice Compression Indices for Simple Model Tests 26

Figures

Figure 1.1.1: Description of Compressive Ice Contact Scenario (Riska et al, 1996). 4
Figure 2.1: Sketch of the towing arrangement (not to scale). 10
Figure 2.2: Typical View of Broken Ice Field. 11
Figure 2.3: Towing winch mounted on tank wall. 12
Figure 2.4: Simple model in tank. 13
Figure 2.5: Schematic showing division of segmented model. 13
Figure 2.6: Segmented model in tank 14
Figure 3.1.1: Instrumentation of simple model. 16
Figure 3.1.2: Instrumentation of segmented model. The circles indicate connections to a framework used to suspend the segments attached to the main hull. It is omitted here for clarity. 16
Figure 4.1.1: Typical force time history for simple model tests 24
Figure 4.1.2: Variation in average force with compaction factor, test series 070696. 24
Figure 4.1.3: Variation in average force with compaction factor, test series 130696. 25
Figure 4.2.1: Typical time histories for Measured Forces in segmented model tests 29
Figure 4.2.2. Typical time histories for Total Resistance in segmented model tests 30
Figure 4.2.3: Typical time histories for Frictional Resistance in segmented model tests 30
Figure 4.2.1.1: Sample bar chart showing each force component 32
Figure 4.2.2.1: Scatter Plot for F_{Bow}, Test Series 040397 34
Figure 4.2.2.2: Scatter Plot for $F_{Compression}$, Test Series 040397. 34
Figure 4.2.2.3: Scatter Plot for $2F_{seg}$, Test Series 040397. 35
Figure 4.2.2.4: Scatter Plot for F_{Model}, Test Series 040397. 35
Figure 4.2.3.1: Influence of ice properties on F_{bow}; ice strength properties for each day are given in Table 3.2.2 and Table 3.2.4 37
Figure 4.2.3.2: Influence of ice properties on $F_{Compression}$; ice strength properties for each day are given in Table 3.2.2 and Table 3.2.4. 38
Figure 4.2.3.3: Influence of ice properties on $2F_{seg}$; ice strength properties for each day are given in Table 3.2.2 and Table 3.2.4 38
Figure 4.2.3.4: Influence of ice properties on F_{Model}; ice strength properties for each day are given in Table 3.2.2 and Table 3.2.4 39
Figure 4.2.4.1: Ratio of Bow and Compressive Forces on A Unit Length of Loading Area Basis 41
Figure 4.2.5.1: Variation in Ratio of Frictional Resistance to Icebreaking Resistance. 43
Figure 4.2.6.1: Variation in Ratio of Frictional Resistance to Compressive Force. 44

Appendices

A.1 Force Histories for Simple Model

A.2 Force Histories for Segmented Model

B.1 Average Forces for Segmented Model

B.2 Bar Charts for Segmented Model

B.3 Variations in Average Forces With Ice Velocity for Segmented Model

B.4 Comparison of Bow and Compressive Forces for Segmented Model

B.5 Bow/Friction Force Variations for Segmented Model

B.6 "Friction Coefficient" Variations for Segmented Model

1. INTRODUCTION

A research project investigating the behaviour of a ship in compressive ice was begun in early 1996. As part of this project model testing was conducted by the Helsinki University of Technology to gain insight into the phenomena involved when a ship is transiting a compressive ice field. This testing focused primarily on the loads developed in the hull and the effect of compression on ship resistance. The current report details the tests carried out, including the experimental set-up, testing procedure, measurements taken, and results obtained. An important difference between the current study and previous projects was the use in this project of small model floes to simulate pack ice rather than large ice sheets simulating level ice. *Level ice* denotes ice that exists as large, flat sheets extending for great distances (e.g. up to hundreds of kilometres) as a single piece of ice, while *pack ice* denotes ice that exists in various sizes and geometries (from smaller than a ship to several hundreds of metres, when the floe can be treated more like level ice). Pack ice is used in this study because it is probable that pack ice would more accurately represent a real compressive ice field than would level ice. When a ship is transiting a large floe of level ice, the ice sheet has to crack into several pieces before they can move against the hull of the ship, i.e. before the ice field can converge. This is not the case in a pack ice field where the ice exists as many smaller pieces which are free to move and collide with the hull of a ship.

Two models were used: the first was a simple icebreaker model used to determine the total resistance of the ship as it transited various compressional ice fields, while the second model was split into three segments to determine the forces on the bow and the parallel midbody in addition to the overall resistance. A general description of the nature of the problem and a review of previous work follows.

1.1. The General Problem

An ice field is compressive if it has internal lateral stresses arising from convergence of floes. *Convergence* refers to the reduction in the area covered by an ice field, i.e. increasing ice concentration, by the closing of leads and channels due to the movement of ice floes. This results eventually in contact among ice floes as leads and channels are completely closed. Convergence of the ice field can continue beyond 100% concentration, as the ice ridges and rafts. *Ice ridging* refers to the formation of large ridges of ice when ice floes collide with one another. Ridges extend above and below the surrounding ice field. Most of the ridged ice exists below the waterline. Ridges are a significant barrier to ships. *Rafting* is the movement of one ice floe over another as they collide. *Compression* is related to convergence in that compressive forces arise in the floes when they are pushed against one another. Compressive forces also arise in anything that the ice is pushed against, such as the hull of a ship. Thus compression arises from the convergence of floes. The driving forces for convergence and compression are primarily due to drag from wind and currents, i.e. frictional forces between the ice, air and water, and are thus dependent on the ice surface roughness (both above and below the waterline) and ice/fluid relative velocity.

Convergence of ice fields can be considered on a global scale as well as on a local scale. *Global* refers to behaviour that occurs over a large area, significantly removed from the *local* situation which is analysed over a smaller geographical region. Global effects are accounted for in local scale analyses but do not change with local changes. The compression induced by currents is of a global scale, i.e. over large geographical areas, while that induced by wind is more local in nature and depends on the wind conditions in a smaller geographical region. For example, the Beaufort Gyro and the Transpolar Drift cause large scale (global) convergence, while compression in the Russian arctic is primarily wind induced and varies over smaller geographical regions, i.e. locally. Wind is by far the most dominant factor influencing compression of ice fields in the Baltic and is the most significant parameter in the development of local compression in the Arctic Ocean ice cover. Thermal and tidal compression may also occur but are considered to have a negligible effect on navigation. Thermal compression is of a static nature, requiring compact level ice and the presence of a confining

shoreline. It is associated with fast and large changes in air temperature. Tidal compression follows the cycle of tides and its occurrence can therefore be predicted and the compressive ice fields avoided.

Generally, in order for an ice field to converge and produce compression it must have a boundary (e.g. land, fast ice, or thicker ice with a different velocity) which restricts the motion of floes. When the ice field encounters a boundary pressure can develop rapidly and reach values high enough to cause local ice sheet failure. This failure can occur by ridge-building, rafting, and consequent crushing and bending failure of floes. It is obvious that these stresses can also affect a ship caught in the ice field - structural failures have occurred under such conditions in the Arctic, Antarctic, and Baltic. Note that the boundary requirement is not absolute as differences in drift velocity or driving forces within a free floating pack ice field can result in internal lateral stresses in the ice field. However, such pressures are probably not as high as those occurring in a situation where a boundary exists. The development of pressure in the ice field is controlled by two factors - the driving forces and the forces required to cause rafting, ridging and failure of the ice. The driving forces causes the motion and the forces required to cause ridging, rafting, or failure set the limit of the compression (Riska *et al*, 1996).

Compressive ice fields pose a risk to navigation. When a ship passes through a level ice field it opens a channel slightly wider than the ship. In a compressive ice field this channel closes due to the convergence of the field. Thus it is possible that the channel may close fast enough to meet the parallel midbody of the ship and begin to exert pressure on the hull. Referring to **Figure 1.1.1** below it can be seen that contact depends on the velocity and length of the vessel, as well as the closure speed and width of the channel (Riska *et al*, 1996).

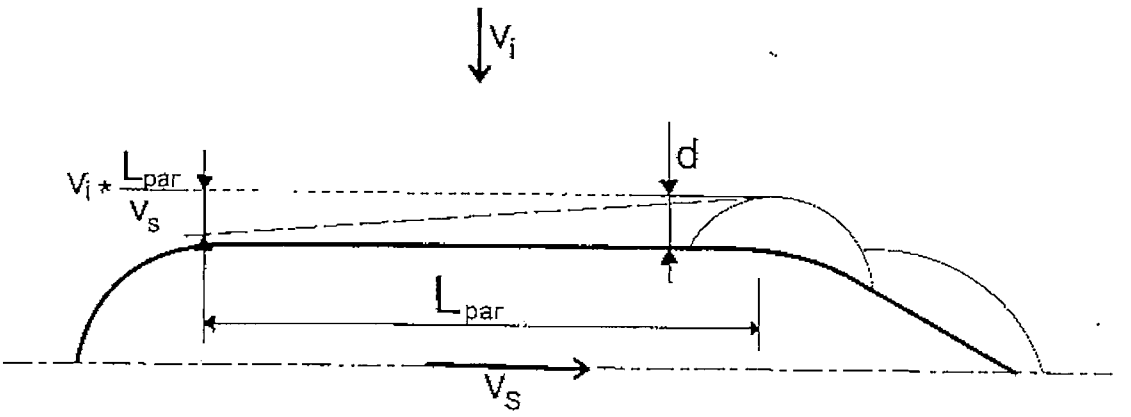

Figure 1.1.1: Description of Compressive Ice Contact Scenario (Riska *et al*, 1996).

Contact will occur if :

$$\frac{d}{v_i} \leq \frac{L_{par}}{v_s} \qquad (1)$$

where d is the transverse dimension of the last ice cusp broken at the shoulder of the vessel, v_i is the channel closure speed, L_{par} is the length of the parallel midbody, and v_s is the ship velocity. This is even more of a problem if the ship is being lead by an icebreaker because the effective length of the convoy (equal to L_{par} above) is equal to the distance from the bow of the icebreaker to the stern of the following vessel, thus increasing the likelihood of contact with the hull of the following vessel. If contact occurs the ship can be stuck in the ice while pressure continues to increase and damage the hull. The increase in pressure occurs because the ice field continues to converge, even beyond 100% concentration. Convergence will continue and the pressure against the ship hull will increase until the ice fails, either by rafting, ridging, bending, or crushing. Failure can occur within the ice field or against the hull of the ship. This is the concept of progressive damage and it is a key facet of the compressive ice problem. Previous studies have shown that local load concentration of ice field pressure is possible, meaning that small areas of the ship hull can be subjected to large stresses (Spencer and Hardiman, 1993). Furthermore, it has been suggested that "ridge" building along the hull is necessary for these load concentrations to occur. The implication of this statement is that high local load concentrations occur only if the ice field

pressure exceeds the ridge-building line load for the ice cover in question, resulting in ridge development against the hull and a localised ice-structure contact.

Compressive ice increases the ice loads on a ship and ice resistance of a ship. According to Spencer and Hardiman the effect on the resistance is considered to be due primarily to the increase in frictional resistance along the parallel midbody. Compression is not believed to have a significant effect on the resistance caused by breaking and sinking of the ice because the stresses involved in breaking are much higher than those needed to generate compression of the ice field (Riska et al, 1996). Visible effects of compression onboard the ship include crushing and turning of the ice floes against the hull, and closing of the channel behind the ship. This last indicator is the most common method to identify ice compression. Ships navigating in the arctic and subarctic areas very often encounter compressive ice fields because most of the shipping routes there are near the coast and the water is shallow. Shallow water is linked to compressive ice fields because the coastline restricts the motion of the ice floes. Additionally, grounded ridges (stamukhas) which occur in shallow water areas also act as a boundary to the motion of floes. Much of the Northern Sea Route lies in waters less than 50 m (Lensu *et al*), and compression has been frequently reported by ships navigating in this area, although the probability of encountering compressional ice is unknown. When a ship encounters compressive ice the most important consideration is the prevention of damage to the ship, especially if compression occurs for an extended period of time and icebreaker assistance is delayed in the event that the ship becomes stuck in the ice field. Thus an understanding of the structural effects of compressional ice fields on a ship is highly desirable. This is not the focus of the current report however, although it is closely related. The increase in ship resistance due to compressive ice, treated herein, has a structural basis, but relates more to navigation. Information about resistance due to compressional ice would be useful in transit simulations like the ones described in Lensu *et al*, (1996) and also in any developments in transit simulation software. Additionally, compressive ice resistance could also be taken into account in developing overall ship resistance formulations and ice trafficability requirements, such as those described in Riska, Englund and Wilhelmson (unpublished).

1.2. Previous Studies

Several articles and studies about ships in compressive ice and problems related to navigation in compressive ice have been published. These have largely been concerned with ice loads and ice failure processes. A reliable method for calculating ship resistance in a compressive ice field still does not exist.

Kujala *et al.* (1991, 1992, 1993, 1994) have conducted a series of model tests in which large floes of level ice were compressed against the parallel midbody of a model ship and another series investigating the ice failure process as the ice was compressed with an instrumented panel. The tests focused on ice loads and ice failure mechanisms, both in the experimental and theoretical treatment. Towing resistance, i.e. total ship resistance, of the model as it was towed through a compressed ice field was also investigated (Kujala *et al*, 1991). The effect of frame angle and friction coefficient are also discussed (Kujala *et al*, 1991). The theoretical side of the research attempted to explain the observations of the experiments, typically from a fracture mechanics approach. The principal outcome of this test series was insight into the process of ice crushing and bending as an ice floe is compressed against a ship hull. It should be reiterated that the analysis and experimentation focused on *large floes of level ice* and thus much of the analytical treatment is inappropriate for the work described in this report. The procedure for testing used in the current study, described in **Section 2**, is largely based on the set-up in Kujala *et al's* work, and the analytical treatment may prove useful with modifications to account for the much smaller floe size.

Based on these tests a method for calculating the resistance in a closing channel is presented by Riska *et al.* (1996). The method is presented as a preliminary result and needs further improvement and validation. Additionally, a new quantity called the ice compression index, κ, is defined. This index is useful in evaluating the occurrence of contact in a compressive ice situation. It is simply a restatement of Equation (1) :

$$\kappa = \frac{dv_s}{v_i L_{par}} \qquad (2)$$

If $\kappa < 1$ contact occurs. In the case of an icebreaker leading another ship the ice compression index would be :

$$\kappa = \frac{B_{eff} - B}{2D} \frac{v_s}{v_i} \tag{3}$$

where B_{eff} is the width of the channel the ice breaker has cleared, B is the breadth of the following vessel, and D is the distance between the ships. Application of this index to a situation involving pack ice is not clear for two reasons: (1) the ice velocity would have to be a bulk characteristic for pack ice fields, as it varies for every floe, and (2) the value used for the ice cusp size d' is not obvious, since a channel through the pack ice field is not the same as a channel cut through a level ice floe. Pack ice floes can close in around the ship whereas level ice must first break along long cracks before floes can move in around the ship. In the pack ice situation the dominating factor in determining loads on the hull is the interaction between ice floes close to the ship. As stated above, the local ice-structure contact is influenced by the driving force and the limiting loads for ridging and rafting as well as bending and crushing failure.

Spencer and Hardiman (1993) have also conducted model ice tests. A ship model was towed through a relatively large compressed ice floe. Elastic hoses filled with air were used to drive the compression. Figure 8 from Spencer and Hardiman clearly shows an increase in both the "Side Force" *and*.the "Breaking Resistance" when the ice is subjected to lateral pressure. In their study "breaking resistance" is the total resistance of the ship as it transits the floe **minus** the "pre-sawn ice resistance". This last term is simply the resistance of the ship as it transits an area of the field which was already broken i.e. the resistance due to clearing of the ice. Therefore breaking resistance is the resistance caused by flexural failing of the ice, *plus* ice frictional resistance along the hull arising from compression. "Side force" is the total force measured by four load cells attached to a plate on one side of the model. They also argued that one test in which a loss of pressure in the hoses resulted in a loss of compression in the ice floe indicated that a **pre**-stressing of the ice does not lead to an increase in the breaking resistance. Spencer and Hardiman's work differs from *Kujala et al*'s studies be-

cause in the former the model was ***inside*** the floe, while the latter simulated a ship in a lead closing under pressure.

Heideman (1996) has published a study about ice compression and its influence on navigation in the Northern Sea Route (NSR). The most significant part of this study was the correlation of wind directions and speeds with reported events of ice compression along the NSR. Furthermore, Heideman describes the Russian "ball" scales used to qualitatively and quantitatively measure ice compression, concentration, and ridging. Ice compression is judged and assigned a ranking from 0 to 3 (0 = no compression, 3 = severe compression). For details the reader is advised to consult Table 4 in the original paper. With respect to ice compression this scale uses signs that can be observed visually, e.g. from a ship or helicopter. Typical signs include the heeling of the ship, colour of the ice and closing speed of the channel behind the ship. The ball scale is not based on any physically measurable units and is therefore very difficult to use for analytical purposes. As it is dependent on visual impressions of the ice field, it is difficult to correlate the ball scale value with non-visual factors, e.g. driving forces and pressure in the ice field. However, because of its extensive use in Russian navigational experience along the NSR, proposals for attempts to correlate the ball scale with measurable physical quantities have been made (Heideman, 1996).

Most recently, Fleet Technology Ltd (1997) of Canada have produced a draft version of a report detailing Phase I of a project to describe the pressurised ice scenario in terms that can be applied in the specification of structural requirements for Polar Class vessels, specifically in compressive pack ice. The report focuses on the loads required to cause load concentrations sufficient to cause reported incidents of damage and the factors involved in developing these loads. This report is the only one cited herein that attempts to explain the pressurised ice scenario from a structural damage standpoint. Ship resistance is not treated by their report, but the analysis of the pressure development in the ice field incorporates much of the work referenced above and makes several insightful suggestions that can be applied to the problem of resistance formulations. This includes an analysis of the global and local load concentration required to produce incidents of reported damage in Baltic navigation studies, and a development of the ridge building load limit required for specific ice thicknesses. The analysis also

suggest that structural damage is the result of ridge building against the ship hull, resulting in a highly varying localised ice-structure contact. This localised contact would result in concentration of field pressures against small sections of the hull area and structural damage.

2. EXPERIMENTAL ARRANGEMENT

Part of the problem in compressive ice testing is the design of a suitable experimental arrangement. Test were conducted in the ice tank of the Helsinki University of Technology (HUT). This tank is 40 m X 40 m in area and is equipped with a moving bridge and carriage spanning the width of the tank. This bridge was used to push the ice floes together to simulate compression. The basic testing procedure consisted of towing a model ice-breaker through a field of broken ice which was compressed by pusher plates attached to the moving bridge. The ice was broken into relatively small floes to simulate a pack ice field. **Figure 2.1** shows a schematic of the towing arrangement. This arrangement was used for a number of reasons. The aim of the experiments was principally to study the influence of ice velocity, model velocity, and ice field concentration on the forces experienced by the model hull and on the overall resistance of the ship. The set-up allowed for variation of these parameters to conduct a systematic investigation of their individual influence on the various components of ship resistance. The work of Kujala *et al* (1991) used the same towing/compression arrangement, so a basis for comparison was laid. The compression of the ice field with all pusher plates attached to the bridge ensured that the entire field was subjected to the same rate of compression. This allowed for specification of an ice velocity for use in the evaluation of the ice compression index.

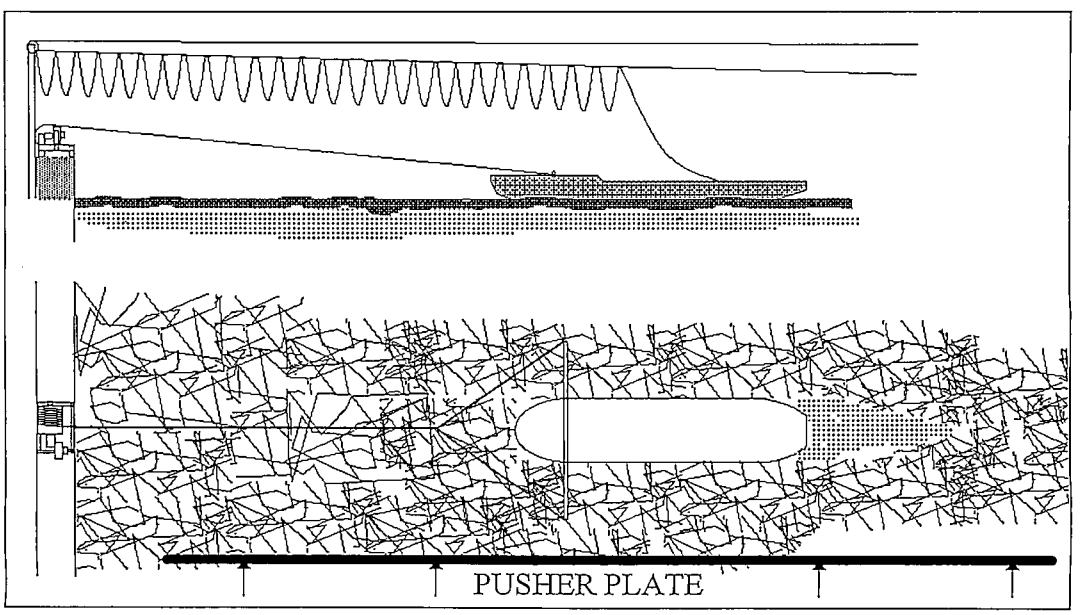

Figure 2.1: Sketch of the towing arrangement (not to scale).

The ice used was granular ethanol model ice, broken by pushing the pusher plates through the ice at regular intervals to achieve a relatively homogeneous ice field at the beginning of each test series. The ice was broken into relatively small pieces to model pack ice. The effect of compression in pack ice conditions has not been investigated in previous experimental studies and the differences in compression of pack ice as opposed to much larger sheets of level ice is unknown. A representative view of the broken ice field is shown in **Figure 2.2**. Ice properties were measured for each ice field before the ice was broken (Li and Riska, 1996).

Figure 2.2: Typical View of Broken Ice Field.

Because the bridge was used to compress the ice a separate towing system was required to pull the model through the ice field. The model towing system consisted of a motor driven drum-type winch mounted on the side of the tank and a cableway across the tank for the instrument cables. The instrument cables were manually winched across the tank so the model would not have to tow them. **Figure 2.3** shows the towing winch mounted on the side of the tank.

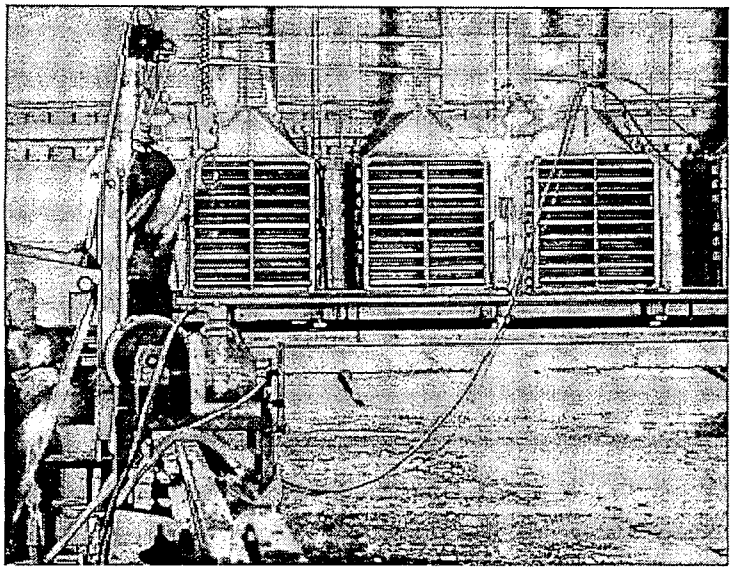

Figure 2.3: Towing winch mounted on tank wall.

Two models were used in the experiments. The first model was a simple icebreaker hull of the Mudyug class with principle dimensions listed in **Table 2.1**. This model was used in preliminary tests to measure the total ship resistance in various compressive pack ice conditions and will be referred to as the *simple model*. The model is shown in **Figure 2.4**.

Table 2.1: Main Dimensions of Simple Model

Dimension	
Length at CWL	3.77 m
Breadth at CWL	0.962 m
Draught at CWL	0.289 m

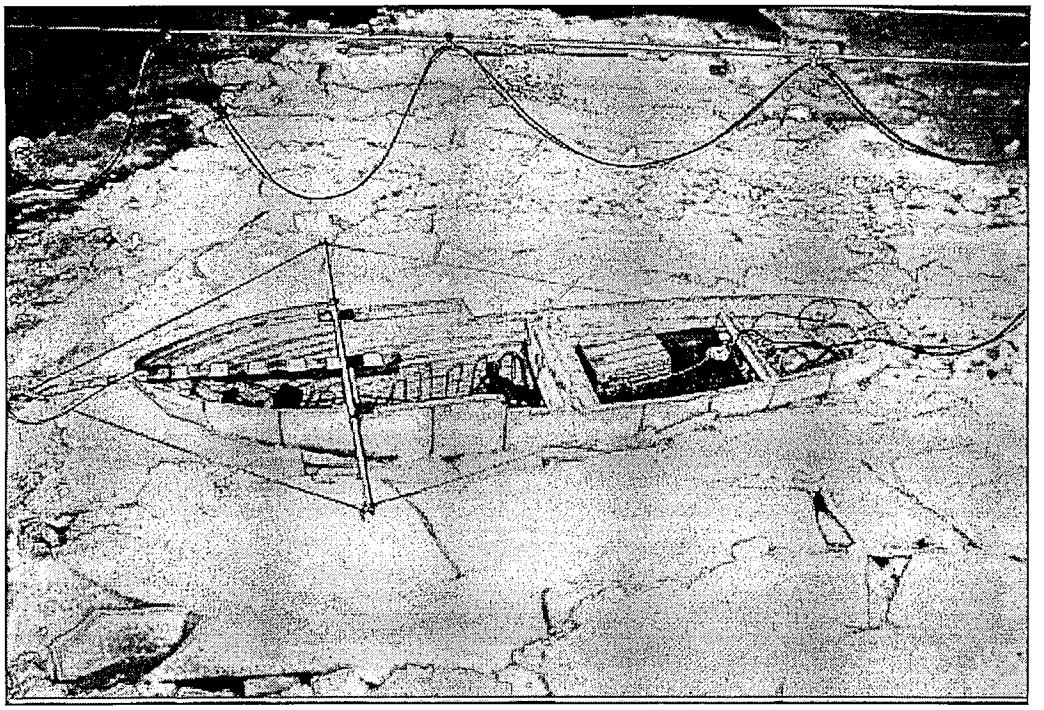

Figure 2.4: Simple model in tank.

The second model was that of an SA-15 vessel. This model was split into three segments as shown in **Figure 2.5**. This was done to determine the forces on the bow and along one side of the parallel midbody in addition to the total resistance. The segments were instrumented separately to measure the principle components of the total ship resistance, namely the icebreaking resistance and the added resistance due to compression. **Figure 2.6** shows the segmented model in the tank. **Table 2.2** lists the main dimensions of the segmented model.

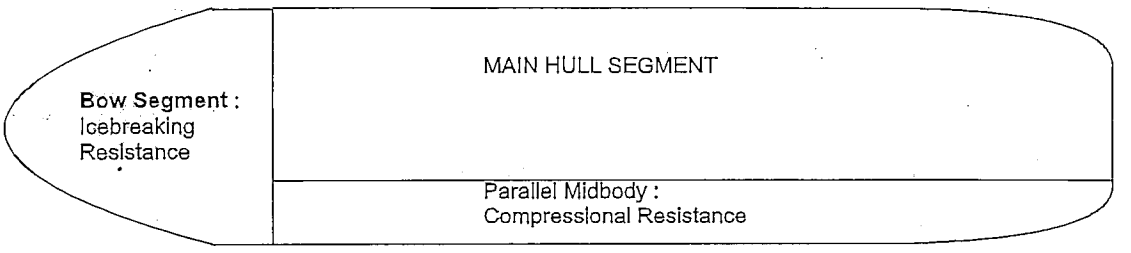

Figure 2.5: Schematic showing division of segmented model.

Table 2.2: Main Dimensions of Segmented Model

Dimension	
Length at CWL	5.88 m
Breadth at CWL	0.88 m
Draught at CWL	0.30 m
Length of Parallel Mid-body Segment at CWL	4.24 m

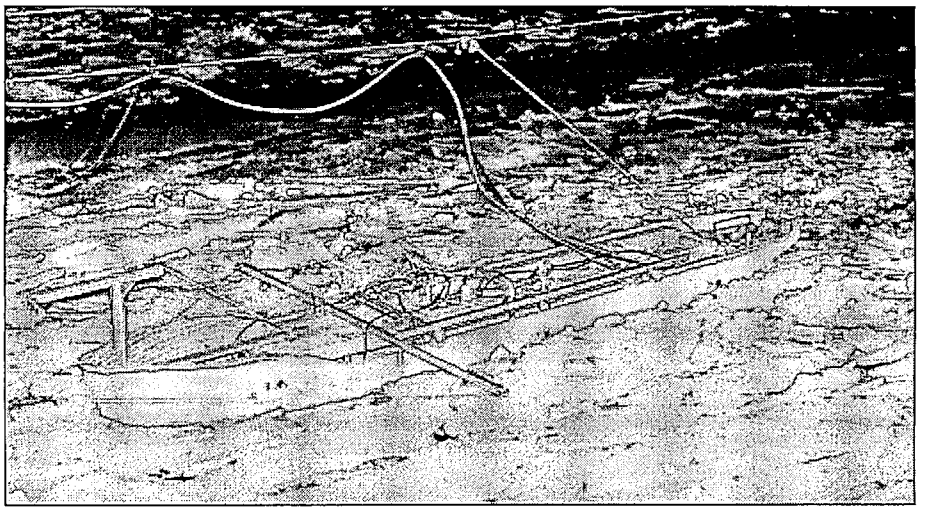

Figure 2.6: Segmented model in tank.

Both models had no propellers installed and their rudders were locked in the zero angle position. The models were free to pitch, roll, yaw, heave, surge and sway. The steering moment required to keep the model on course was developed by a straight rod connected across the model perpendicular to the hull at frame eight. The towing line was connected in a "Y" arrangement as shown in Figure 2.1.

3. TESTS CONDUCTED

Two sets of tests were conducted, one with a simple model used to measure the total resistance in compressive pack ice, and another with a segmented model used to examine the contribution of icebreaking and compressive forces to total resistance in compressive pack ice. The first set of tests were thus, in a sense, of a preliminary nature. Initially, two ice sheets were used to determine the most appropriate experimental set-up. The results from these two series of tests are not included here. Additionally, some tests with the segmented model were problematic and produced clearly unreliable results. They are also left out of the present discussion. A detailed listing of the successful tests is included below.

3.1. Measurements

The basic measurements taken were as follows :

1. Time
2. Pusher Plate Location
3. Force(s) measured with a load cell(s)
4. Winch rpm

The principle result of these measurements was a force time series for each load cell used in the test. In the simple model tests only one load cell was used, connected as shown in **Figure 3.1.1**. This load cell measured the total towing force required to pull the model through the ice field, thus indicating the total ship resistance. The segmented model was instrumented with seven load cells, as shown in **Figure 3.1.2**. Three load cells on the parallel midbody segment were used to measure the compressive force, two on the bow measured the bow force, one on the tow rope measured the total resistance, and the last load cell measured the ship resistance in the parallel midbody, i.e. the resistance caused by compression. As stated above the reason for this more complicated arrangement was to isolate the effects of compression from the effects of icebreaking and clearing. Winch rpm was recorded to compare target model velocities with actual model velocities. Pusher plate location was used to determine the degree of ice field compression (see **Section 4.1** below) and to compare target ice field velocities (i.e. desired velocity) with actual ice field velocities as determined

from the recorded speed of the ice tank bridge. Video recordings were taken of all tests.

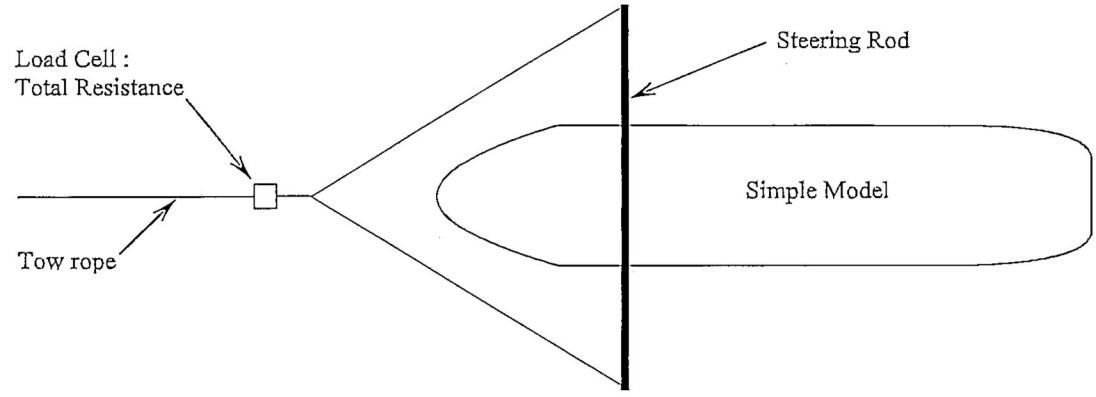

Figure 3.1.1: Instrumentation of simple model.

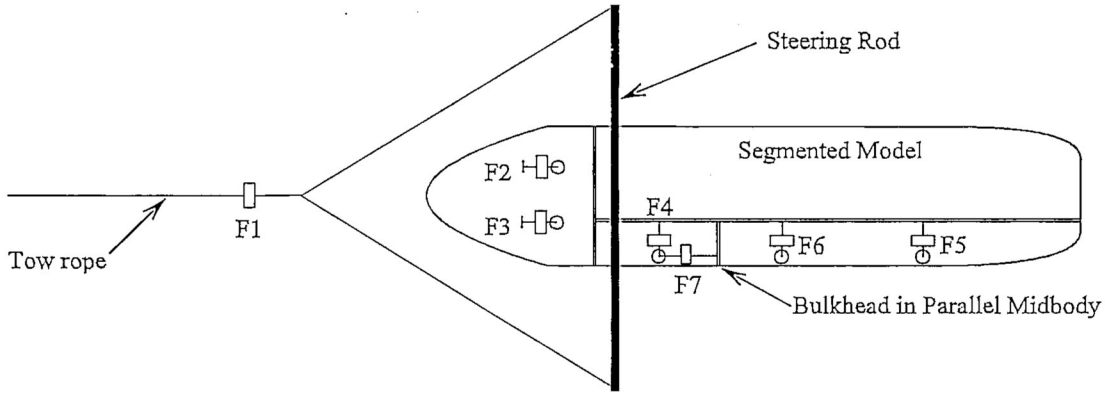

Figure 3.1.2: Instrumentation of segmented model. The circles indicate connections to a framework used to suspend the segments attached to the main hull. It is omitted here for clarity.

3.2. Summary of Tests

The parameters varied during the tests were the velocity of the model and the velocity of the ice, i.e. the rate of compression. Other factors such as ice thickness, floe size, and ice mechanical properties also varied due to the use of different ice sheets on different days. This allows for comparison of model behaviour based on ice properties.

Table 3.2.1 summarises the tests conducted using the simple model. A test series is identified by the date (dd.mm.yy) on which it was conducted and the number of the test. This is used to link the tests to the ice properties measured for that day of testing, i.e. that particular ice sheet. Tests with an ice velocity of zero indicate no compression. Note that actual model velocity is not included in this table. Winch rpm could have been used to calculate the actual model velocity. However, the use of a non-rigid tow rope allowed for possibly significant variation in model velocity as the rope alternately slackened and tightened as the model encountered an obstacle or change in resistance. This is clear from the videotape recordings of the tests. This problem complicates the evaluation of overall resistance during the tests. Thus it can only be assumed that the measured force histories are representative of the actual resistance forces. More will be said about this problem in **Section 4**, where the test results are discussed.

Note also that the test containing A, B, or C as an identifier in their title show more variation between target and ice model velocities. This is because these tests were done with one "pull" of the model through the ice. The ice was compressed at velocity "A" for a certain length of time, then accelerated to velocity "B" and then to velocity "C".

Table 3.2.1: Test Parameters for Simple Model

Test (ddmmyy_#)	Target Model Velocity (m/s)	Target Ice Velocity (m/s)	Actual Ice Velocity (m/s)
070696_3	0.1	0.01	0.010
070696_4	0.25	0.01	0.010
070696_5	0.5	0.01	0.010
070696_6	0.1	0.01	0.010
070696_7	0.25	0.01	0.010
070696_8	0.5	0.01	0.011
070696_9	0.1	0.01	0.010
070696_10	0.1	0.00	0.000
070696_11	0.25	0.01	0.010
070696_12	0.25	0.00	0.000
070696_13	0.25	0.01	0.010
130696_1A	0.25	0.01	0.010
130696_1B	0.25	0.02	0.026
130696_1C	0.25	0.04	0.047
130696_2A	0.25	0.01	0.011
130696_2B	0.25	0.02	0.027
130696_2C	0.25	0.04	0.048
130696_3A	0.25	0.01	0.015
130696_3B	0.25	0.02	0.026
130696_3C	0.25	0.04	0.040
130696_4A	0.25	0.01	0.016
130696_4B	0.25	0.02	0.024
130696_4C	0.25	0.04	0.041

Table 3.2.2 lists the ice properties for each test series conducted with the simple model. The broken ice area is the size of the ice sheet that was used in the testing. It represents the dimensions of the ice field when the coverage is 100%. This is the concentration at the beginning of each test series, i.e. the first test for each day starts with a concentration of 100%.

Table 3.2.2: Ice Properties for Simple Model Tests

Test Series	Broken Ice Area	26.4m x 40m
070696	Thickness	39 mm
	Strength, Compressive	22.9 kPa
	Strength, Bending Up	53.5 kPa
	Strength, Bending Down	51.5 kPa
Test Series	Broken Ice Area	26.4m x 40m
130696	Thickness	50 mm
	Strength, Compressive	11.8 kPa
	Strength, Bending Up	26.2 kPa
	Strength, Bending Down	21.4 kPa

Similarly, the test parameters for the segmented model tests are listed in **Table 3.2.3** and the corresponding ice properties in **Table 3.2.4**. The broken ice area.was 25 m X 40 m for the segmented model tests. In the first three segmented model test series the ice was initially broken by dropping the pusher plates through the ice every 0.5 m, while the last two ice fields were initially broken into 1.5 m X 1.5 m floes.

Table 3.2.3: Test Parameters for Segmented Model

Test	Model Velocity (m/s)	Target Ice Velocity (m/s)	Actual Ice Velocity (m/s)	Test	Model Velocity (m/s)	Ice Velocity (m/s)	Actual Ice Velocity (m/s)
				040397_1A	0.25	0.02	0.021
051296_3	0.25	0.04	0.044	040397_1B	0.25	0	0.000
051296_4	0.25	0.01	0.009	040397_2A	0.25	0.02	0.022
				040397_2B	0.25	0	0.000
101296_1A	0.1	0.04	0.046	040397_3A	0.25	0.02	0.021
101296_1B	0.1	0.02	0.026	040397_3B	0.25	0	0.000
101296_1C	0.1	0.01	0.017	040397_4A	0.25	0.02	0.021
101296_2A	0.1	0.04	0.042	040397_4B	0.25	0	0.000
101296_2B	0.1	0.02	0.026	040397_5A	0.25	0.02	0.021
101296_2C	0.1	0.01	0.015	040397_5B	0.25	0	0.000
101296_3	0.1	0.02	0.020	040397_6A	0.25	0.02	0.020
				040397_6B	0.25	0	0.000
270297_1A	0.25	0.02	0.022	060397_1	0.25	0.02	0.022
270297_1B	0.25	0.01	0.015	060397_2A	0.25	0.02	0.022
270297_2A	0.25	0.02	0.021	060397_2B	0.25	0.01	0.010
270297_2B	0.25	0.01	0.009	060397_3A	0.25	0.02	0.021
270297_3A	0.25	0.02	0.022	060397_3B	0.25	0.01	0.009

Test	Model Velocity (m/s)	Target Ice Velocity (m/s)	Actual Ice Velocity (m/s)	Test	Model Velocity (m/s)	Ice Velocity (m/s)	Actual Ice Velocity (m/s)
270297_3B	0.25	0.01	0.009	060397_4A	0.25	0.02	0.021
270297_4A	0.25	0.02	0.021	060397_4B	0.25	0.01	0.009
270297_4B	0.25	0.01	0.009	060397_5A	0.25	0.02	0.021
270297_5A	0.25	0.01	0.009	060397_5B	0.25	0.01	0.009
270297_5B	0.25	0.00	0.000	060397_6A	0.25	0.02	0.021
				060397_6B	0.25	0.01	0.009

Tests with a letter A, B, or C indicate that the testing was done with one pull of the model through the ice field, accelerating the ice field from velocity A to velocity B and velocity C. From a comparison of the various target and actual ice velocities in Table 3.2.3, it appears that this process resulted in greater differences between target and model velocities than testing at a single velocity.

Table 3.2.4: Ice Properties for Segmented Model Tests

Test Series (dd.mm.yy)	Thickness (mm)	Strength Bending Down (kPa)	Strength Bending Up (kPa)	Strength Compression (kPa)	Elastic Modulus (MPa)
05.12.96	40	56.9	47.6	107.7	46.7
10.12.96	49	33.7	20.5	57.8	24.0
27.02.97	38	42.7	32.0	58.9	32.0
04.03.97	40	42.3	32.9	43.9	29.9
06.03.97	40	77.2	62.2	90.0	113.8

4. RESULTS

It is clearly seen from the video recordings that compression occurred in the ice fields during testing. Deformation was obvious including rafting and the formation of ridges. Deformation was spread throughout the field. Closing of the channel behind the model as it was towed and crushing of the ice against the hull was clear. Bending of floes against the hull was evident as well as turning and sinking of floes. Large floes were seldom turned by the model but instead experienced crushing or bending failure.

The essential result of the tests was a history of the force measured by each load cell during the test. Typical time histories for each model are included in the relevant section below. From the video recordings it appears that variations or trends in the forces can be attributed to a number of factors :

- inhomogeneities in the ice field, e.g. variation in floe size, mechanical properties, existence of open water areas, leading to peaks in the force time history

- increasing compaction during the test, as compression increases the average thickness of the ice field and would thus be expected to generate an increasing trend in the force history.

- tightening and slackening of the tow rope as the model encounters an ice floe, stops and then surges forward creating a peak in the force history. The placement of the load cell in the tow rope also results in smoothing of the force history measured by this load cell

Some explanation regarding the treatment of the results is required. Because of the obvious complexity in analytically or numerically modelling a compressive field of pack ice, variations in model behaviour are examined based on the average force ex-

perienced by the load cell during the test. The focus of the current study was on ship *resistance*. Generally this resistance is "referenced to power requirements for maintaining effectively constant forward motion" thus ***power requirement correspond to average load, not peak loads*** (Sanderson, p.137). The high momentum of a ship allows it to sustain high global forces of short duration without coming to a complete stop. This averaging of forces represents bulk characteristics for each test, which greatly simplifies the analysis, and still captures the essential variations in resistance forces with variations in model velocity and compression rate. Results for a test series are presented as the average force versus a **compaction factor C** for the ice field, with model and ice velocities as parameters. The compaction factor of the ice field is defined as :

$$C = \frac{1}{2}\left[\frac{A_0}{A_{initial}} + \frac{A_0}{A_{final}}\right] = \frac{1}{2}\left[\frac{1}{1-\frac{l_i}{L}} + \frac{1}{1-\frac{l_f}{L}}\right] \qquad (4)$$

where:

C	Compaction factor during test
A_0	Broken ice area before testing
$A_{initial}$	Area of ice at beginning of test
A_{final}	Area of ice at end of test
L	Length of broken ice area (width of broken ice area does not change)
l_i	Pusher plate location at beginning of test
l_f	Pusher plate location at end of test

Thus the compaction factor represents the extent to which the ice field has been compressed from the broken ice areas[1]. This is calculated using the location of the pusher plate. Essentially this is a measure of the increase in the nominal thickness of the ice field. This must be viewed as a rough measure of the ice field compression as it does not directly indicate the extent of any rafting or ridging.

[1]The term "concentration" would seem applicable to this situation. It is the opinion of the author that the term "compaction factor" more clearly denotes the physical situation being studied than would "concentration" as it makes little sense to talk of concentrations greater than 100% or 1.

4.1. Simple Model

Two test series (070696 and 130696) were conducted for the simple model. As stated above the result of the simple model tests was a force time series for the total towing force, that is, the total ship resistance. **Figure 4.1.1** shows a typical time history from these tests. Complete time histories for all the tests are included in **Appendix A.1**. (Those tests identified by "A", "B", or "C", being continuations of the same model run through the ice field, do not start at time t = 0, thus the rather high values used along the time axis shown in Appendix A.1. This is also the case for the segmented model time series in Appendix A.2). These total resistance forces were averaged for each test and plotted versus average concentration for each test series, using model velocity and ice velocity as parameters. **Table 4.1.1** lists the average forces and concentrations for each test. **Figure 4.1.2** shows the average forces for test series 070696 while **Figure 4.1.3** shows the results for test series 130696.

Table 4.1.1: Average Forces for Simple Model Tests

Test ddmmyy_#)	Average Force (N)	Compaction Factor	Test (ddmmyy_#)	Average Force (N)	Compaction Factor
070696_3	40.37	1.18	130696_1A	29.40	1.17
070696_4	48.76	1.23	130696_1B	35.86	1.20
070696_5	62.77	1.30	130696_1C	53.01	1.27
070696_6	47.46	1.41	130696_2A	70.68	1.45
070696_7	70.25	1.49	130696_2B	93.88	1.49
070696_8	105.32	1.61	130696_2C	92.04	1.60
070696_9	85.71	1.75	130696_3A	89.44	1.81
070696_10	53.83	1.79	130696_3B	120.07	1.89
070696_11	73.52	2.05	130696_3C	181.43	2.04
070696_12	80.74	2.13	130696_4A	125.61	2.57
070696_13	106.61	2.35	130696_4B	122.17	2.73
			130696_4C	176.81	3.05

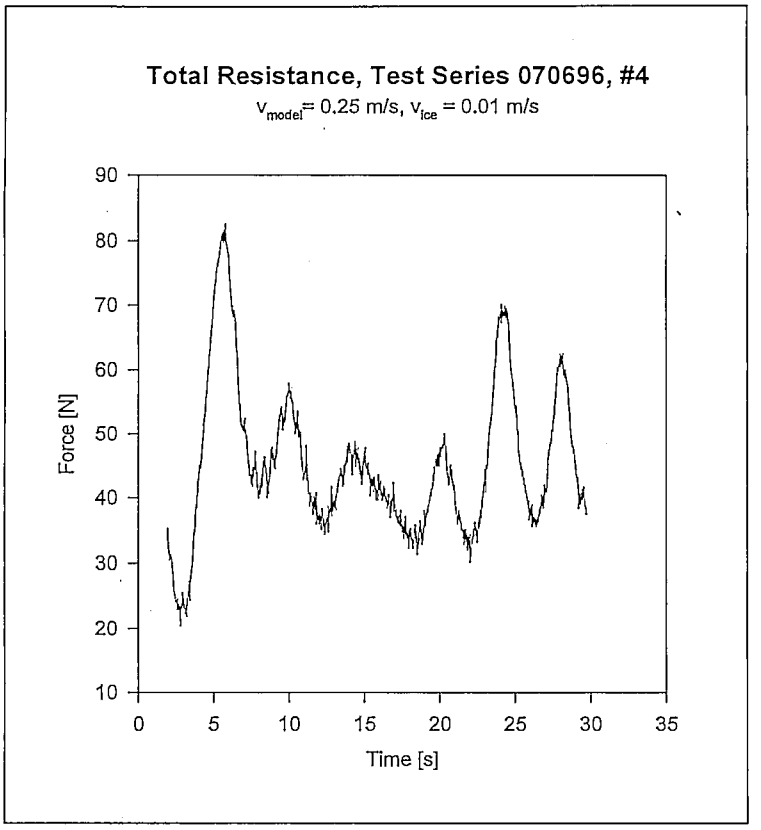

Figure 4.1.1: Typical force time history for simple model tests.

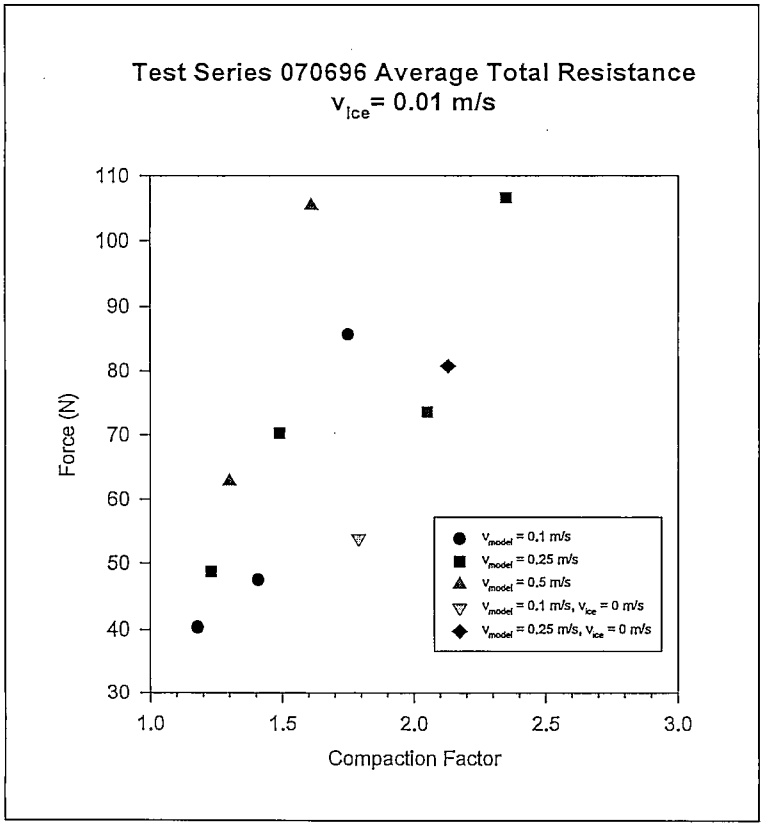

Figure 4.1.2: Variation in average force with compaction factor, test series 070696.

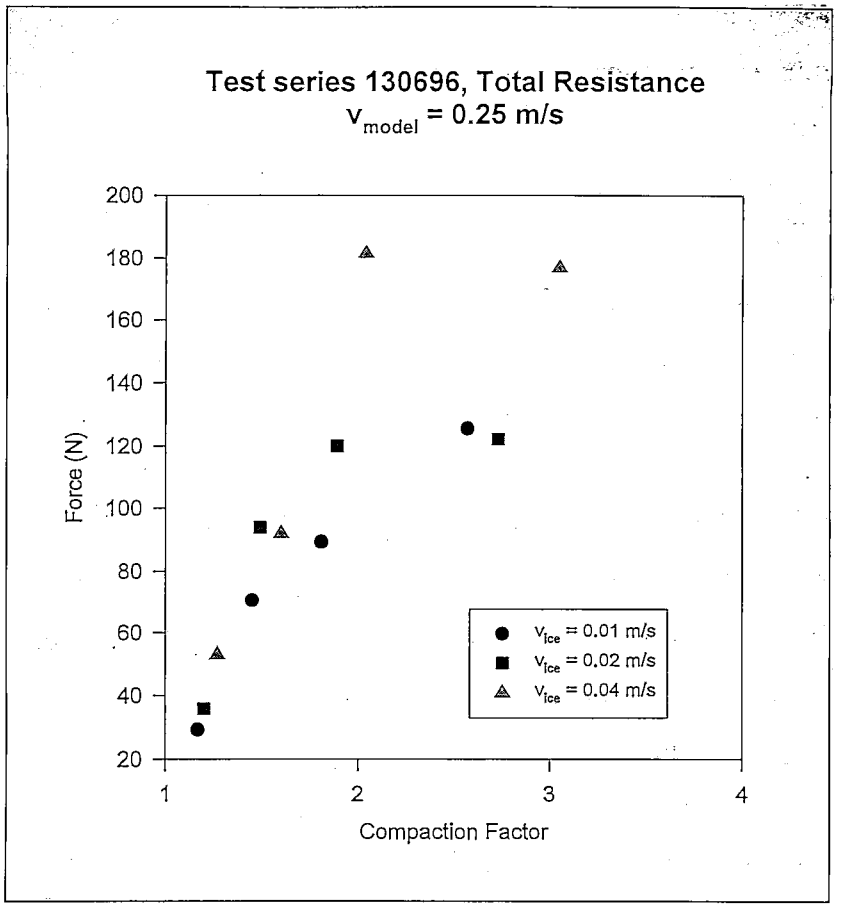

Figure 4.1.3: Variation in average force with compaction factor, test series 130696.

Figures 4.1.2 and 4.1.3 show: **(1)** increasing resistance with increasing compaction, and **(2)** increasing resistance with increasing ice velocity. Figure 4.1.2 also shows that **(3)** resistance is significantly greater with compression than without (the result for test 070696_11 at C = 2.05, Force = 73.52 N is considered an errant point). Also, it can be seen from Figure 4.1.2 that **(4)** higher model velocities tend to produce higher resistances. Figure 4.1.3 shows another feature of the model tests results - **(5)** a maximum resistance force seems to be reached, the value of this maximum resistance force increasing with ice velocity (i.e. compression rate). These observations can be explained rather simply. Model speed will increase resistance since the icebreaking and ice clearing forces would be greater as the acceleration of ice mass occurs in a shorter period of time. Thus a higher force is required to move through the field at a higher rate. Ice velocity would increase the rate of crushing and bending of floes against the hull, as well as the impact forces of ice floes against the model, thus increasing the normal force against the hull and the friction-induced resistance. Because the ice moves

faster, the ice would have to pile up against the ship hull at a higher rate of accumulation, requiring a greater number of failures in the ice field over a shorter period of time. The rate of loading in the ice could affect both the failure mechanisms in the ice and the nature of the loading on the ship hull. The limiting of resistance force shown in Figure 4.1.3 may be due to rafting in the ice field at higher compactions, with ice ridging and pile-up reducing the force transmitted from the pusher plates to the model hull. These explanations should be viewed as tentative, as the data is limited and subject to stochastic variations that may arise with more testing.

The relative effects of ice and model velocity can be examined using the ice compression index κ, to provide a means of assessing resistance independent of the velocities and lengths involved. The only parameter that needs to be estimated is d, the ice cusp size formed at the bow shoulder. For the simple model test series this is estimated as 0.25 m, a value equal to half the average ice floe diameter, estimated from Figure 2.1 and the video tape recordings of the tests. Using L = 3.77 m (from Table 2.1) and v_{ice} and v_{model} values from Table 3.1, the ice compression index can be calculated for each test. **Table 4.1.2** shows the values of κ for the simple model tests.

Table 4.1.2: Ice Compression Indices for Simple Model Tests

Test (ddmmyy_#)	Ice Compression Index κ	Maximum *d* required for contact (m)	Test (ddmmyy_#)	Ice Compression Index κ	Maximum *d* required for contact (m)
070696_3	0.6631	0.3770	130696_1A	1.6578	0.1508
070696_4	1.6578	0.1508	130696_1B	0.6376	0.3921
070696_5	3.3156	0.0754	130696_1C	0.3527	0.7088
070696_6	0.6631	0.3770	130696_2A	1.5071	0.1659
070696_7	1.6578	0.1508	130696_2B	0.6140	0.4072
070696_8	3.0142	0.0829	130696_2C	0.3454	0.7238
070696_9	0.6631	0.3770	130696_3A	1.1052	0.2262
070696_10			130696_3B	0.6376	0.3921
070696_11	1.6578	0.1508	130696_3C	0.4145	0.6032
070696_12			130696_4A	1.0361	0.2413
070696_13	1.6578	0.1508	130696_4B	0.6908	0.3619
			130696_4C	0.4043	0.6183

It is clear from this table that evaluation of the ice compression index for pack ice fields makes no physical sense. Contact against the hull occurs for all tests, yet values for the ice compression index greater than 1, indicating no contact, occur. Additionally,.the third and sixth columns of this table show the maximum value of *d* for which contact will occur. These values are not supported by the visual observations of the ice field during the tests. Furthermore, the use of the pusher plate velocity to represent the ice field velocity is questionable because the transmission of forces from the plates to the ice floes is not necessarily consistent throughout the field. Ice floe velocities away from the plates could differ considerably from that at the plates as the ice field fails by rafting and ridging, allowing rafted and ridged floes to remain relatively stationary. This suggests that the compressive ice problem must be treated in a different manner than that of level ice. The severity of compression must be non-dimensionalized in a physically meaningful way which is currently lacking. This is beyond the scope of the current project and is a potential area for future work.

4.2 Segmented Model

The treatment of data obtained from the segmented model tests was slightly more involved. Referring to Figure 3.1.2, the following forces were calculated for purposes of analysis of the model behaviour :

$\mathbf{F_{Rope} = F_1}$	This represents the total model resistance measured in the compressive ice field by the load cell in the rope.
$\mathbf{F_{Bow} = F_2 + F_3}$	This measures the total force in the bow segment, i.e. the "icebreaking" resistance.
$\mathbf{F_{Compression} = F_4 + F_5 + F_6}$	Total compressive force on one side of the parallel midbody.
$\mathbf{F_{seg} = F7}$	The component of total model resistance measured in the parallel midbody segment.

$\mathbf{F_{Model} = F_{Bow} + 2F_{seg}}$ This is the total ship resistance calculated from the forces experienced by the hull of the model. The parallel midbody segment force is doubled to include resistance along the side of the ship model that was not instrumented.

$\mathbf{F_{Friction} = F_{Rope} - F_{Bow}}$ This is the frictional resistance calculated as the total measured resistance minus icebreaking forces. It thus represents the contribution to the total resistance due to compressive forces and any other forces not measured.

From these equations it is clear that the following relations *should be* true, neglecting forces along the bottom of the main hull segment:

$$\mathbf{F_{Rope} \approx F_{Model} = F_{Bow} + 2F_{seg}}$$
$$\mathbf{F_{Friction} = F_{Rope} - F_{Bow} \approx .2F_{seg}}$$

The results of the segmented tests were plotted as time histories for $\mathbf{F_{Rope}}$, $\mathbf{F_{Bow}}$, $\mathbf{F_{Compression}}$, and $\mathbf{F_{seg}}$, collectively referred to as the *Measured Forces*. Typical time histories for these forces are shown in **Figure 4.2.1**. Furthermore, using the approximate relationships for $\mathbf{F_{Rope} \approx F_{Model}}$ and $\mathbf{F_{Friction} \approx .2F_{seg}}$, comparative plots of *Total Resistance* and *Frictional Resistance* were generated. **Figures 4.2.2** and **4.2.3** show typical plots for each of these comparisons. Complete time histories for all tests are included in **Appendix A.2**. Several things are worth noting regarding these sample histories that are typical of all time histories for the segmented tests. First, in tests where compression occurs, compressive forces are the highest forces measured, indicating there is substantial pressure on the midbody of the model, much more than icebreaking forces on the bow. This is examined in greater detail below, see **Section 4.2.1**. Second, the longitudinal force in the parallel midbody is clearly non-zero, indicating that frictional resistance due to compression is evident and measurable. Third, as stated in

section 4.1, the total resistance measured shows a markedly smoother time history than the total resistance calculated from the bow and midbody forces. Finally, there are clear discrepancies between the forces $\mathbf{F_{Rope}}$ and $\mathbf{F_{Model}}$ and between the forces $\mathbf{F_{Friction}}$ and $\mathbf{2F_{seg}}$, as shown in Figures 4.2.2 and 4.2.3. This is most probably due to the use of a non-rigid tow rope and the subsequent effects of slackening, tightening, pitching and surging that this causes.

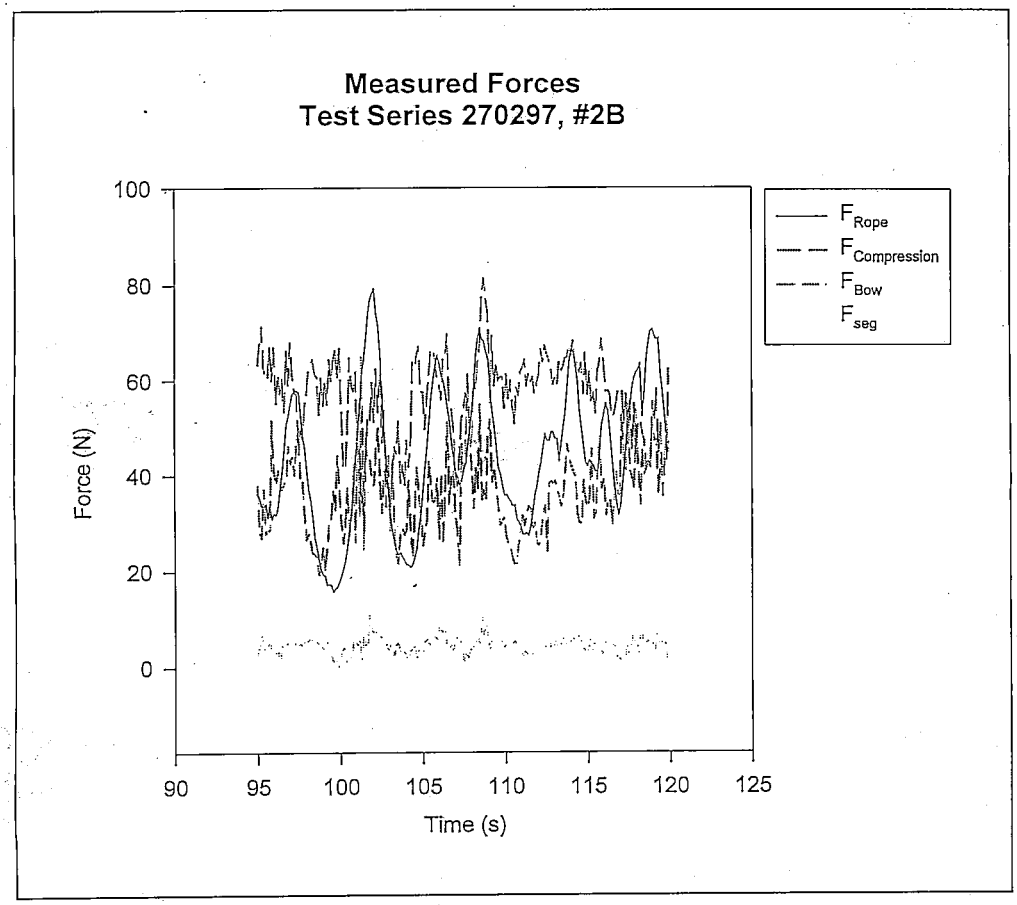

Figure 4.2.1: Typical time histories for Measured Forces in segmented model tests.

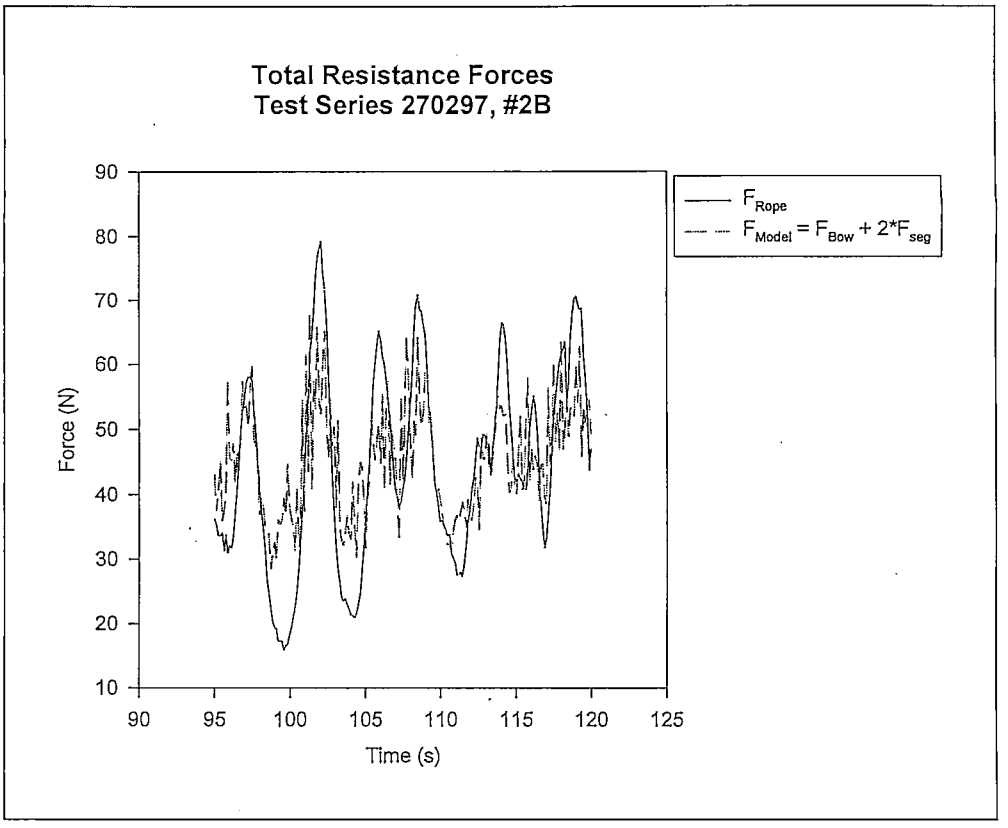

Figure 4.2.2. Typical time histories for Total Resistance in segmented model tests.

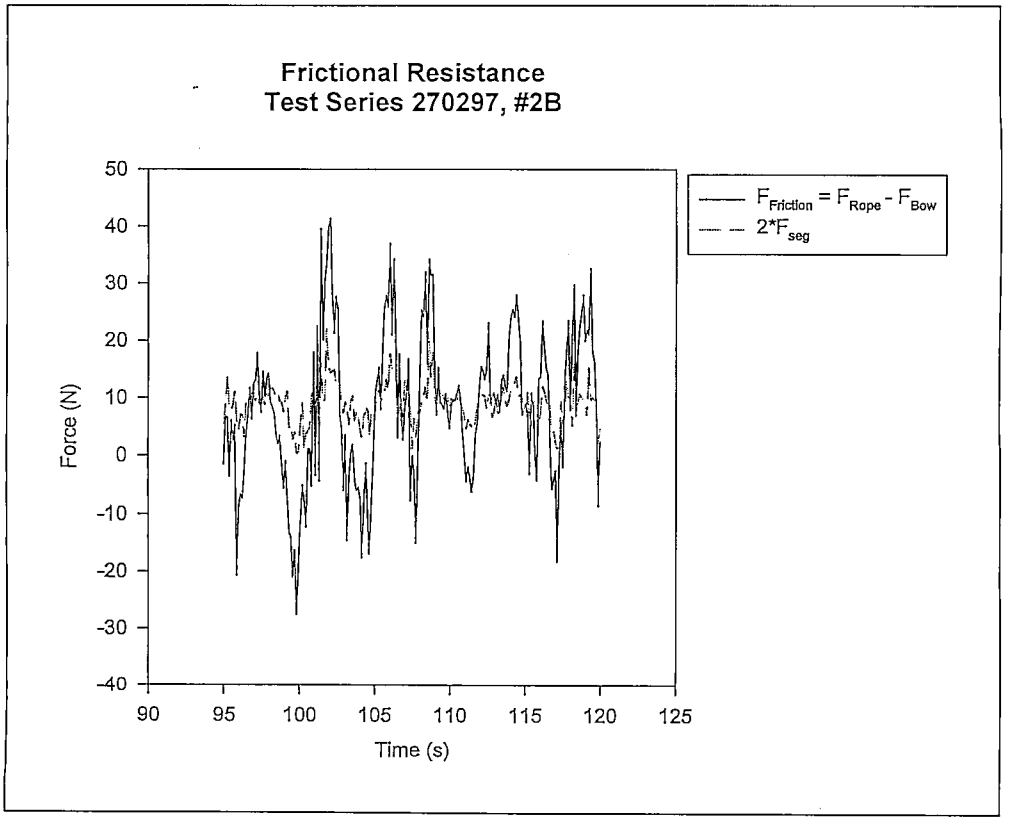

Figure 4.2.3: Typical time histories for Frictional Resistance in segmented model tests.

This tow rope effect does create some problems, but these discrepancies manifest themselves primarily as extremes in the time histories. Examination of Figures 4.2.2 and 4.2.3 show that on average the approximate relationships hold, with large discrepancies being due to the force measured by the load cell in the tow rope (F_1, total resistance measured, i.e. F_{Rope}). Examination of the time histories in Appendix A.2 indicate that this is usually the case. Additionally, forces in the main body segment were not measured. This means the assumptions that *(a)* drag on the bottom is negligible and *(b)* the frictional resistance on the un-instrumented side of the parallel midbody is the same as F_{seg}, are not necessarily true. These may have contributed to the differences between F_{Rope} and F_{Model}. Examination of the results is conducted in the same manner as for the simple model, using average forces and compaction factors to examine parametric trends in the force behaviour. **Appendix B.1** summarises the average forces for the tests conducted using the segmented model.

4.2.1. Comparison of Force Magnitudes

Bar charts of the relevant average forces were made to examine the relative magnitudes of the various force components for each test. Groups are ordered by increasing compaction. **Figure 4.2.1.1** shows a sample bar chart. **Appendix B.2** contains the charts for each of the test series for the segmented model.

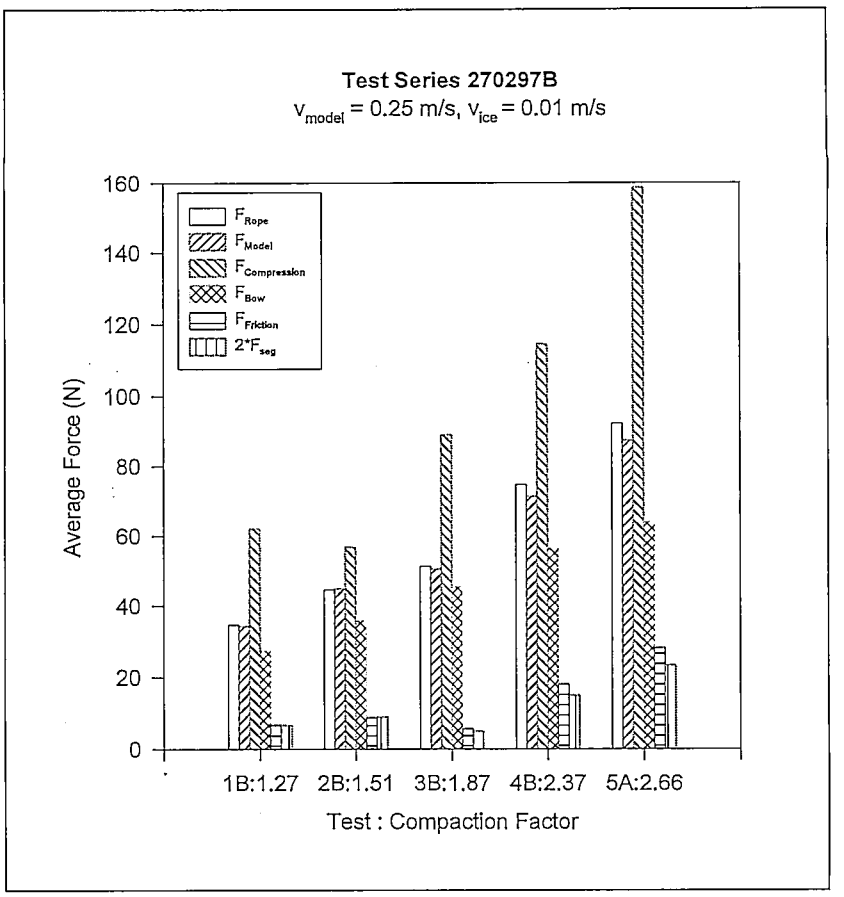

Figure 4.2.1.1: Sample bar chart showing each force component.

Examination of these charts show a number of distinct trends :

- Forces increase with compaction.

- Unmeasured forces, e.g. drag on the bottom, appear to be negligible. F_{Rope} is (in about all cases) slightly greater than F_{Model}. This indicates that other forces are noticeable, but insignificant.

- $F_{Compression}$ is always significantly greater than the other forces, notably F_{Bow}, the bow force. This indicates that compressional forces can be of large magnitudes, yet not be reflected in large increases in ship resistance. However, the compression force is measured over a larger area than the bow force. This prompted the examination of their magnitudes

base on the load per unit length of the projected contact area, discussed in detail in **Section 4.2.4**.

- $2F_{seg}$, the measured frictional resistance in the parallel midbody, is generally less than 40% of the bow force, F_{Bow}. This means that the major component of ship resistance appears to be the icebreaking force, but frictional resistance is significant. Similar to the preceding point, this should be examined on a load per unit length basis. Furthermore, as these two forces are used in calculating a value for total resistance it is worthwhile to examine the changes in the ratio of these forces with compaction. This is discussed in **Section 4.2.5**.

- In tests with no compression there are still significant ($F_{Compression} \approx F_{Bow}$) forces on the parallel midbody. This may be due to compression from previous tests resulting in pile up of ice floes that have not been re-ordered to relieve stresses in the ice field. The use of pusher plates in the experiment meant that piling up of ice could not be relieved because the plates restricted the motion of the floes.

4.2.2. Variations in Average Forces with Compaction Rate

Further analysis of the average forces was conducted on the basis of variations due to compaction rate, i.e. v_{ice}. Four forces were examined for each test series - F_{Bow}, $F_{Compression}$, $2F_{seg}$, and F_{Model}. Scatter plots of all of these forces vs. compaction factor as a function of ice compaction rate are included in **Appendix B.3. Figures 4.2.2.1-4.2.2.4** show sample plots for each of these forces.

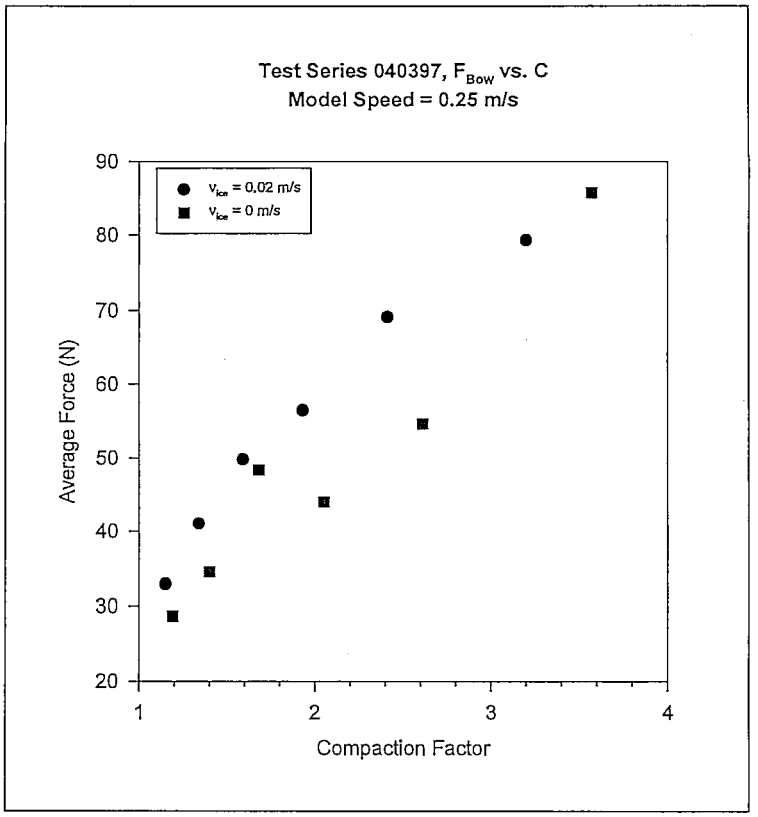

Figure 4.2.2.1: Scatter Plot for F_{Bow}, Test Series 040397.

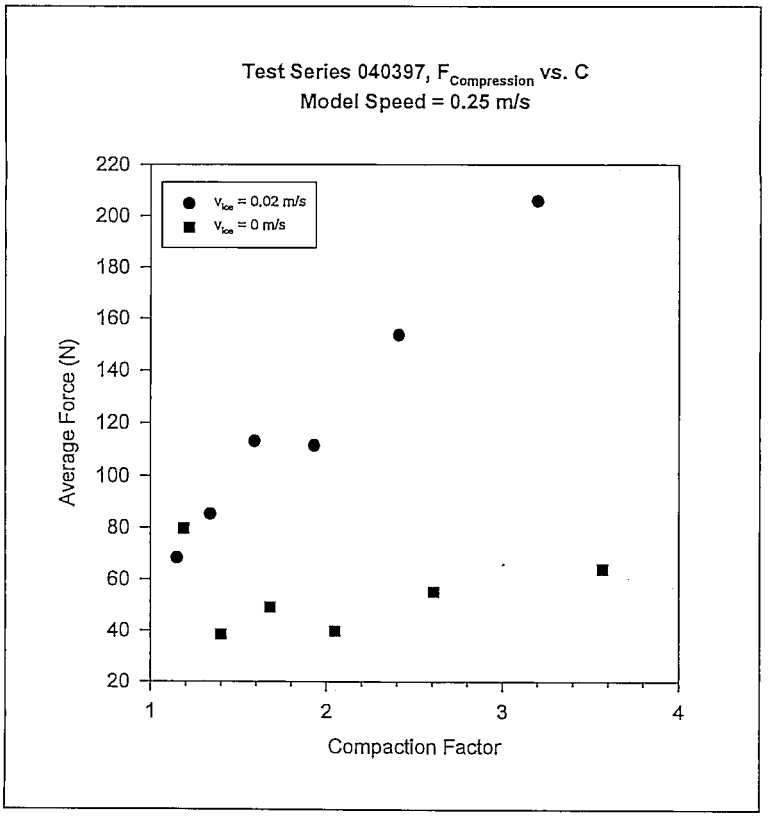

Figure 4.2.2.2: Scatter Plot for $F_{Compression}$, Test Series 040397.

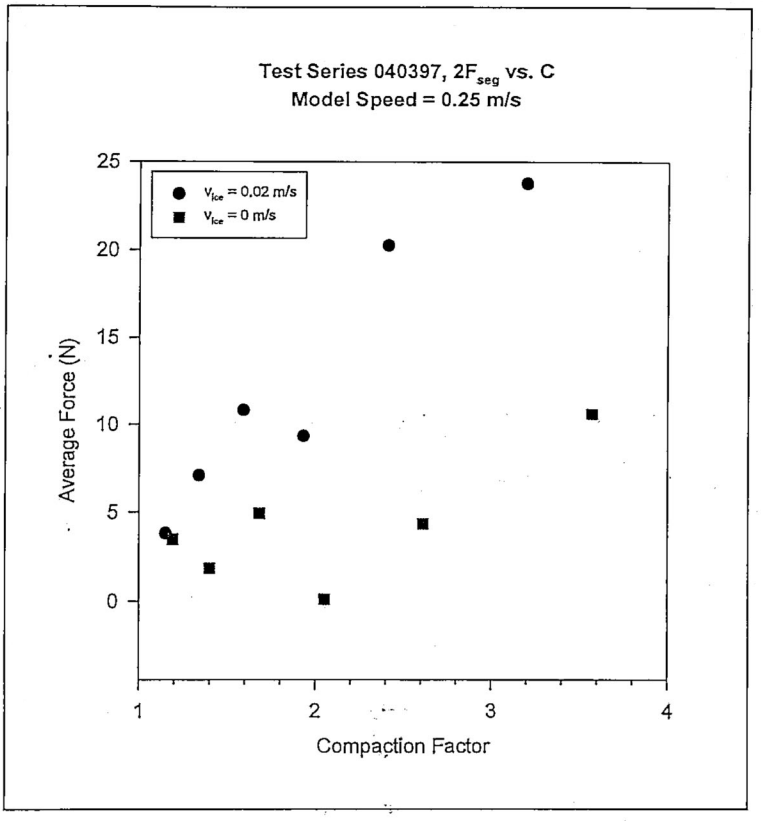

Figure 4.2.2.3: Scatter Plot for $2F_{seg}$, Test Series 040397.

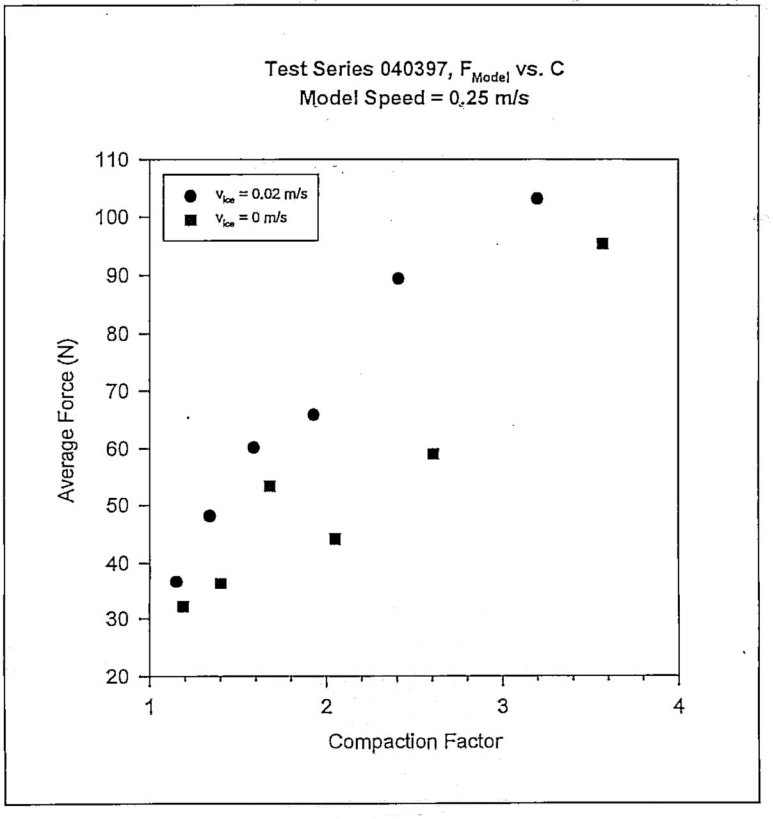

Figure 4.2.2.4: Scatter Plot for F_{Model}, Test Series 040397.

Referring to Appendix B.3, a number of trends are apparent :

- All forces increase with increasing compaction factor. This is expected as the compaction factor is effectively a measure of the thickness of the ice field.

- All forces increase when compression occurs. This includes the bow (ice-breaking) force because of the longitudinal component of compression on the curved bow.

- Compaction rate appears to have a different influence on different forces. Bow force is seen to increase with compaction rate, while compression force does not. The influence of compaction rate on frictional resistance (F_{seg}) is much more difficult to ascertain. Because of the small magnitudes recorded for F_{seg} it is difficult to tell if the variations are due to a high noise level or if the complexity of the ice field allows for high variations in frictional forces.

These trends are supported by most of the test results. Errant points do occur, but these may be due to statistical scatter, the influence of fundamental laws governing the system behaviour, or systematic error in the experiment.

4.2.3. Influence of Ice Mechanical Properties

The use of different ice sheets in the testing allows for a comparison of the influence of ice mechanical properties on the forces measured. This was done for the test series 270297, 040397, and 060397. Referring to Table 3.2.4, it is shown that these ice sheets had *approximately* the same thickness. Ice from test series 270297 and 040397 also have very similar strength characteristics, the only significant difference being in compressive strength. Ice from 060397 shows significantly greater values for all strength parameters and can thus be used for "overall" ice strength comparisons to the other two test series. **Figures 4.2.3.1 - 4.2.3.4** show the variations in forces for the compaction rate of 0.02 m/s.

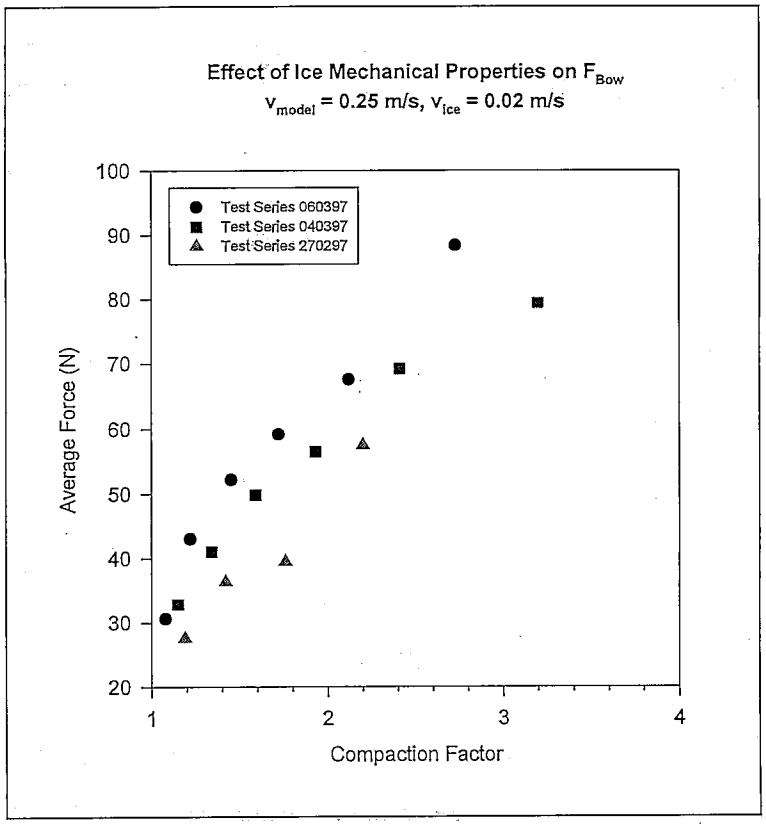

Figure 4.2.3.1: Influence of ice properties on F_{bow}; ice strength properties for each day are given in Table 3.2.2 and Table 3.2.4.

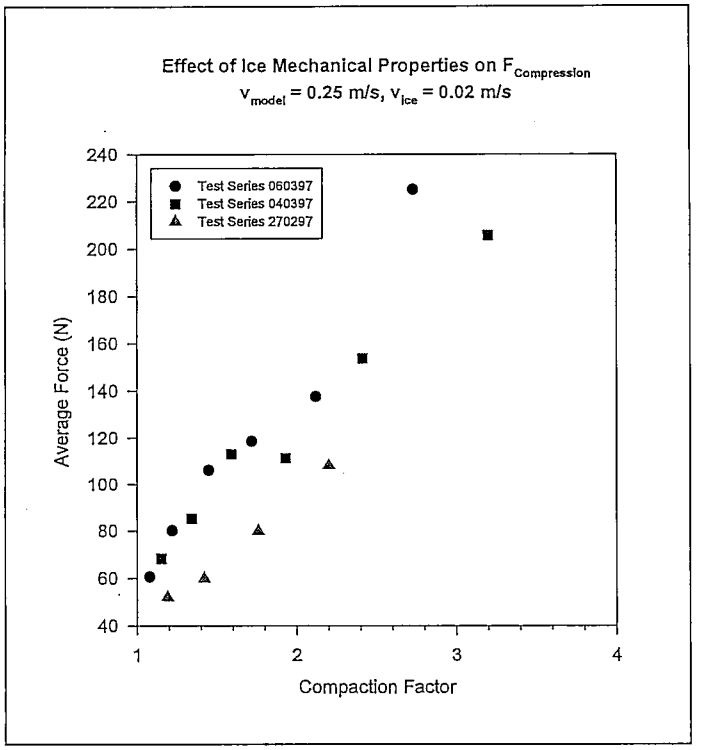

Figure 4.2.3.2: Influence of ice properties on $F_{Compression}$; ice strength properties for each day are given in Table 3.2.2 and Table 3.2.4.

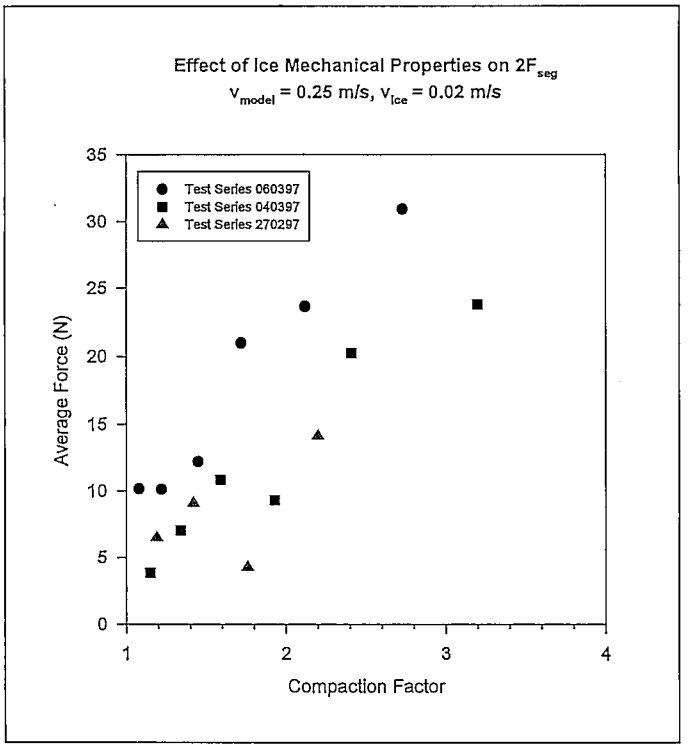

Figure 4.2.3.3: Influence of ice properties on $2F_{seg}$; ice strength properties for each day are given in Table 3.2.2 and Table 3.2.4.

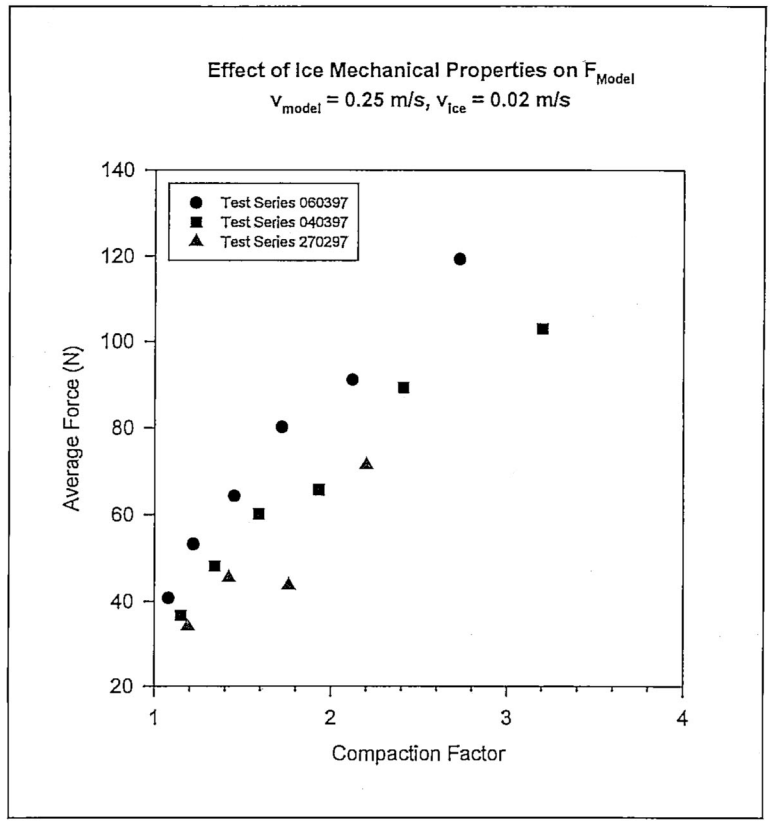

Figure 4.2.3.4: Influence of ice properties on F_{Model}; ice strength properties for each day are given in Table 3.2.2 and Table 3.2.4.

There are several things that these plots exhibit with respect to the influence of ice mechanical properties on the forces plotted.

the test series 060397, which had consistently higher values for the ice strengths measured, shows consistently higher forces, except in the case of the compression force. In this case the test series 060397 and 040397 show similar forces, even though the various measures of ice strength are much greater for 060397. This suggests that compression forces could be only slightly dependent on ice strength. A wider range of ice strength values would help define this behaviour more clearly. Furthermore, this is counter to the results shown for.the frictional component of resistance, $2F_{seg}$. This plot shows quite clearly that the higher strength ice has the highest forces for frictional resistance. One

would expect the behaviour of the friction force to reflect that of the compression forces, yet it does not do this.

- A comparison of test series 270297 and 040397 show consistently higher forces for 040397, but 040397 has a lower compressive strength. This may be due to a number of influences, primarily inaccuracies in the measurement of compressive strength of ice and the assumption that the influence of a 2 mm difference in ice thickness would be minimal.

Quite clearly the influence of ice properties on ship resistance is discernible using the limited results and the simple experimental arrangement in the current study. The significance of variations in ice properties should be examined in more detail than the current test results allow.

4.2.4. Comparison of F_{Bow} and $F_{Compression}$

Given the different loading areas over which these two forces acted, a valid comparison of their relative magnitudes should be made on a force per unit length basis. This was done using the values reported in Table 2.2, dividing the bow force by the breadth at CWL and the compression force by the length of the parallel midbody segment at the waterline. Plots of the ratio of these.forces per unit length are reported in **Appendix B.4**. Figure 4.2.4.1 shows a sample plot of the variation in ($F_{Bow}/F_{Compression}$) ratio with ice velocity and compaction factor.

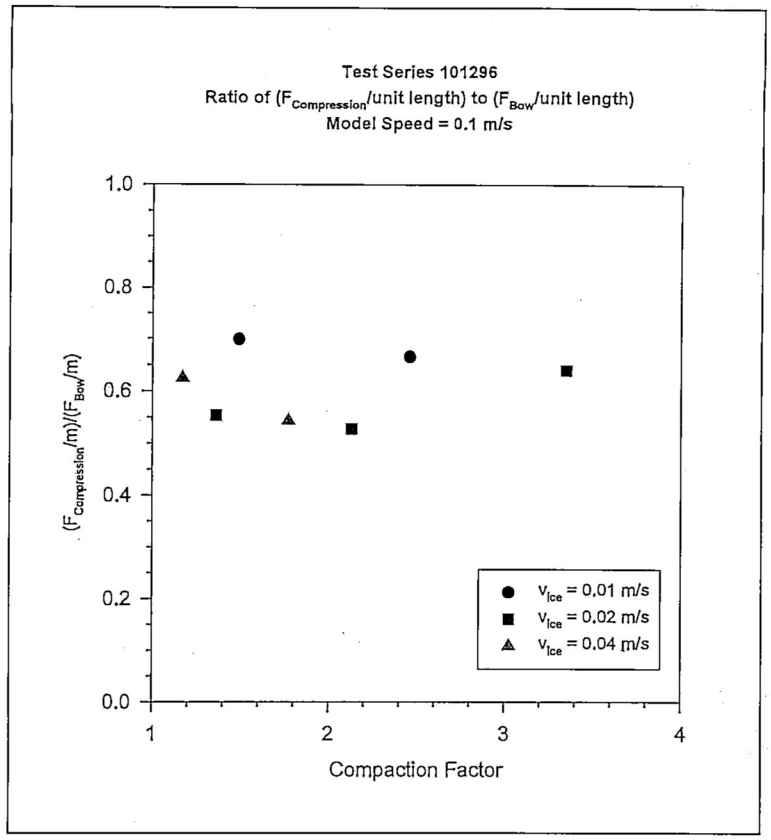

Figure 4.2.4.1: Ratio of Bow and Compressive Forces on A Unit Length of Loading Area Basis.

Referring to Appendix B.4, we see that:

> on a unit length basis, compressive force is actually less than the bow force, a result which is not obvious from the analysis in Section 4.2.1. Compressive force per unit length also shows sensitivity to model speed, as the ratios are higher for the slower model speed of 0.10 m/s in test series 101296, at around 60-70%. The speed of the model in the other three test series was 0.25 m/s, and the ratios of compressive force to bow force are significantly lower, averaging around 40-50%. This supports the argument that slower ship speeds will allow greater development of compressive forces.
>
> test series 040397, in which no compression occurred for half the tests, show that compressive forces still occur at about 20% the magnitude of the bow forces. As stated above in Section

4.2.1 this may be due to an unrealistic restriction placed on the "uncompressed" ice field by the pusher plates.

- No significant variation in the ratio of these forces seems to occur with either ice velocity or compaction factor. This suggests a non-dimensionalized constant relation between bow force and compressive force for a given ship velocity. The verification of this would require more testing of the influence of both ice velocity and compaction factor on these forces.

4.2.5. Comparison of F_{Bow} and $2F_{seg}$

The relationship of compressive force to bow force is significant from both a structural and a total resistance point of view. To examine the influence of compressive forces on resistance, however, requires the analysis of the component of resistance caused by compression, $2F_{seg}$. This was done again on a unit length basis to more realistically determine the relative importance of icebreaking and frictional resistance. Plots of the variation in the bow force/frictional resistance ratio are shown in **Appendix B.5**, with a sample plot shown in **Figure 4.2.5.1**.

From Appendix B.5, it is clear that the increase in resistance on a per unit length basis is less than 10% of the bow force resistance. However, given the length of the parallel midbody of some ships, this would result in a significant increase in overall resistance. The ratio of these forces shows no visible dependency on model speed or ice velocity, although more testing would be recommended to investigate this influence more thoroughly. As the overall variations among the test series are around 5% for cases in which compression occurred, this is probably due to statistical variation rather than some deterministic element. The frictional resistance as determined from these tests is small enough to cause some problems in determining parametric influences, given the rough nature of the experimental arrangement.

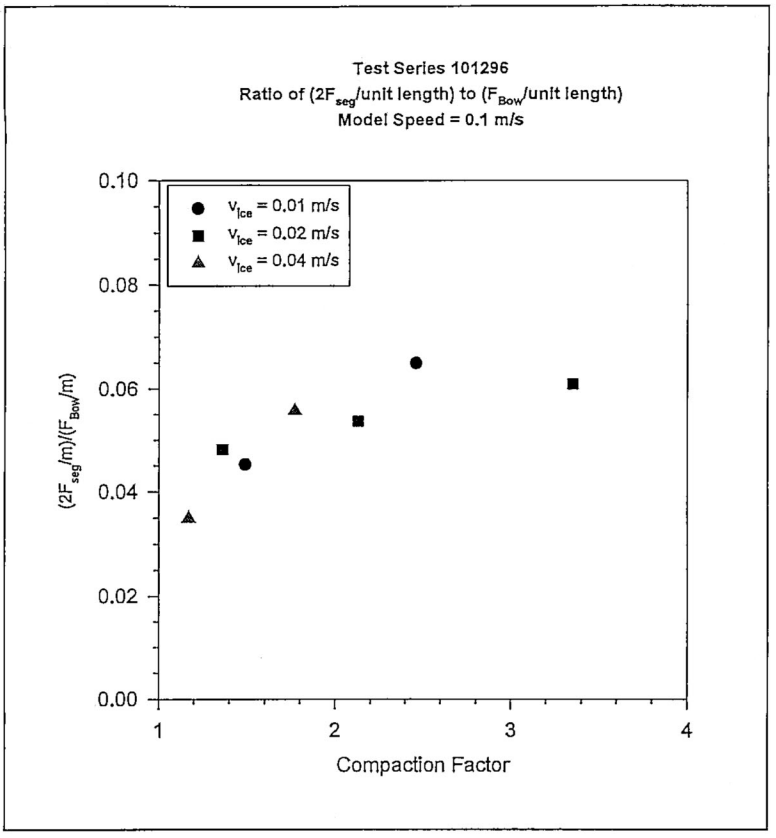

Figure 4.2.5.1: Variation in Ratio of Frictional Resistance to Icebreaking Resistance.

4.2.6. Friction Coefficient Variation

Given the compressive force measurements and the frictional resistance measurements, it is possible to investigate the variation of a "friction coefficient" with ice velocity and compaction factor by examining the ratio of friction force, F_{seg}, and compression force, $F_{Compression}$. The plots of the ratios of these forces are shown in **Appendix B.6**, with a sample plot given in **Figure 4.2.6.1**.

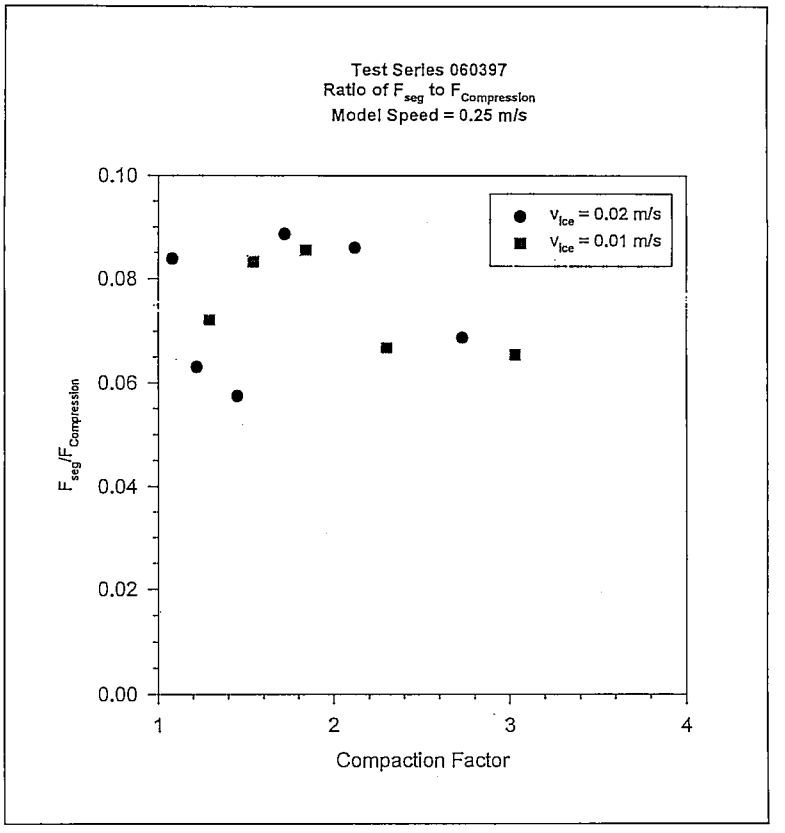

Figure 4.2.6.1: Variation in Ratio of Frictional Resistance to Compressive Force.

From the plots in Appendix B.6, several points are apparent :

- no variation in friction coefficient with ice or model velocity is discernible from these figures.
- at low compaction factors, for cases in which compression occurred, there seems to be an increase in the friction coefficient with increasing compaction factor.
- the friction coefficients for compressive tests are all under 0.1, with the majority between 0.05 and 0.1.

The plots for test series 040397 and 060397 show significant scatter in the data. This is similar to the problems encountered in Section 4.2.5, in that the force measured in the parallel midbody segment is small enough that sensitivity to parameter variations is indistinguishable from what could be stochastic effects. The influence of ice compaction velocity on the frictional resistance is thus still a problematic issue.

5. CONCLUSIONS

Quite clearly there are practical limitations involved in the experimental arrangement as described in this report that have a not insignificant effect on the ability to distinguish parametric influences of ice and model velocities on the ship resistance forces. This problem needs to be addressed before more testing should be done. The use of the rope to tow the model results in inconsistent model velocities. If this system is not replaced, then at least the model velocity should be measured during the test. Further, the ice compression velocity shows a significant difference at times between target and measured compaction rates, due to the motion of the bridge. This makes it more difficult to distinguish trends in resistance forces with ice velocities. A means of dealing with this should be developed. Finally, the dimensions of the ice tank make the extent of testing (i.e. range of compaction factors) using a single ice sheet limited. Thus a large number of ice sheets, with similar characteristics, would be required to investigate stochastic variations in ship resistance forces.

In spite of these problems with the experimental set-up, many valid conclusions have been obtained from the test series :

1. Testing of ship resistance in compressive pack ice is feasible in an experimental ice tank. Refinements to the experimental set-up in this report are required for detailed investigation of ship resistance in compressive pack ice.

2. The use of the **compaction factor** as a measure of severity of compression is supported by its usefulness in defining behaviour of ship resistance forces. This factor is a characteristic measure of the ice field which clearly shows variations in measured forces. It can loosely be interpreted as an indication of the increase in ice field nominal thickness. However, the usefulness of the compaction factor as a measure of compression severity should be more rigidly examined.

3. Variations in time histories for measured forces appear to be mainly influenced by inhomogeneities in the ice field, increasing compaction, and problems in the

experimental set-up. The influence of the experimental set-up should be minimised by a refined testing arrangement.

4. Testing the influence of compaction rate should not be done by varying the ice velocity during a single pull of the model through the ice field, as this consistently showed deviations in target and actual ice velocities. The bridge should be stopped, then accelerated to the desired ice velocity and then the model should be pulled through. Target and actual ice velocities of test series 070696 support this procedure, as do those of 040397.

5. Variations in resistance forces with ice velocity need to examined over a wider range of ice velocities. This range should correspond to predicted full scale forces, thus a model for predicting ice field stresses, such as that described in **Fleet Technology Ltd, 1997**, should be pursued.

6. The forces experienced by a ship in compressive ice increase as the compression grows more severe, as measured by the compaction factor of the ice field. This includes the resistance encountered at the bow as it breaks through the ice field as the compression generates a longitudinal force (i.e. along the longitudinal axis of the model) due to the curved bow surface.

7. Tests in which the ice was compressed at a given compaction rate showed consistently higher forces than those in which no compaction occurred

8. Total ship resistance increases with compaction factor, ice velocity and model velocity. Quantification of this increase should be rigorously defined, both through further model tests, and development of mathematical models to predict full scale resistance in real compressive ice fields.

9. While compressive forces are always much greater than those measured in the bow, on a per unit length basis they are still only about 60% of the bow force. Thus the compressive force is much more significant from a ship resistance standpoint than from a ship structural standpoint.

10. No visible dependency on ice velocity or compaction factor was seen for the ratios of frictional resistance to bow resistance or compression force to bow force. These ratios are defined on a "per unit length of loaded area" basis. This suggests that some direct relationship exists for each pair of these forces.

11. The frictional resistance as measured by the load cell in the parallel midbody segment showed significant scatter. Thus it is very difficult to ascertain whether the variations in this force are due to statistical influences, or parametric variations controlled by the experimenter.

12. Ice strength has a discernible effect on the forces experienced by the model, with the exception of compressive force. However, as the influence of ice strength was incidental to the study, it was not pursued in greater detail. The effect of greater ice strength is to increase the forces experienced by the model, with the exception of compressive force in which no effect was observed.

13. More testing should be done to refine the dependency of ship hull forces and ship resistance on compaction rate. The testing should reflect realistic compressive pack ice situations.

REFERENCES

"Definition of Ice Loads Under the Pressured Ice Scenario.".**DRAFT REPORT**. Fleet Technology Ltd. Report #4643A6. Kanata, Ontario, Canada. August 14, 1997.

Heideman, T. "Influence of Ice Compression on Feasible Navigation on the Northern Sea Route". INSROP Working Paper No. 39-1996, I.1.8

Kujala, P., R. Goldstein, N. Osipenko, V. Danilenko. "A Ship In Compressive Ice: Preliminary Model Test Results and Analysis of The Problem." Report From The Joint Finnish-Soviet Research Project. Helsinki University of Technology/USSR Academy of Sciences. M-111. Otaniemi, 1991.

Kujala, P. & J. Kuukoski. "Compressive Ice Model Tests with a Pusher Plate Attached to The Carriage of The Ice Tank." Report From The Joint Finnish-Soviet Research Project. Helsinki University of Technology, Ship Laboratory. M-118. Otaniemi 1992.

Kujala, P., R. Goldstein, N. Osipenko, V. Danilenko. "A Ship In Compressive Ice: Analysis of the Ice Failure Process." Report From The Joint Finnish-Soviet Research Project. Helsinki University of Technology/USSR Academy of Sciences. M-165. Otaniemi, 1993.

Kujala P., & S. Ralph. "A Ship in Compressive Ice: Results of Model Scale Tests to Study Pile-Up Process of Ice." Report From The Joint Finnish-Soviet Research Project. Helsinki University of Technology, Ship Laboratory. M-191. Otaniemi, 1994.

Lensu, M. Stephanie Heale, Kaj Riska and Pentti Kujala. "Ice Environment and Ship Hull Loading along the NSR.".INSROP Working Paper No. 66-1996, I.1.10. 1996.

Li, Z, & K. Riska. "Preliminary Study of Physical and Mechanical Properties of Model Ice." Helsinki University of Technology, Ship Laboratory. M-212. Otaniemi, 1996.

Riska, K., P. Kujala, R. Goldstein, N. Osipenko, V. Danilenko. "Application of Results from the Research Project A Ship In Compressive Ice' to Ship Operability". Helsinki University of Technology, Ship Laboratory. M-209. Otaniemi, 1996.

Riska, K., M. Wilhelmson, K. Englund. "Performance of Merchant Vessels in Ice in the Baltic." Helsinki University of Technology, Ship Laboratory. To be published in 1997.

Sanderson, T.J.O. Ice Mechanics: Risks to Offshore Structures. Graham & Trotman Ltd. London, UK. 1988.

Spencer, D. & K. Hardiman. "Effect of Lateral Ice Pressure on Ship Resistance.".12th International Conference on Port and Ocean Engineering Under Arctic Conditions. Hamburg, Germany. 1993.

Voevodin, V.A. "To The Problem of Ice Compression Effect on Navigation.".Transactions of AANII (Arctic and Antarctic Research Institute). Vol. 384, 1981. In Russian.

APPENDIX A.1

FORCE HISTORIES FOR SIMPLE MODEL

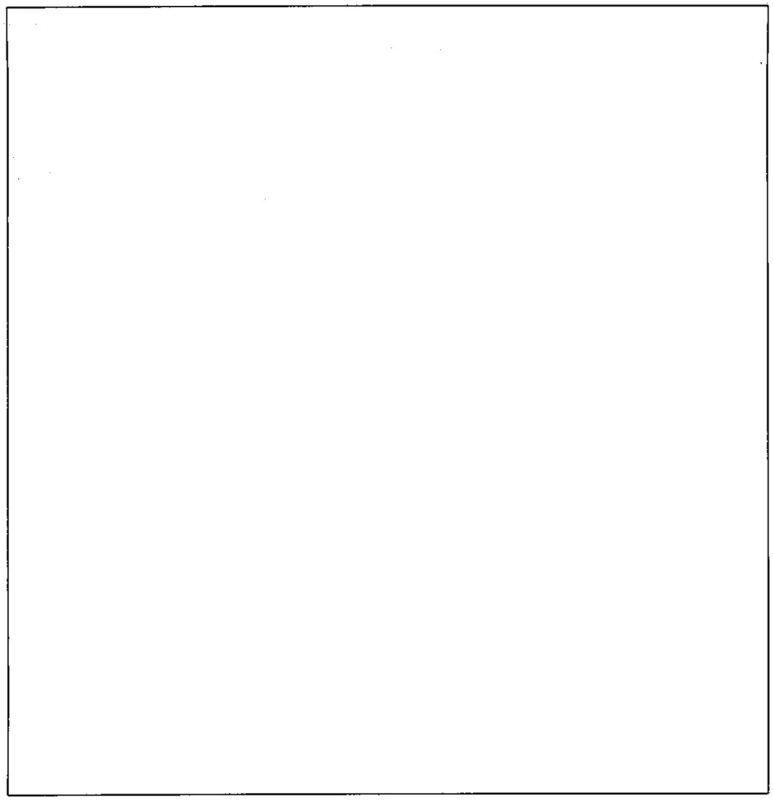

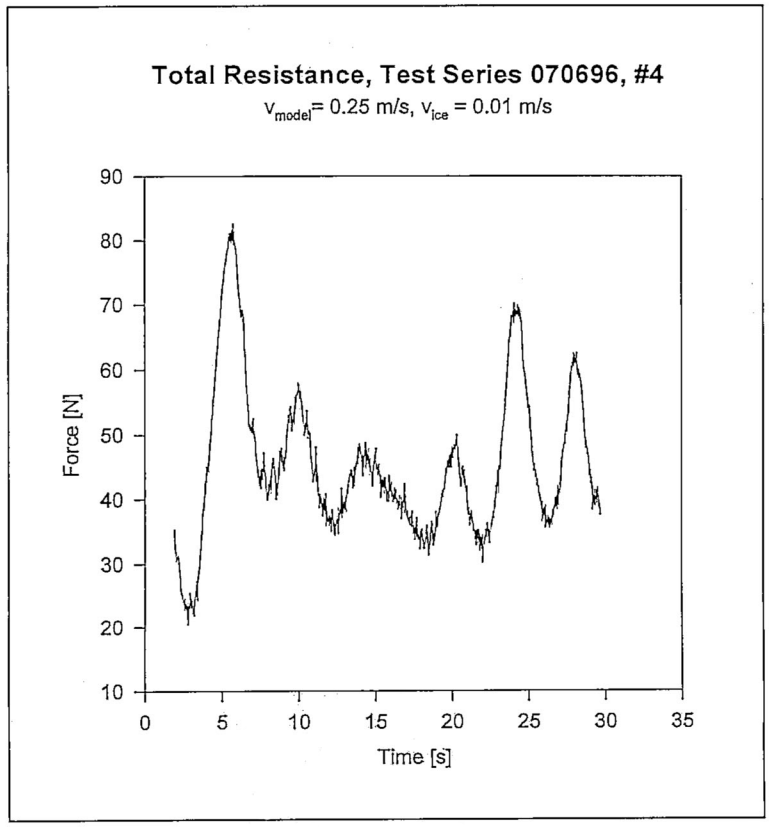
Total Resistance, Test Series 070696, #4
v_{model}= 0.25 m/s, v_{ice} = 0.01 m/s
Force [N]
90
80
70
60
50
40
30
20
10
0
5
10
15
20
25
30
35
Time [s]

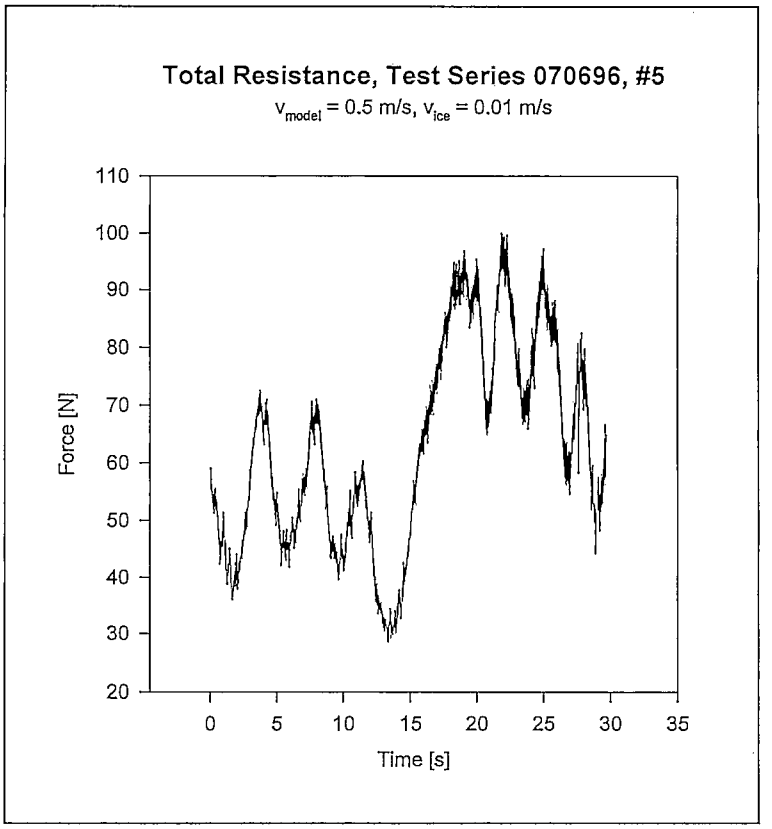
Total Resistance, Test Series 070696, #5
v_{model} = 0.5 m/s, v_{ice} = 0.01 m/s
Force [N]
110
100
90
80
70
60
50
40
30
20
0
5
10
15
20
25
30
35
Time [s]

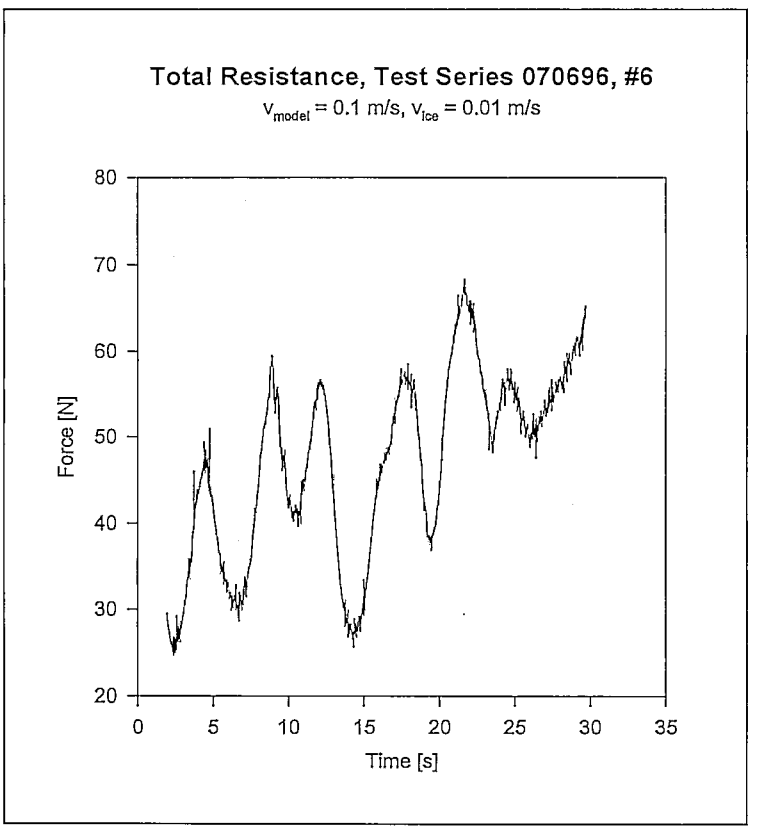
Total Resistance, Test Series 070696, #6
v_{model} = 0.1 m/s, v_{ice} = 0.01 m/s
Force [N]
80
70
60
50
40
30
20
0
5
10
15
20
25
30
35
Time [s]

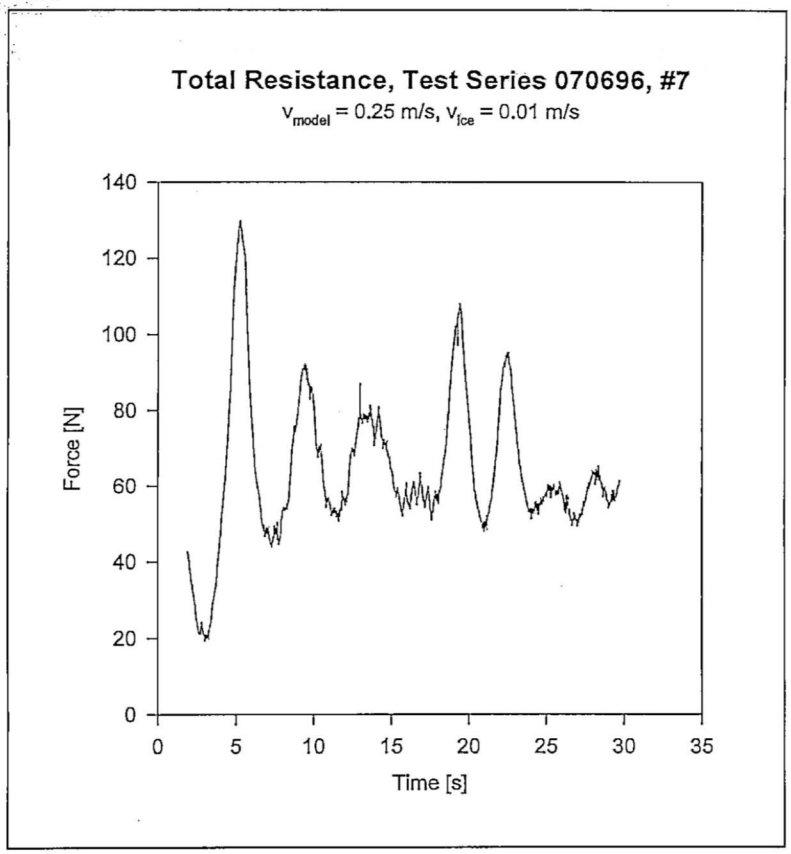
Total Resistance, Test Series 070696, #7
v_{model} = 0.25 m/s, v_{ice} = 0.01 m/s
Force [N]
Time [s]
0
20
40
60
80
100
120
140
0
5
10
15
20
25
30
35

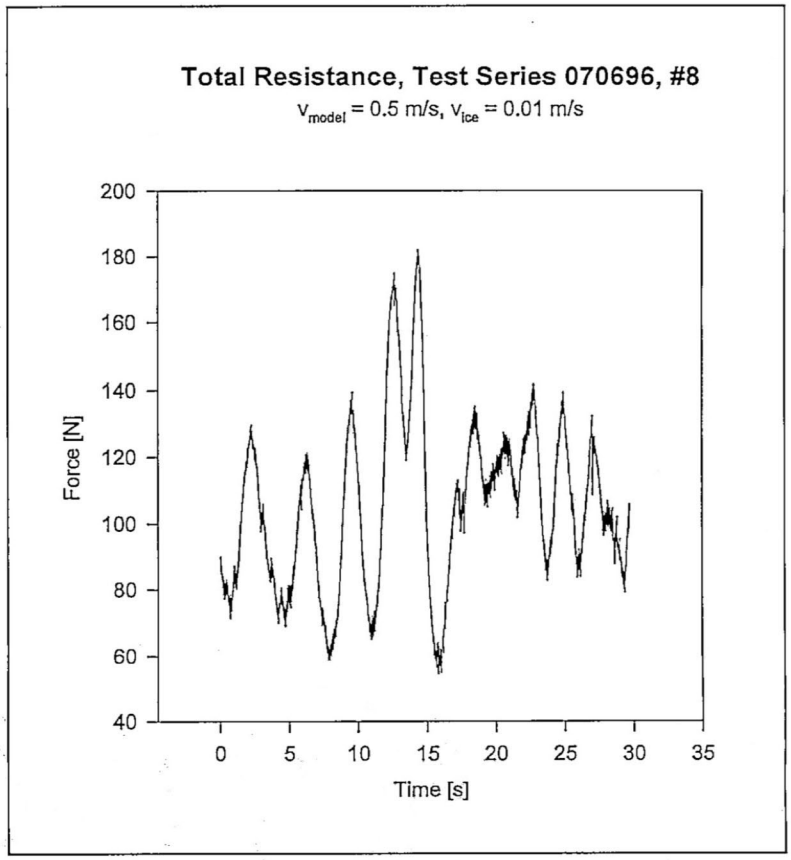
Total Resistance, Test Series 070696, #8
v_{model} = 0.5 m/s, v_{ice} = 0.01 m/s
Force [N]
Time [s]
40
60
80
100
120
140
160
180
200
0
5
10
15
20
25
30
35

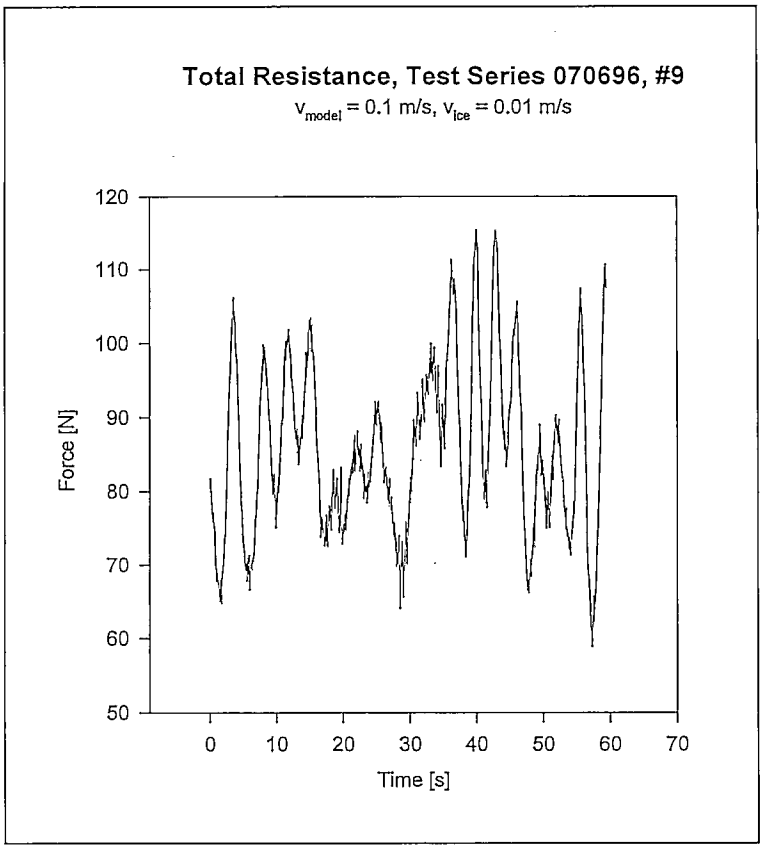
Total Resistance, Test Series 070696, #9
v_{model} = 0.1 m/s, v_{ice} = 0.01 m/s
Force [N]
120
110
100
90
80
70
60
50
0
10
20
30
40
50
60
70
Time [s]

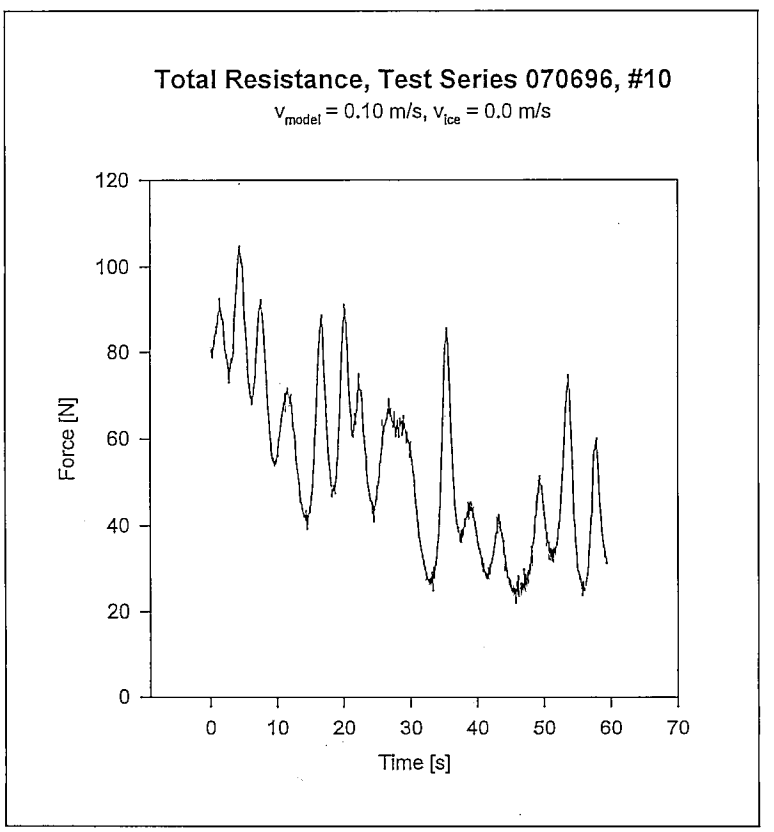
Total Resistance, Test Series 070696, #10
v_{model} = 0.10 m/s, v_{ice} = 0.0 m/s
Force [N]
120
100
80
60
40
20
0
0
10
20
30
40
50
60
70
Time [s]

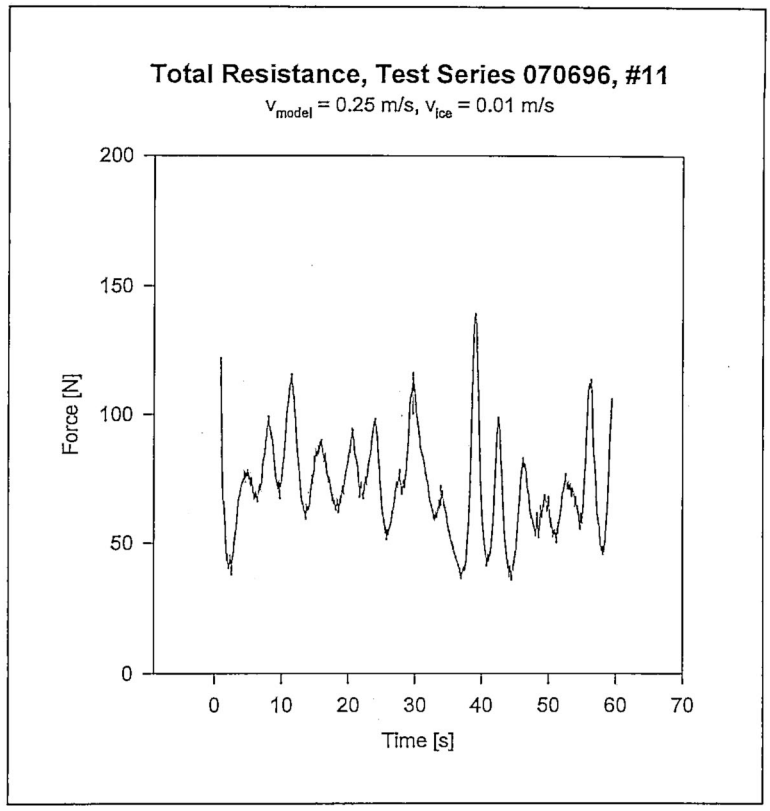
Total Resistance, Test Series 070696, #11
v_{model} = 0.25 m/s, v_{ice} = 0.01 m/s
Force [N]
200
150
100
50
0
0
10
20
30
40
50
60
70
Time [s]

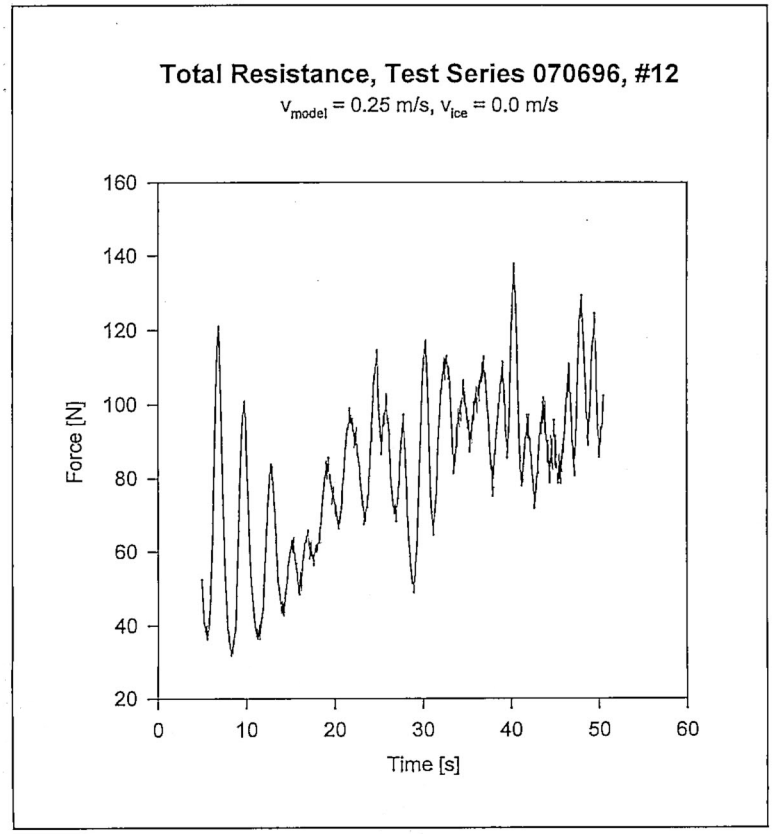
Total Resistance, Test Series 070696, #12
v_{model} = 0.25 m/s, v_{ice} = 0.0 m/s
Force [N]
160
140
120
100
80
60
40
20
0
10
20
30
40
50
60
Time [s]

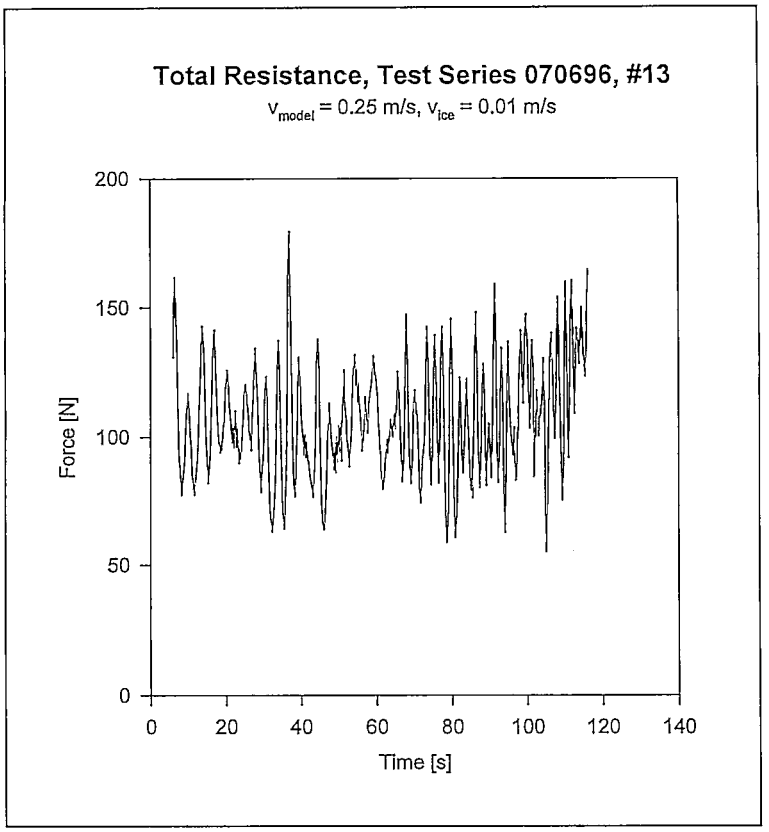
Total Resistance, Test Series 070696, #13
v_{model} = 0.25 m/s, v_{ice} = 0.01 m/s
Force [N]
200
150
100
50
0
0
20
40
60
80
100
120
140
Time [s]

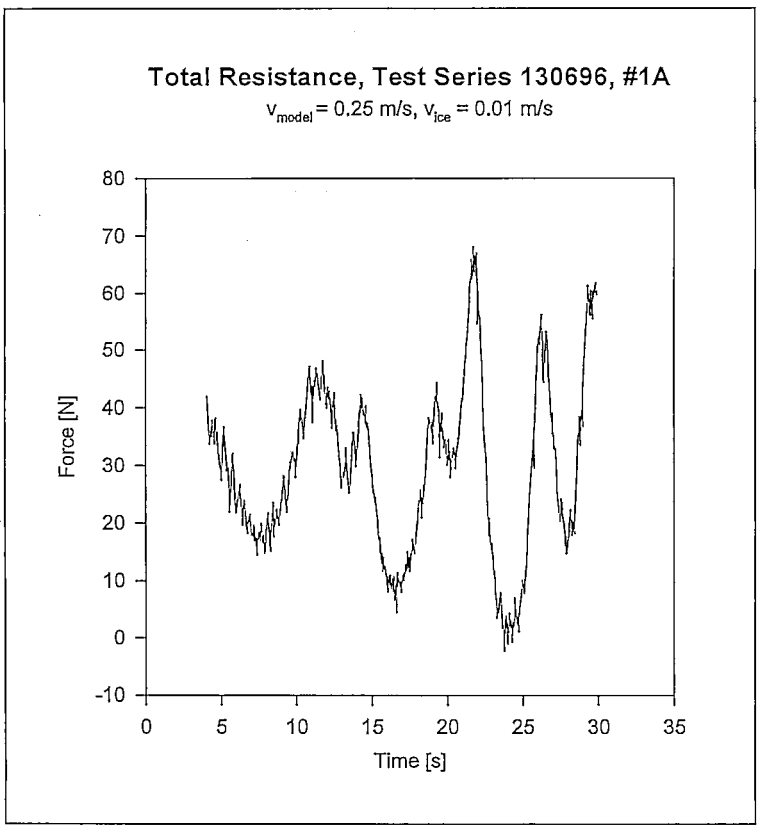
Total Resistance, Test Series 130696, #1A
v_{model} = 0.25 m/s, v_{ice} = 0.01 m/s
Force [N]
80
70
60
50
40
30
20
10
0
-10
0
5
10
15
20
25
30
35
Time [s]

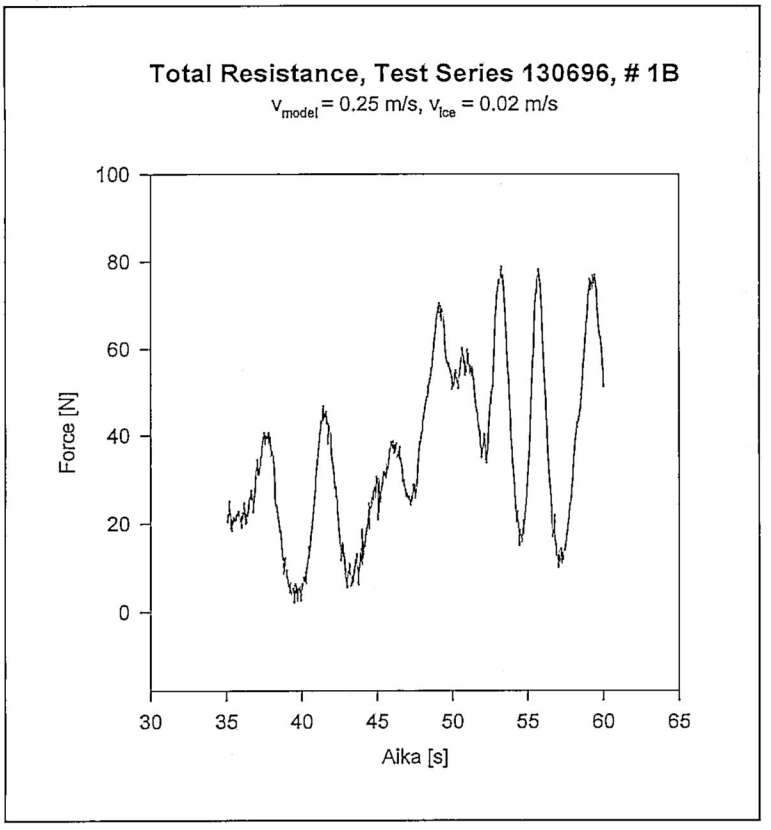
Total Resistance, Test Series 130696, # 1B
v_{model} = 0.25 m/s, v_{Ice} = 0.02 m/s
Force [N]
100
80
60
40
20
0
30
35
40
45
50
55
60
65
Aika [s]

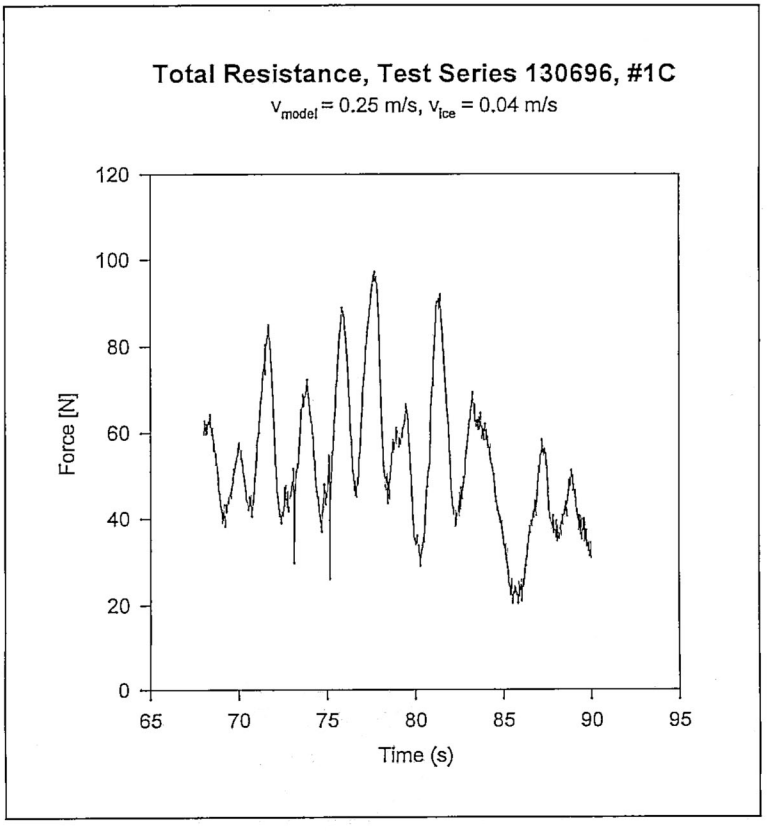
Total Resistance, Test Series 130696, #1C
v_{model} = 0.25 m/s, v_{Ice} = 0.04 m/s
Force [N]
120
100
80
60
40
20
0
65
70
75
80
85
90
95
Time (s)

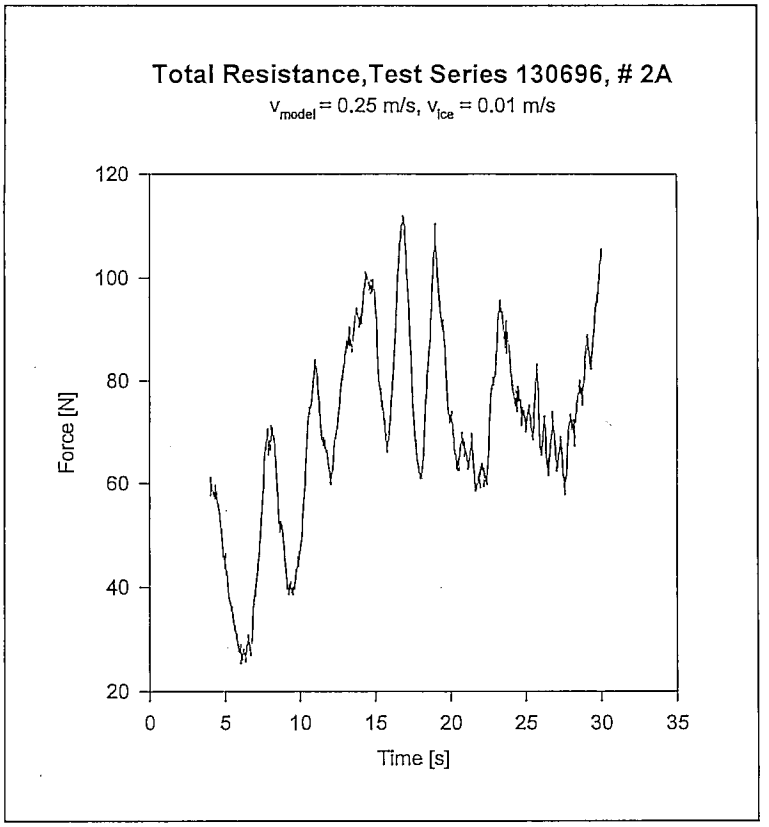
Total Resistance,Test Series 130696, # 2A
v_{model} = 0.25 m/s, v_{ice} = 0.01 m/s
Force [N]
120
100
80
60
40
20
0
5
10
15
20
25
30
35
Time [s]

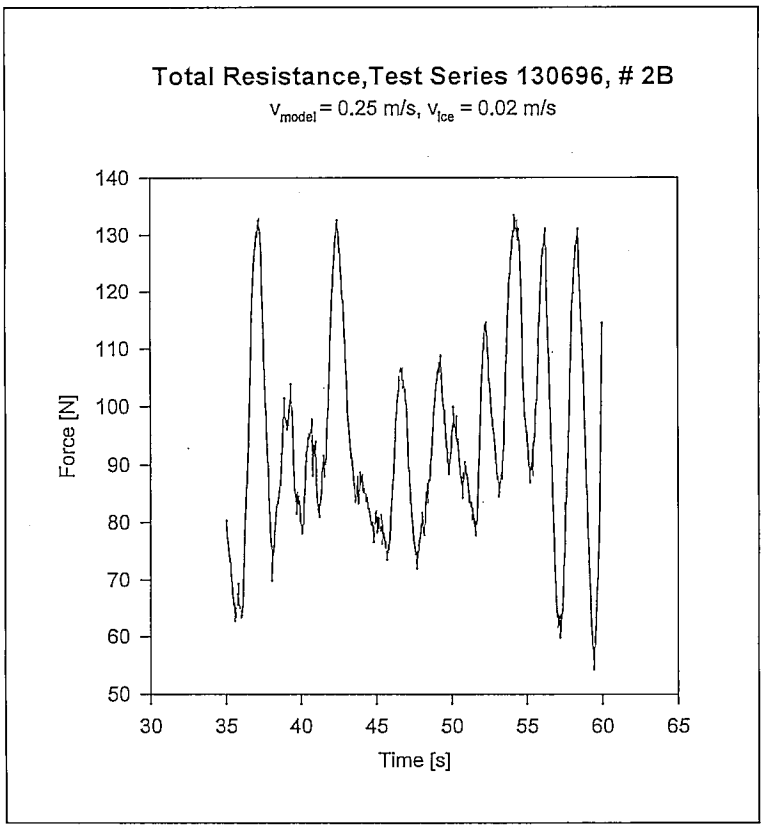
Total Resistance,Test Series 130696, # 2B
v_{model} = 0.25 m/s, v_{ice} = 0.02 m/s
Force [N]
140
130
120
110
100
90
80
70
60
50
30
35
40
45
50
55
60
65
Time [s]

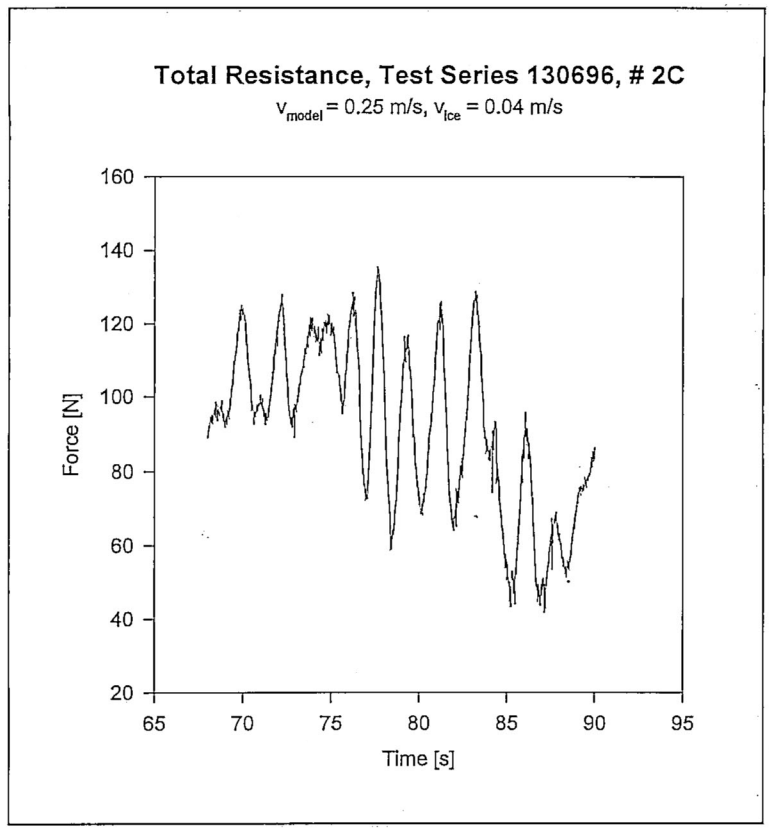
Total Resistance, Test Series 130696, # 2C
v_{model} = 0.25 m/s, v_{Ice} = 0.04 m/s
Force [N]
160
140
120
100
80
60
40
20
65
70
75
80
85
90
95
Time [s]

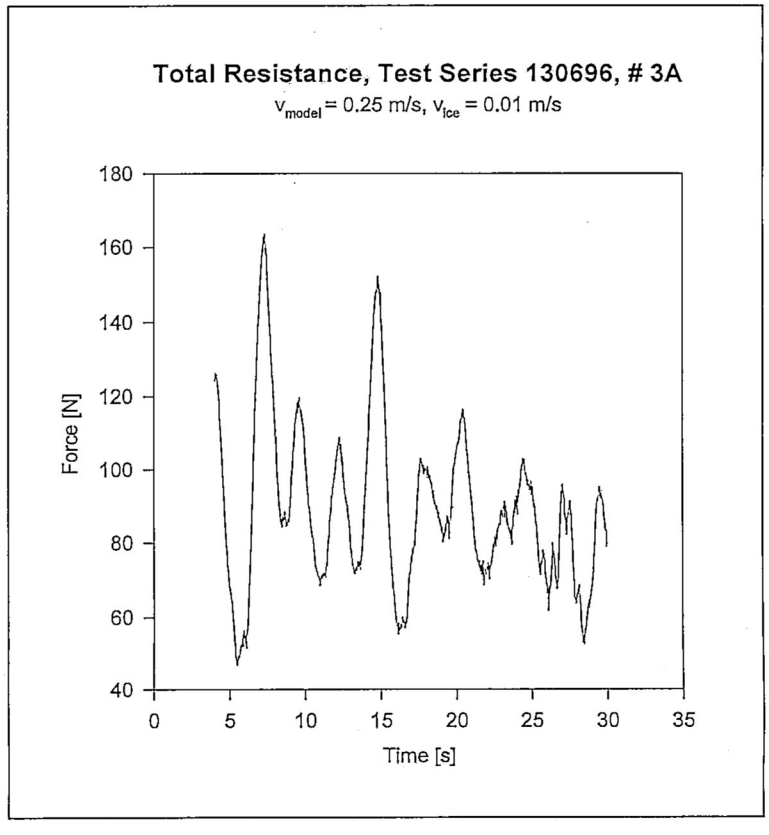
Total Resistance, Test Series 130696, # 3A
v_{model} = 0.25 m/s, v_{Ice} = 0.01 m/s
Force [N]
180
160
140
120
100
80
60
40
0
5
10
15
20
25
30
35
Time [s]

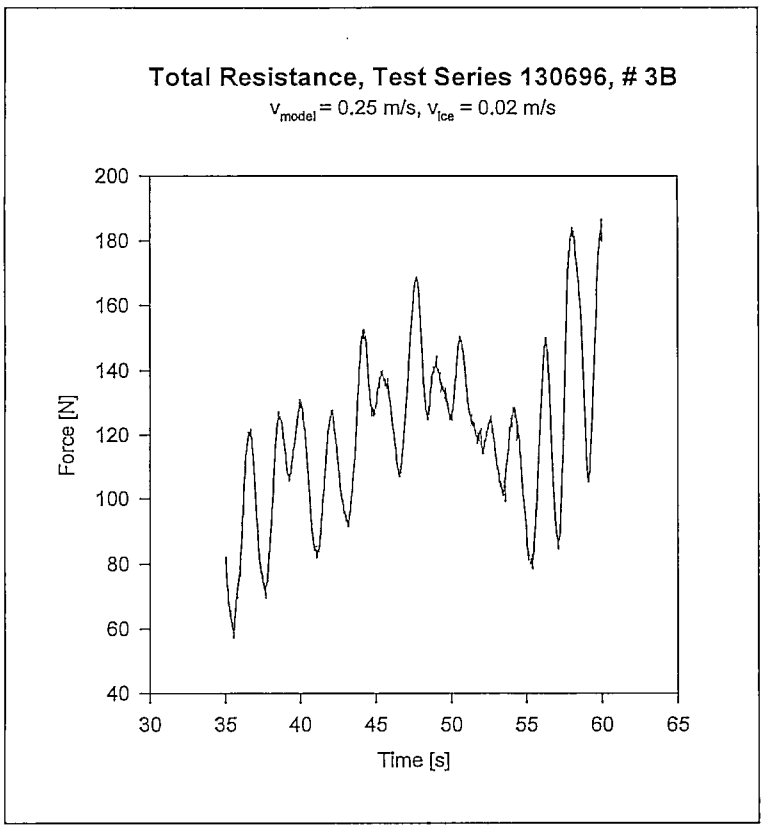
Total Resistance, Test Series 130696, # 3B
v_{model} = 0.25 m/s, v_{ice} = 0.02 m/s
Force [N]
200
180
160
140
120
100
80
60
40
30
35
40
45
50
55
60
65
Time [s]

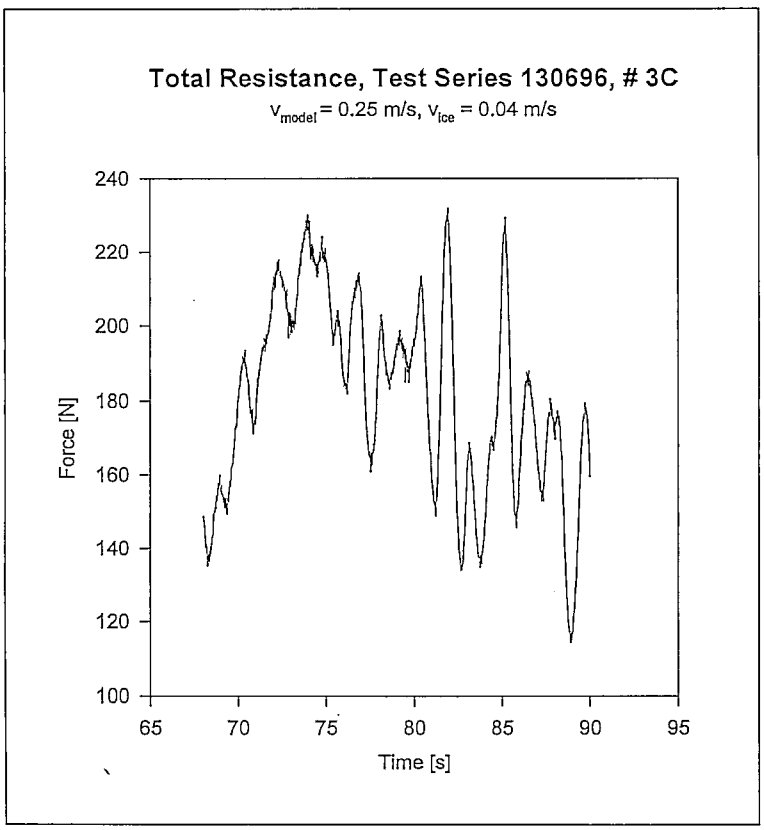
Total Resistance, Test Series 130696, # 3C
v_{model} = 0.25 m/s, v_{ice} = 0.04 m/s
Force [N]
240
220
200
180
160
140
120
100
65
70
75
80
85
90
95
Time [s]

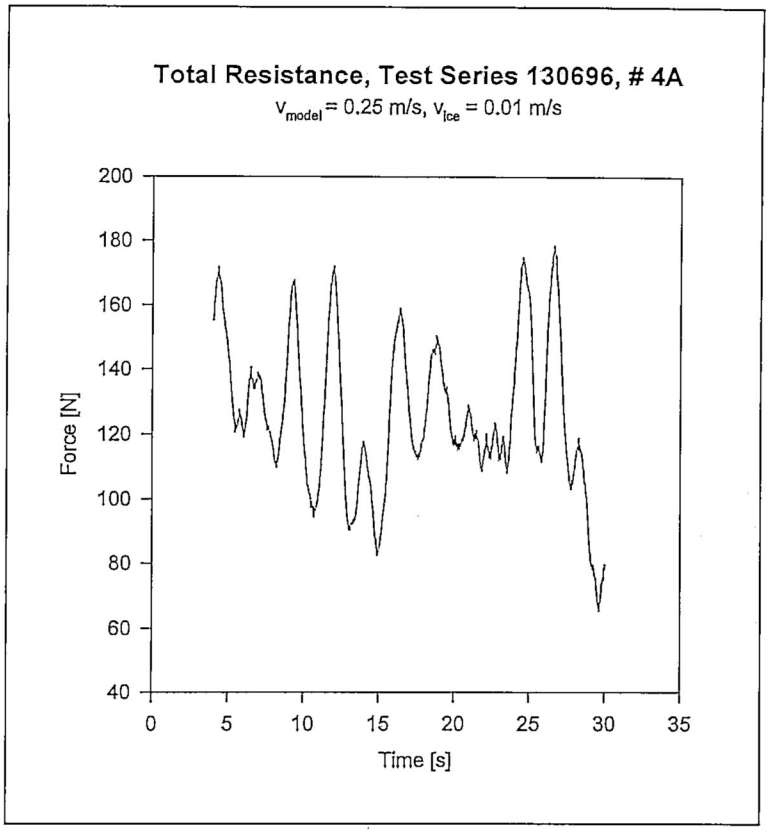
Total Resistance, Test Series 130696, # 4A
v_{model} = 0.25 m/s, v_{Ice} = 0.01 m/s
Force [N]
200
180
160
140
120
100
80
60
40
0
5
10
15
20
25
30
35
Time [s]

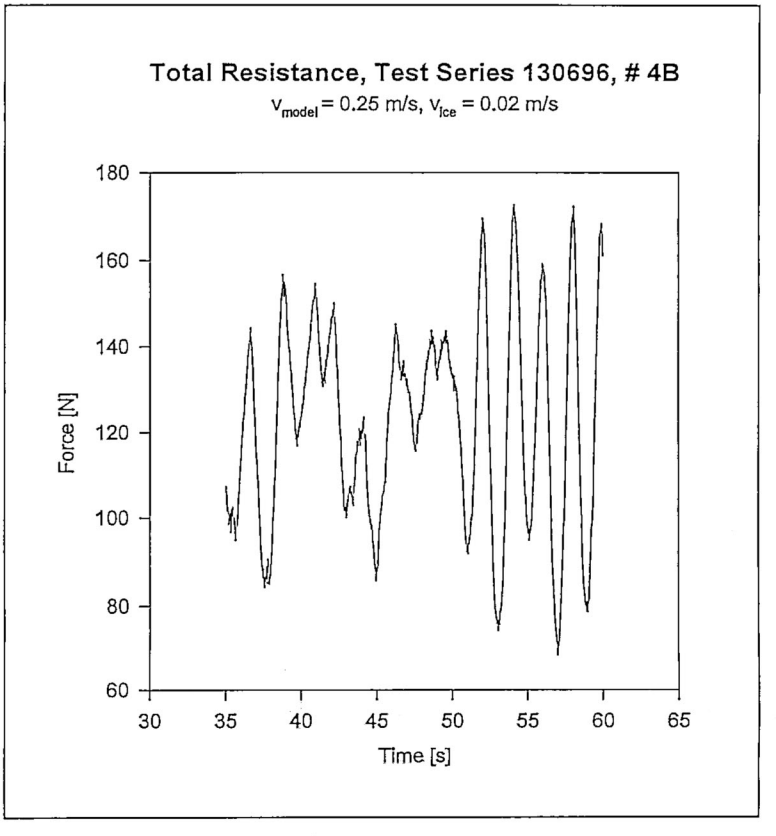
Total Resistance, Test Series 130696, # 4B
v_{model} = 0.25 m/s, v_{Ice} = 0.02 m/s
Force [N]
180
160
140
120
100
80
60
30
35
40
45
50
55
60
65
Time [s]

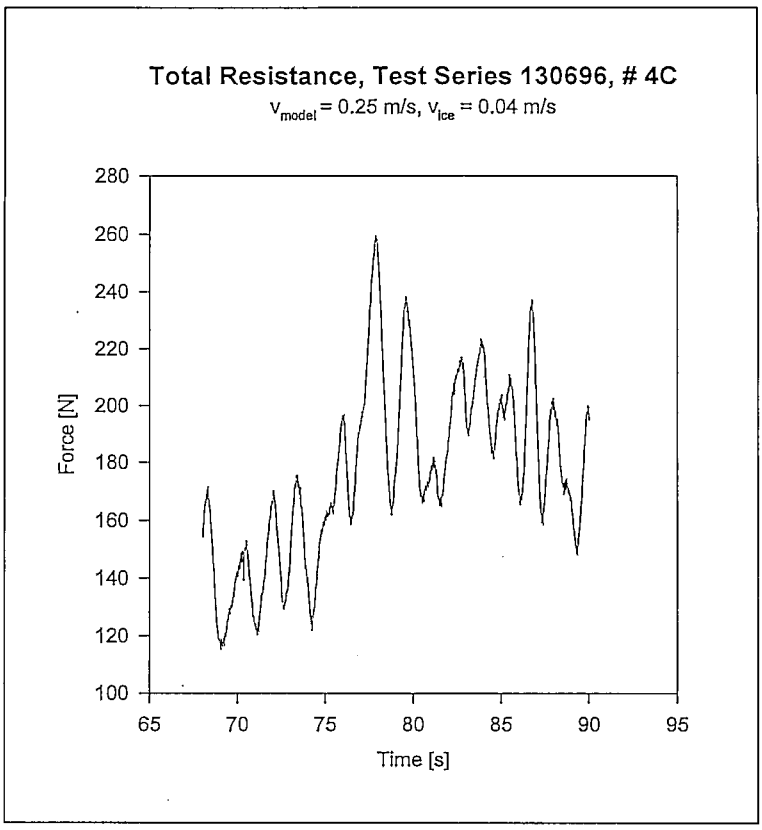
Total Resistance, Test Series 130696, # 4C
v_{model} = 0.25 m/s, v_{ice} = 0.04 m/s
Force [N]
280
260
240
220
200
180
160
140
120
100
65
70
75
80
85
90
95
Time [s]

APPENDIX A.2

FORCE HISTORIES FOR SEGMENTED MODEL

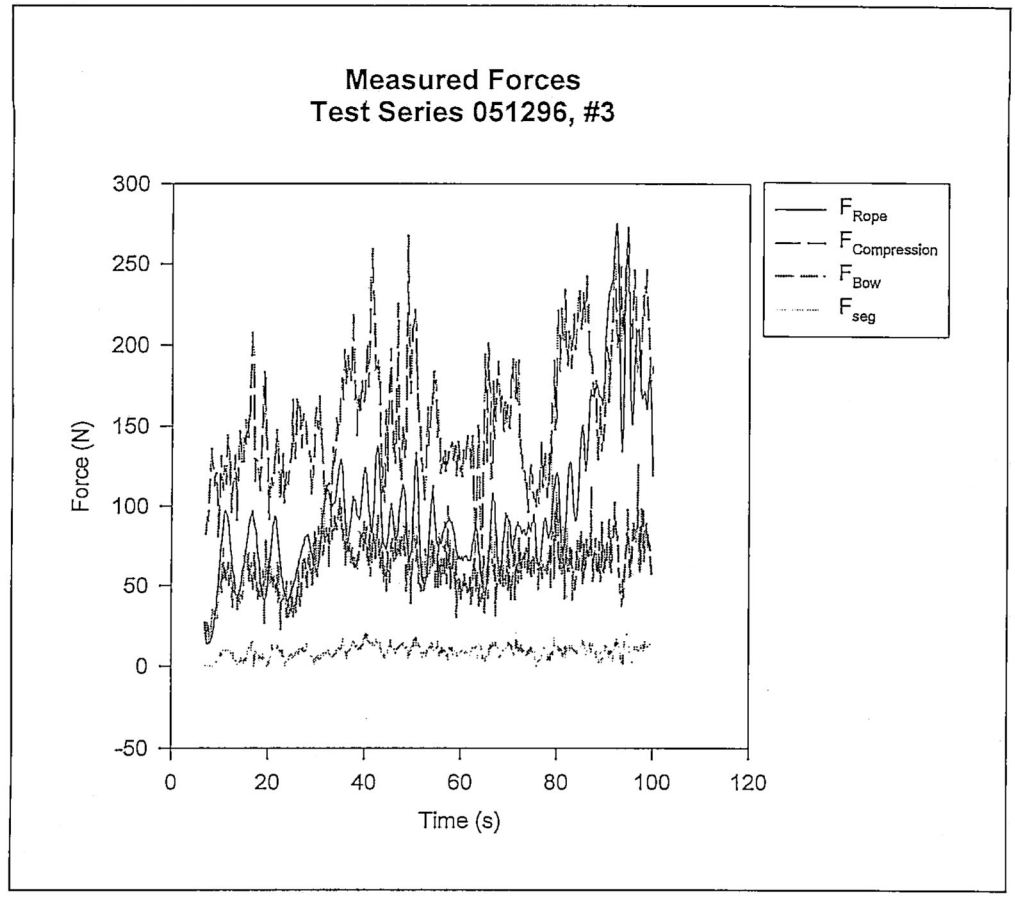
Measured Forces
Test Series 051296, #3
Force (N)
Time (s)
300
250
200
150
100
50
0
-50
0
20
40
60
80
100
120
F Rope
F Compression
F Bow
F seg

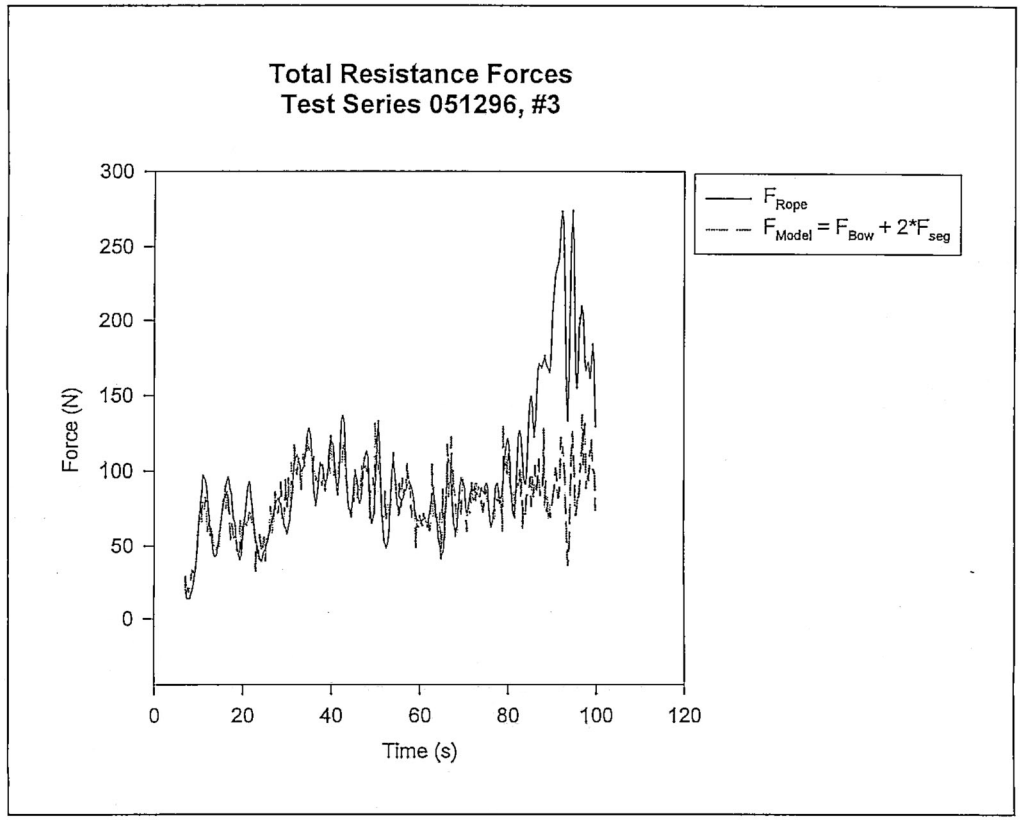
Total Resistance Forces
Test Series 051296, #3
Force (N)
Time (s)
300
250
200
150
100
50
0
0
20
40
60
80
100
120
F Rope
F Model = F Bow + 2*F seg

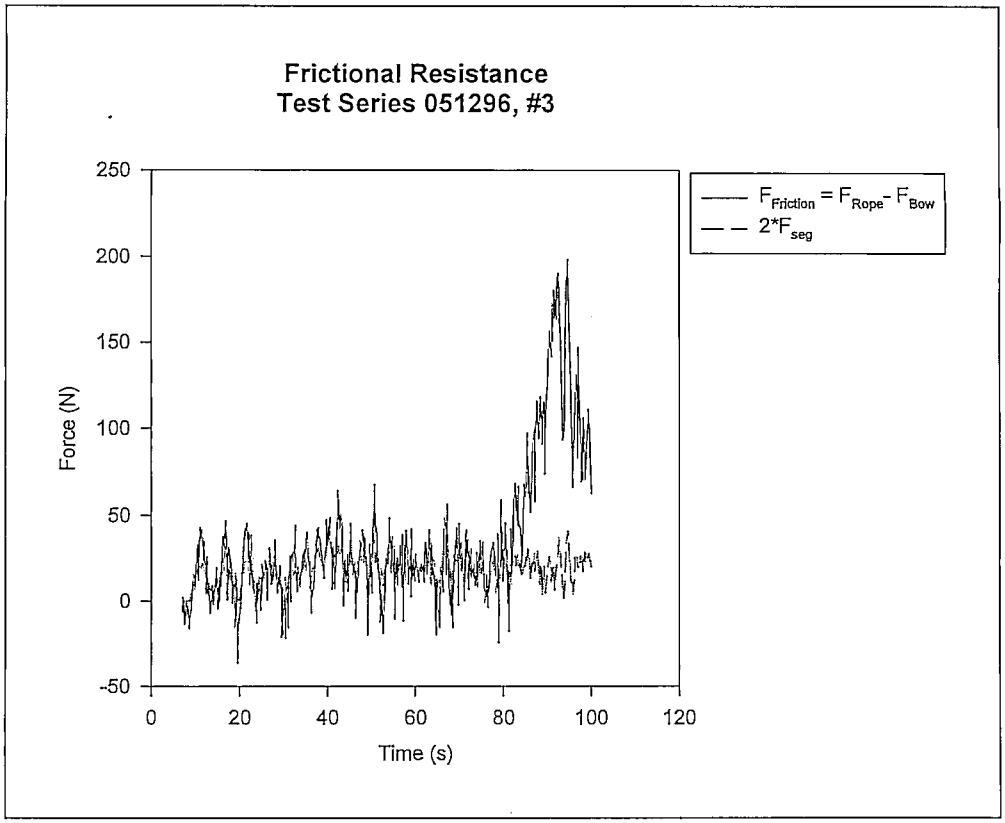
Frictional Resistance
Test Series 051296, #3
Force (N)
Time (s)
250
200
150
100
50
0
-50
0
20
40
60
80
100
120
F Friction = F Rope - F Bow
2*F seg

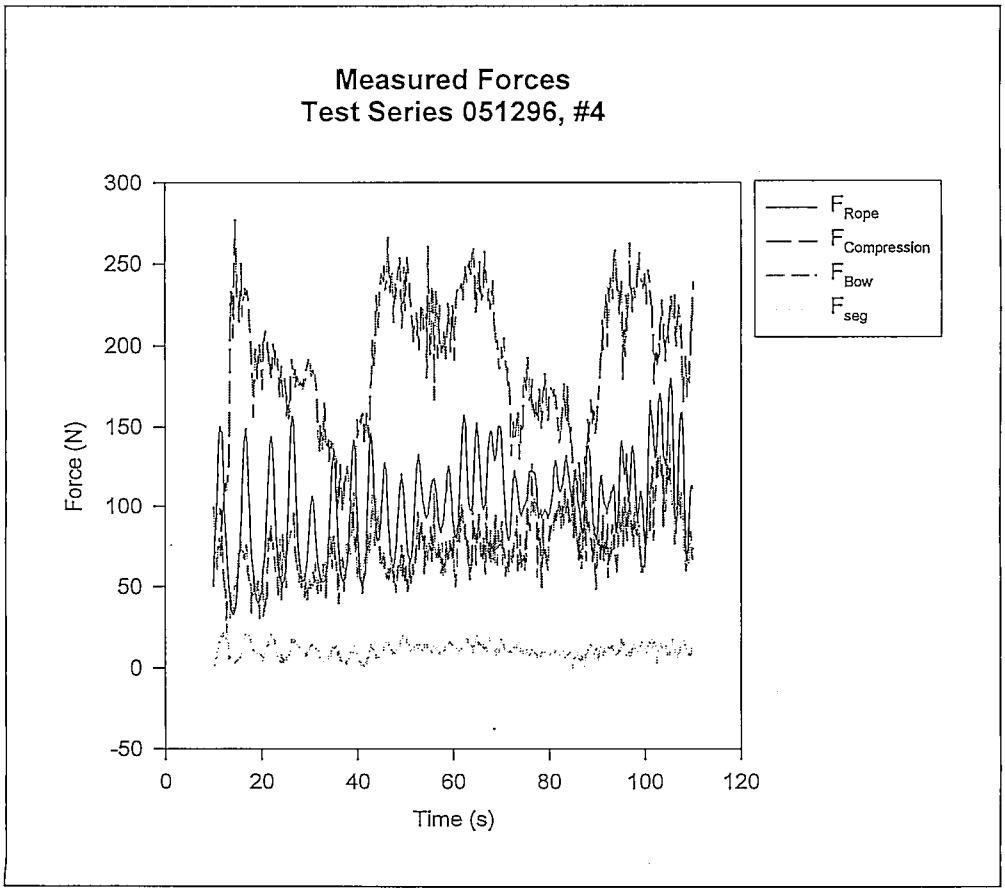
Measured Forces
Test Series 051296, #4
Force (N)
Time (s)
300
250
200
150
100
50
0
-50
0
20
40
60
80
100
120
F Rope
F Compression
F Bow
F seg

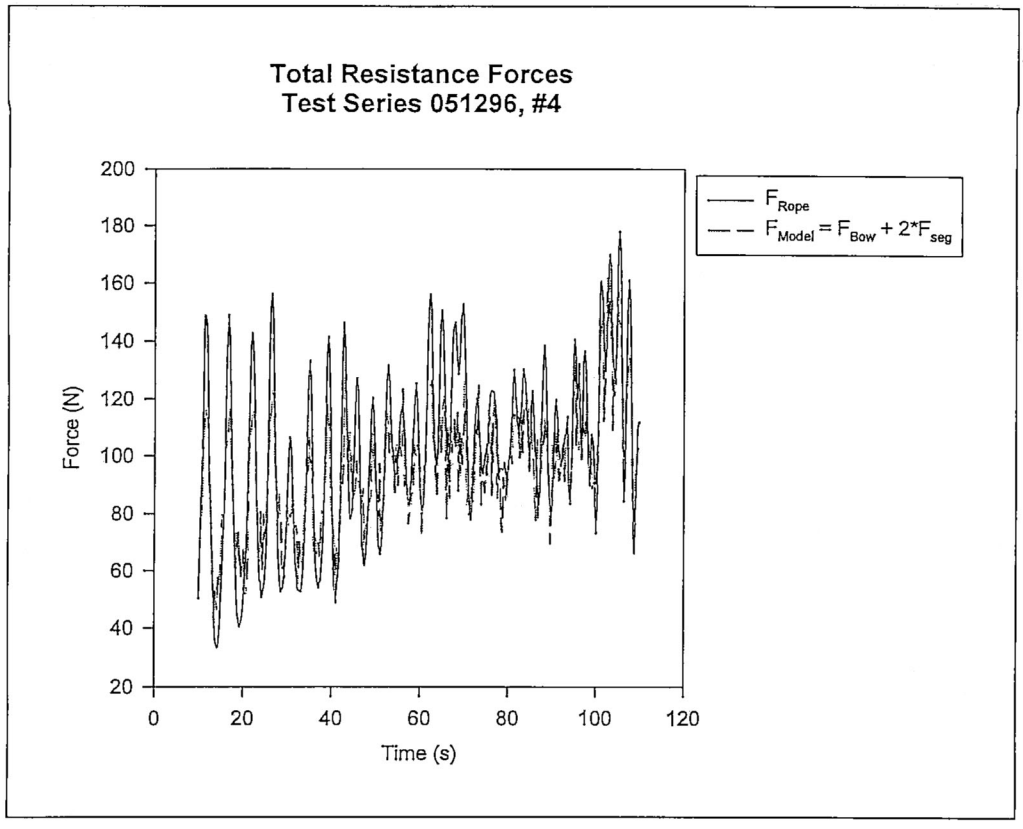
Total Resistance Forces
Test Series 051296, #4
Force (N)
Time (s)
200
180
160
140
120
100
80
60
40
20
0
20
40
60
80
100
120
F_Rope
F_Model = F_Bow + 2*F_seg

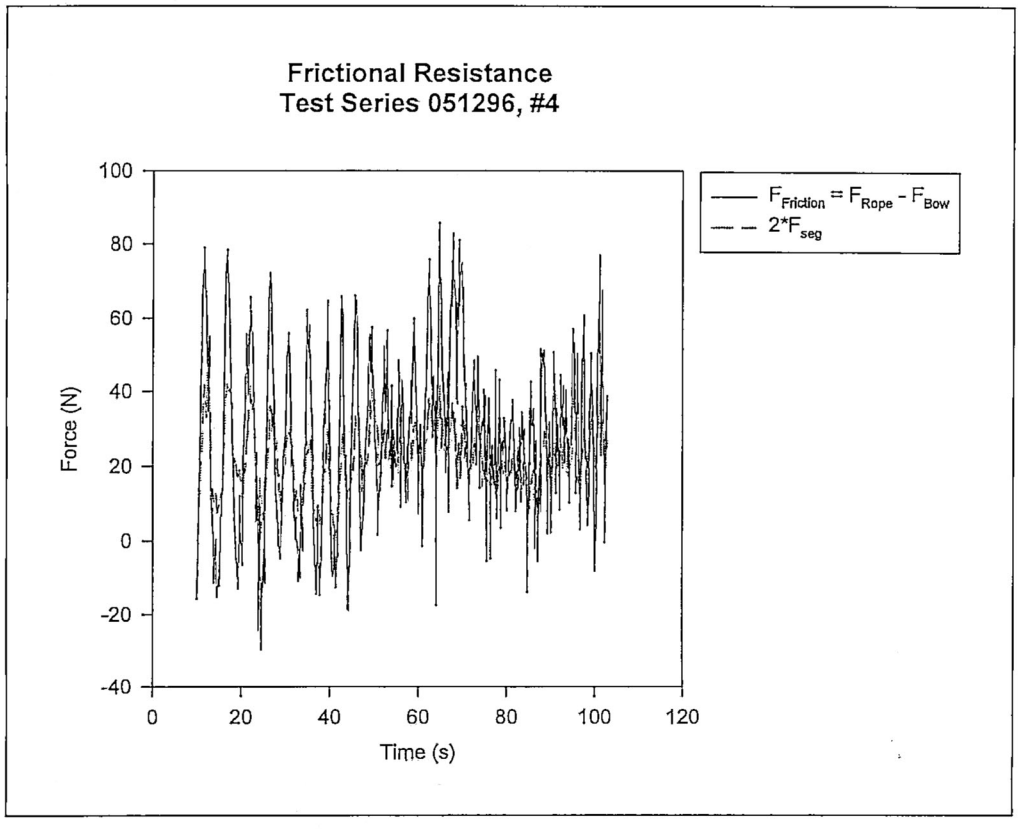
Frictional Resistance
Test Series 051296, #4
Force (N)
Time (s)
100
80
60
40
20
0
-20
-40
0
20
40
60
80
100
120
F_Friction = F_Rope - F_Bow
2*F_seg

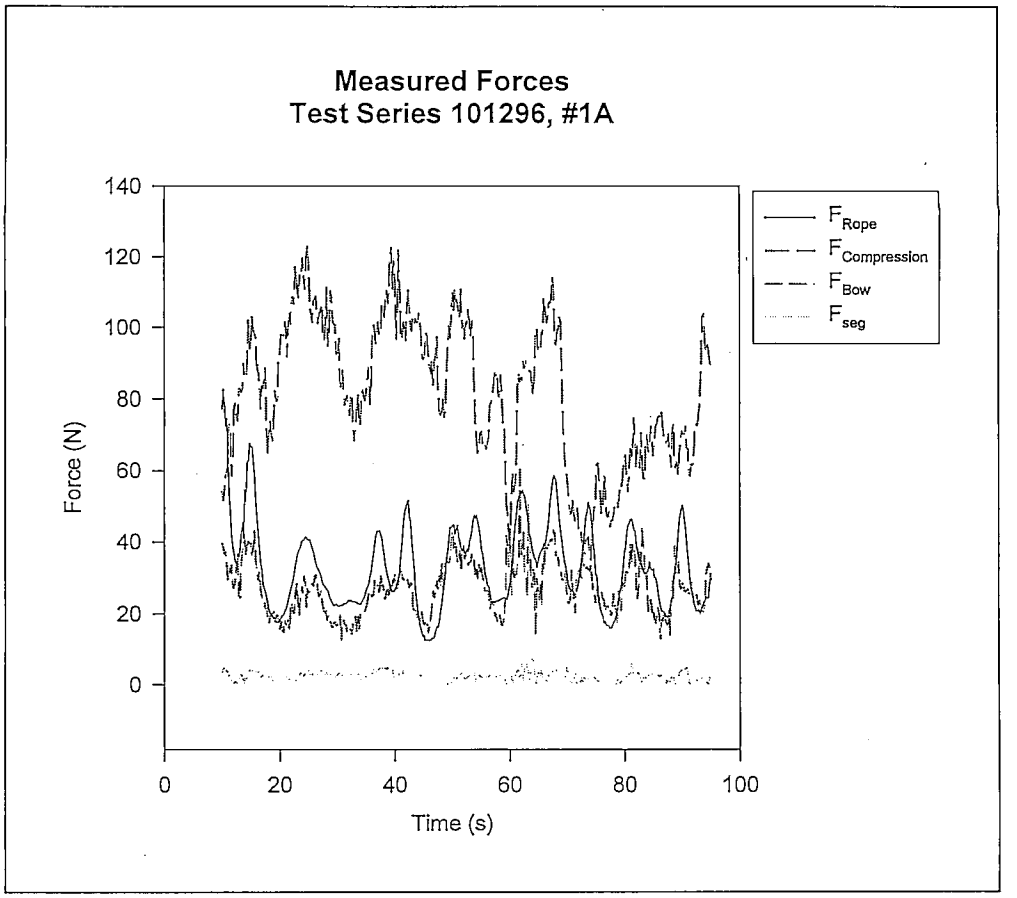
Measured Forces
Test Series 101296, #1A
Force (N)
Time (s)
0
20
40
60
80
100
120
140
F_{Rope}
$F_{Compression}$
F_{Bow}
F_{seg}

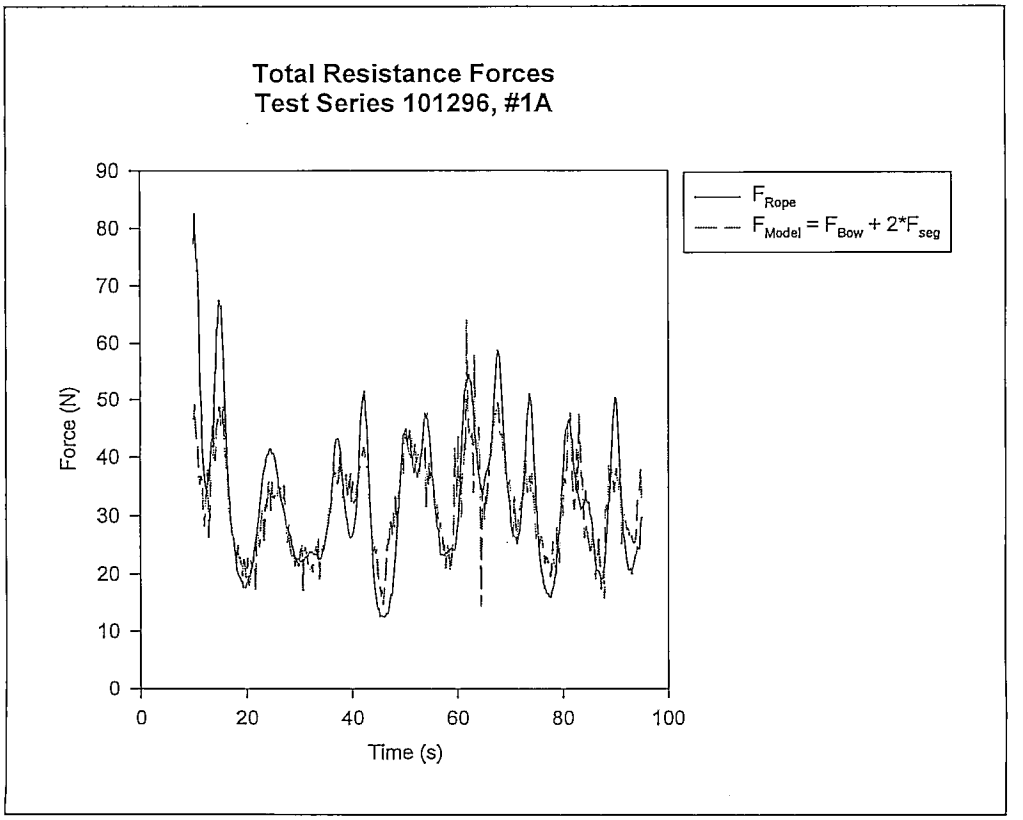
Total Resistance Forces
Test Series 101296, #1A
Force (N)
Time (s)
0
10
20
30
40
50
60
70
80
90
F_{Rope}
$F_{Model} = F_{Bow} + 2*F_{seg}$

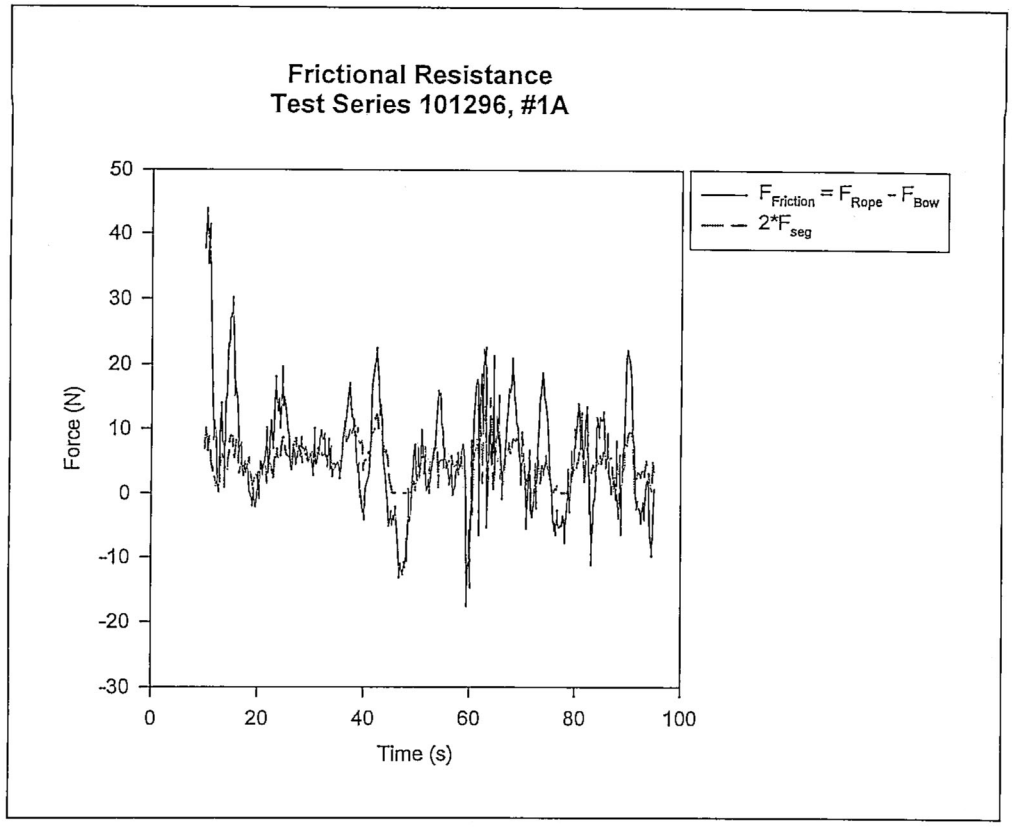
Frictional Resistance
Test Series 101296, #1A
Force (N)
Time (s)
$F_{Friction} = F_{Rope} - F_{Bow}$
$2*F_{seg}$

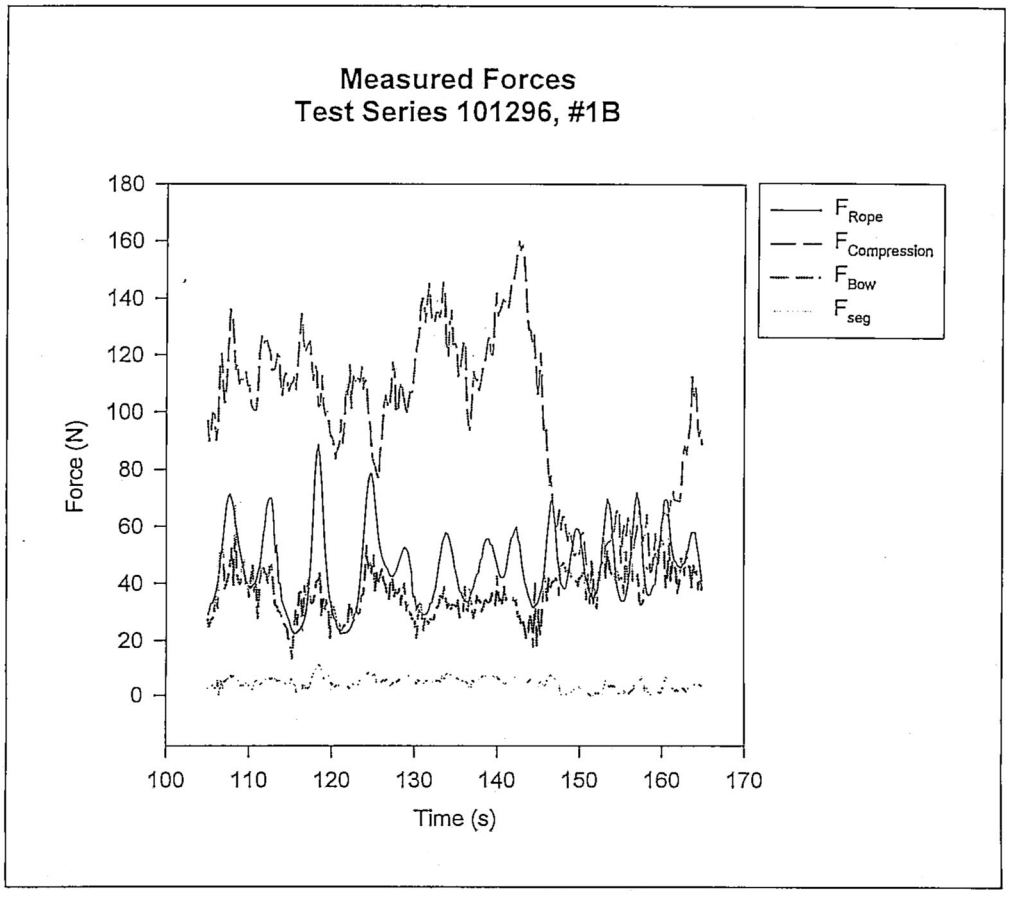
Measured Forces
Test Series 101296, #1B
Force (N)
Time (s)
F_{Rope}
$F_{Compression}$
F_{Bow}
F_{seg}

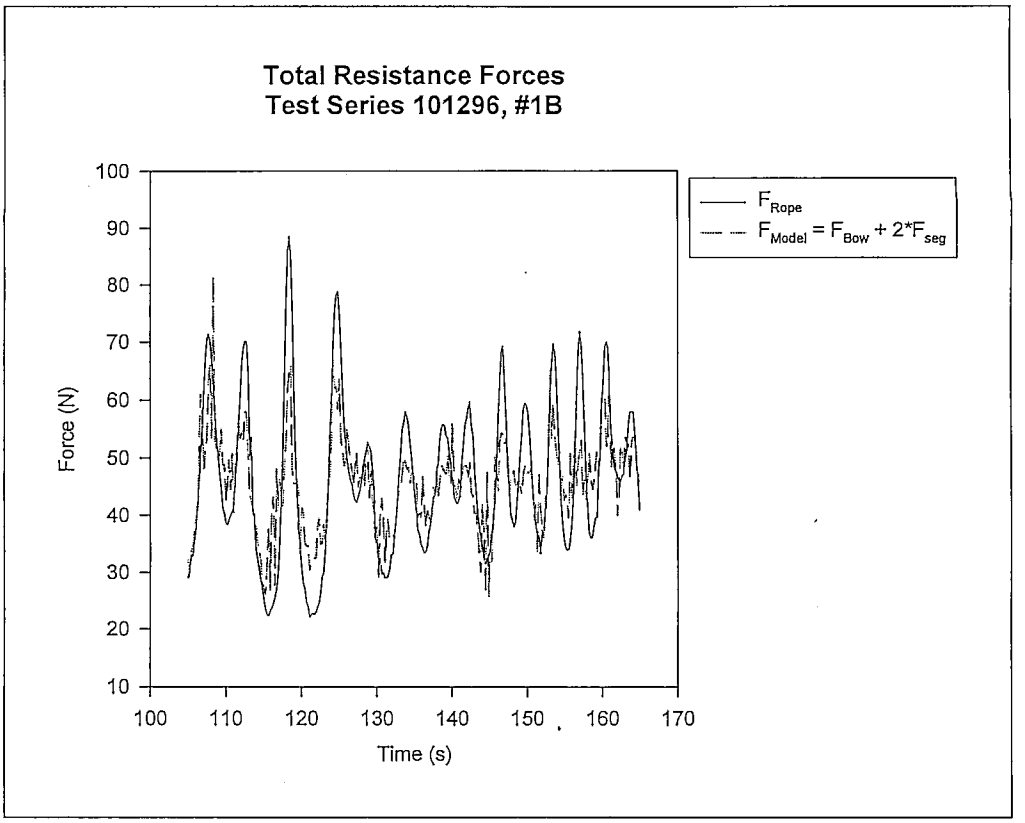
Total Resistance Forces
Test Series 101296, #1B
Force (N)
Time (s)
100
90
80
70
60
50
40
30
20
10
100
110
120
130
140
150
160
170
F_Rope
F_Model = F_Bow + 2*F_seg

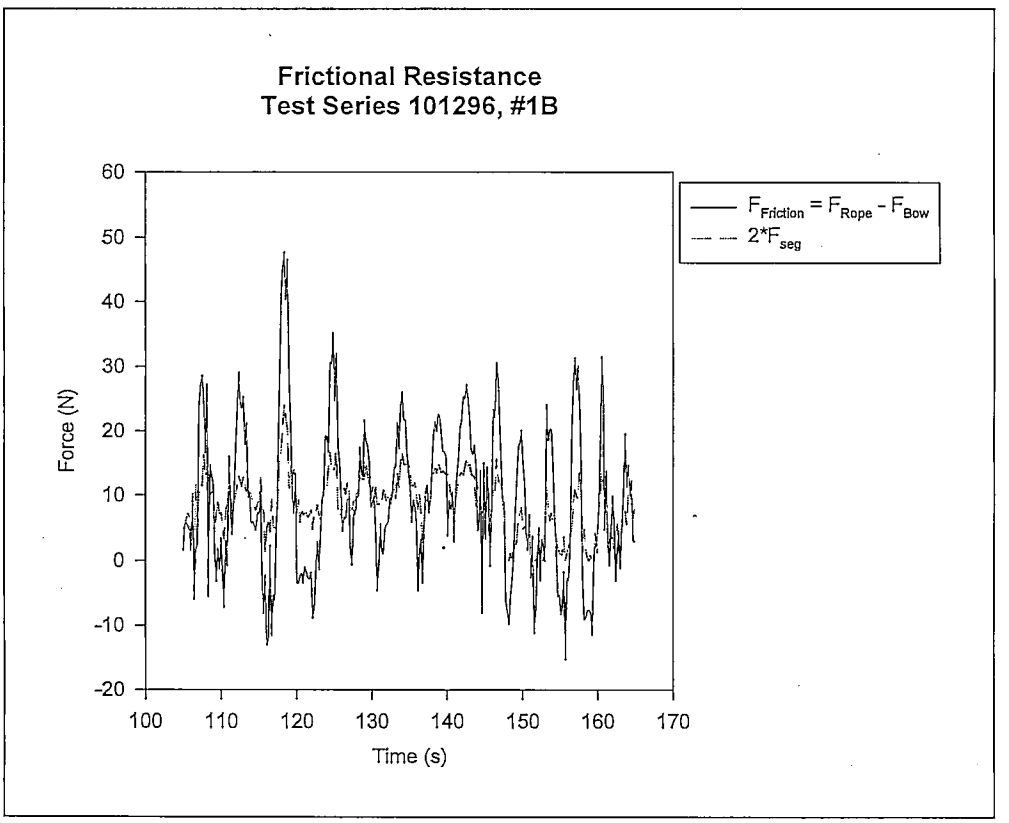
Frictional Resistance
Test Series 101296, #1B
Force (N)
Time (s)
60
50
40
30
20
10
0
-10
-20
100
110
120
130
140
150
160
170
F_Friction = F_Rope - F_Bow
2*F_seg

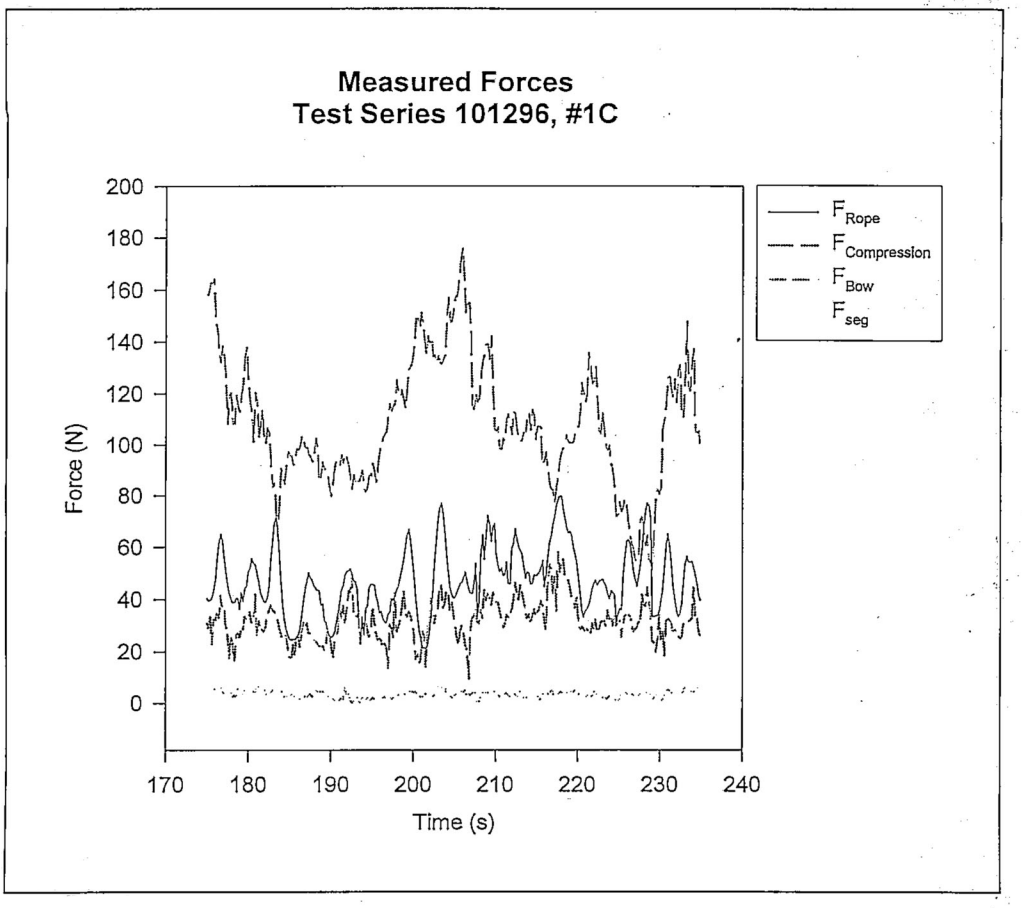
Measured Forces
Test Series 101296, #1C
Force (N)
Time (s)
200
180
160
140
120
100
80
60
40
20
0
170
180
190
200
210
220
230
240
F Rope
F Compression
F Bow
F seg

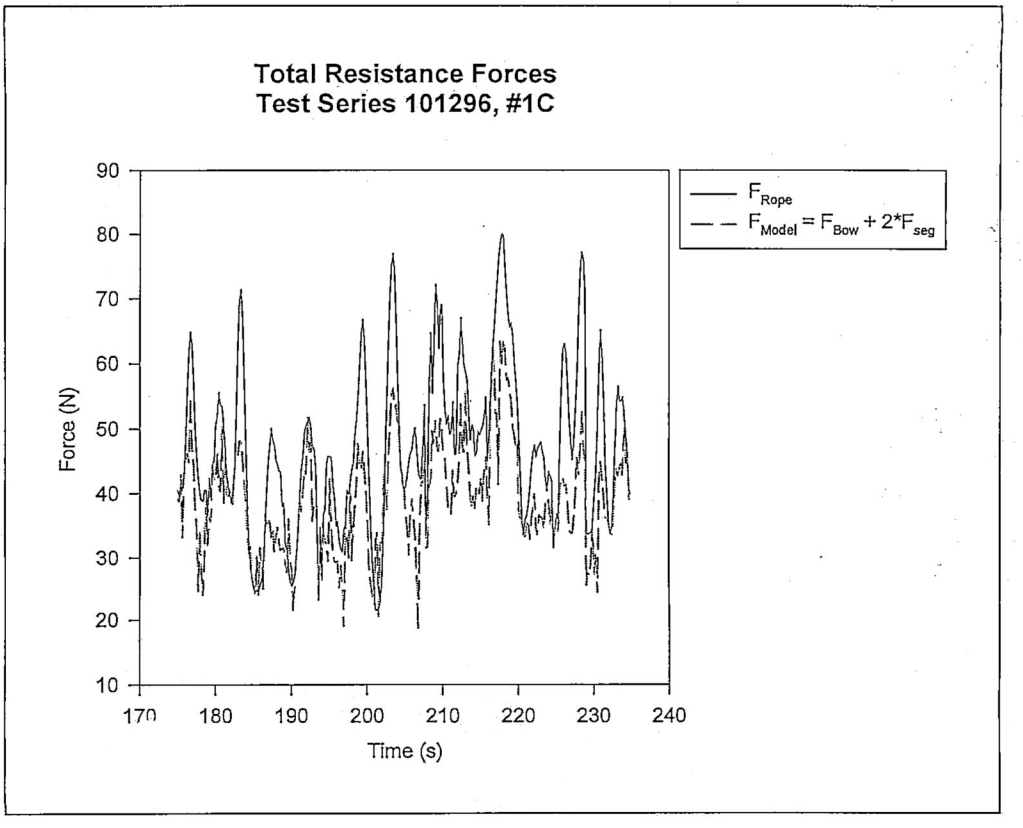
Total Resistance Forces
Test Series 101296, #1C
Force (N)
Time (s)
90
80
70
60
50
40
30
20
10
170
180
190
200
210
220
230
240
F Rope
F Model = F Bow + 2*F seg

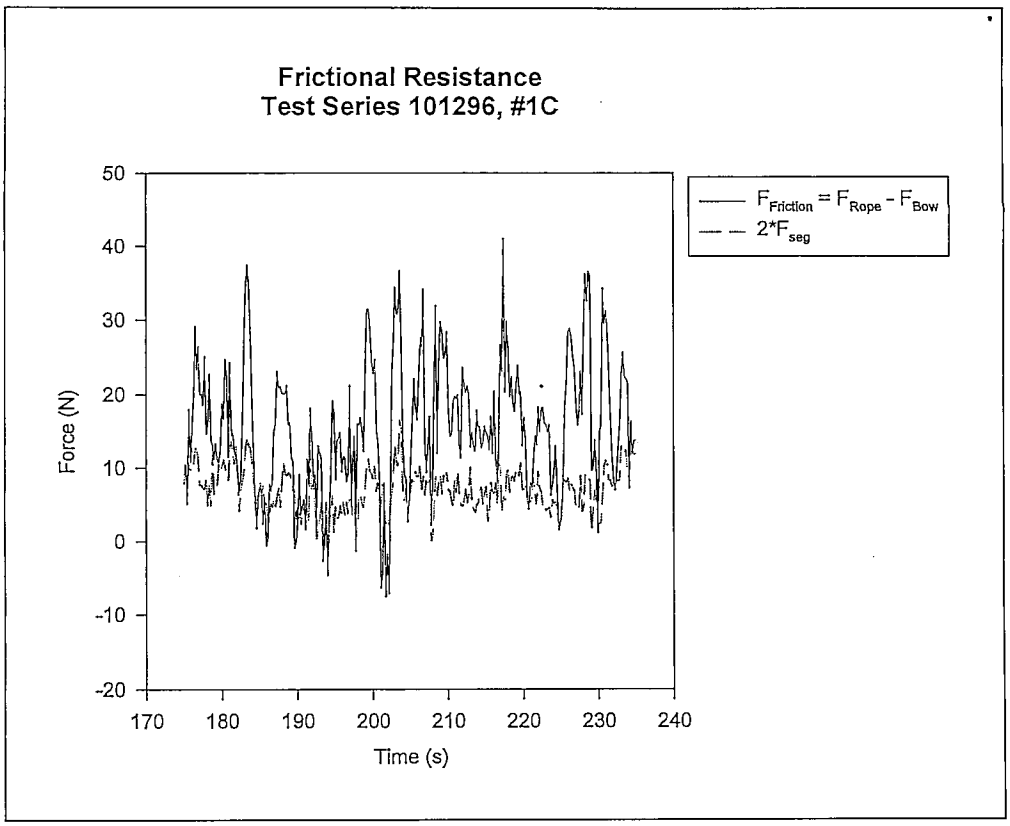
Frictional Resistance
Test Series 101296, #1C
Force (N)
Time (s)
50
40
30
20
10
0
-10
-20
170
180
190
200
210
220
230
240
$F_{Friction} = F_{Rope} - F_{Bow}$
$2*F_{seg}$

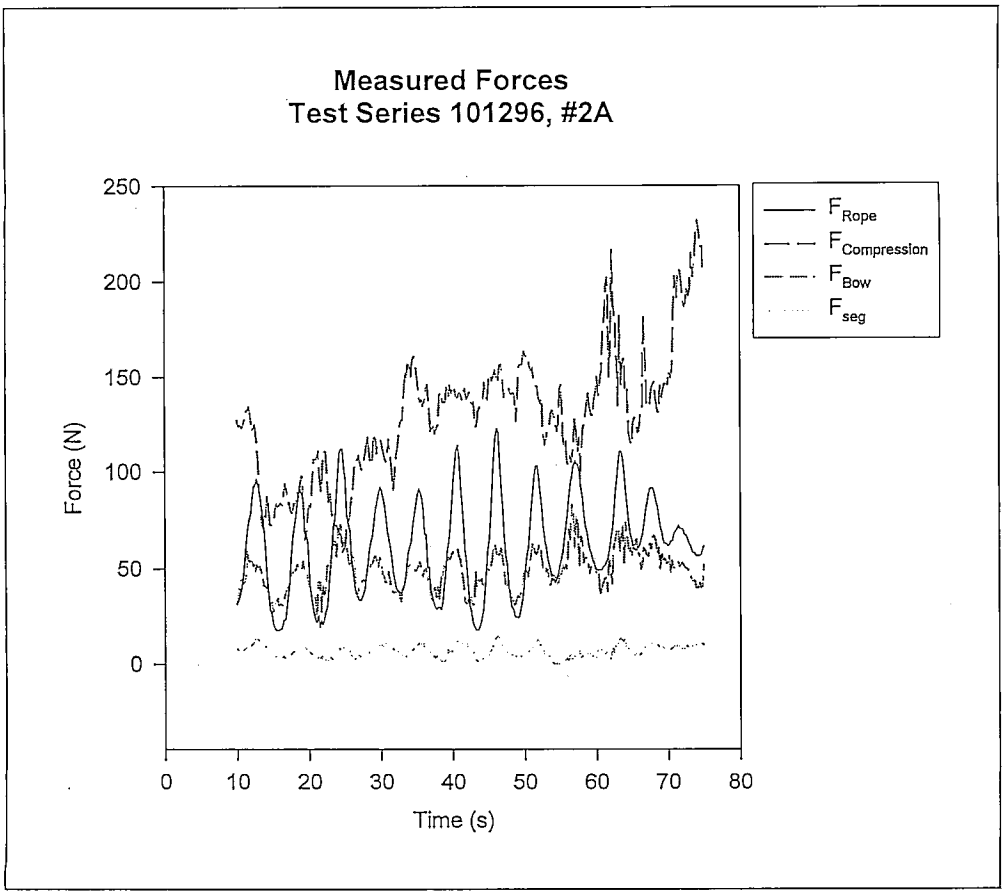
Measured Forces
Test Series 101296, #2A
Force (N)
Time (s)
250
200
150
100
50
0
0
10
20
30
40
50
60
70
80
F_{Rope}
$F_{Compression}$
F_{Bow}
F_{seg}

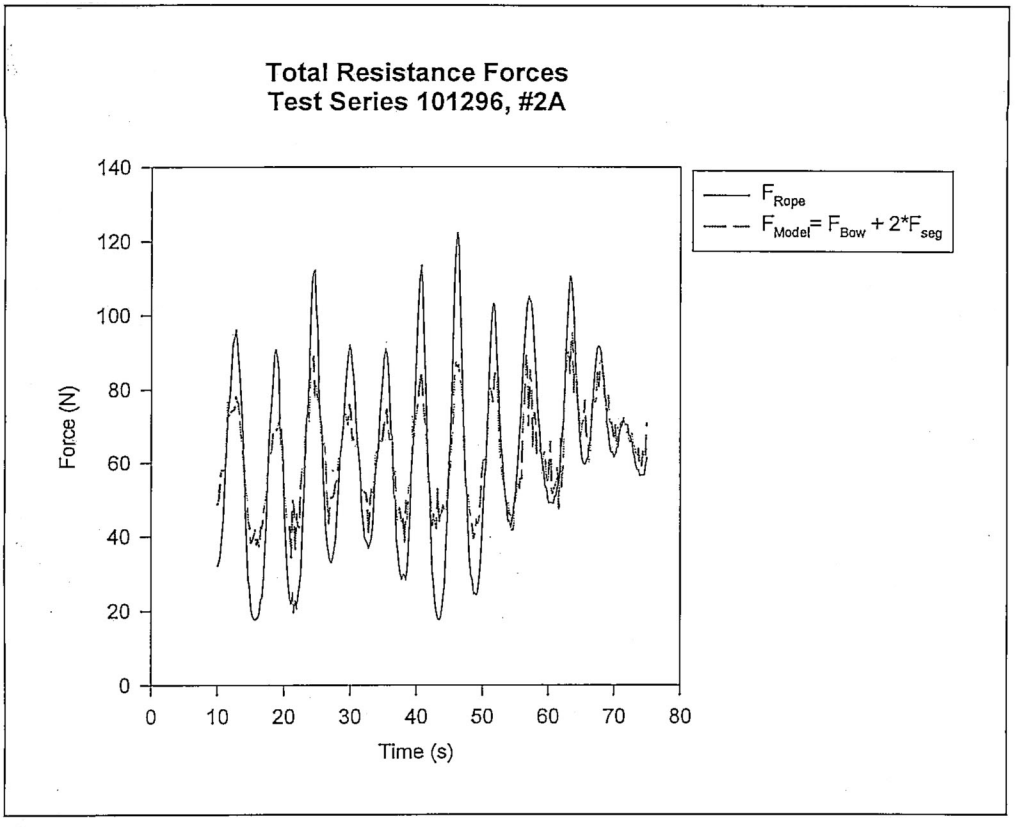
Total Resistance Forces
Test Series 101296, #2A
Force (N)
Time (s)
0
20
40
60
80
100
120
140
0
10
20
30
40
50
60
70
80
F_Rope
F_Model = F_Bow + 2*F_seg

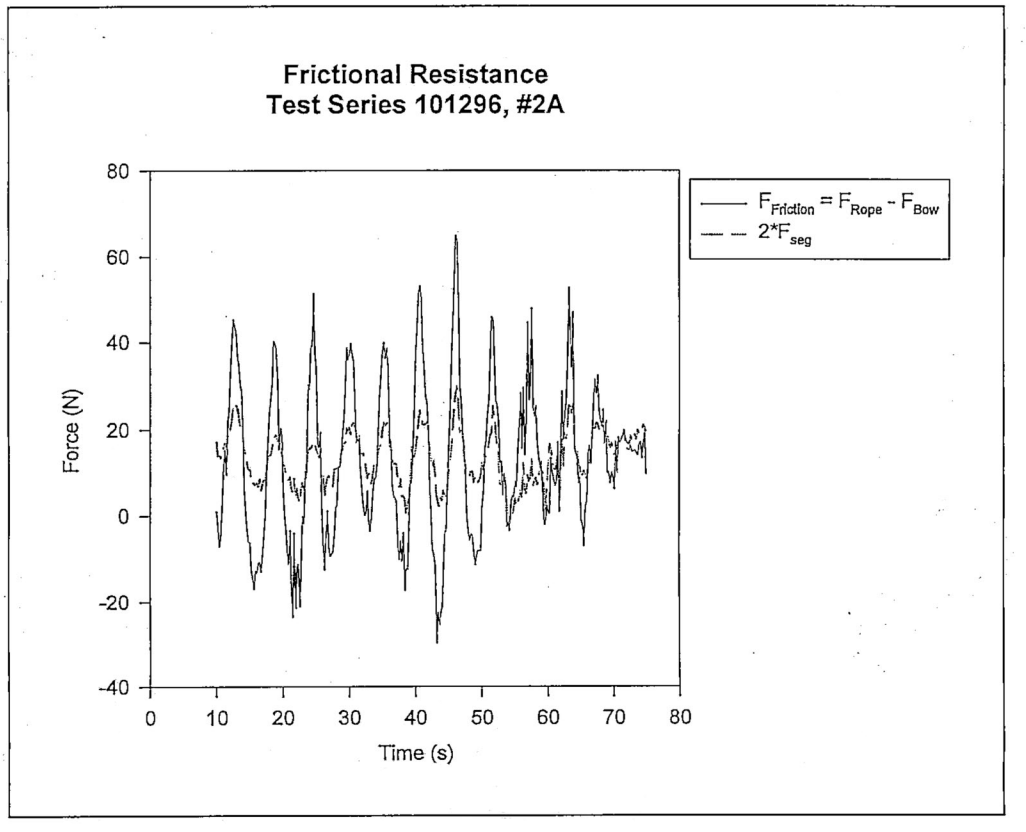
Frictional Resistance
Test Series 101296, #2A
Force (N)
Time (s)
-40
-20
0
20
40
60
80
0
10
20
30
40
50
60
70
80
F_Friction = F_Rope - F_Bow
2*F_seg

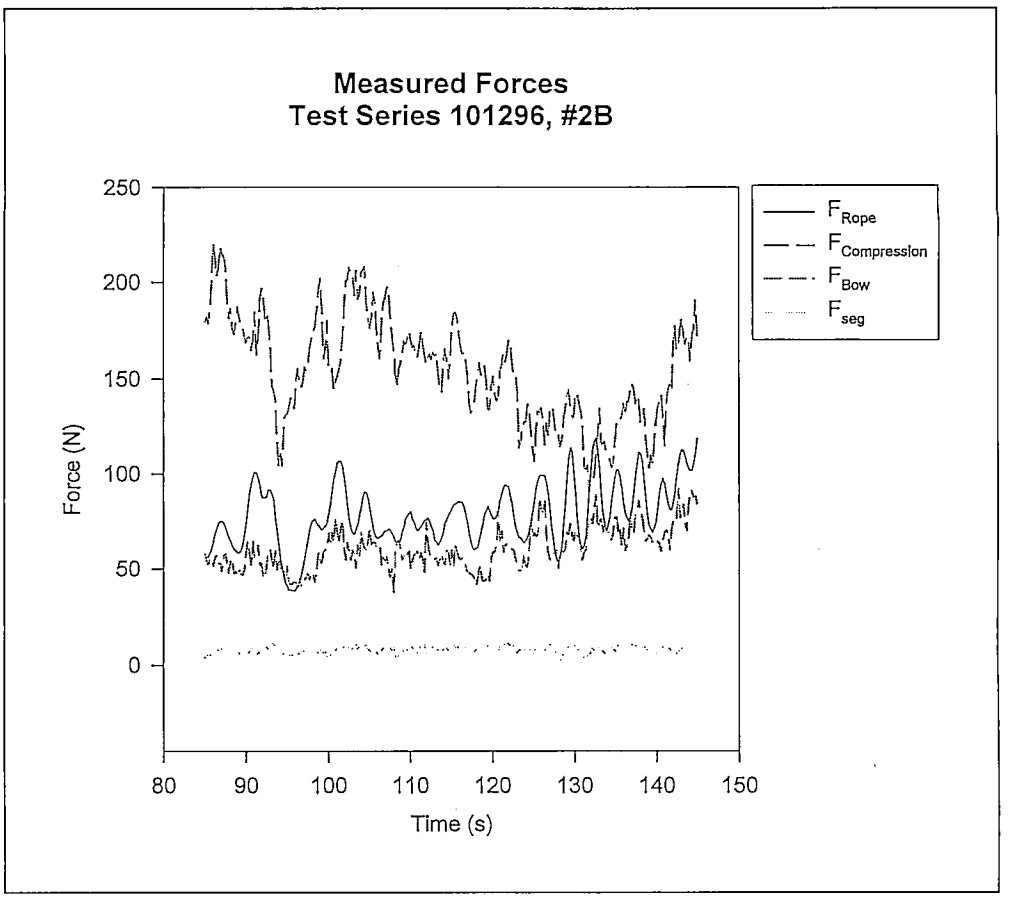
Measured Forces
Test Series 101296, #2B
250
200
150
100
50
0
Force (N)
80
90
100
110
120
130
140
150
Time (s)
F Rope
F Compression
F Bow
F seg

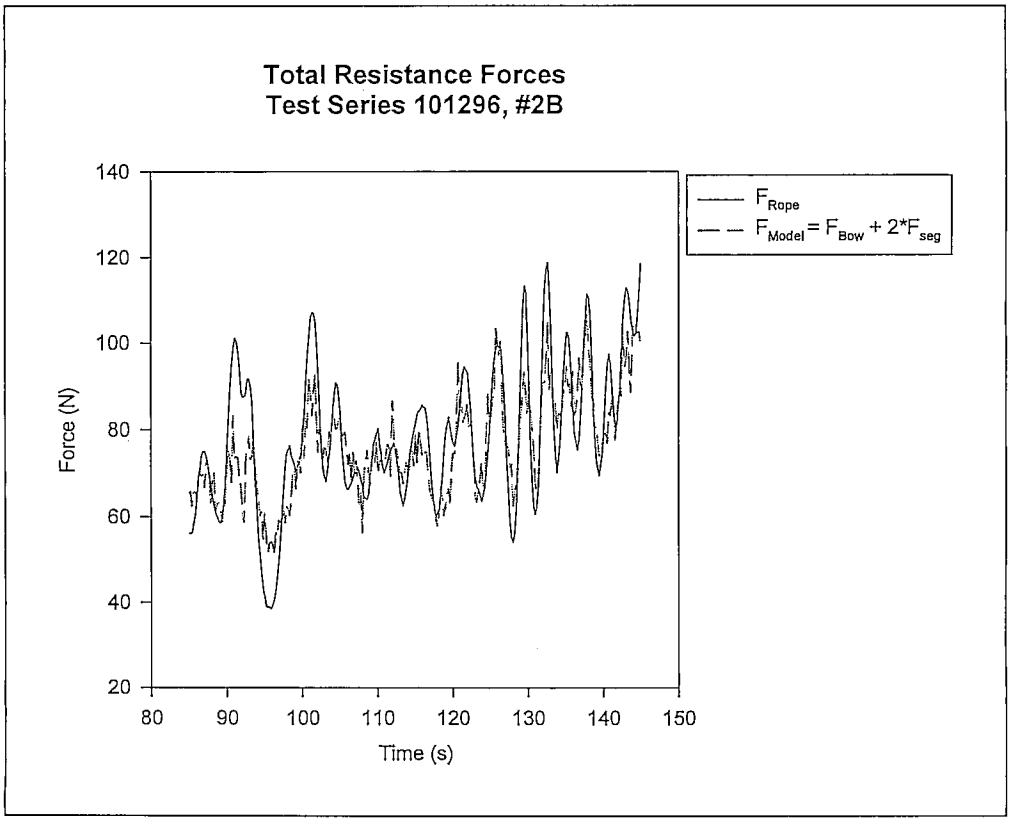
Total Resistance Forces
Test Series 101296, #2B
140
120
100
80
60
40
20
Force (N)
80
90
100
110
120
130
140
150
Time (s)
F Rope
F Model = F Bow + 2*F seg

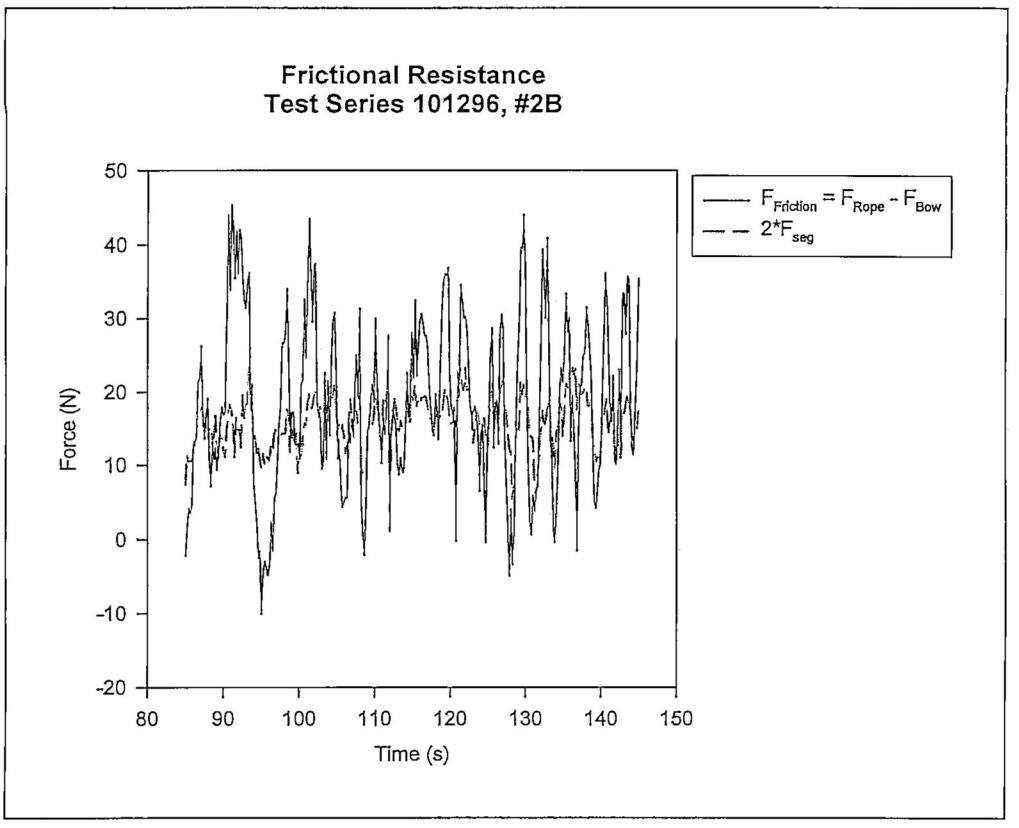
Frictional Resistance
Test Series 101296, #2B
Force (N)
Time (s)
50
40
30
20
10
0
-10
-20
80
90
100
110
120
130
140
150
$F_{Friction} = F_{Rope} - F_{Bow}$
$2*F_{seg}$

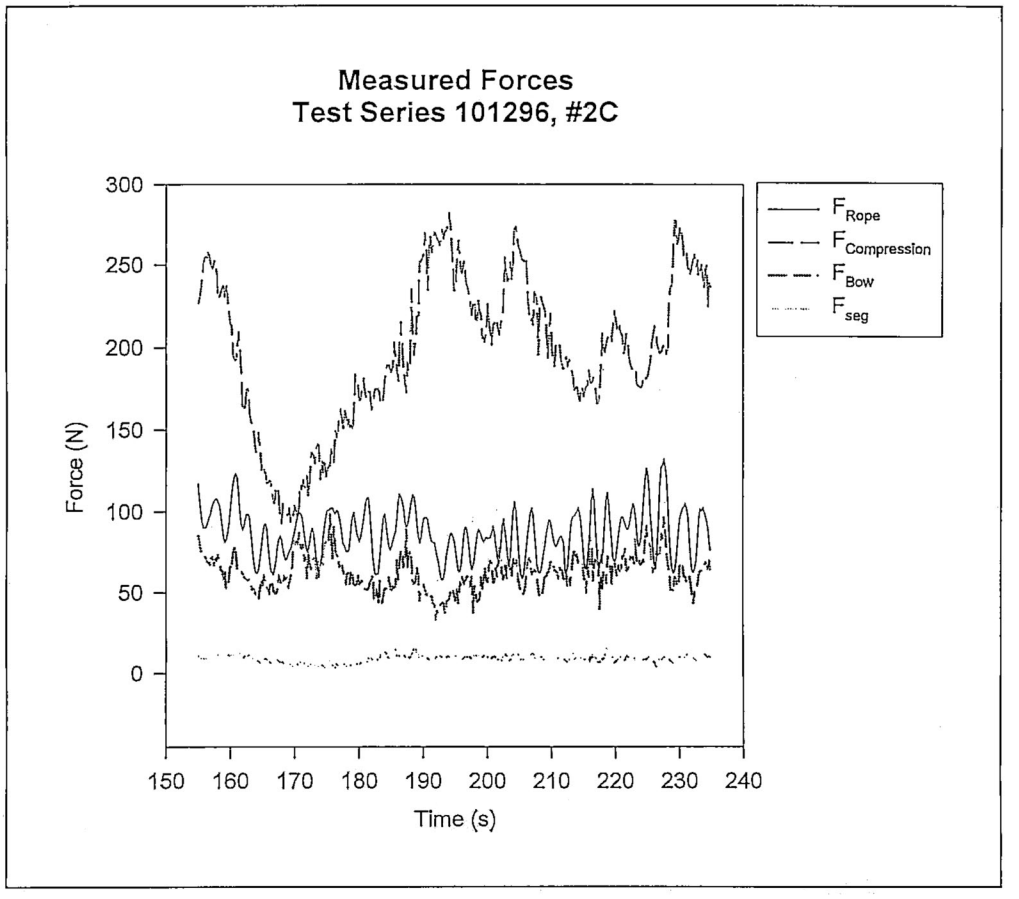
Measured Forces
Test Series 101296, #2C
Force (N)
Time (s)
300
250
200
150
100
50
0
150
160
170
180
190
200
210
220
230
240
F_{Rope}
$F_{Compression}$
F_{Bow}
F_{seg}

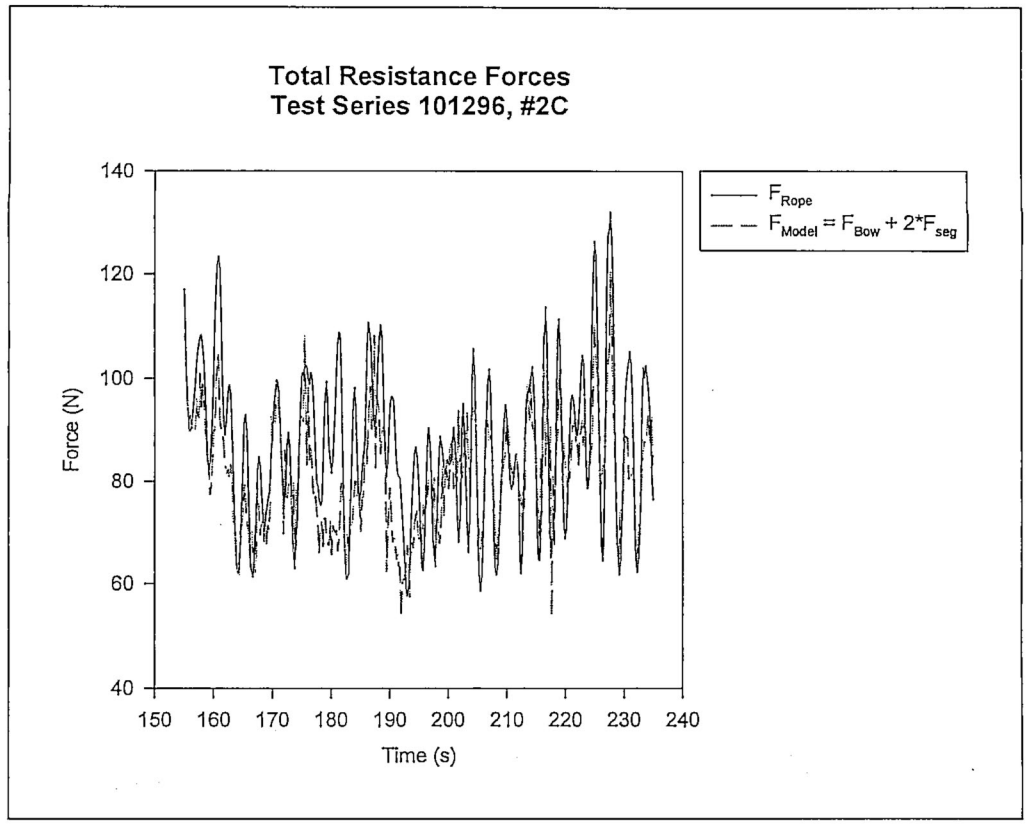
Total Resistance Forces
Test Series 101296, #2C
Force (N)
Time (s)
140
120
100
80
60
40
150
160
170
180
190
200
210
220
230
240
F_Rope
F_Model = F_Bow + 2*F_seg

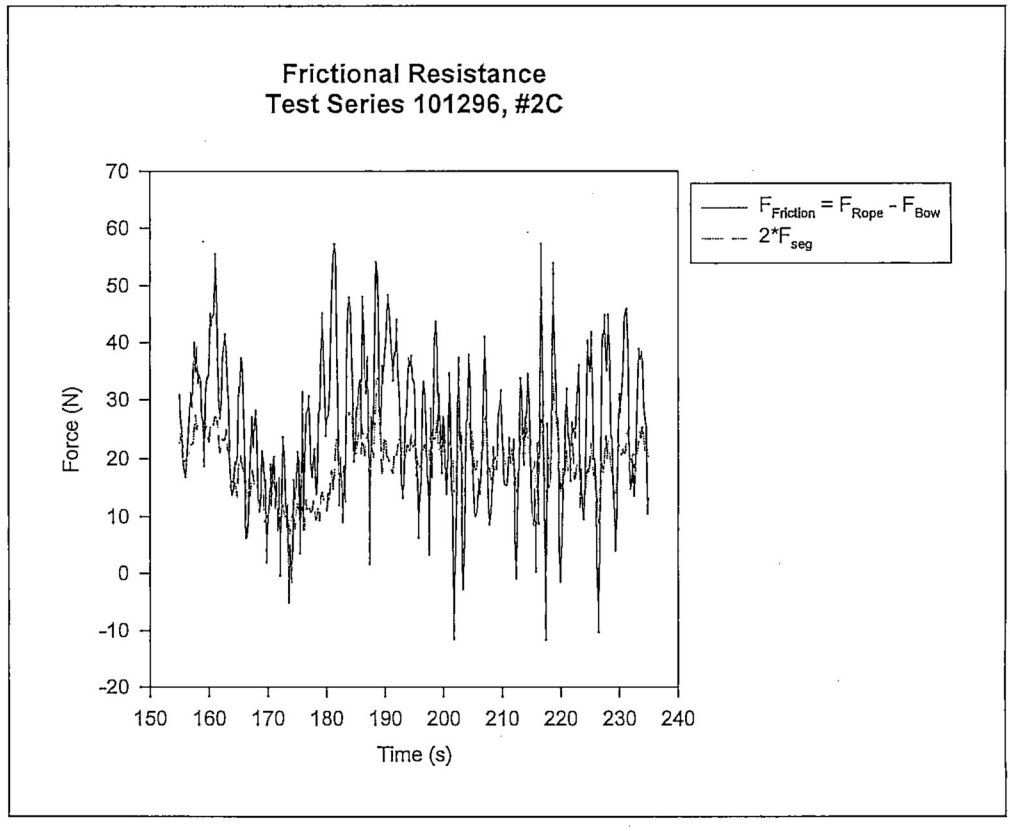
Frictional Resistance
Test Series 101296, #2C
Force (N)
Time (s)
70
60
50
40
30
20
10
0
-10
-20
150
160
170
180
190
200
210
220
230
240
F_Friction = F_Rope - F_Bow
2*F_seg

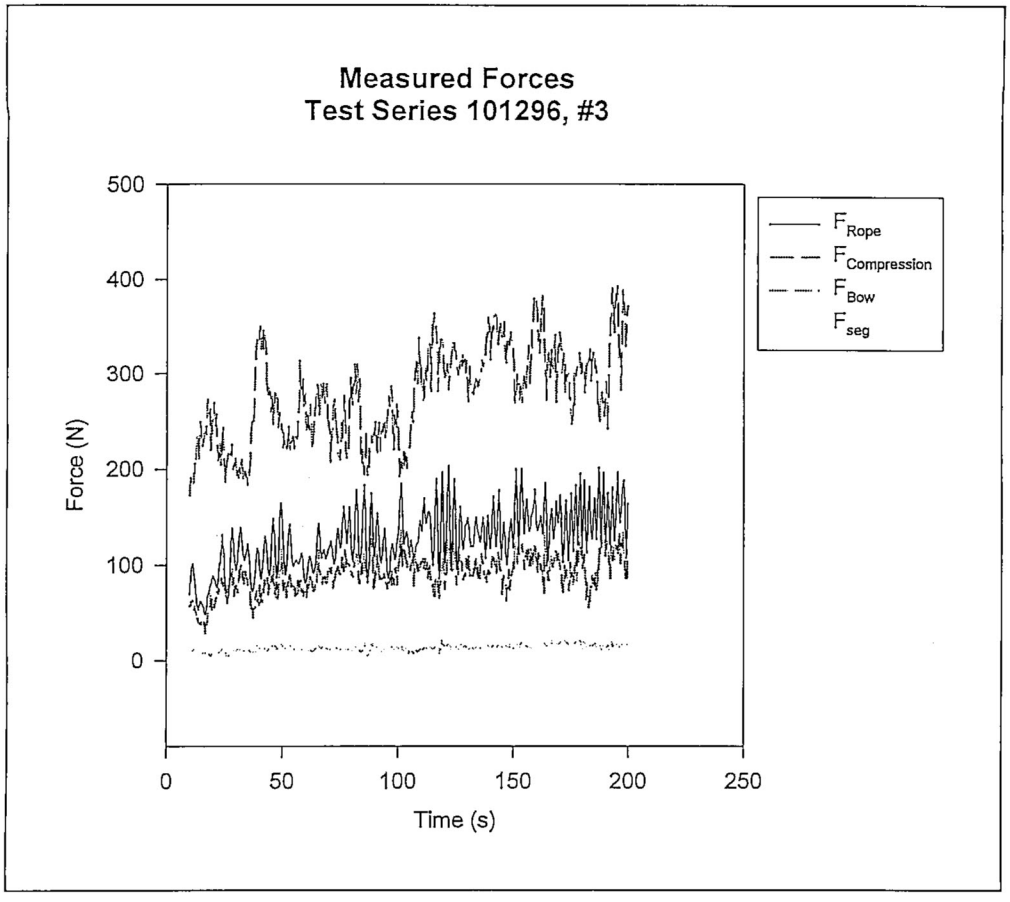
Measured Forces
Test Series 101296, #3
Force (N)
Time (s)
500
400
300
200
100
0
0
50
100
150
200
250
F Rope
F Compression
F Bow
F seg

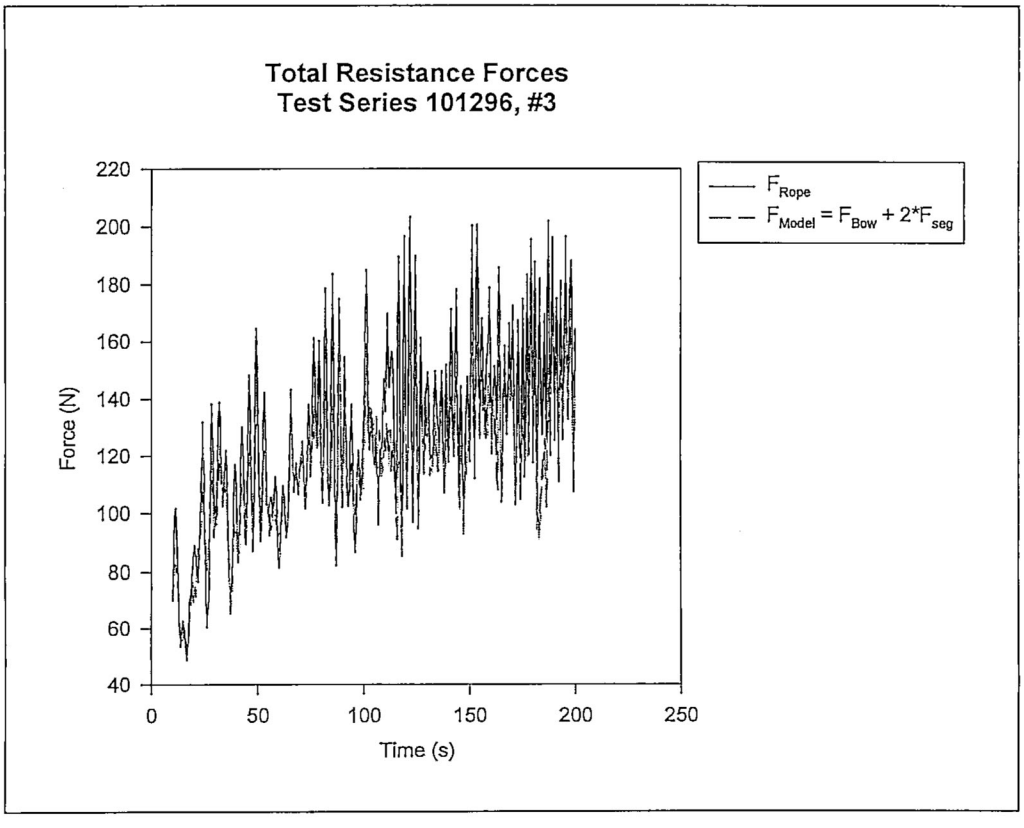
Total Resistance Forces
Test Series 101296, #3
Force (N)
Time (s)
220
200
180
160
140
120
100
80
60
40
0
50
100
150
200
250
F Rope
F Model = F Bow + 2*F seg

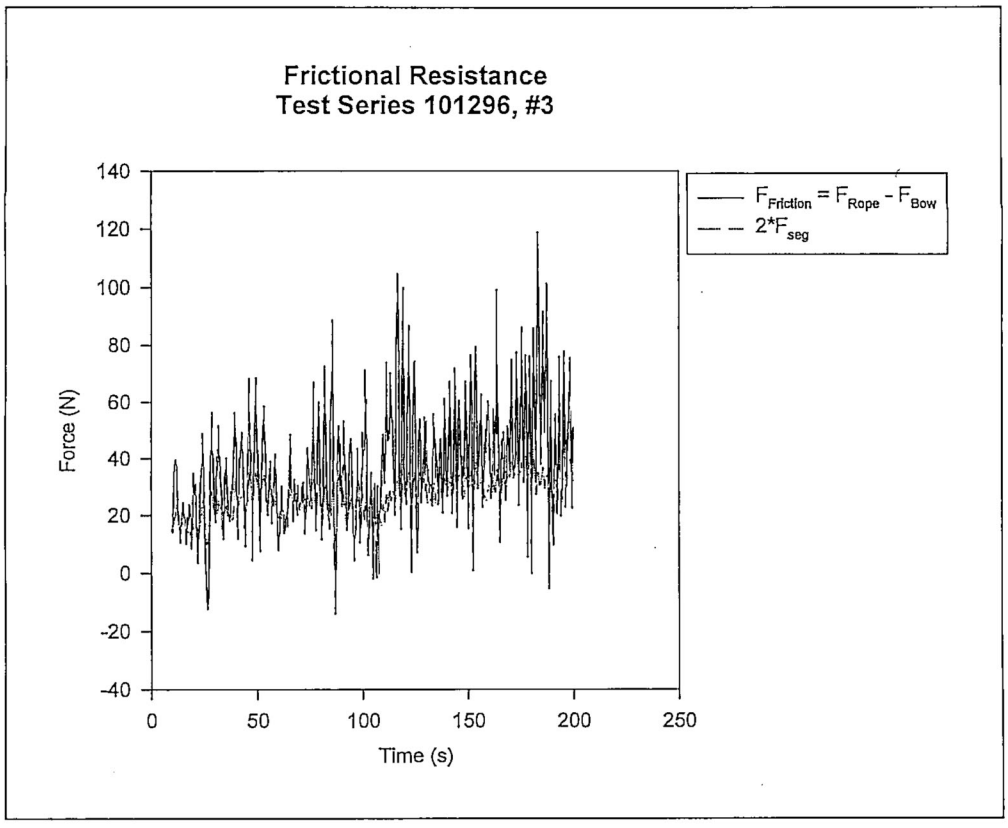
Frictional Resistance
Test Series 101296, #3
Force (N)
Time (s)
$F_{Friction} = F_{Rope} - F_{Bow}$
$2*F_{seg}$

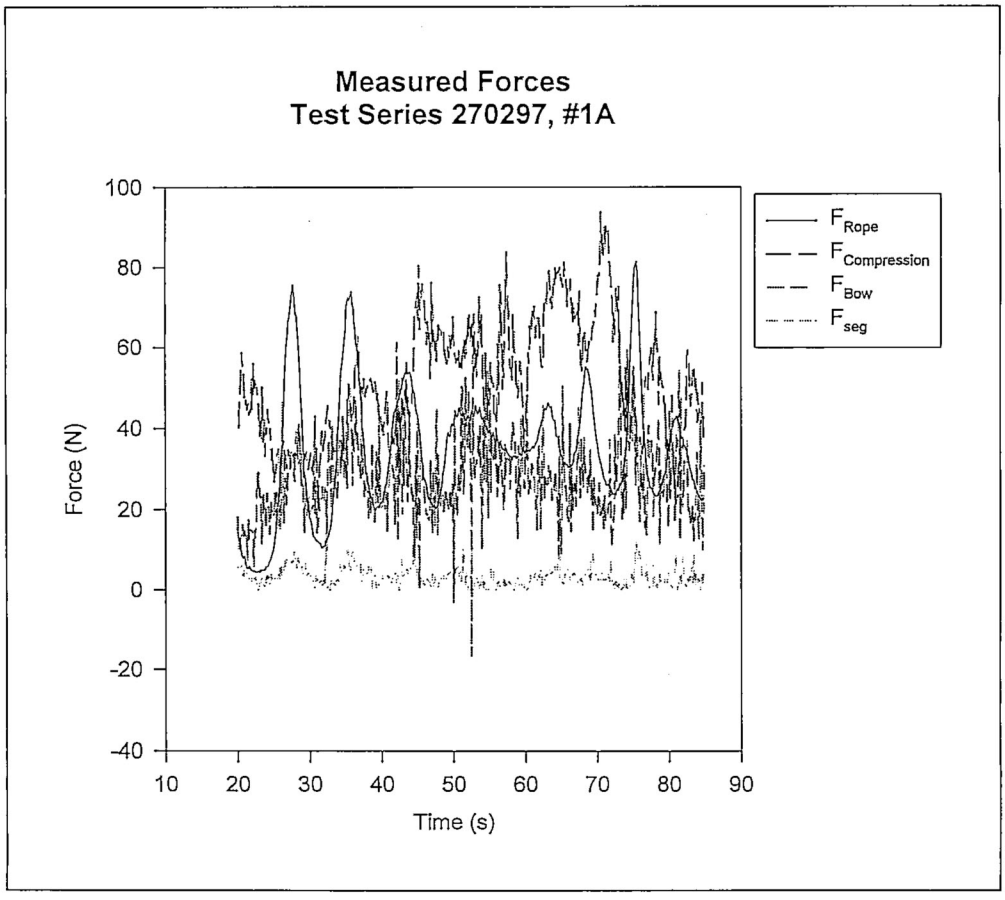
Measured Forces
Test Series 270297, #1A
Force (N)
Time (s)
F_{Rope}
$F_{Compression}$
F_{Bow}
F_{seg}

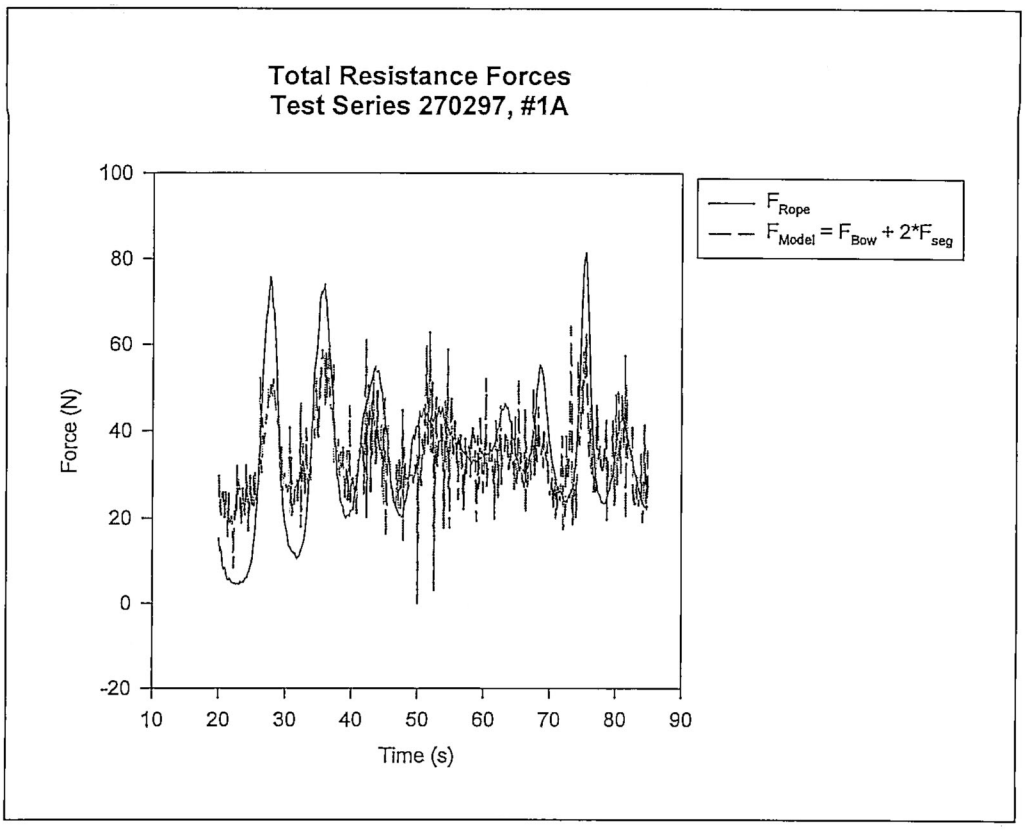
Total Resistance Forces
Test Series 270297, #1A
Force (N)
Time (s)
100
80
60
40
20
0
-20
10
20
30
40
50
60
70
80
90
F_Rope
F_Model = F_Bow + 2*F_seg

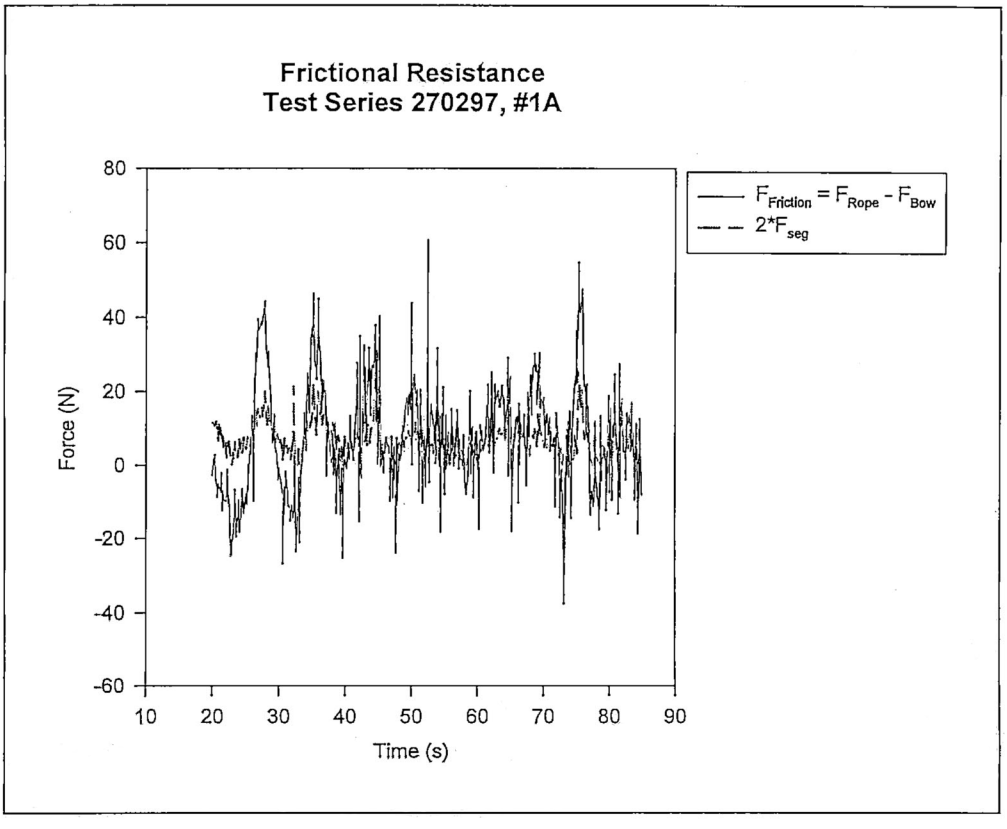
Frictional Resistance
Test Series 270297, #1A
Force (N)
Time (s)
80
60
40
20
0
-20
-40
-60
10
20
30
40
50
60
70
80
90
F_Friction = F_Rope - F_Bow
2*F_seg

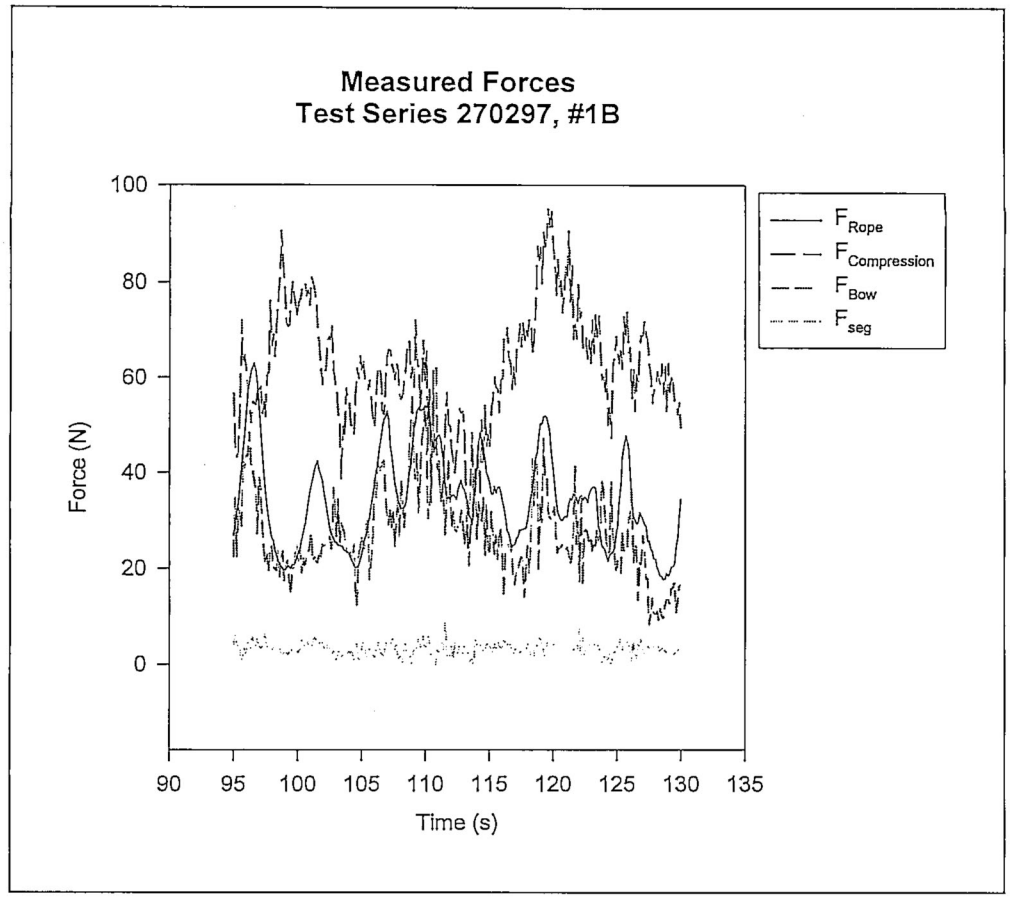
Measured Forces
Test Series 270297, #1B
Force (N)
Time (s)
100
80
60
40
20
0
90
95
100
105
110
115
120
125
130
135
F Rope
F Compression
F Bow
F seg

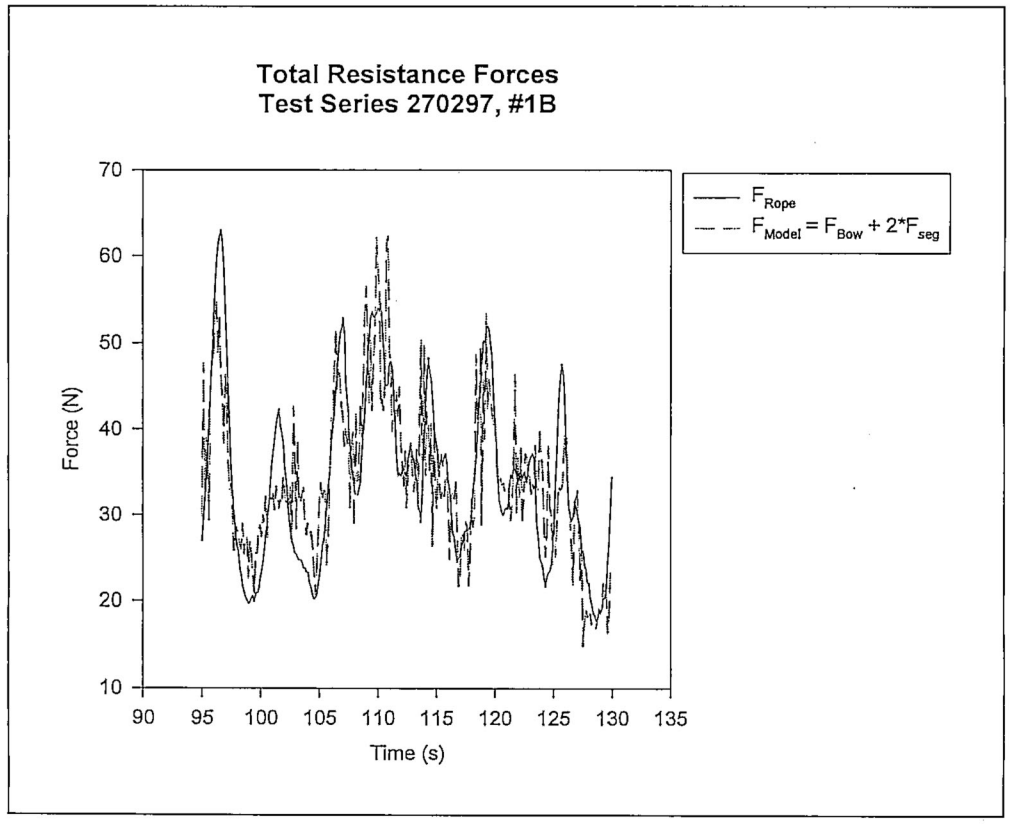
Total Resistance Forces
Test Series 270297, #1B
Force (N)
Time (s)
70
60
50
40
30
20
10
90
95
100
105
110
115
120
125
130
135
F Rope
F Model = F Bow + 2*F seg

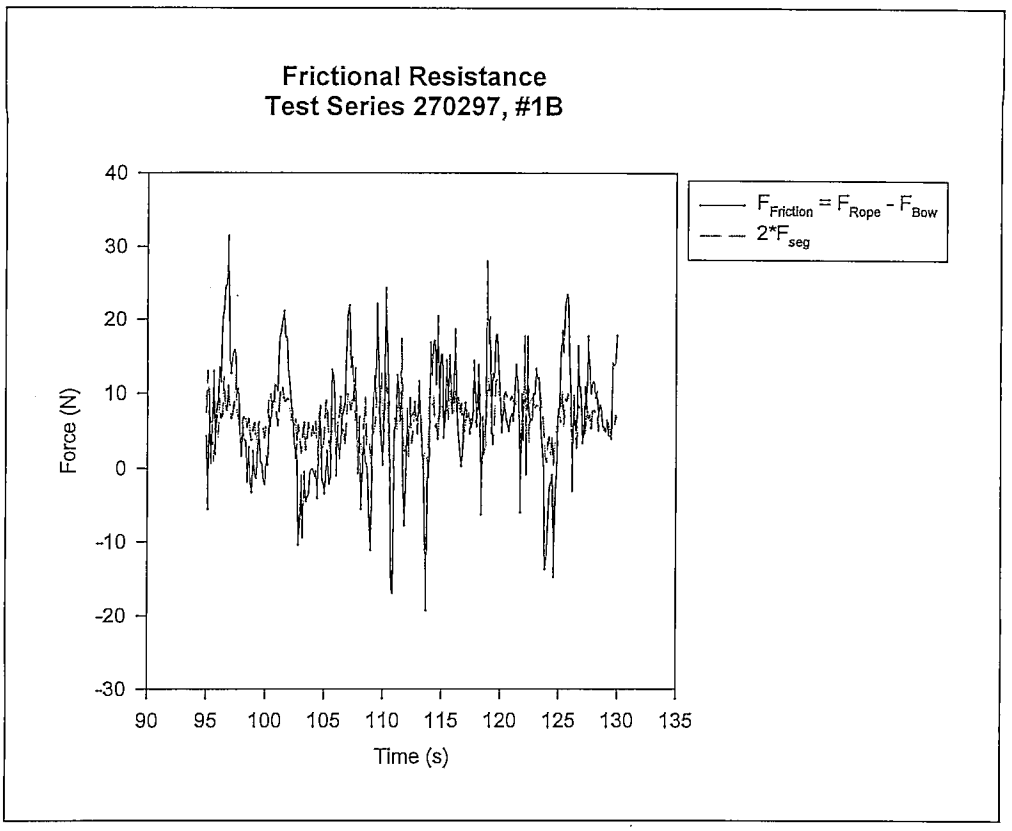
Frictional Resistance
Test Series 270297, #1B
Force (N)
Time (s)
$F_{Friction} = F_{Rope} - F_{Bow}$
$2*F_{seg}$

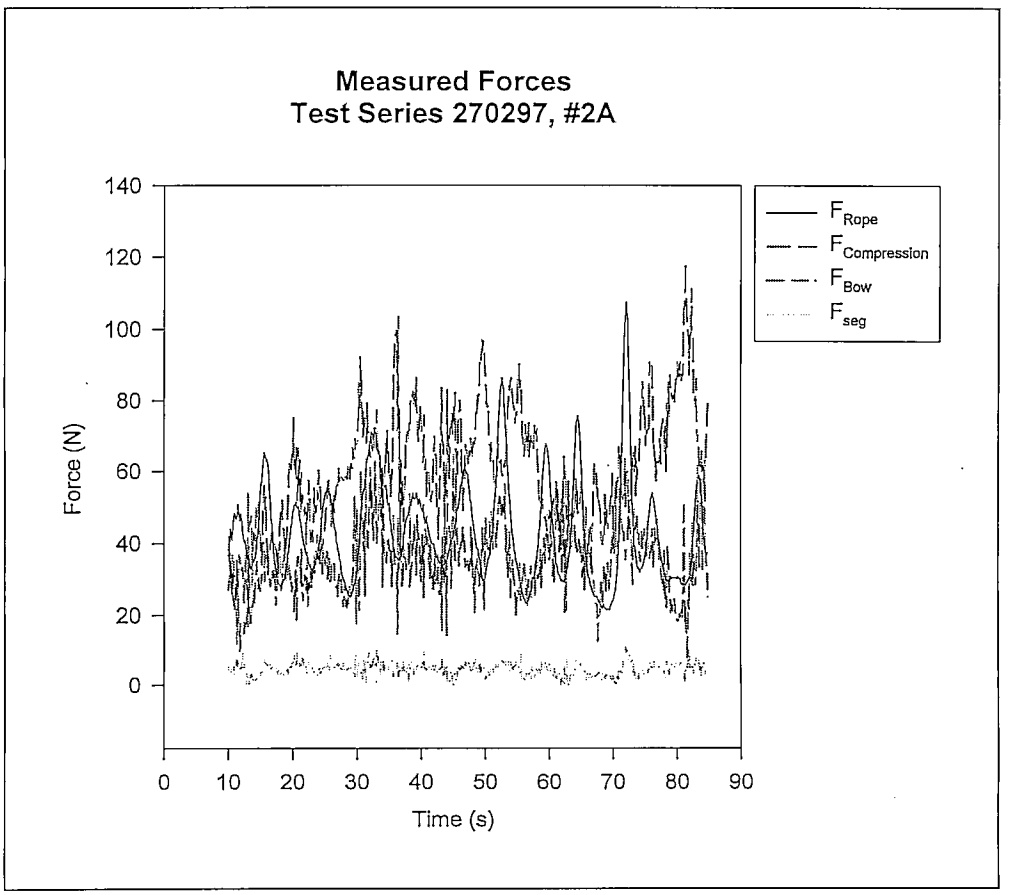
Measured Forces
Test Series 270297, #2A
Force (N)
Time (s)
F_{Rope}
$F_{Compression}$
F_{Bow}
F_{seg}

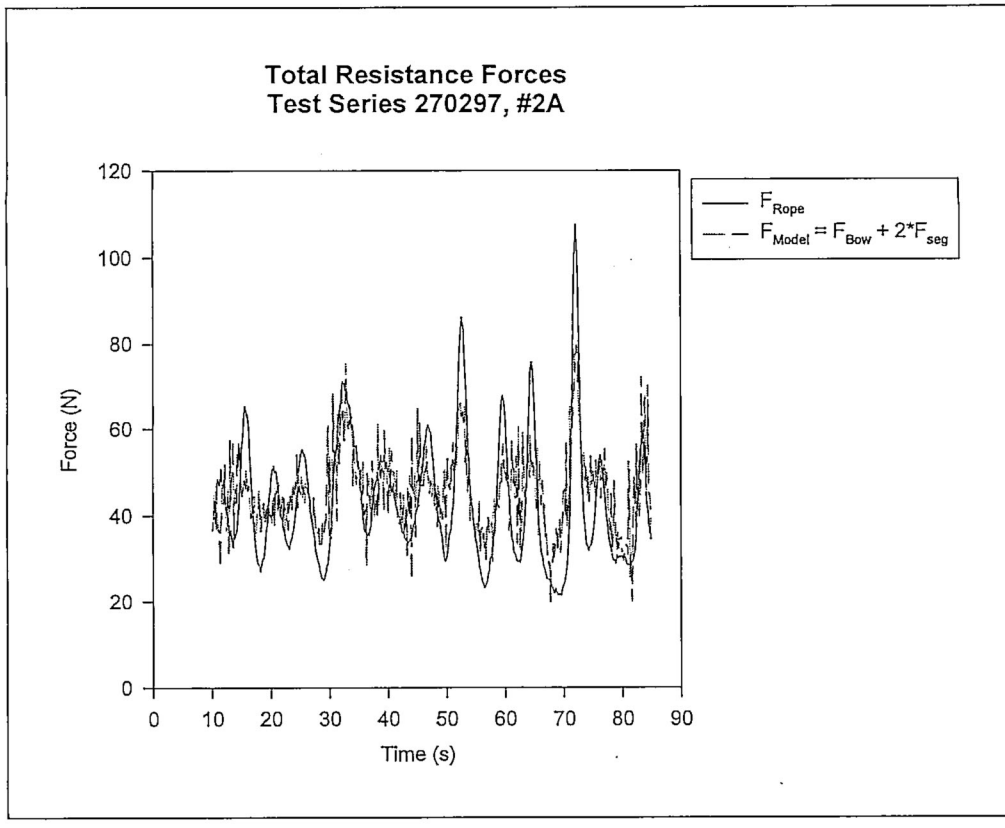
Total Resistance Forces
Test Series 270297, #2A
Force (N)
Time (s)
F_Rope
F_Model = F_Bow + 2*F_seg
0
20
40
60
80
100
120
0
10
20
30
40
50
60
70
80
90

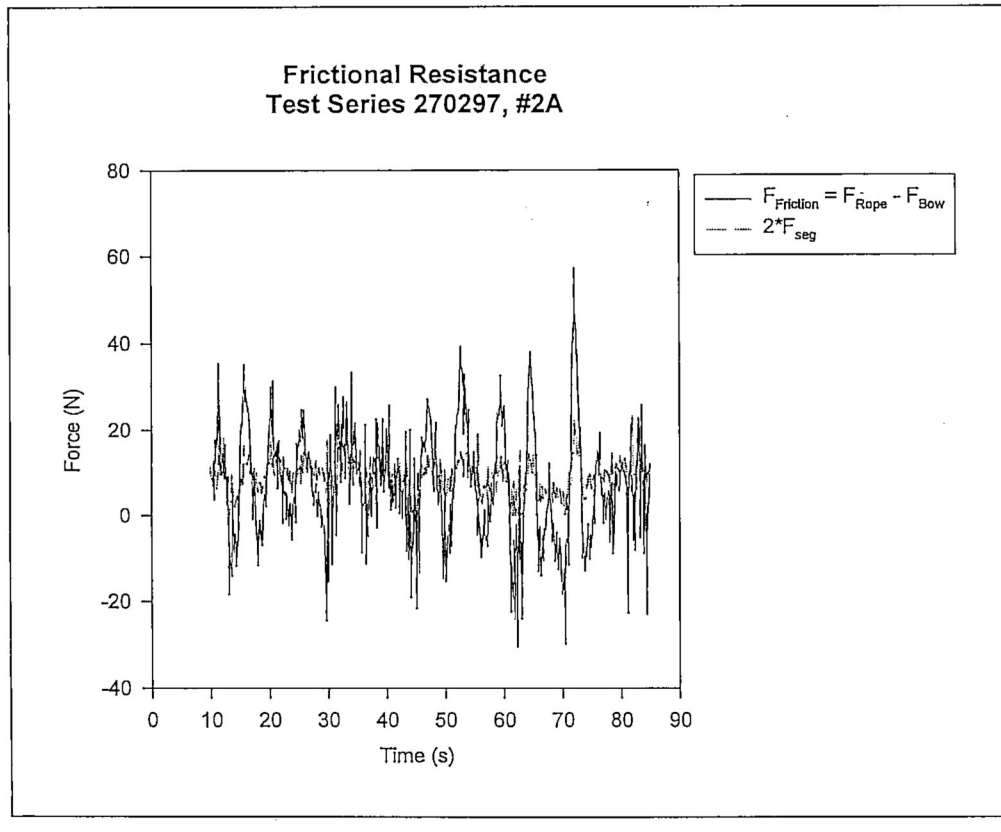
Frictional Resistance
Test Series 270297, #2A
Force (N)
Time (s)
F_Friction = F_Rope - F_Bow
2*F_seg
-40
-20
0
20
40
60
80
0
10
20
30
40
50
60
70
80
90

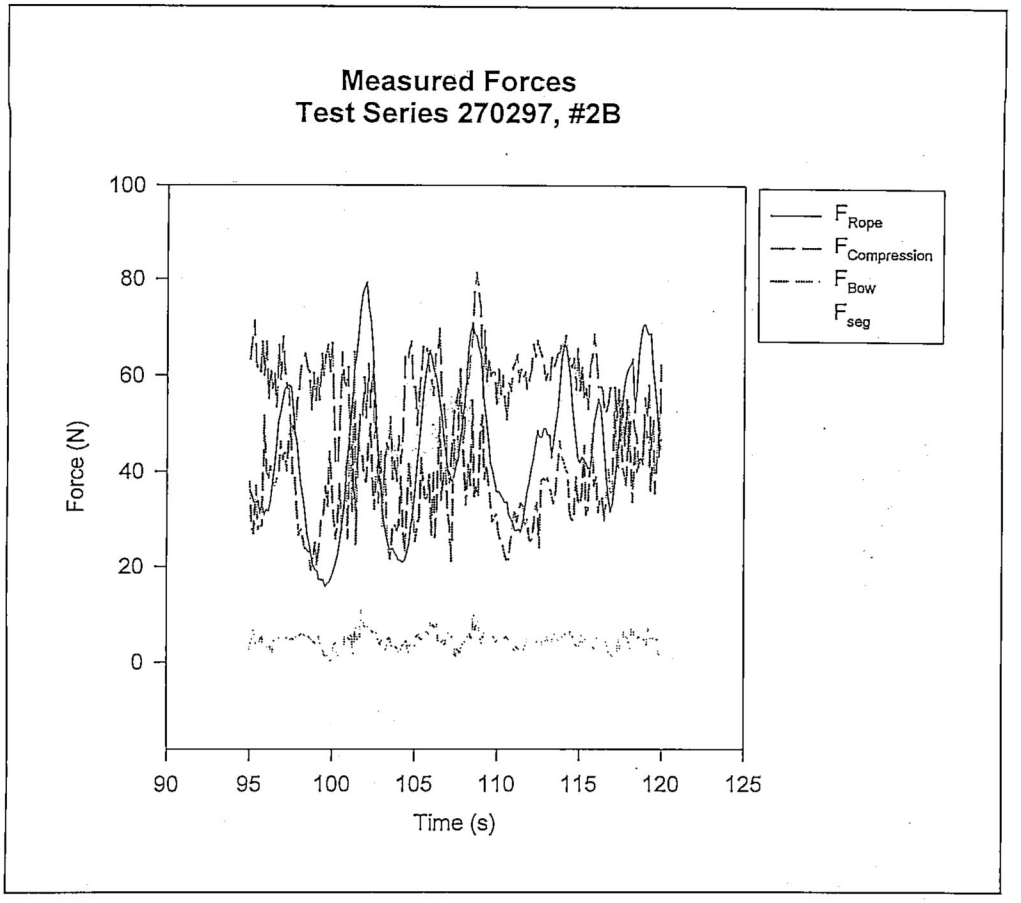
Measured Forces
Test Series 270297, #2B
Force (N)
Time (s)
100
80
60
40
20
0
90
95
100
105
110
115
120
125
F Rope
F Compression
F Bow
F seg

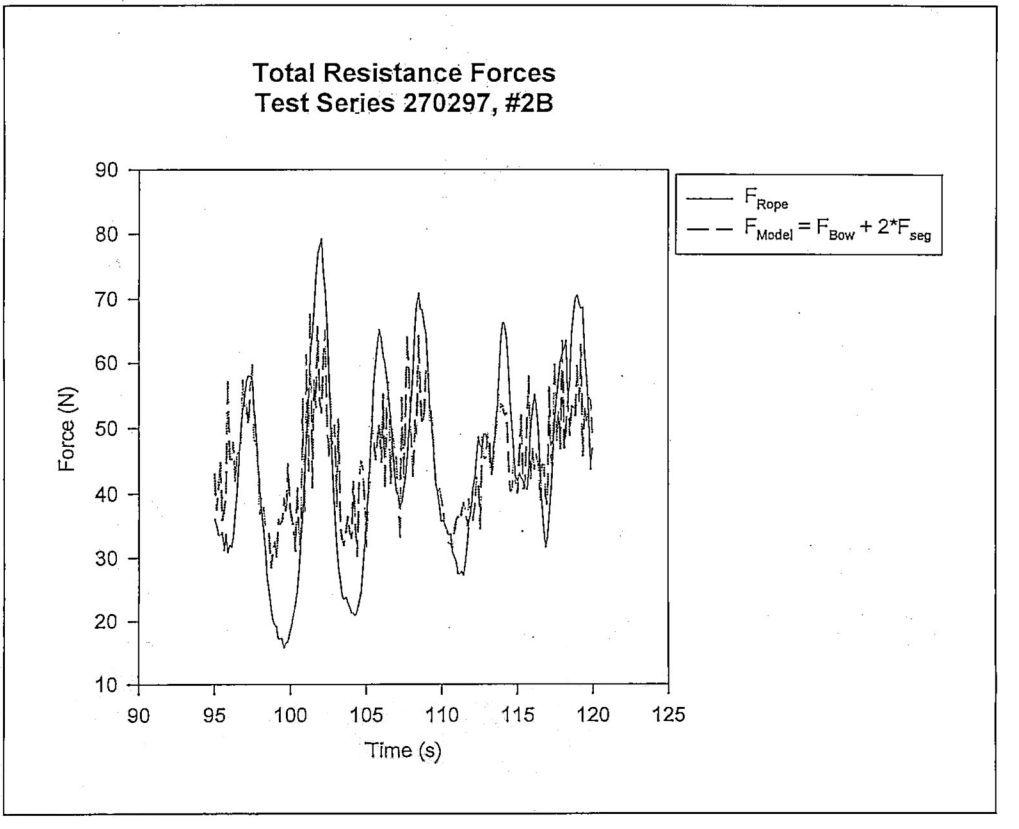
Total Resistance Forces
Test Series 270297, #2B
Force (N)
Time (s)
90
80
70
60
50
40
30
20
10
90
95
100
105
110
115
120
125
F Rope
F Model = F Bow + 2*F seg

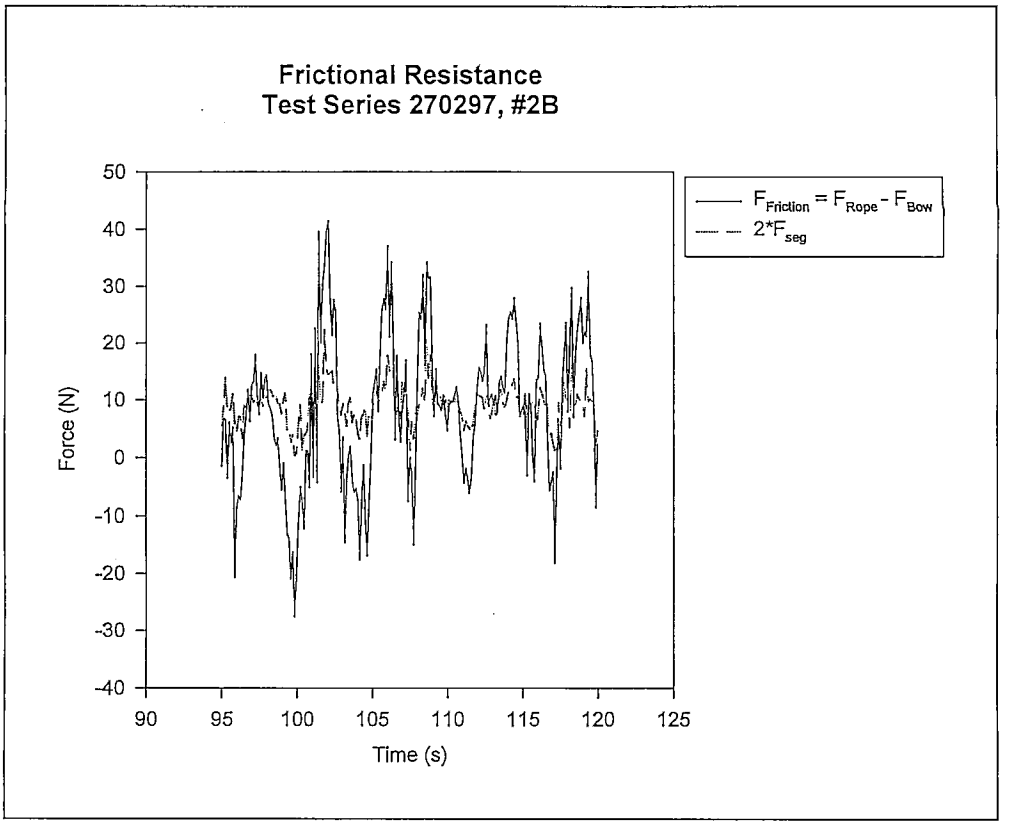
Frictional Resistance
Test Series 270297, #2B
Force (N)
Time (s)
$F_{Friction} = F_{Rope} - F_{Bow}$
$2*F_{seg}$

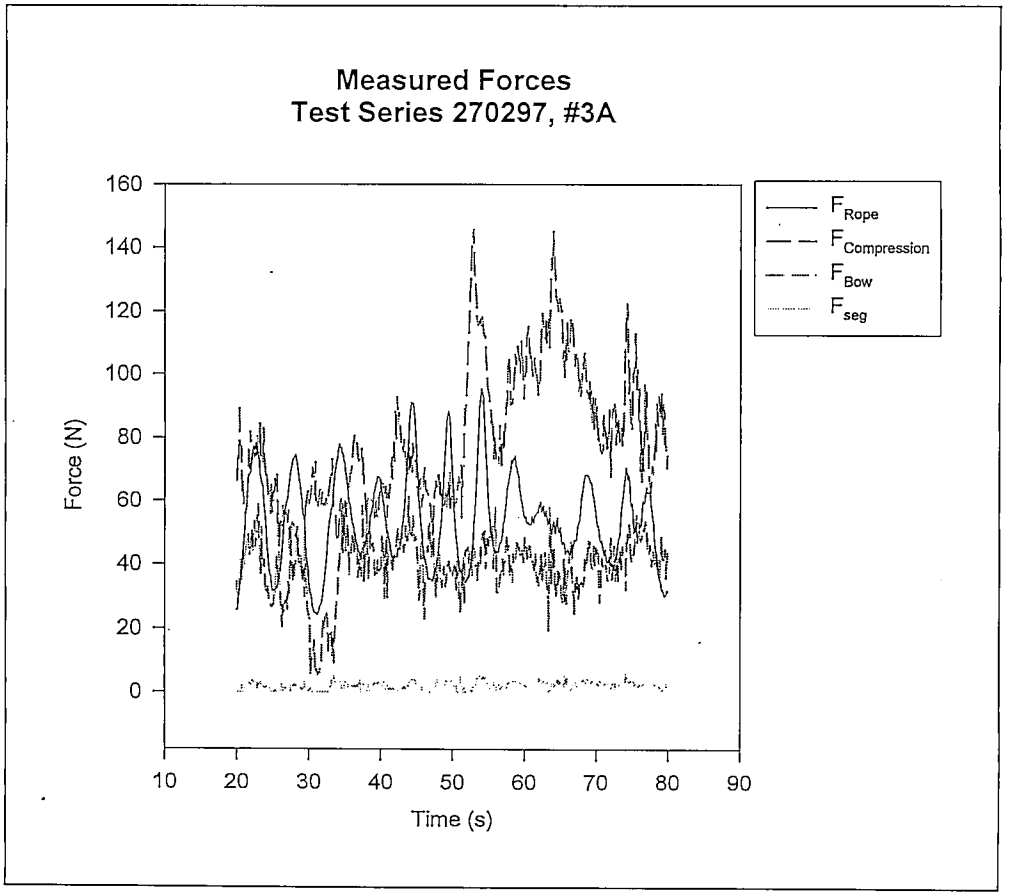
Measured Forces
Test Series 270297, #3A
Force (N)
Time (s)
F_{Rope}
$F_{Compression}$
F_{Bow}
F_{seg}

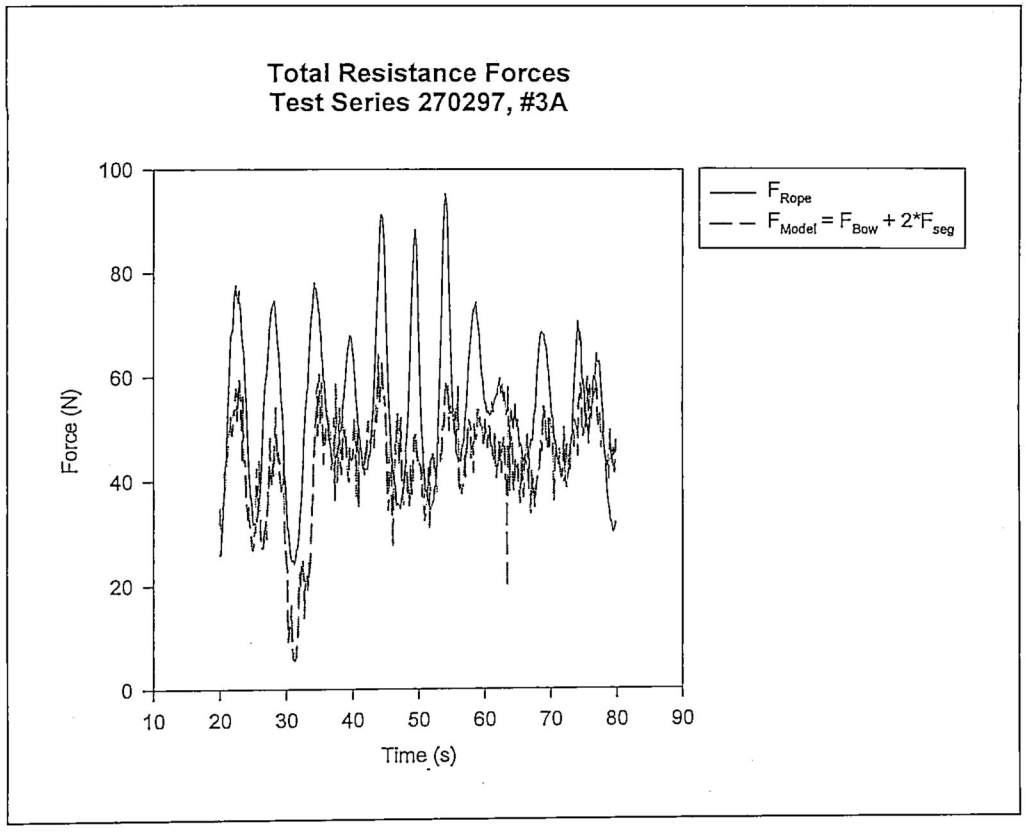
Total Resistance Forces
Test Series 270297, #3A
Force (N)
Time (s)
100
80
60
40
20
0
10
20
30
40
50
60
70
80
90
F_Rope
F_Model = F_Bow + 2*F_seg

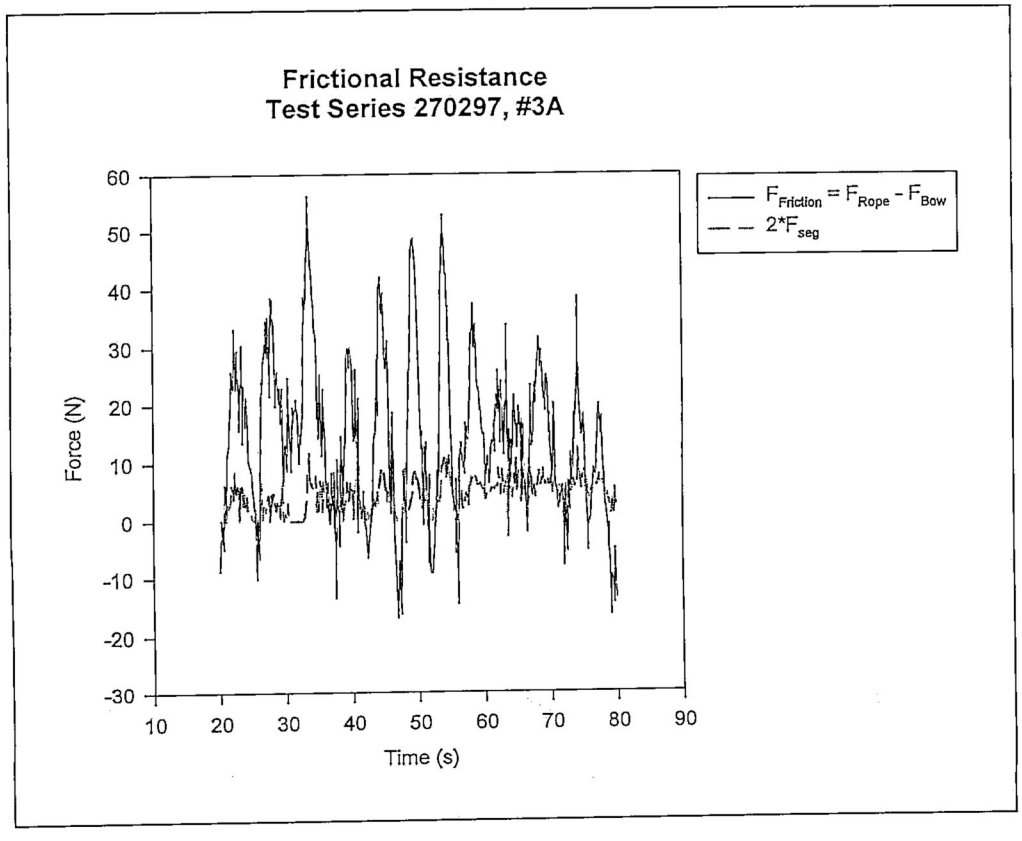
Frictional Resistance
Test Series 270297, #3A
Force (N)
Time (s)
60
50
40
30
20
10
0
-10
-20
-30
10
20
30
40
50
60
70
80
90
F_Friction = F_Rope - F_Bow
2*F_seg

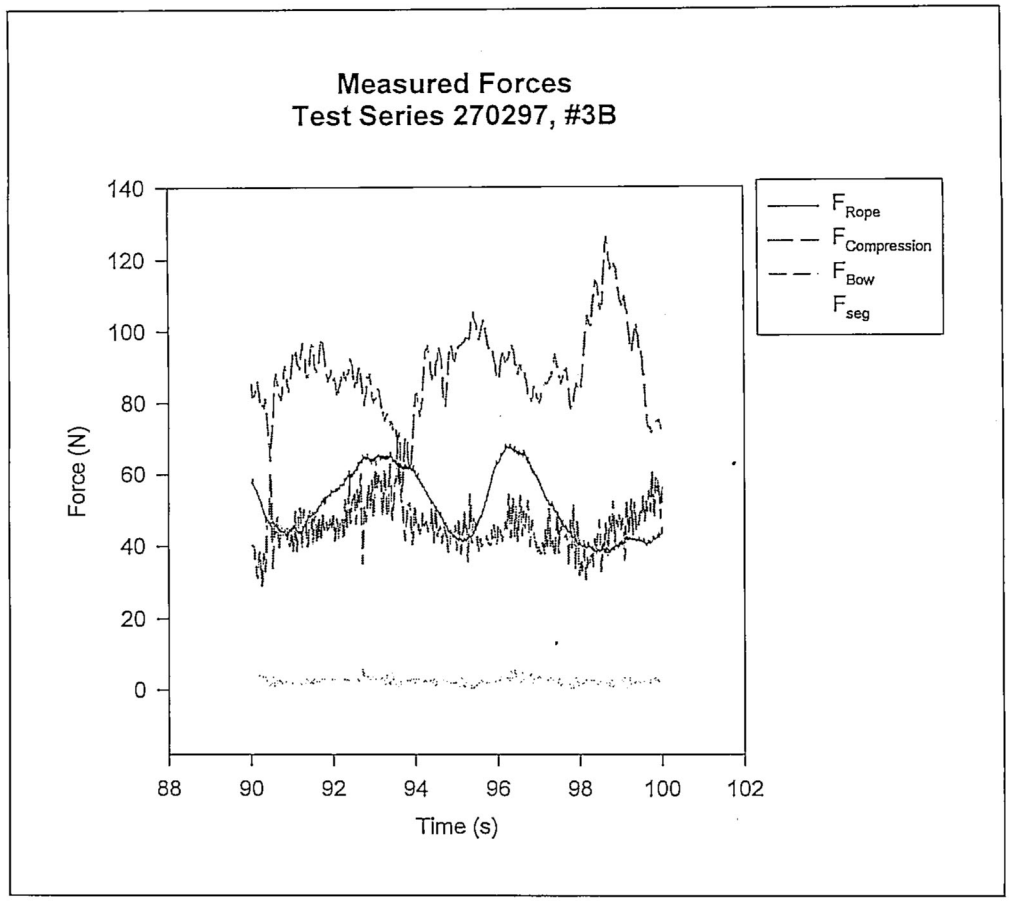
Measured Forces
Test Series 270297, #3B
Force (N)
Time (s)
F_{Rope}
$F_{Compression}$
F_{Bow}
F_{seg}

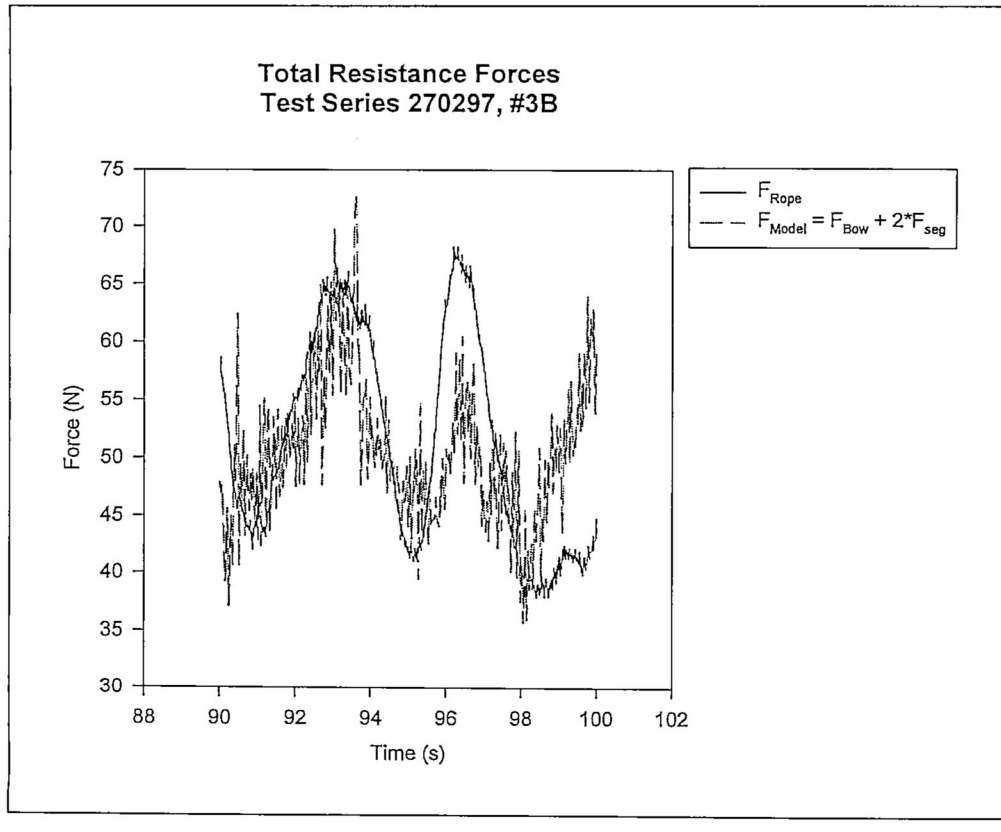
Total Resistance Forces
Test Series 270297, #3B
Force (N)
Time (s)
F_{Rope}
$F_{Model} = F_{Bow} + 2*F_{seg}$

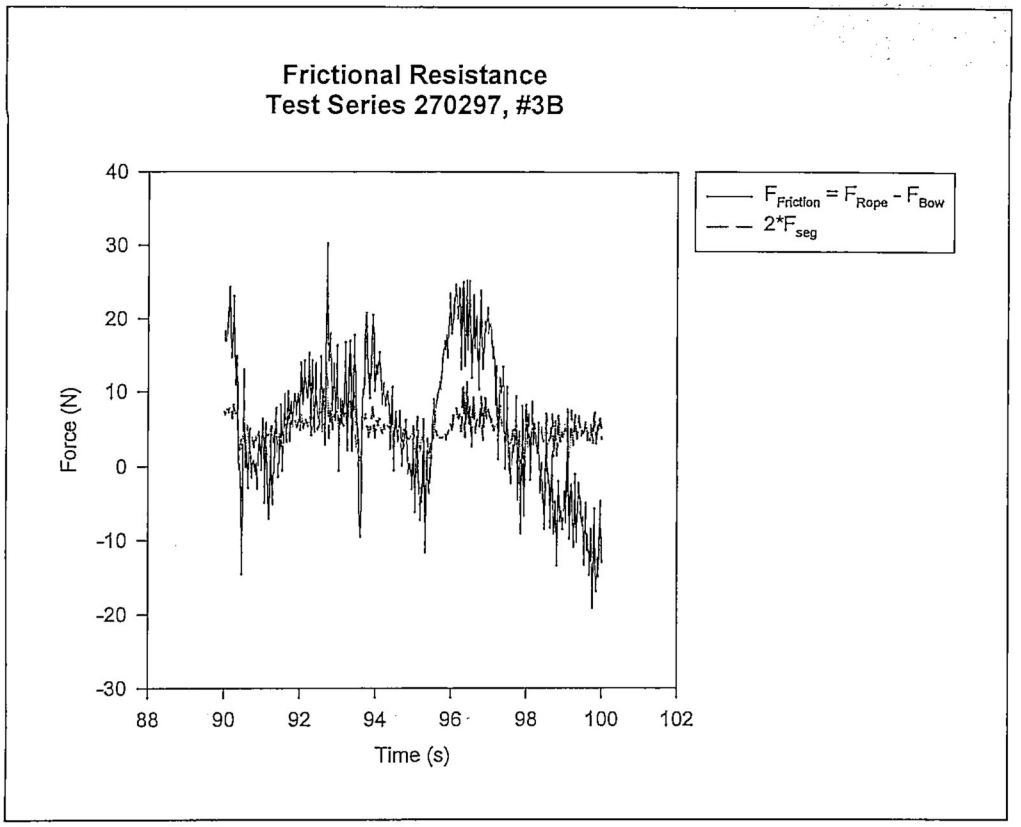
Frictional Resistance
Test Series 270297, #3B
Force (N)
Time (s)
40
30
20
10
0
-10
-20
-30
88
90
92
94
96
98
100
102
F_Friction = F_Rope - F_Bow
2*F_seg

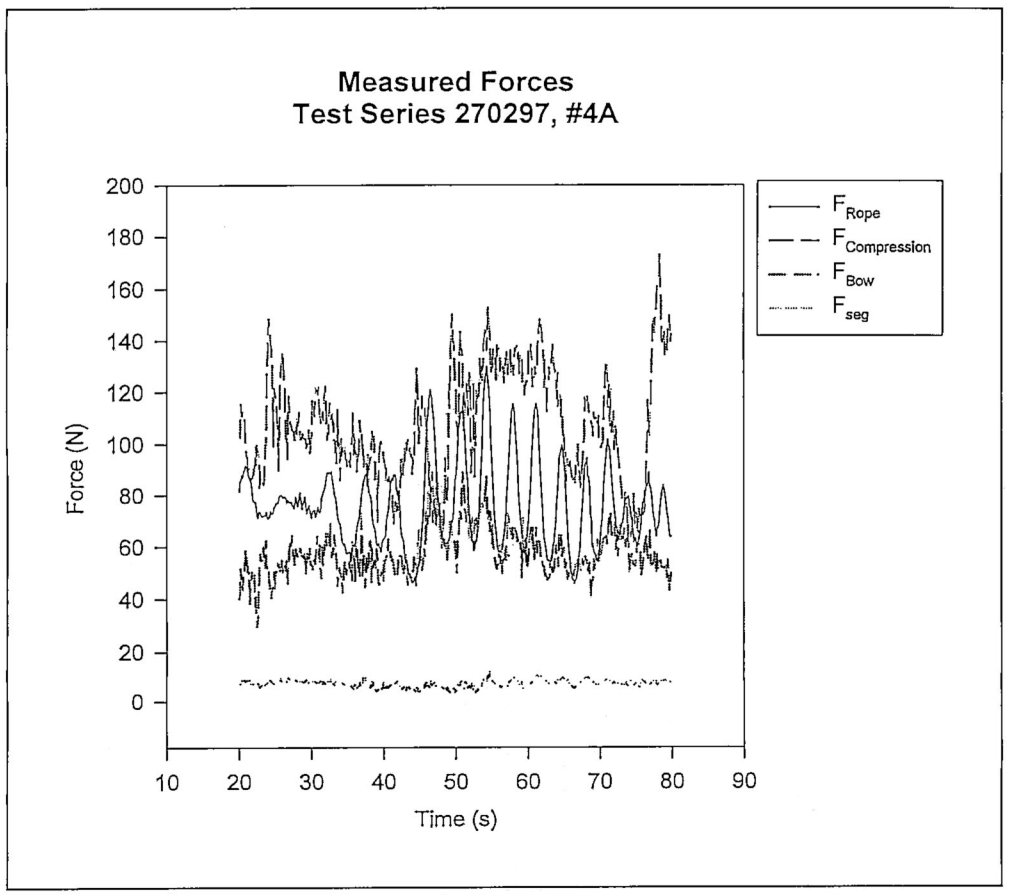
Measured Forces
Test Series 270297, #4A
Force (N)
Time (s)
200
180
160
140
120
100
80
60
40
20
0
10
20
30
40
50
60
70
80
90
F_Rope
F_Compression
F_Bow
F_seg

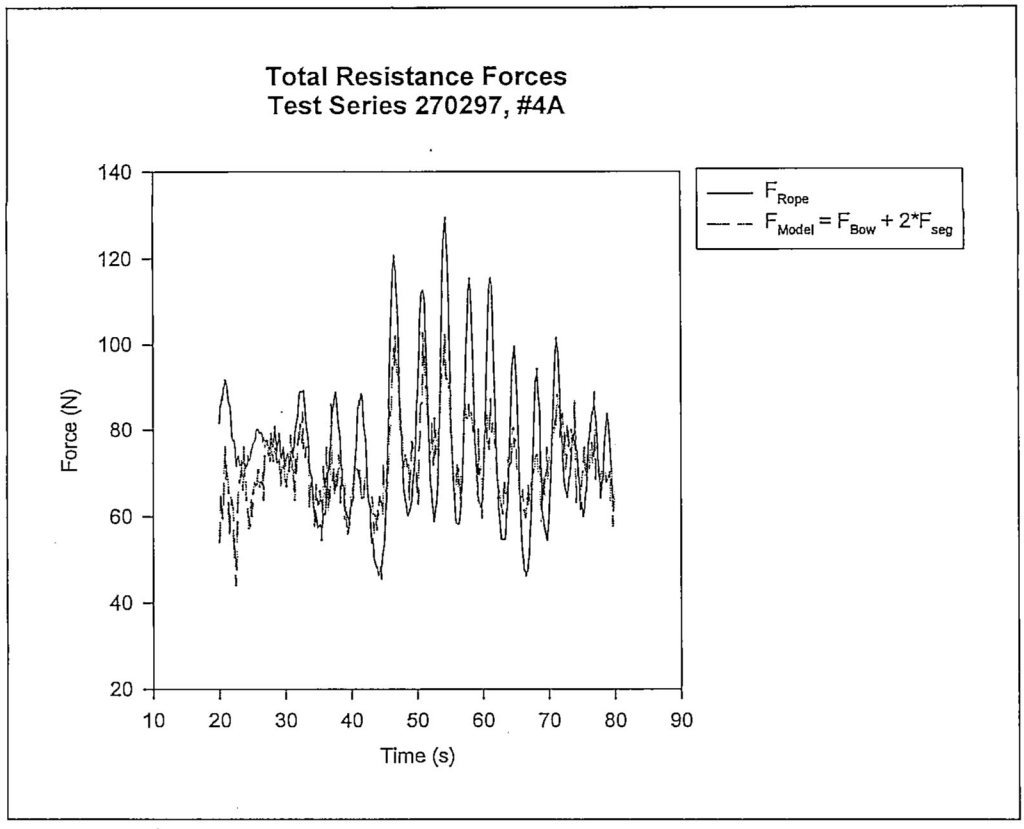
Total Resistance Forces
Test Series 270297, #4A
Force (N)
Time (s)
F_{Rope}
$F_{Model} = F_{Bow} + 2*F_{seg}$

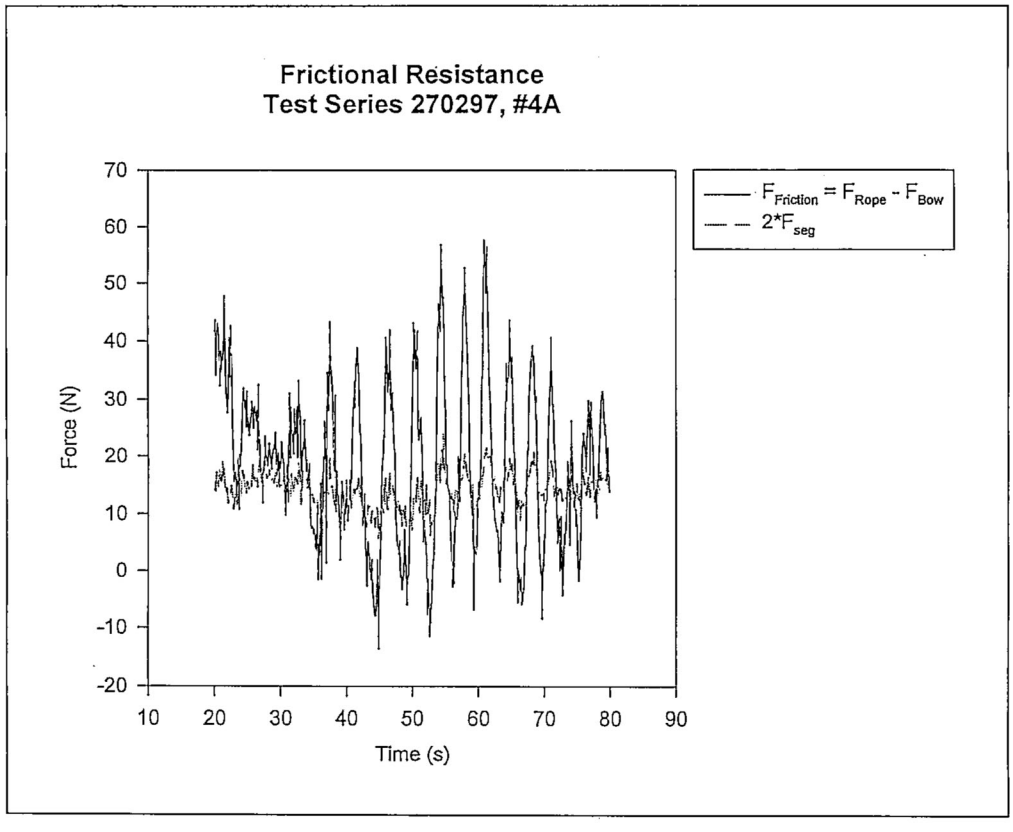
Frictional Resistance
Test Series 270297, #4A
Force (N)
Time (s)
$F_{Friction} = F_{Rope} - F_{Bow}$
$2*F_{seg}$

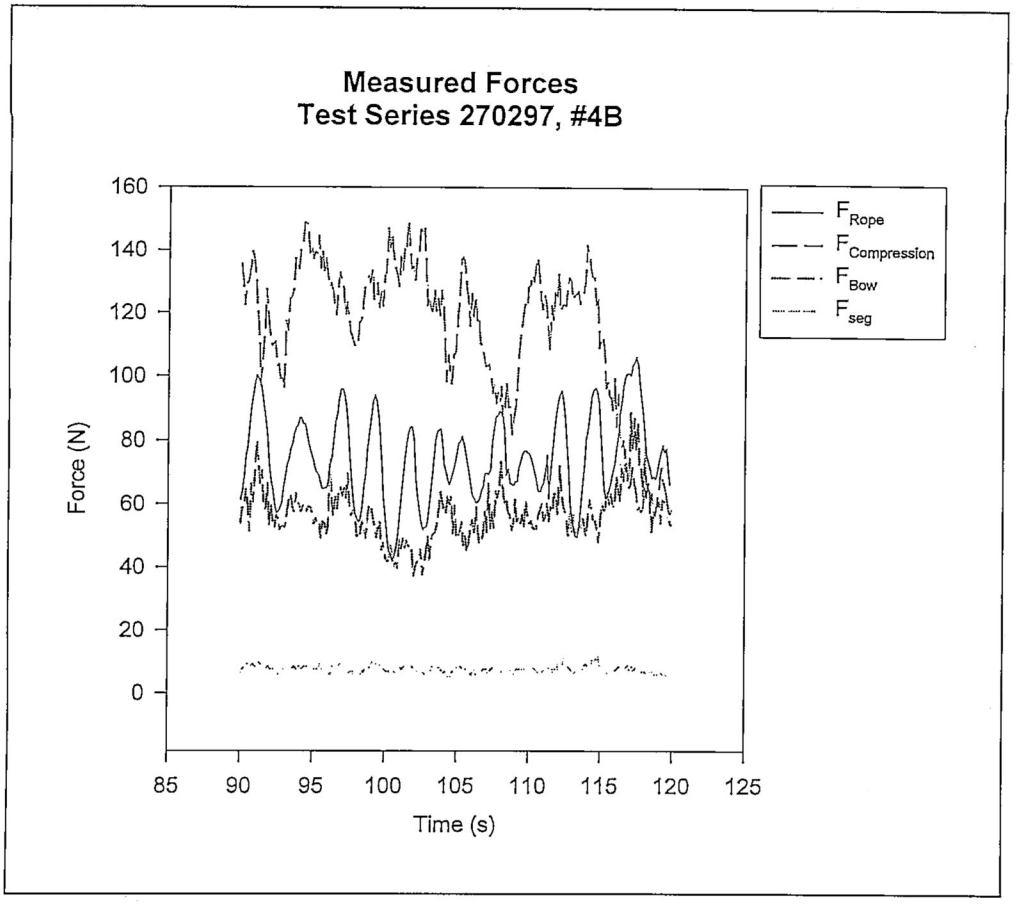
Measured Forces
Test Series 270297, #4B
Force (N)
Time (s)
160
140
120
100
80
60
40
20
0
85
90
95
100
105
110
115
120
125
F Rope
F Compression
F Bow
F seg

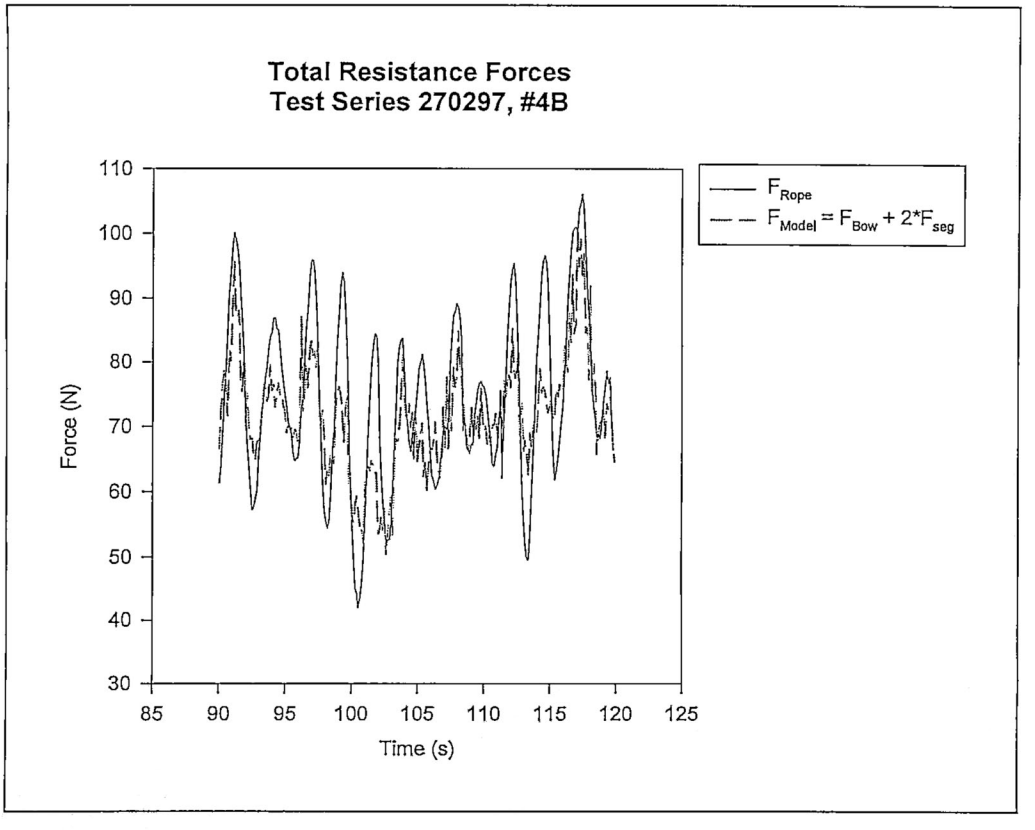
Total Resistance Forces
Test Series 270297, #4B
Force (N)
Time (s)
110
100
90
80
70
60
50
40
30
85
90
95
100
105
110
115
120
125
F Rope
F Model = F Bow + 2*F seg

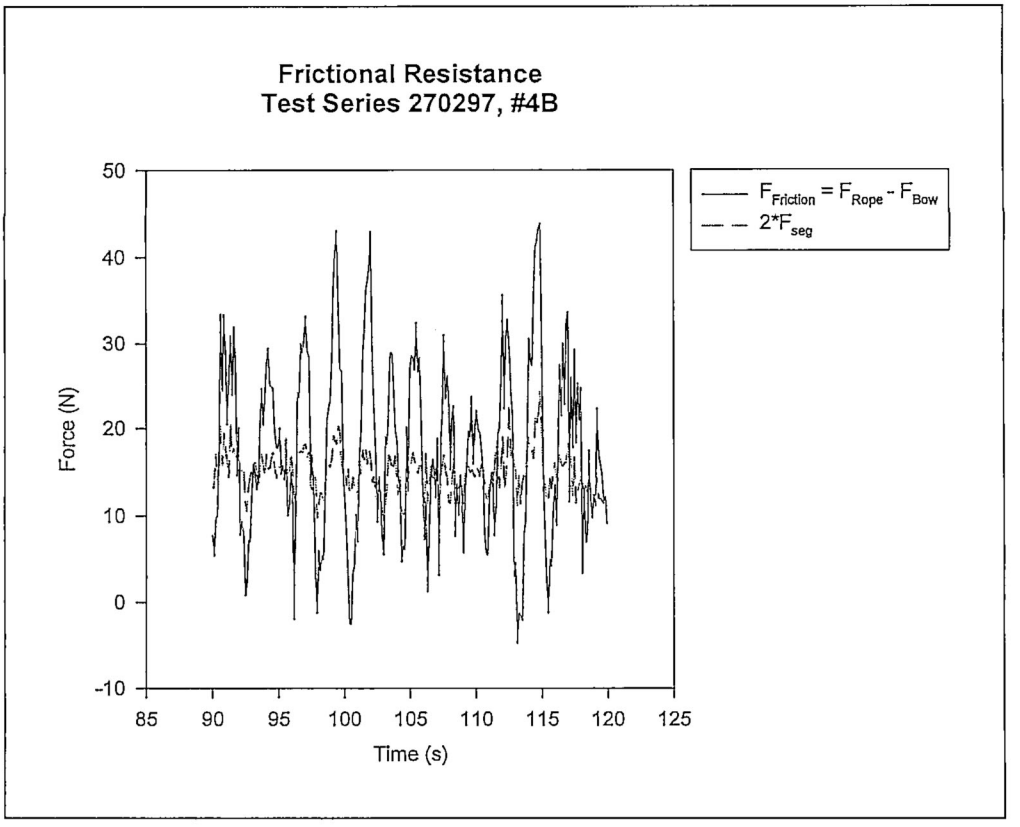
Frictional Resistance
Test Series 270297, #4B
$F_{Friction} = F_{Rope} - F_{Bow}$
$2*F_{seg}$
Force (N)
Time (s)
50
40
30
20
10
0
-10
85
90
95
100
105
110
115
120
125

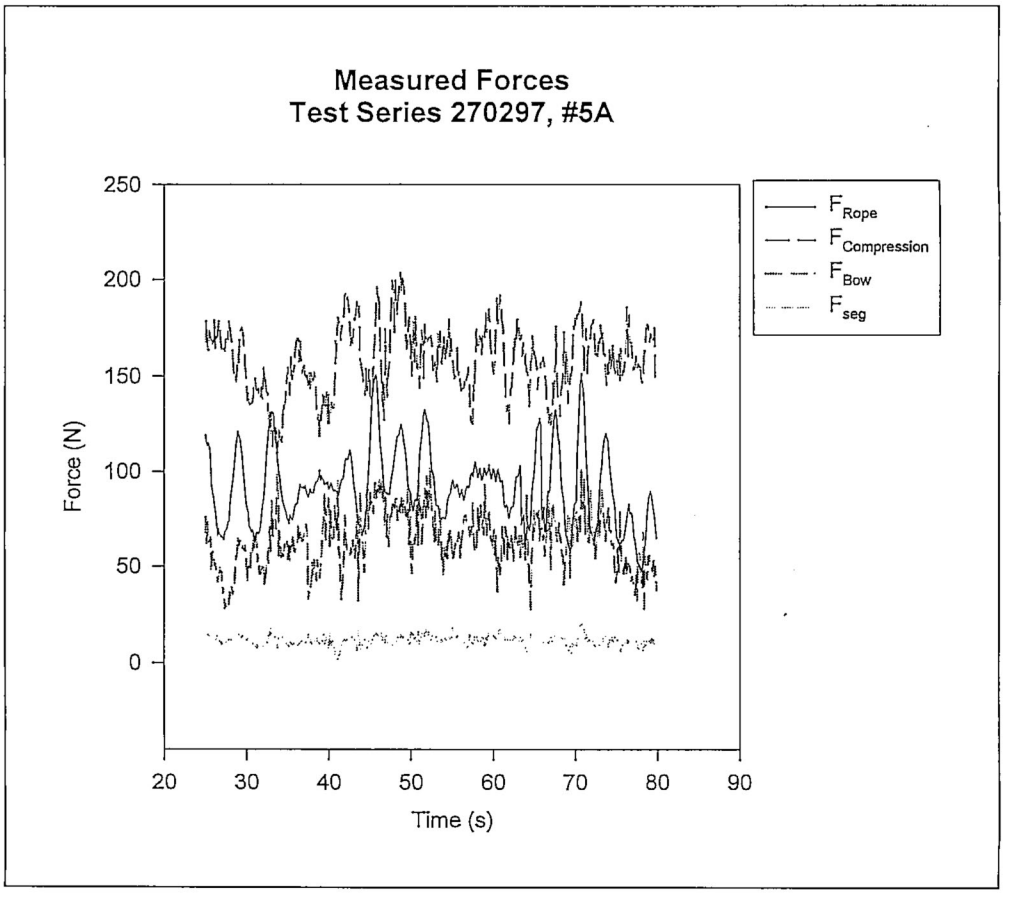
Measured Forces
Test Series 270297, #5A
F_{Rope}
$F_{Compression}$
F_{Bow}
F_{seg}
Force (N)
Time (s)
250
200
150
100
50
0
20
30
40
50
60
70
80
90

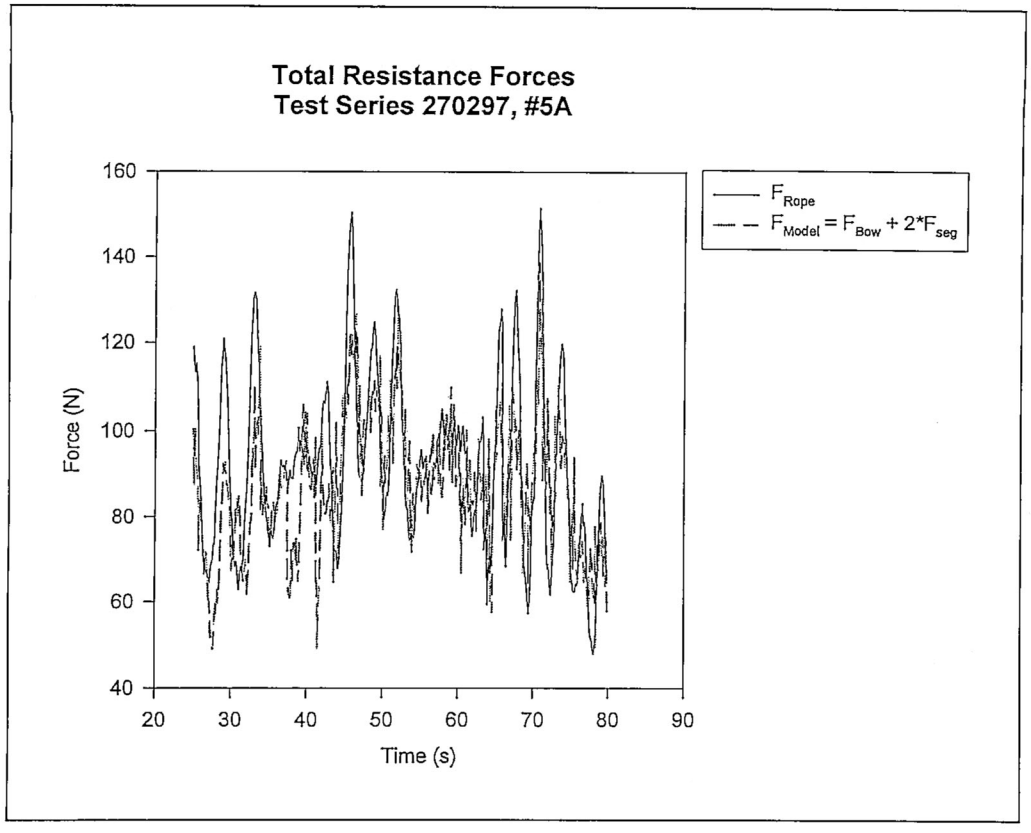
Total Resistance Forces
Test Series 270297, #5A
Force (N)
Time (s)
160
140
120
100
80
60
40
20
30
40
50
60
70
80
90
F_Rope
F_Model = F_Bow + 2*F_seg

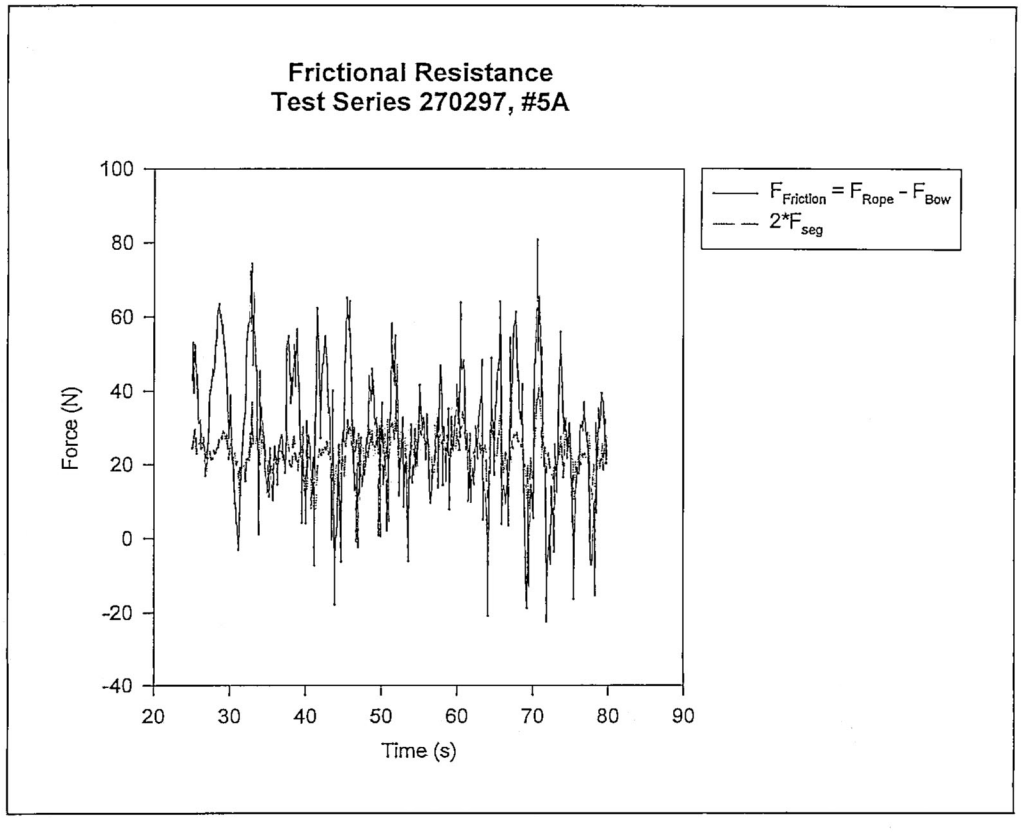
Frictional Resistance
Test Series 270297, #5A
Force (N)
Time (s)
100
80
60
40
20
0
-20
-40
20
30
40
50
60
70
80
90
F_Friction = F_Rope - F_Bow
2*F_seg

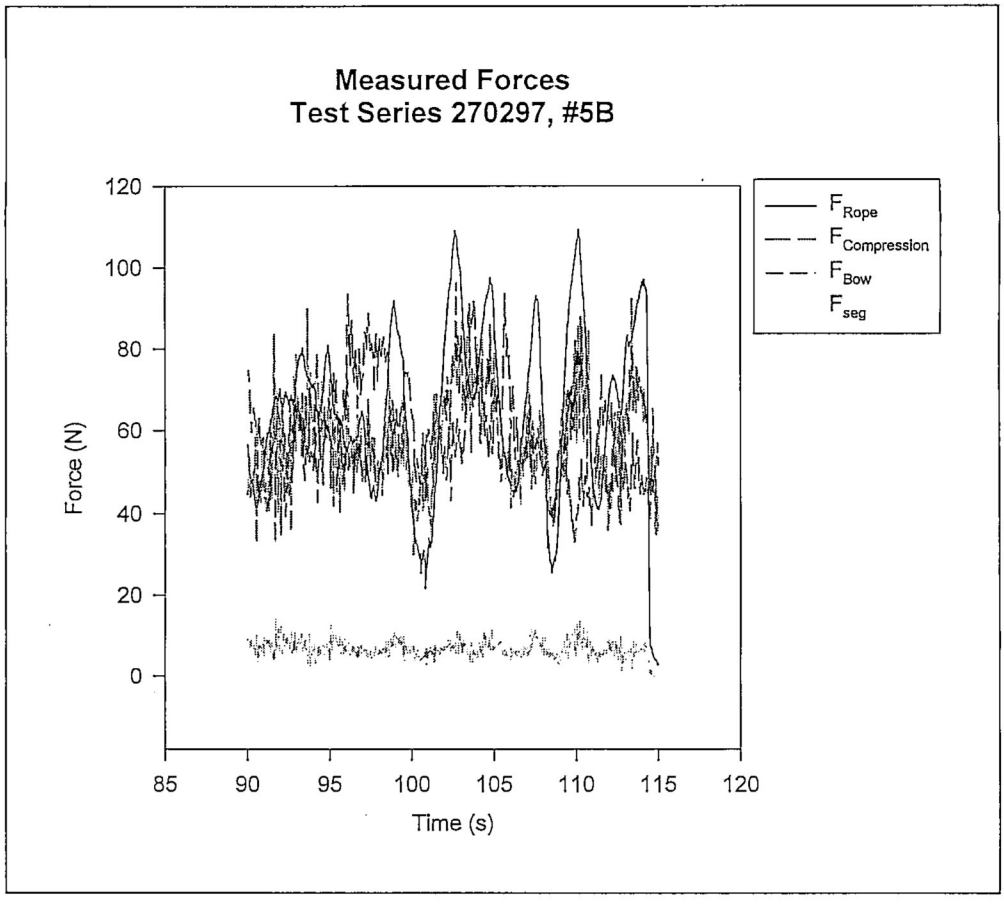
Measured Forces
Test Series 270297, #5B
Force (N)
Time (s)
120
100
80
60
40
20
0
85
90
95
100
105
110
115
120
F Rope
F Compression
F Bow
F seg

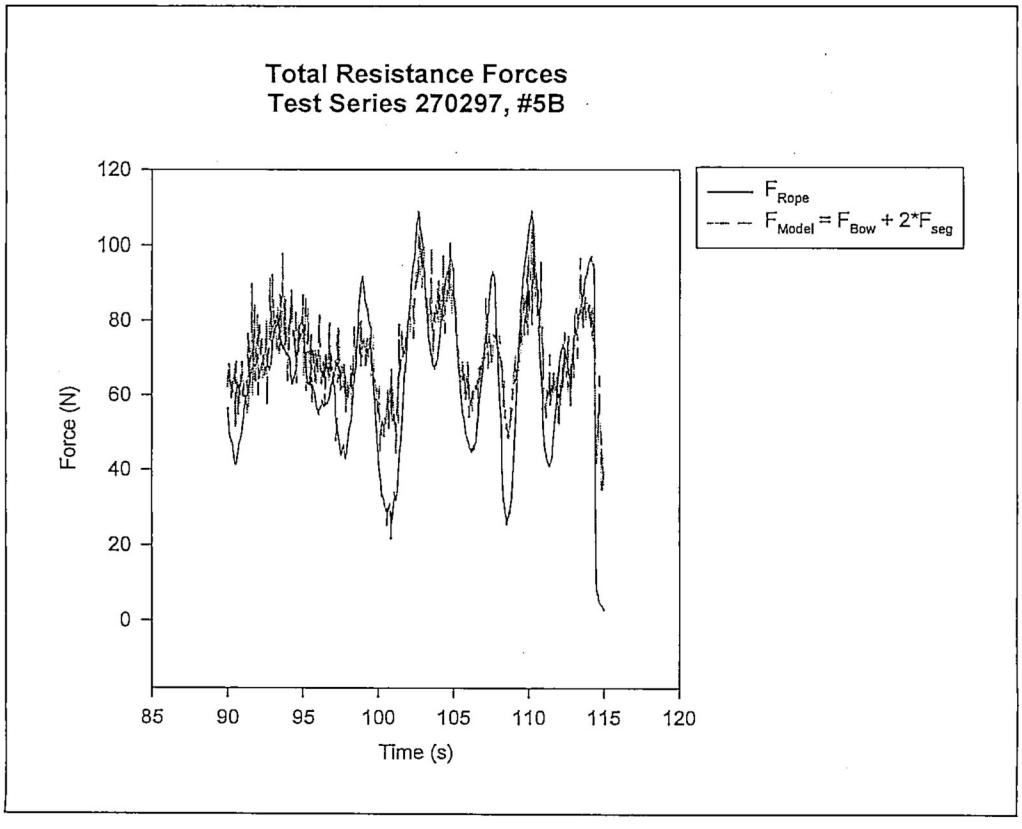
Total Resistance Forces
Test Series 270297, #5B
Force (N)
Time (s)
120
100
80
60
40
20
0
85
90
95
100
105
110
115
120
F Rope
F Model = F Bow + 2*F seg

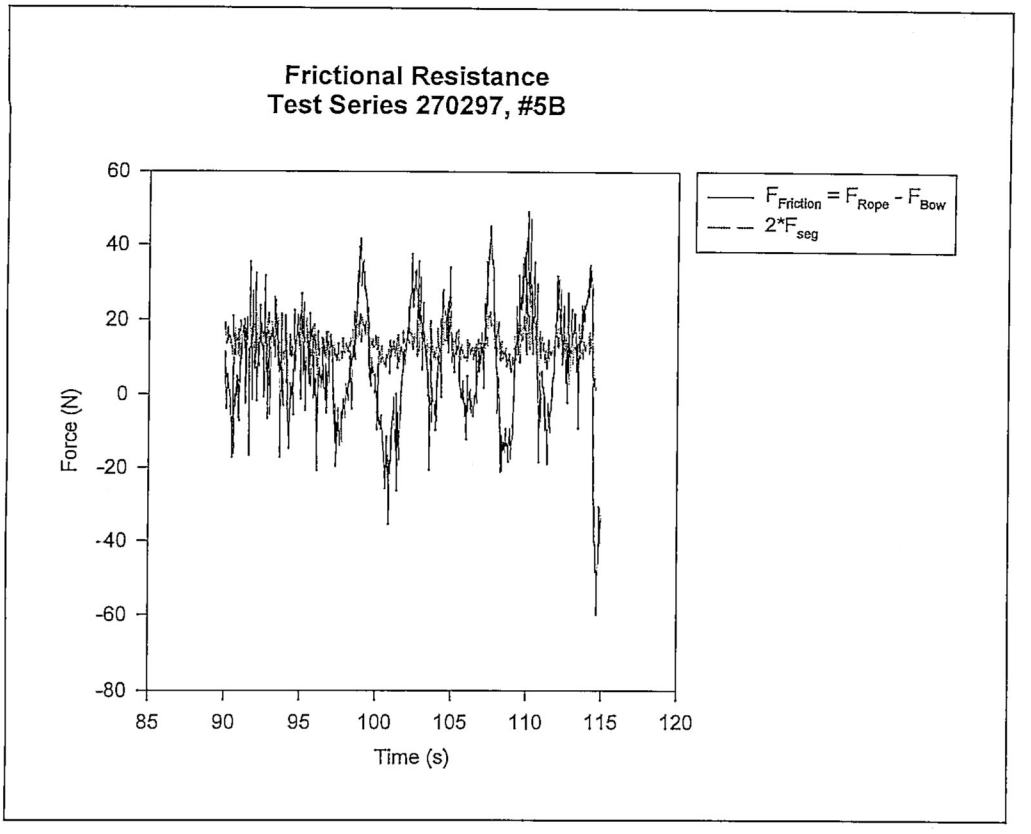
Frictional Resistance
Test Series 270297, #5B
Force (N)
Time (s)
60
40
20
0
-20
-40
-60
-80
85
90
95
100
105
110
115
120
F Friction = F Rope - F Bow
2*F seg

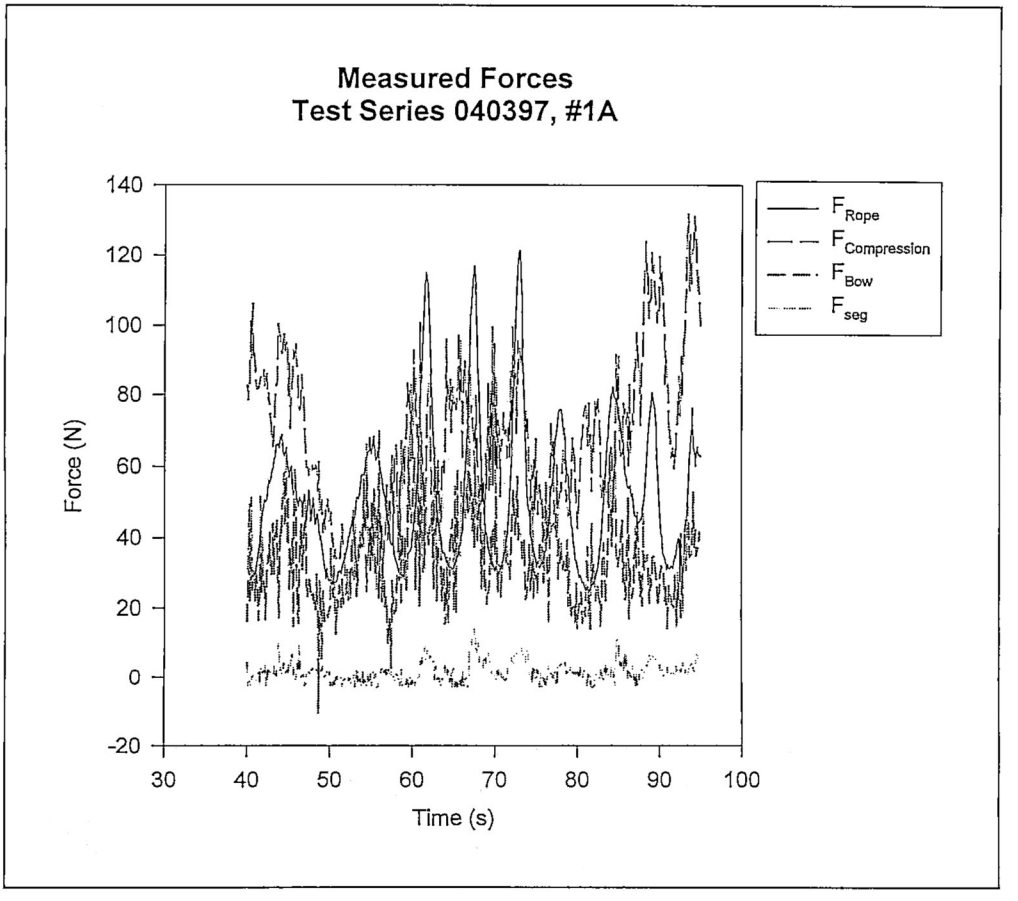
Measured Forces
Test Series 040397, #1A
Force (N)
Time (s)
140
120
100
80
60
40
20
0
-20
30
40
50
60
70
80
90
100
F Rope
F Compression
F Bow
F seg

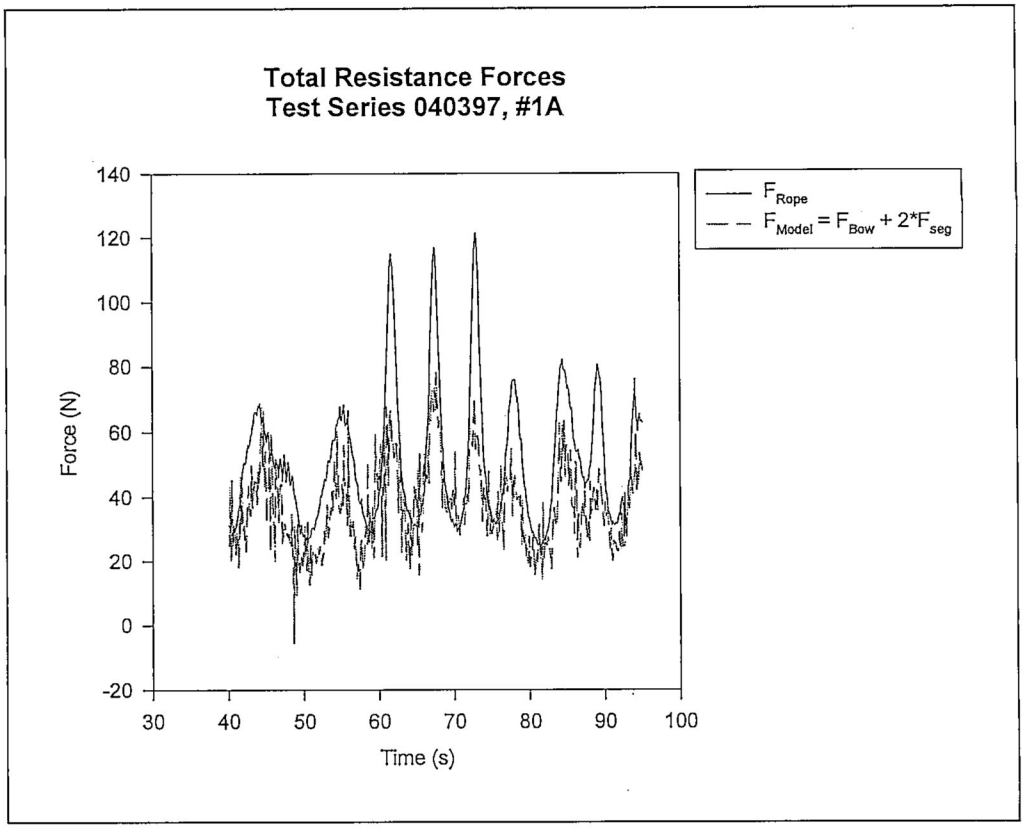
Total Resistance Forces
Test Series 040397, #1A
Force (N)
Time (s)
140
120
100
80
60
40
20
0
-20
30
40
50
60
70
80
90
100
F_Rope
F_Model = F_Bow + 2*F_seg

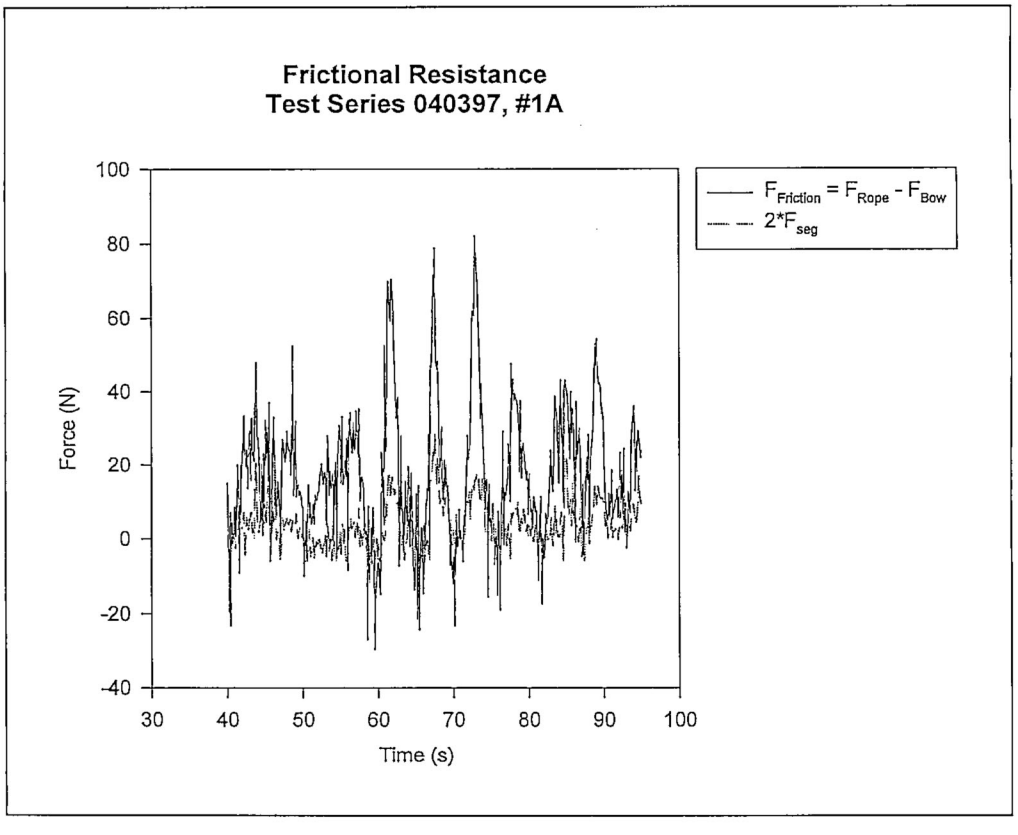
Frictional Resistance
Test Series 040397, #1A
Force (N)
Time (s)
100
80
60
40
20
0
-20
-40
30
40
50
60
70
80
90
100
F_Friction = F_Rope - F_Bow
2*F_seg

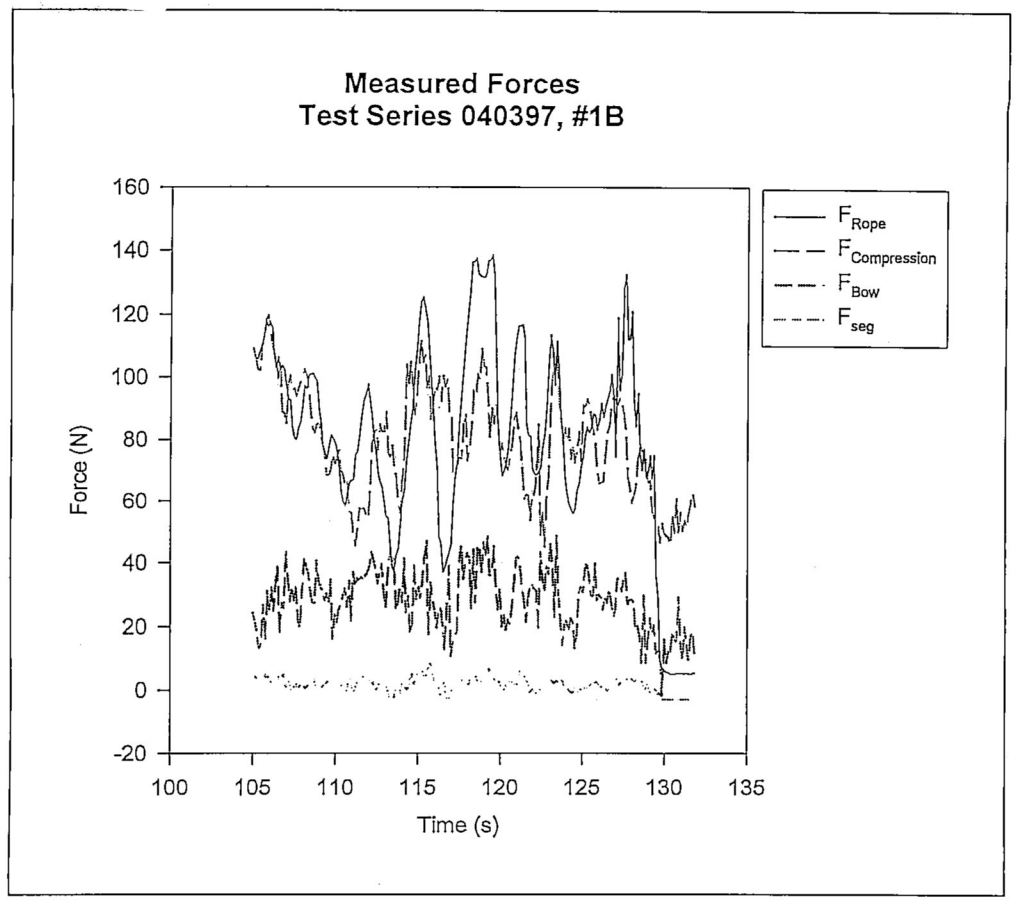
Measured Forces
Test Series 040397, #1B
Force (N)
Time (s)
160
140
120
100
80
60
40
20
0
-20
100
105
110
115
120
125
130
135
F_Rope
F_Compression
F_Bow
F_seg

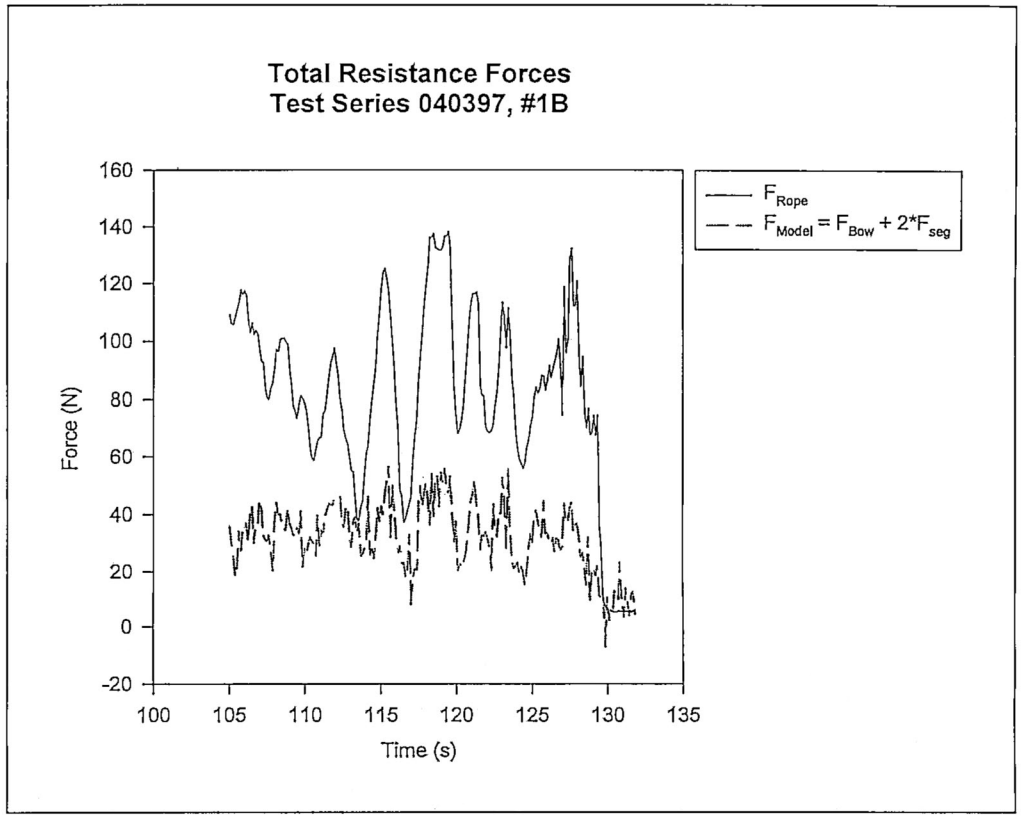
Total Resistance Forces
Test Series 040397, #1B
Force (N)
Time (s)
160
140
120
100
80
60
40
20
0
-20
100
105
110
115
120
125
130
135
F_Rope
F_Model = F_Bow + 2*F_seg

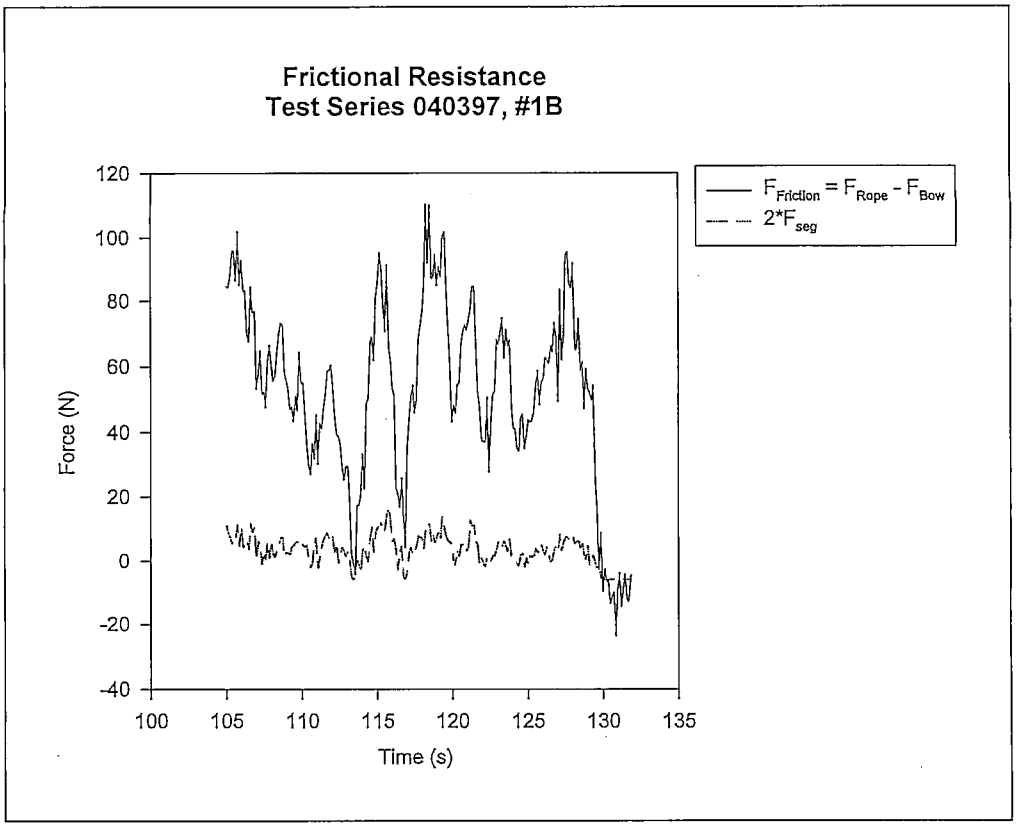
Frictional Resistance
Test Series 040397, #1B
Force (N)
Time (s)
120
100
80
60
40
20
0
-20
-40
100
105
110
115
120
125
130
135
F Friction = F Rope - F Bow
2*F seg

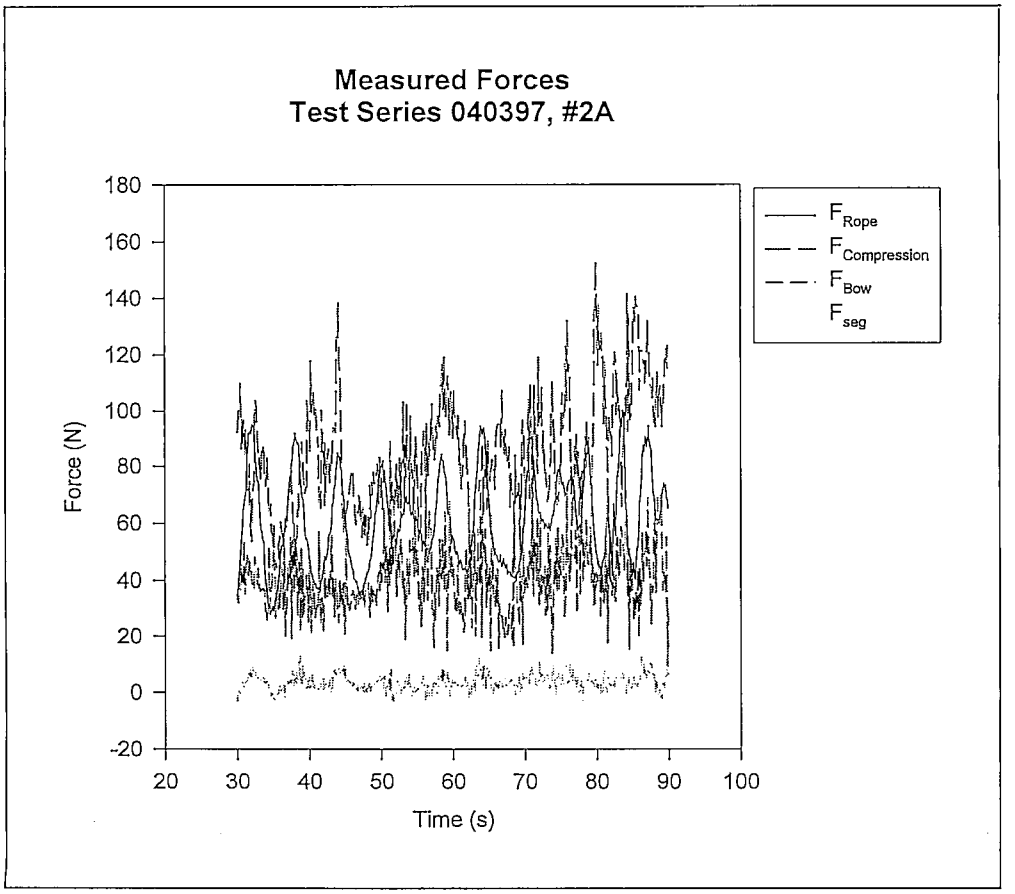
Measured Forces
Test Series 040397, #2A
Force (N)
Time (s)
180
160
140
120
100
80
60
40
20
0
-20
20
30
40
50
60
70
80
90
100
F Rope
F Compression
F Bow
F seg

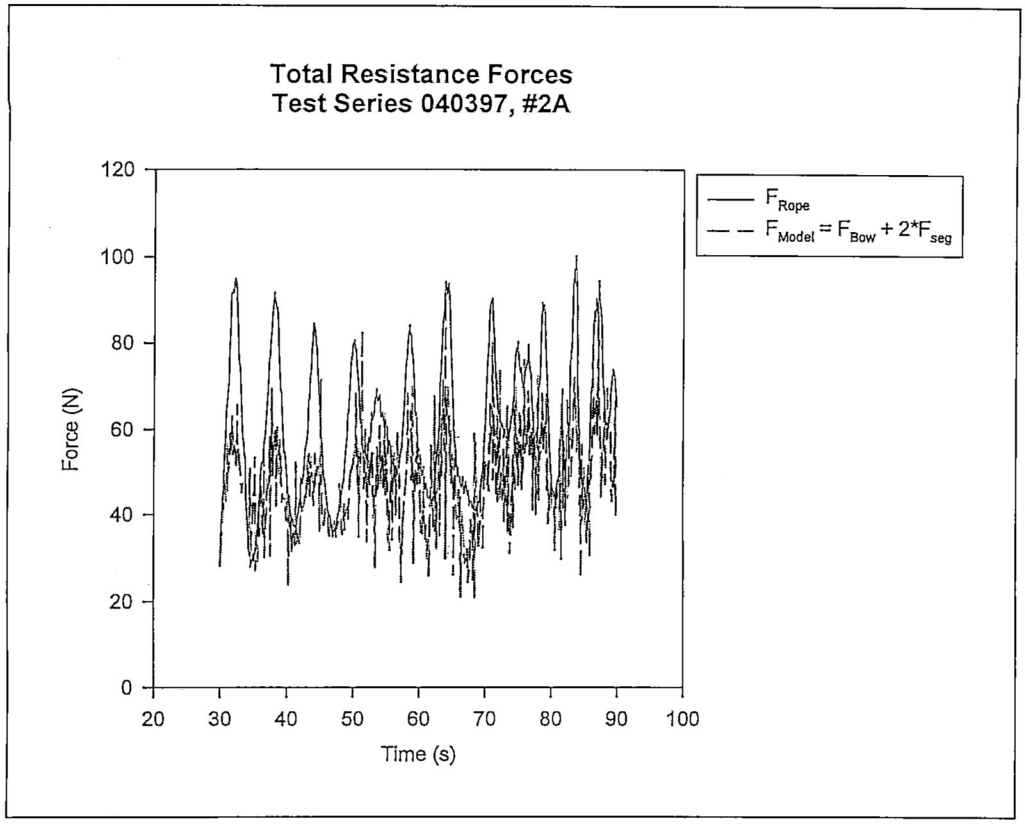
Total Resistance Forces
Test Series 040397, #2A
Force (N)
Time (s)
120
100
80
60
40
20
0
20
30
40
50
60
70
80
90
100
F_Rope
F_Model = F_Bow + 2*F_seg

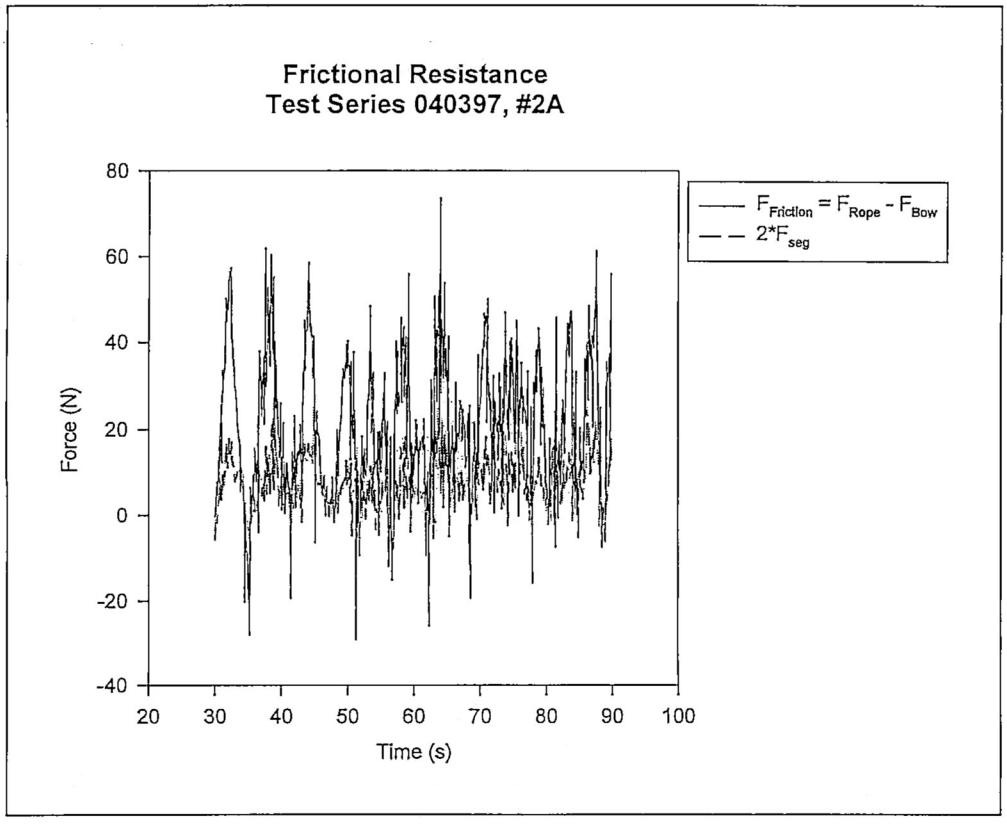
Frictional Resistance
Test Series 040397, #2A
Force (N)
Time (s)
80
60
40
20
0
-20
-40
20
30
40
50
60
70
80
90
100
F_Friction = F_Rope - F_Bow
2*F_seg

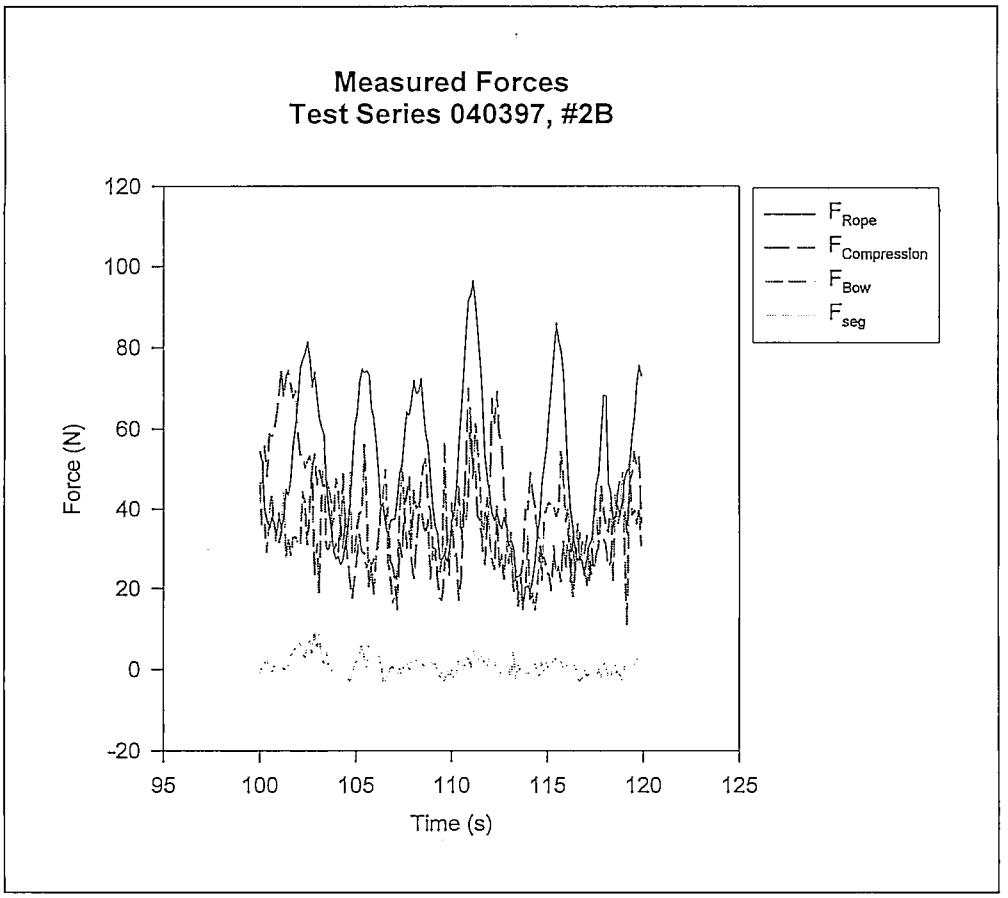
Measured Forces
Test Series 040397, #2B
120
100
80
60
40
20
0
-20
Force (N)
95
100
105
110
115
120
125
Time (s)
F Rope
F Compression
F Bow
F seg

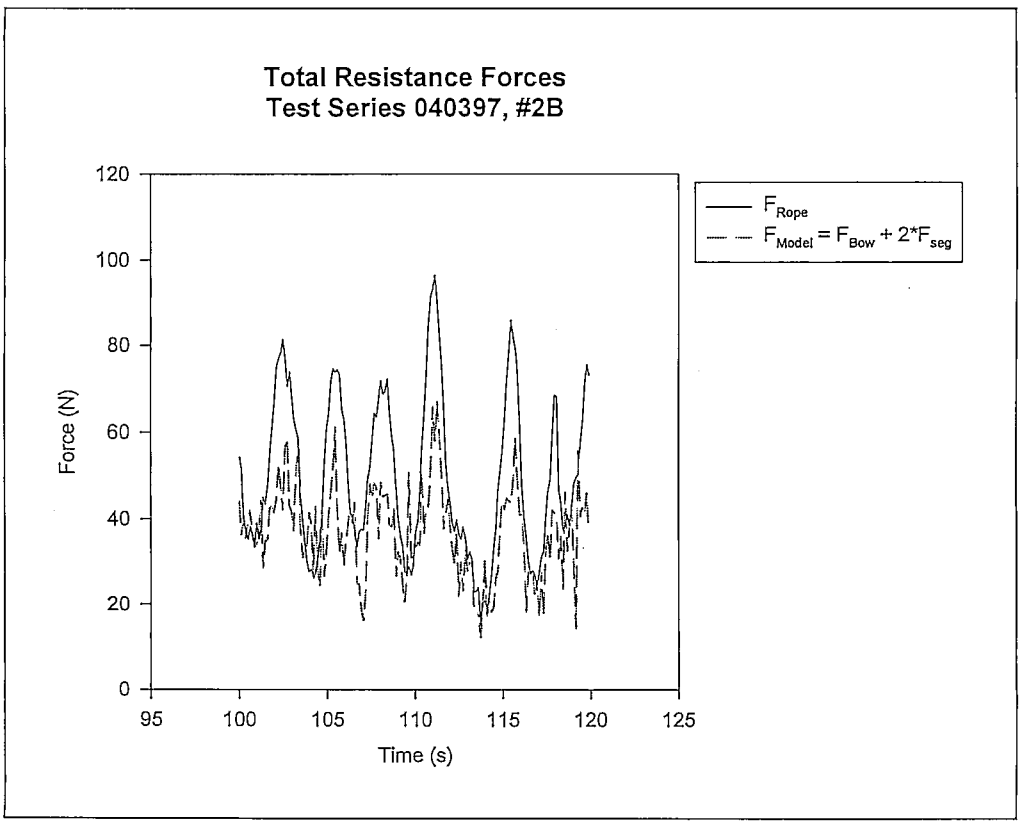
Total Resistance Forces
Test Series 040397, #2B
120
100
80
60
40
20
0
Force (N)
95
100
105
110
115
120
125
Time (s)
F Rope
F Model = F Bow + 2*F seg

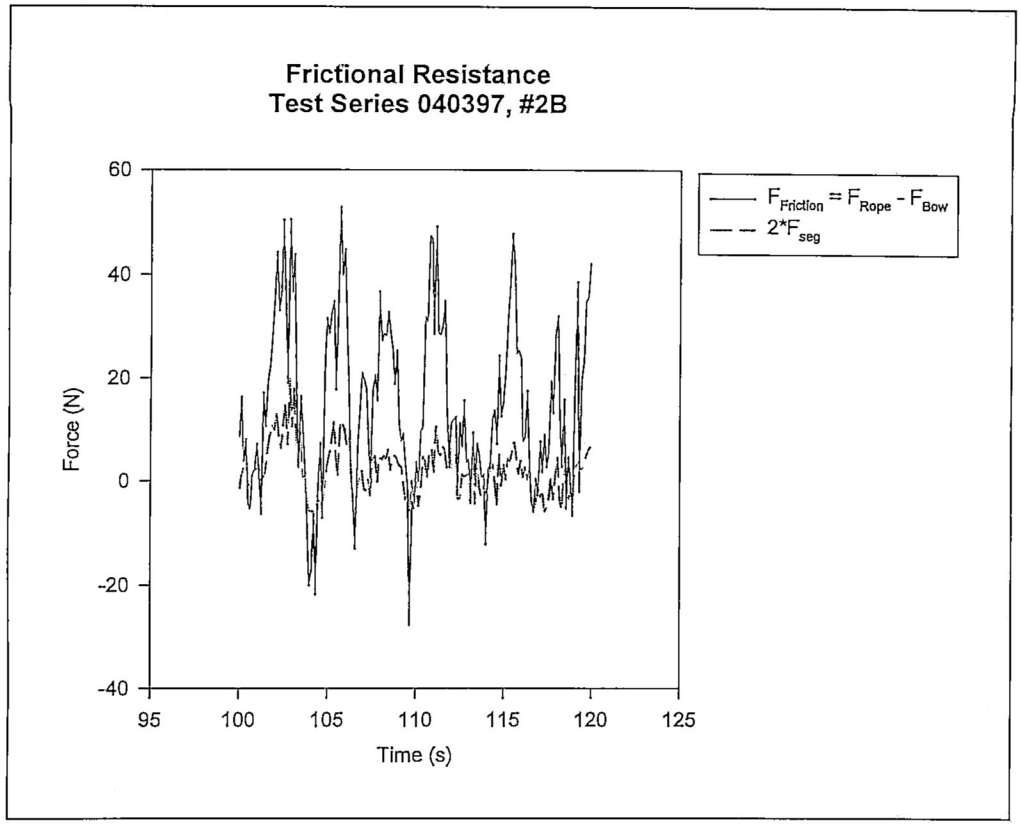
Frictional Resistance
Test Series 040397, #2B
Force (N)
Time (s)
60
40
20
0
-20
-40
95
100
105
110
115
120
125
F_Friction = F_Rope - F_Bow
2*F_seg

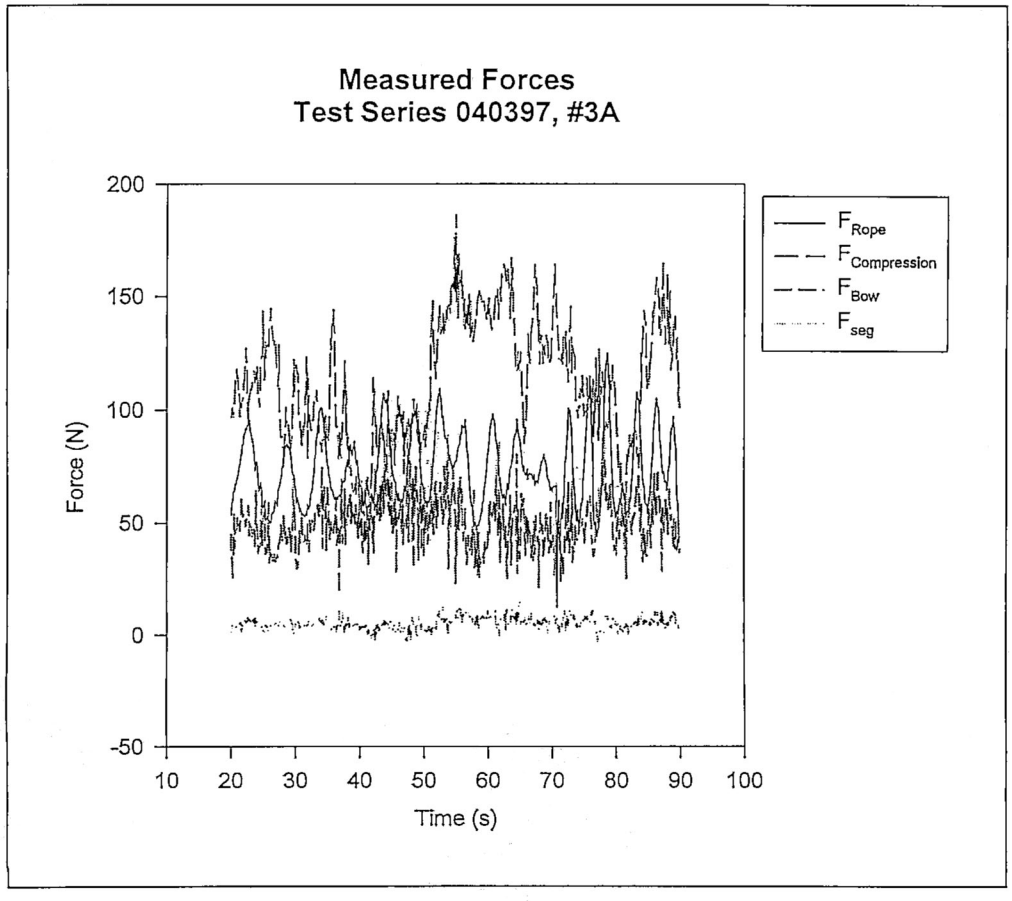
Measured Forces
Test Series 040397, #3A
Force (N)
Time (s)
200
150
100
50
0
-50
10
20
30
40
50
60
70
80
90
100
F_Rope
F_Compression
F_Bow
F_seg

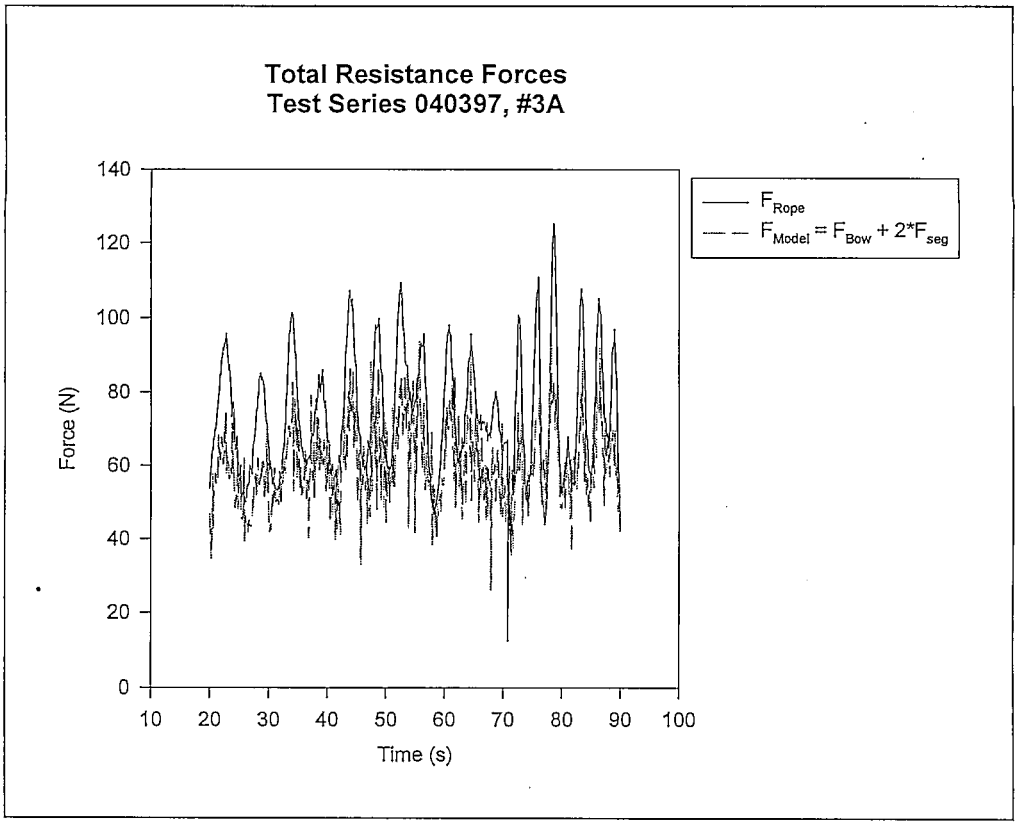
Total Resistance Forces
Test Series 040397, #3A
Force (N)
Time (s)
0
20
40
60
80
100
120
140
10
20
30
40
50
60
70
80
90
100
F_Rope
F_Model = F_Bow + 2*F_seg

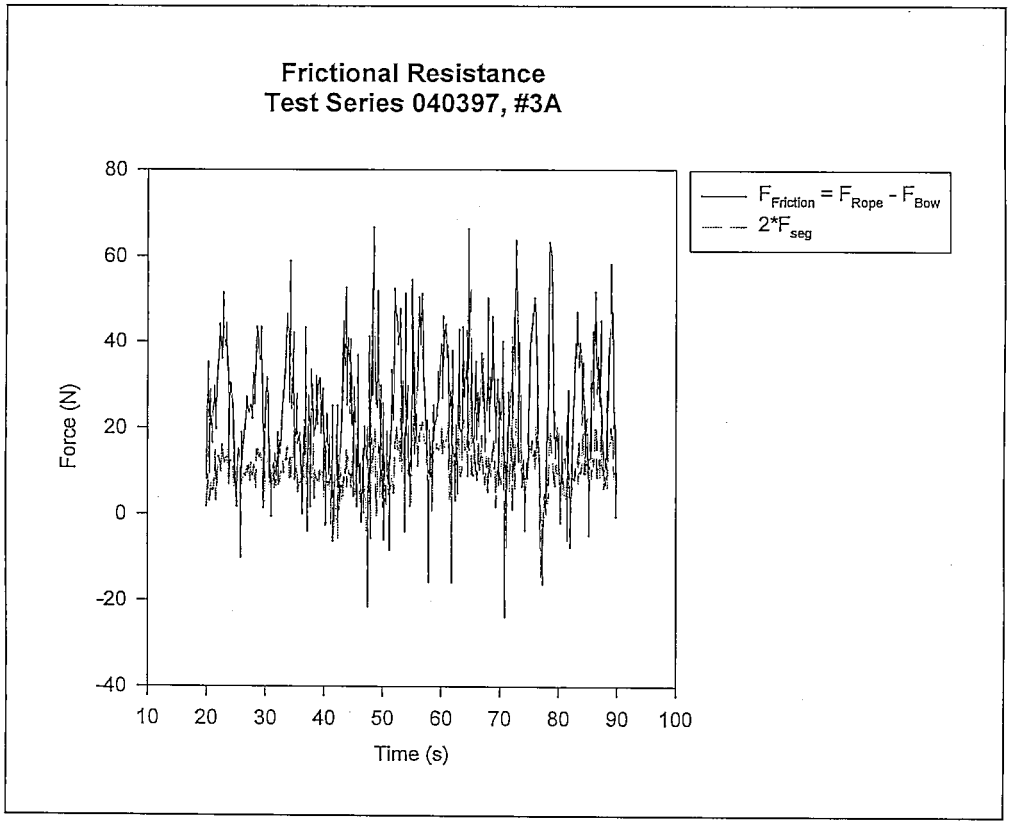
Frictional Resistance
Test Series 040397, #3A
Force (N)
Time (s)
-40
-20
0
20
40
60
80
10
20
30
40
50
60
70
80
90
100
F_Friction = F_Rope - F_Bow
2*F_seg

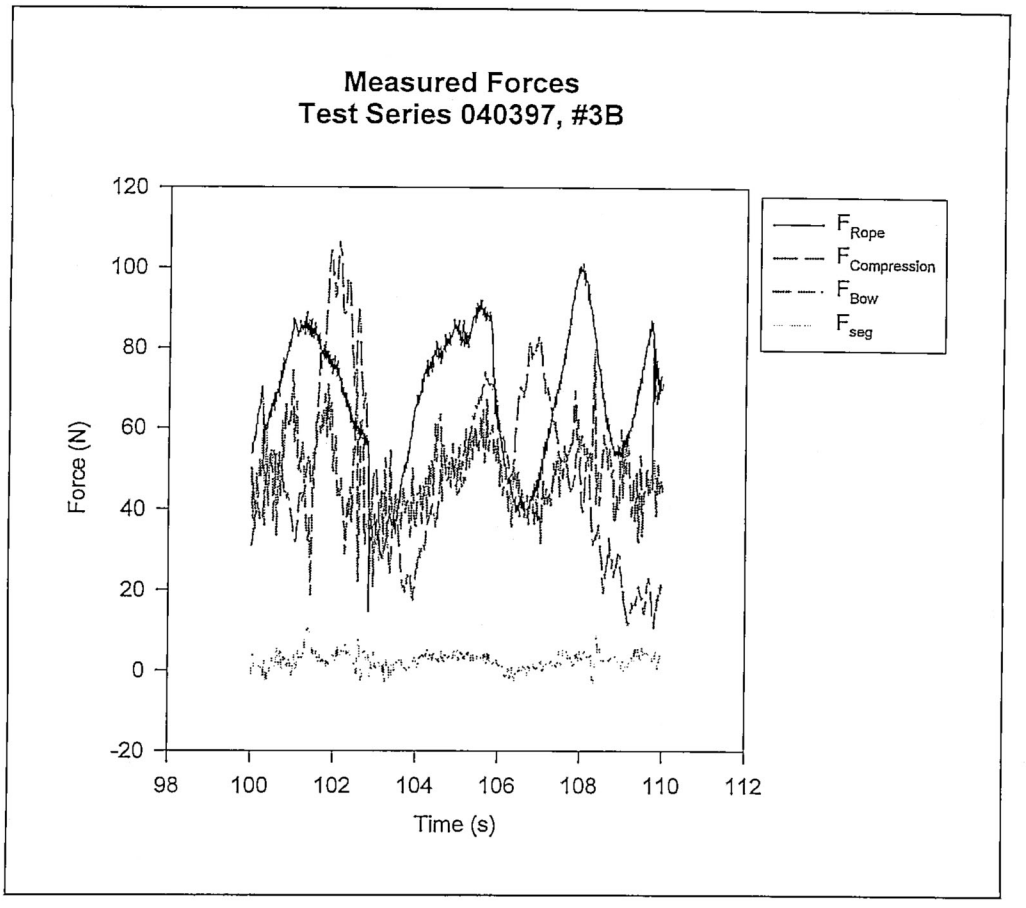
Measured Forces
Test Series 040397, #3B
Force (N)
Time (s)
120
100
80
60
40
20
0
-20
98
100
102
104
106
108
110
112
F Rope
F Compression
F Bow
F seg

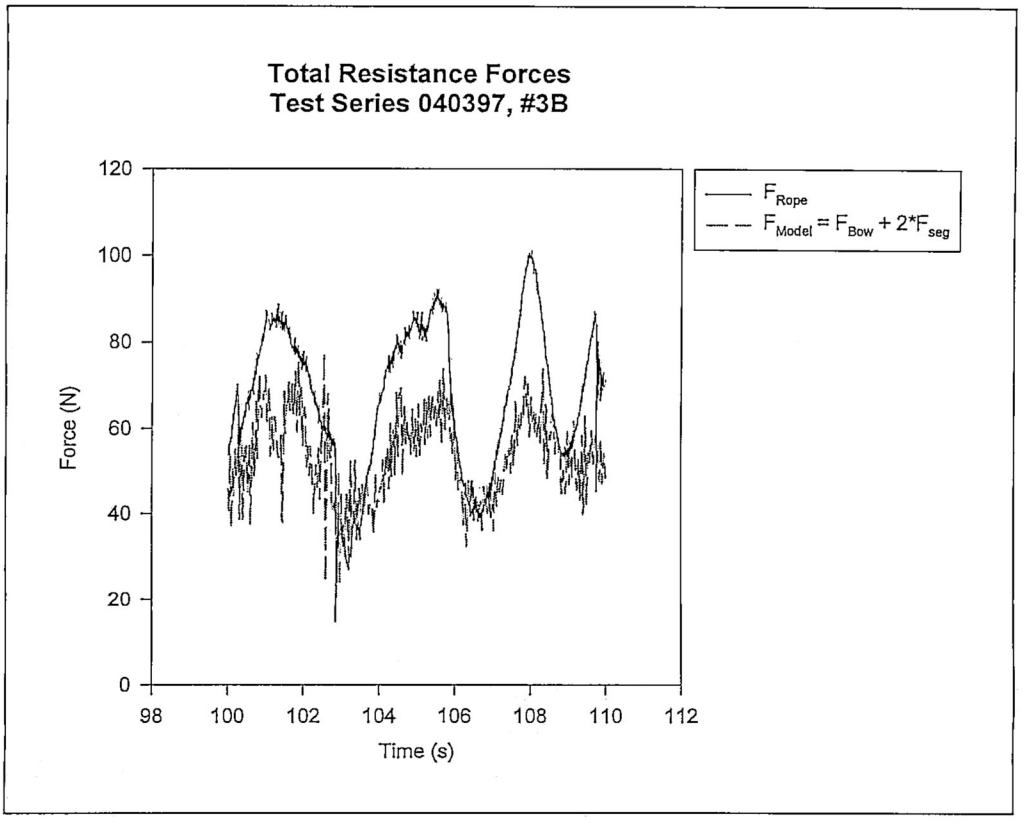
Total Resistance Forces
Test Series 040397, #3B
Force (N)
Time (s)
120
100
80
60
40
20
0
98
100
102
104
106
108
110
112
F Rope
F Model = F Bow + 2*F seg

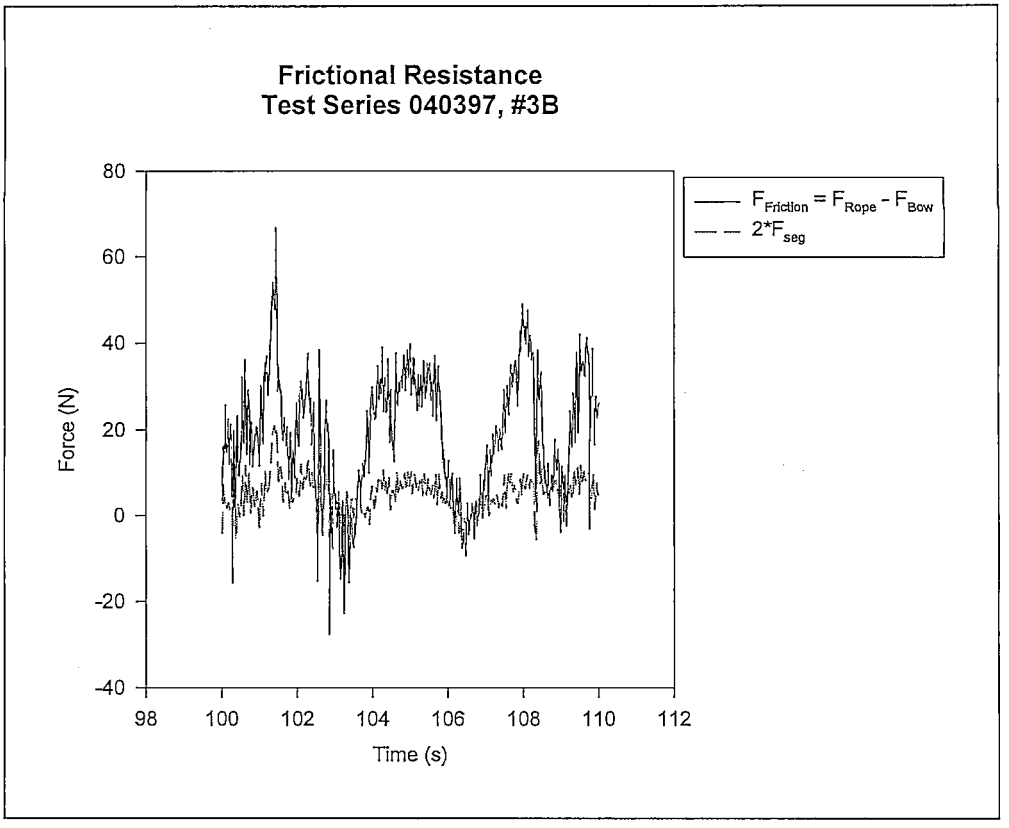
Frictional Resistance
Test Series 040397, #3B
80
60
40
20
0
-20
-40
Force (N)
98
100
102
104
106
108
110
112
Time (s)
F_Friction = F_Rope - F_Bow
2*F_seg

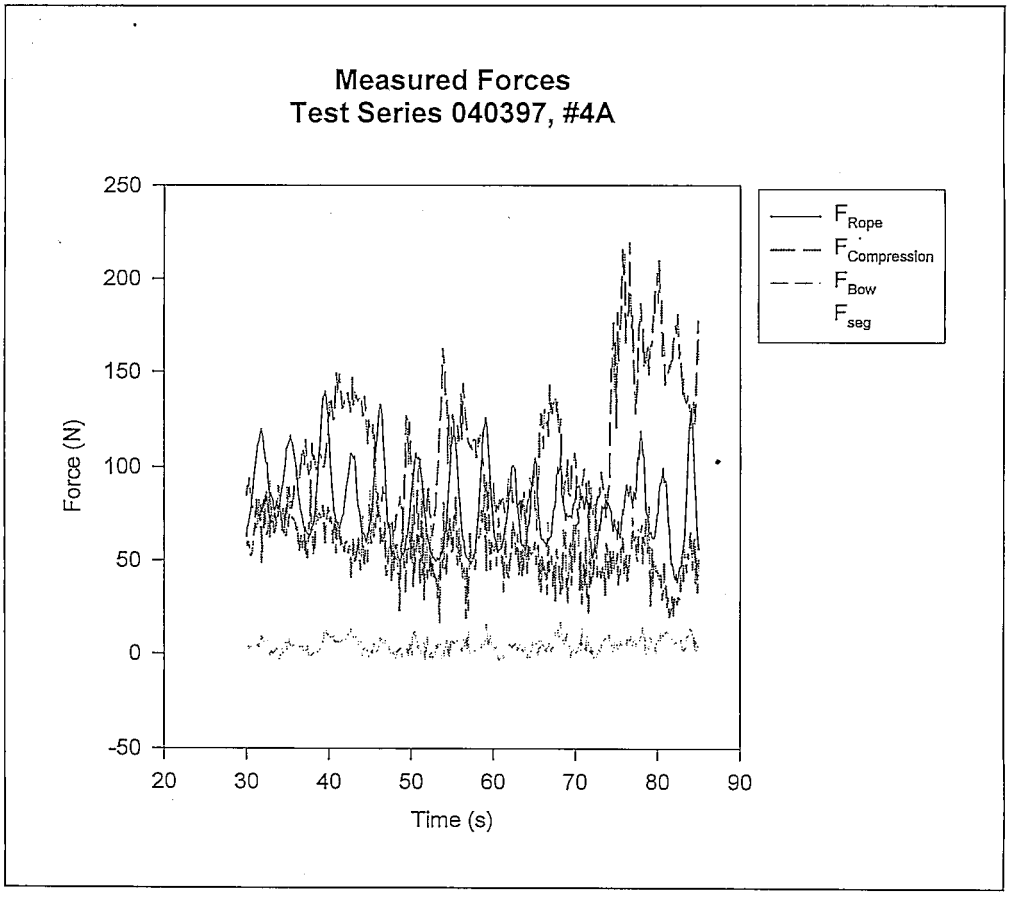
Measured Forces
Test Series 040397, #4A
250
200
150
100
50
0
-50
Force (N)
20
30
40
50
60
70
80
90
Time (s)
F_Rope
F_Compression
F_Bow
F_seg

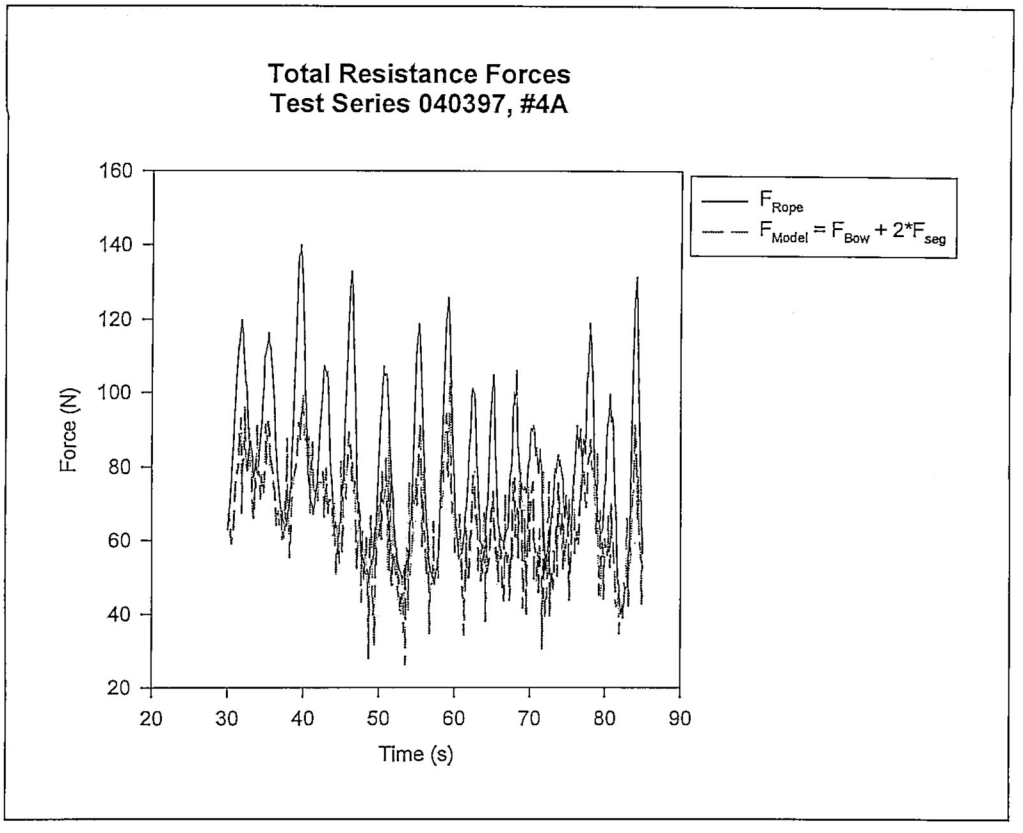
Total Resistance Forces
Test Series 040397, #4A
Force (N)
Time (s)
160
140
120
100
80
60
40
20
20
30
40
50
60
70
80
90
F_Rope
F_Model = F_Bow + 2*F_seg

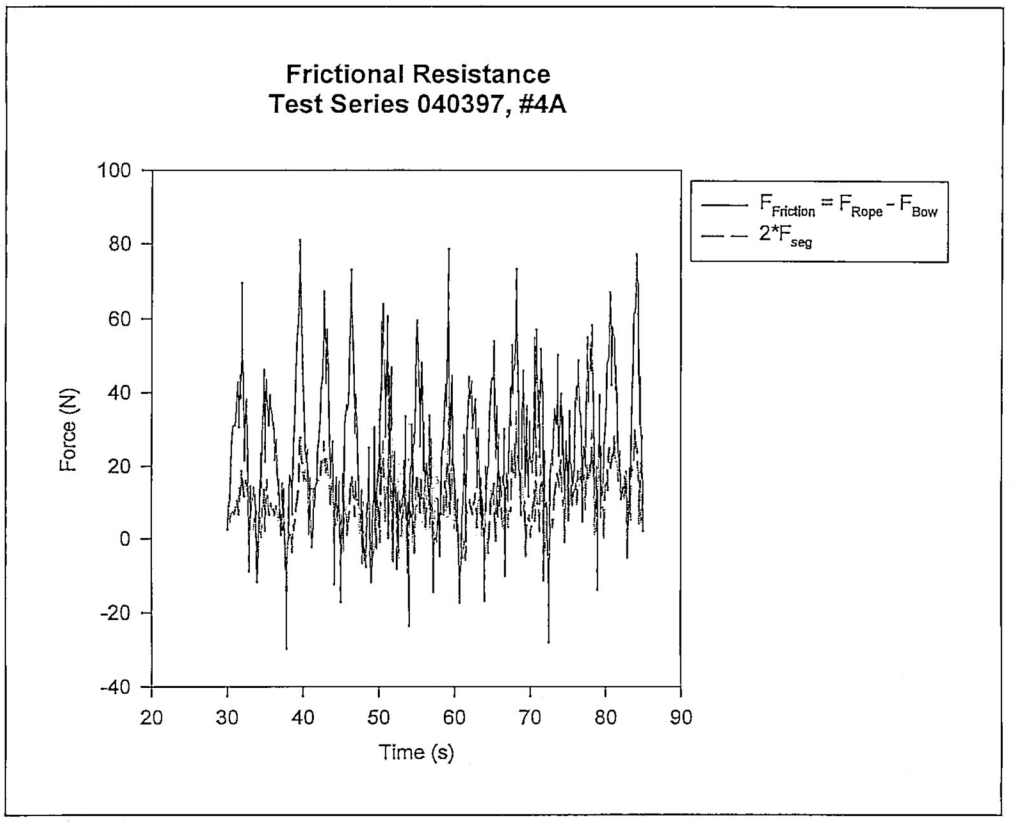
Frictional Resistance
Test Series 040397, #4A
Force (N)
Time (s)
100
80
60
40
20
0
-20
-40
20
30
40
50
60
70
80
90
F_Friction = F_Rope - F_Bow
2*F_seg

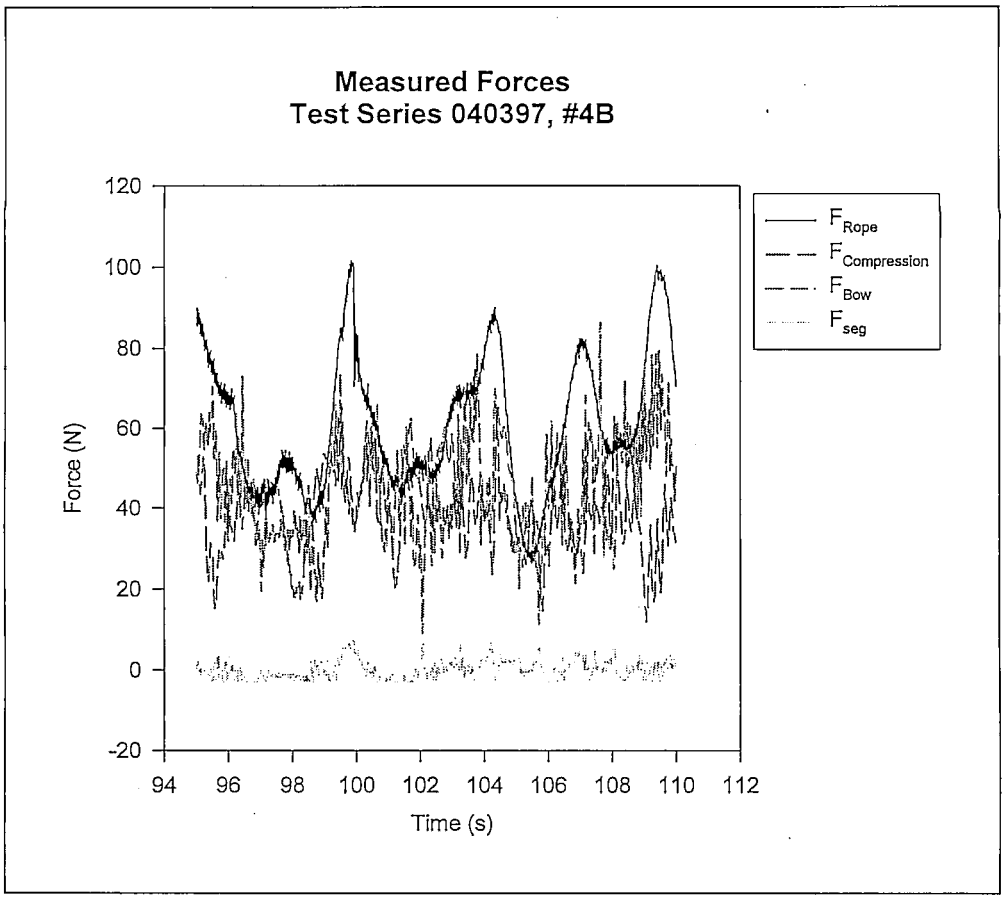
Measured Forces
Test Series 040397, #4B
Force (N)
Time (s)
120
100
80
60
40
20
0
-20
94
96
98
100
102
104
106
108
110
112
F Rope
F Compression
F Bow
F seg

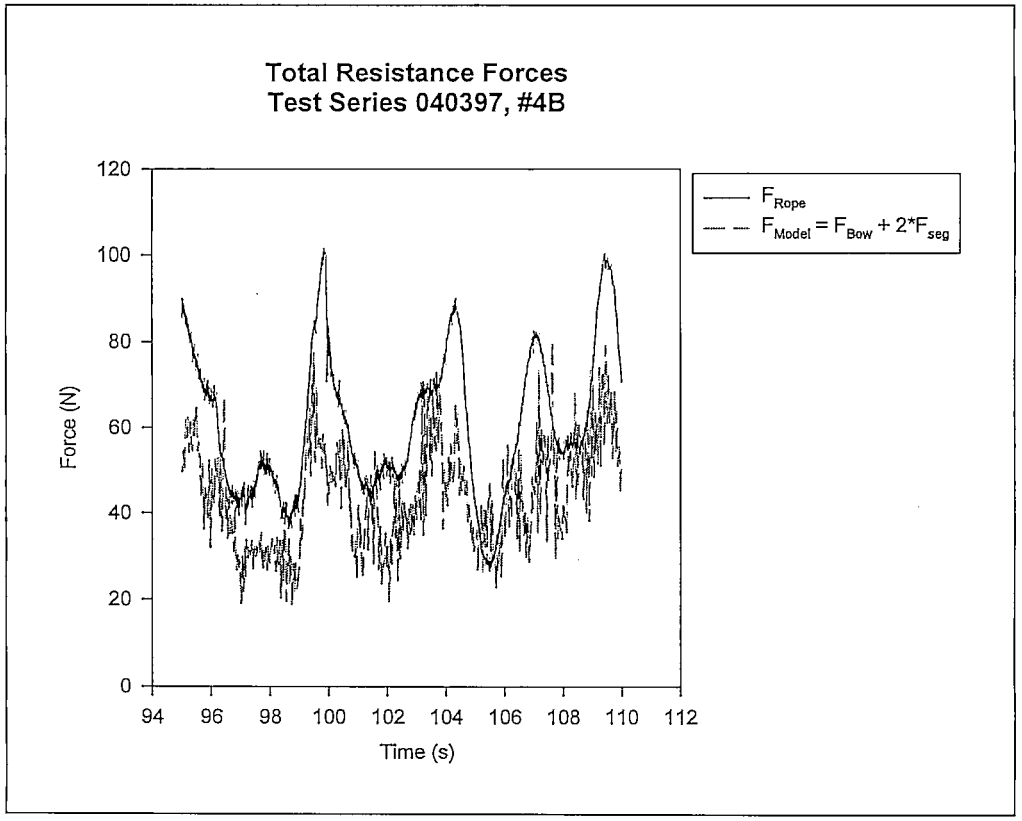
Total Resistance Forces
Test Series 040397, #4B
Force (N)
Time (s)
120
100
80
60
40
20
0
94
96
98
100
102
104
106
108
110
112
F Rope
F Model = F Bow + 2*F seg

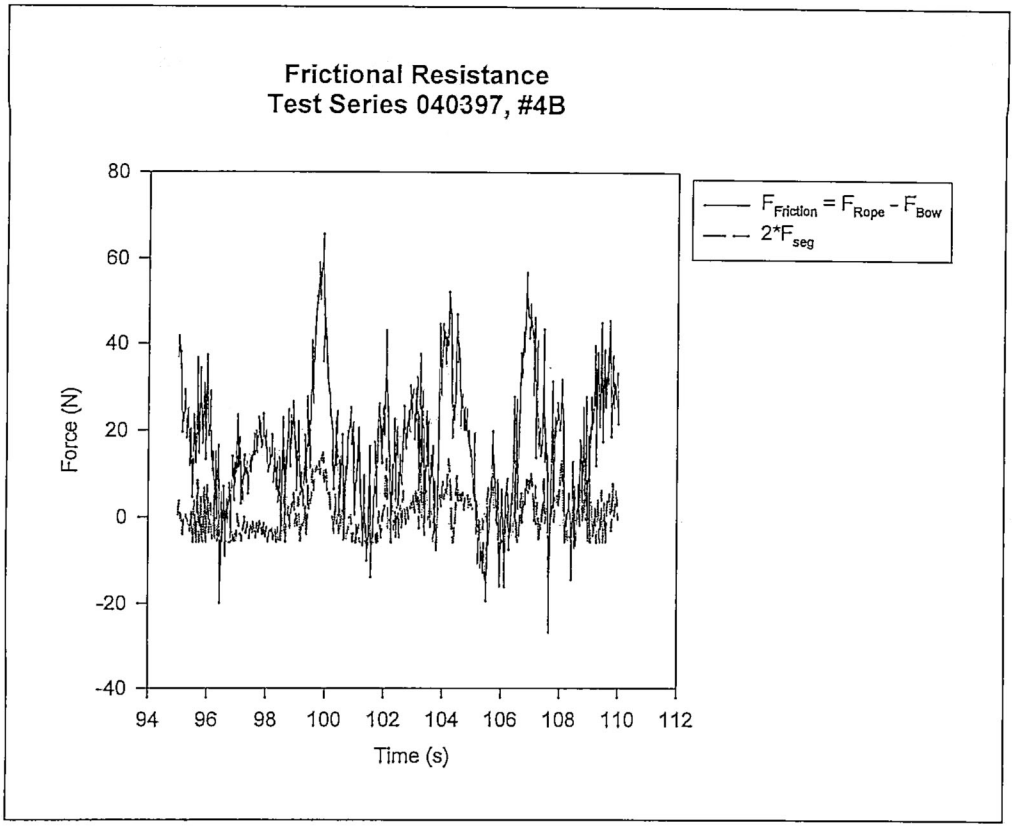
Frictional Resistance
Test Series 040397, #4B
Force (N)
Time (s)
80
60
40
20
0
-20
-40
94
96
98
100
102
104
106
108
110
112
F_Friction = F_Rope - F_Bow
2*F_seg

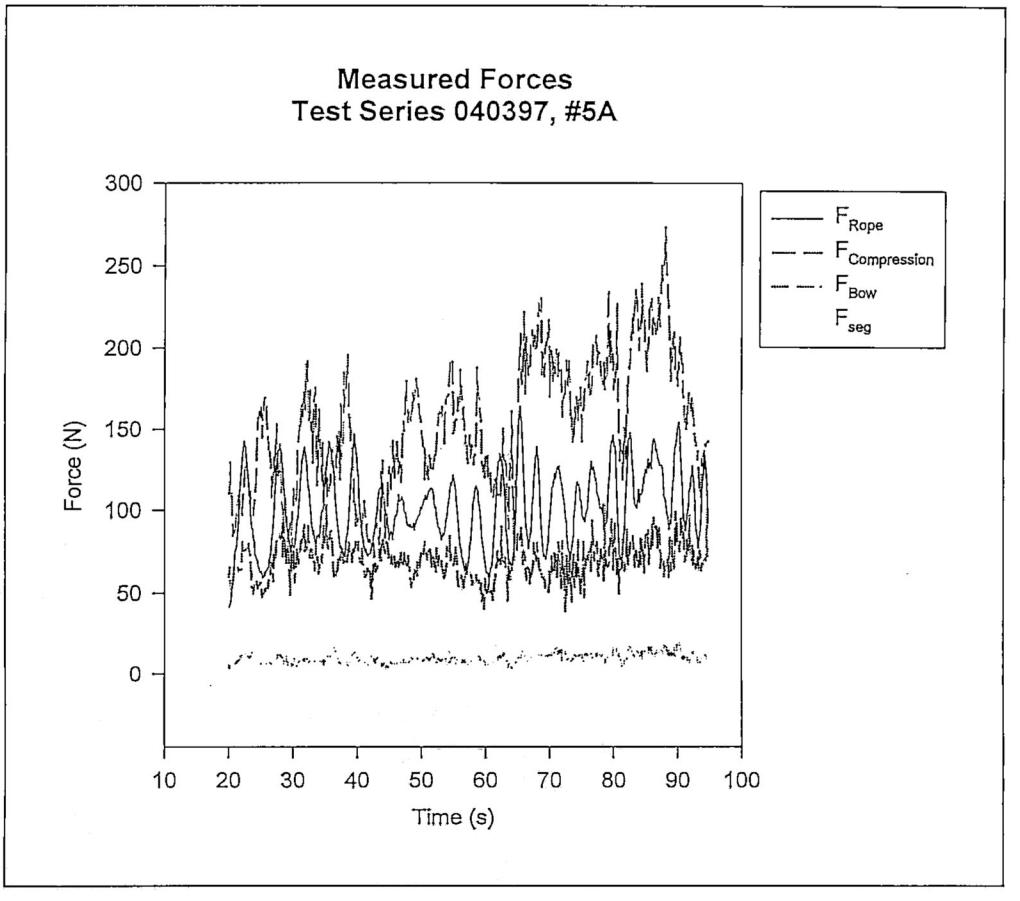
Measured Forces
Test Series 040397, #5A
Force (N)
Time (s)
300
250
200
150
100
50
0
10
20
30
40
50
60
70
80
90
100
F_Rope
F_Compression
F_Bow
F_seg

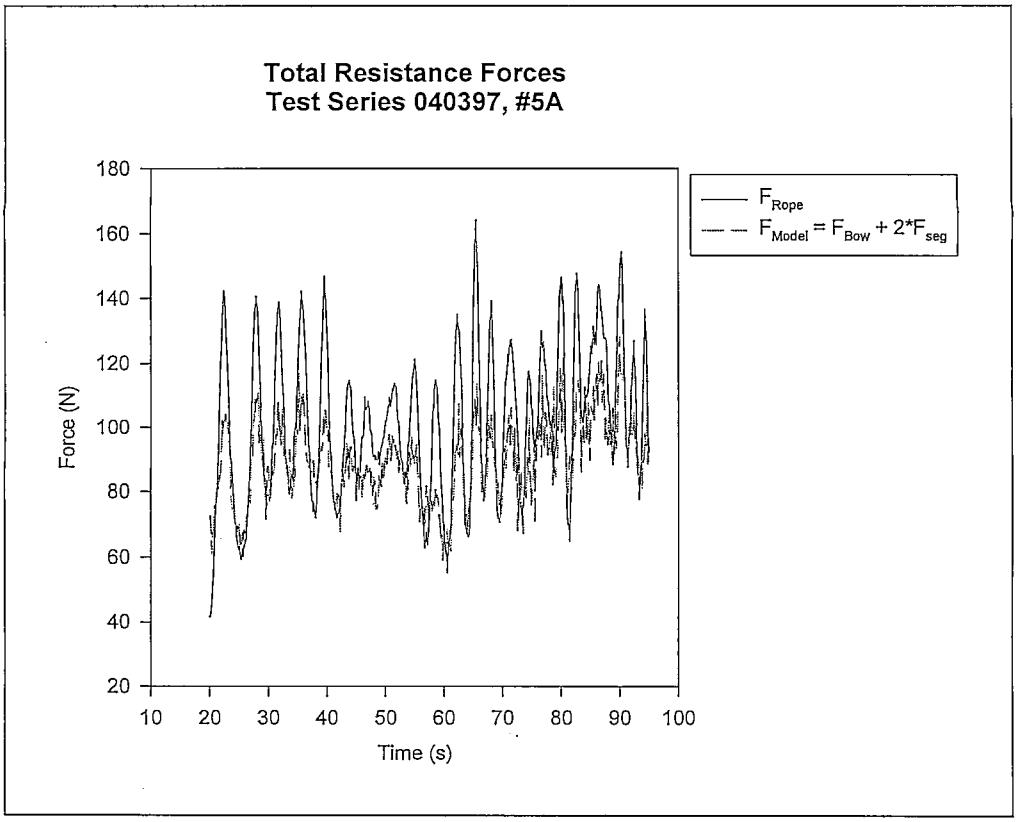
Total Resistance Forces
Test Series 040397, #5A
Force (N)
Time (s)
180
160
140
120
100
80
60
40
20
10
20
30
40
50
60
70
80
90
100
F_Rope
F_Model = F_Bow + 2*F_seg

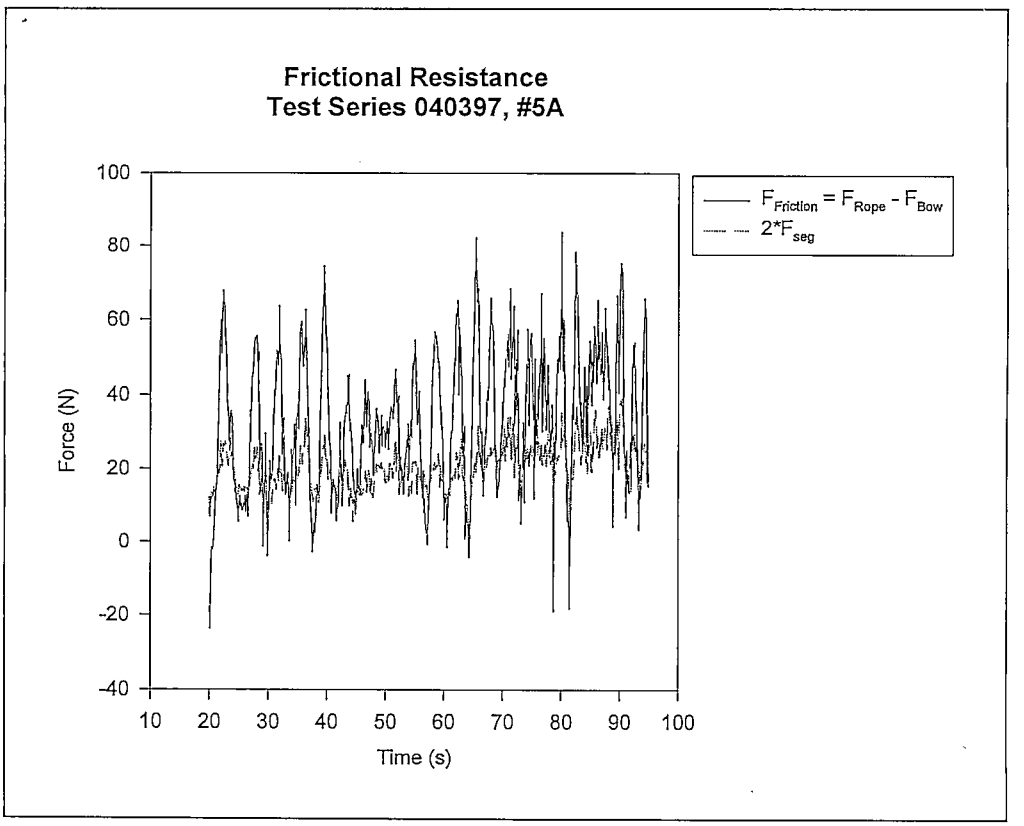
Frictional Resistance
Test Series 040397, #5A
Force (N)
Time (s)
100
80
60
40
20
0
-20
-40
10
20
30
40
50
60
70
80
90
100
F_Friction = F_Rope - F_Bow
2*F_seg

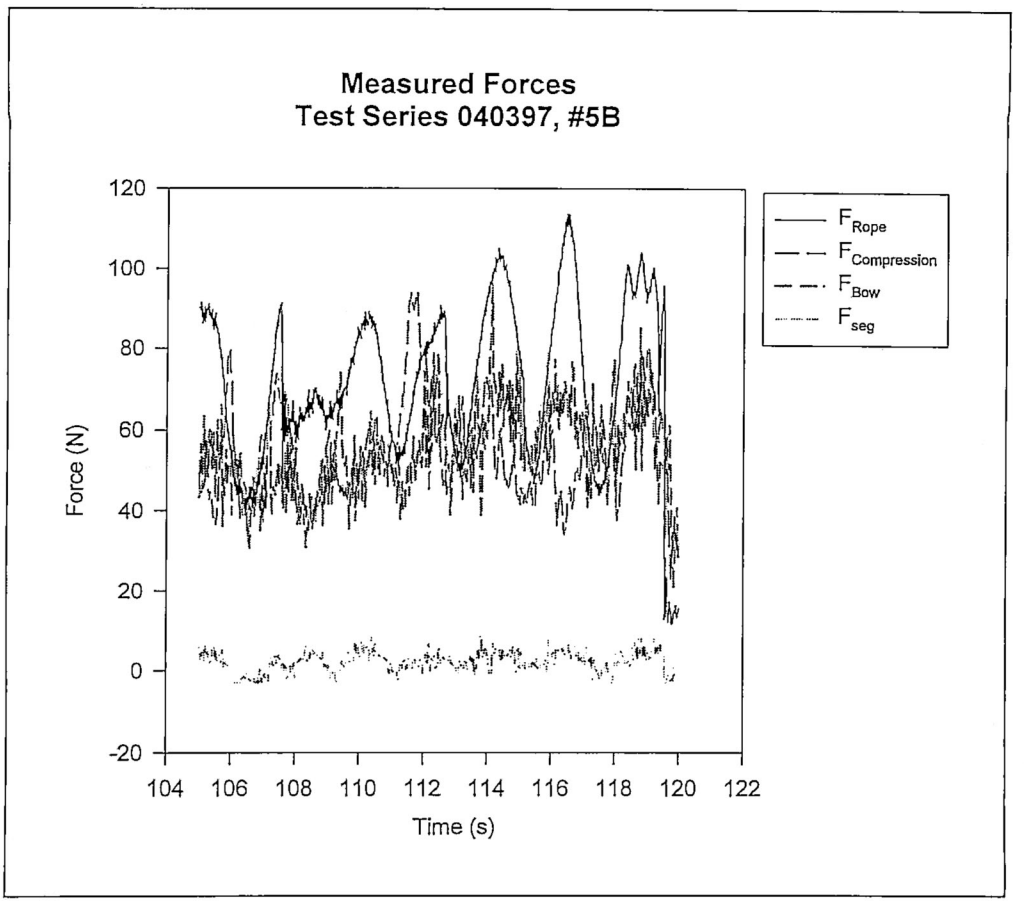
Measured Forces
Test Series 040397, #5B
Force (N)
Time (s)
120
100
80
60
40
20
0
-20
104
106
108
110
112
114
116
118
120
122
F Rope
F Compression
F Bow
F seg

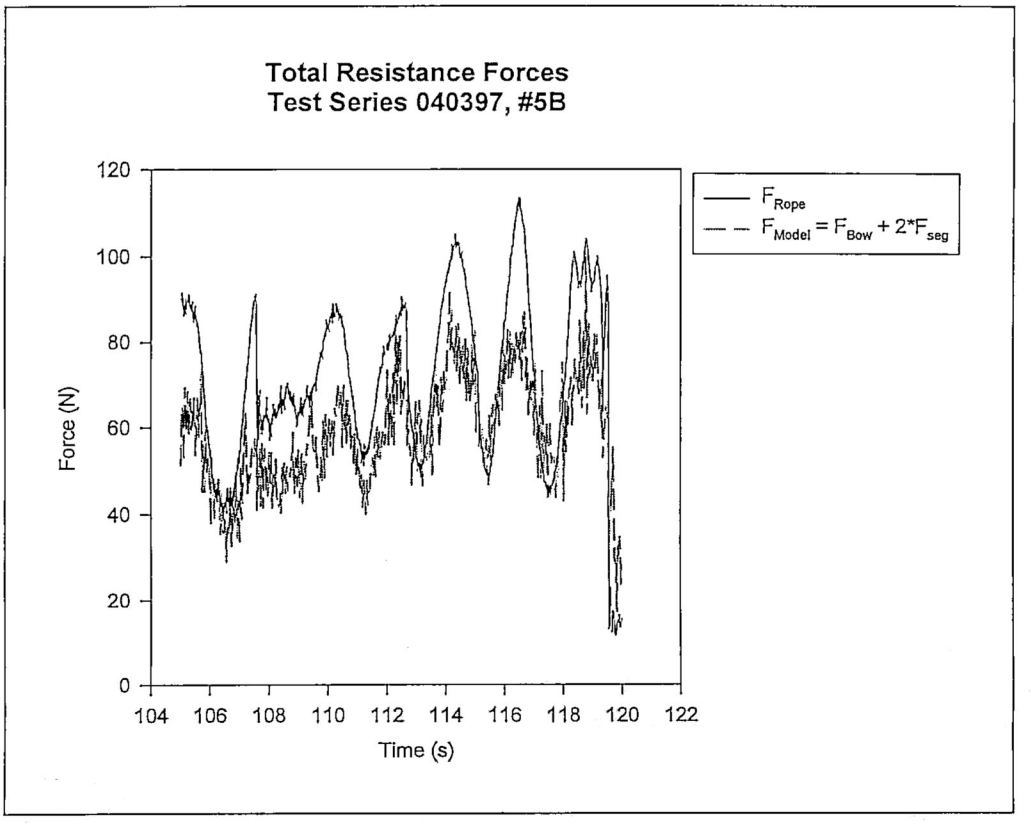
Total Resistance Forces
Test Series 040397, #5B
Force (N)
Time (s)
120
100
80
60
40
20
0
104
106
108
110
112
114
116
118
120
122
F Rope
F Model = F Bow + 2*F seg

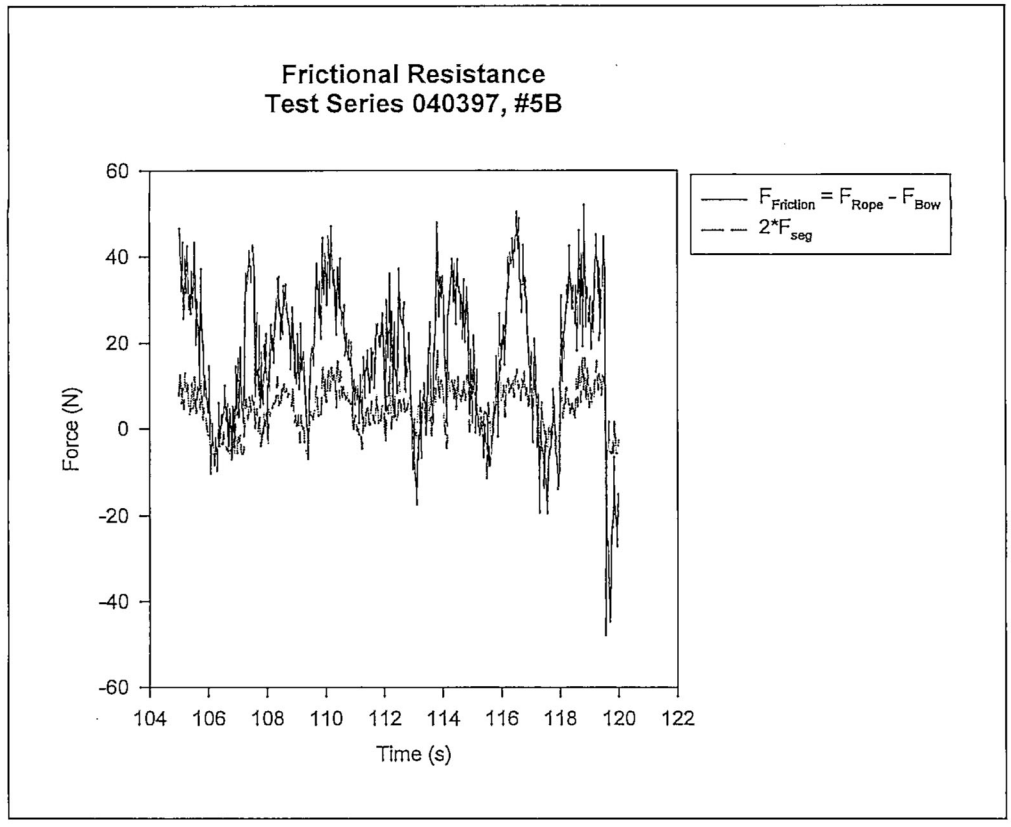
Frictional Resistance
Test Series 040397, #5B
Force (N)
Time (s)
60
40
20
0
-20
-40
-60
104
106
108
110
112
114
116
118
120
122
$F_{Friction} = F_{Rope} - F_{Bow}$
$2*F_{seg}$

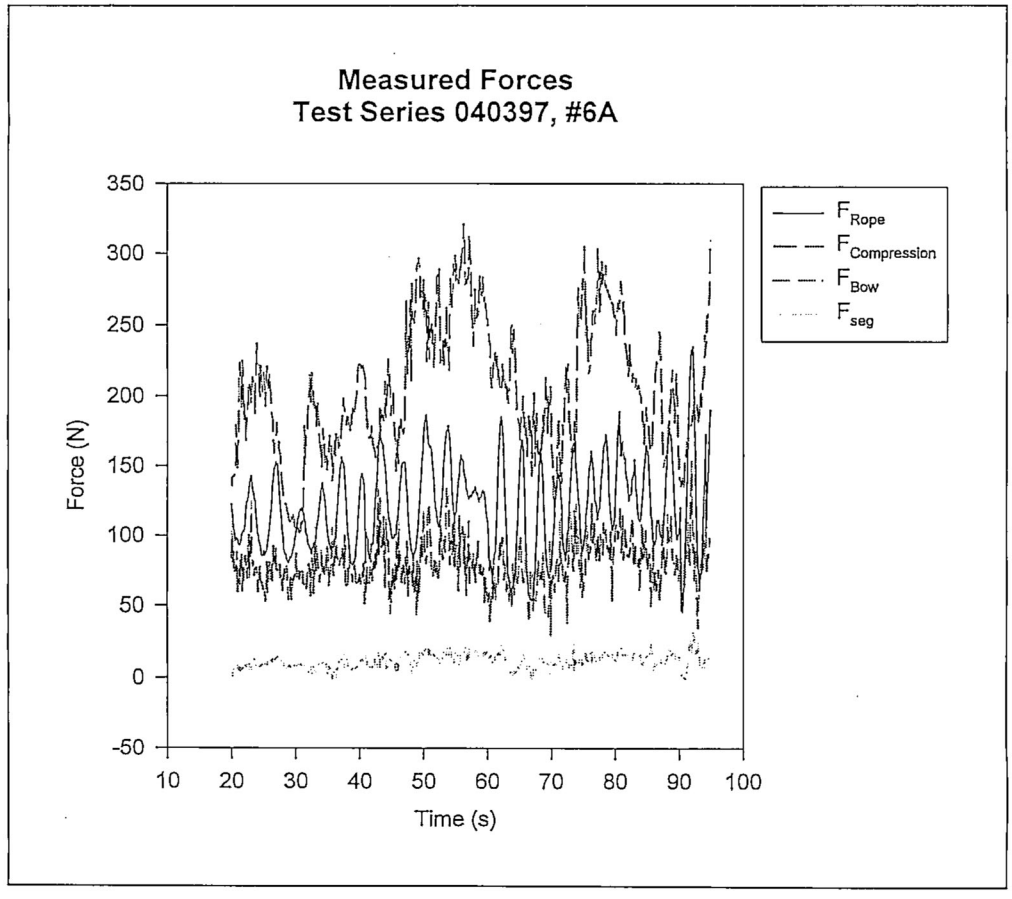
Measured Forces
Test Series 040397, #6A
Force (N)
Time (s)
350
300
250
200
150
100
50
0
-50
10
20
30
40
50
60
70
80
90
100
F_{Rope}
$F_{Compression}$
F_{Bow}
F_{seg}

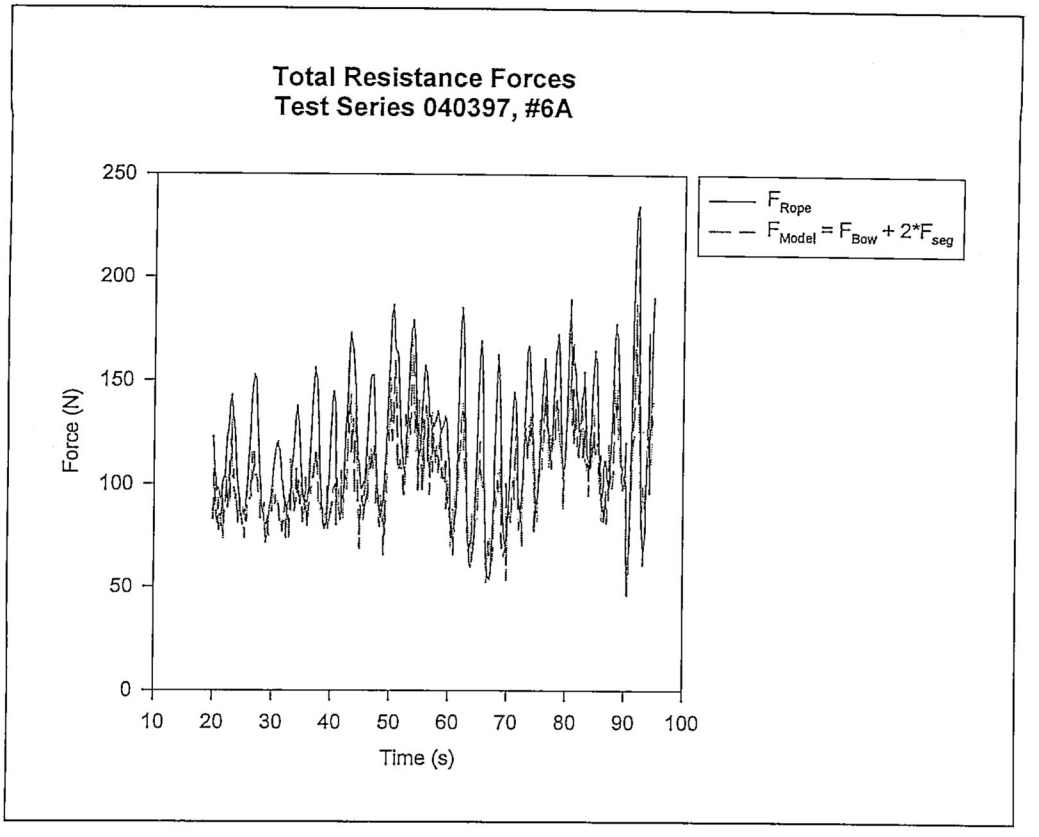
Total Resistance Forces
Test Series 040397, #6A
Force (N)
Time (s)
250
200
150
100
50
0
10
20
30
40
50
60
70
80
90
100
F_Rope
F_Model = F_Bow + 2*F_seg

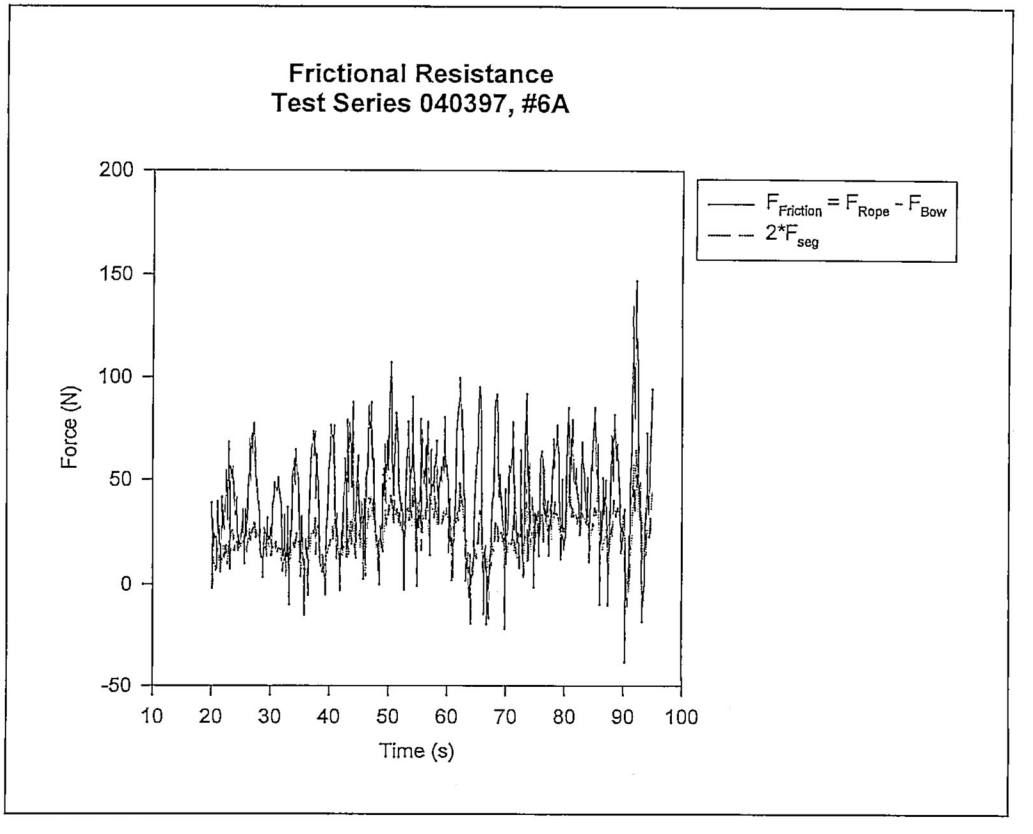
Frictional Resistance
Test Series 040397, #6A
Force (N)
Time (s)
200
150
100
50
0
-50
10
20
30
40
50
60
70
80
90
100
F_Friction = F_Rope - F_Bow
2*F_seg

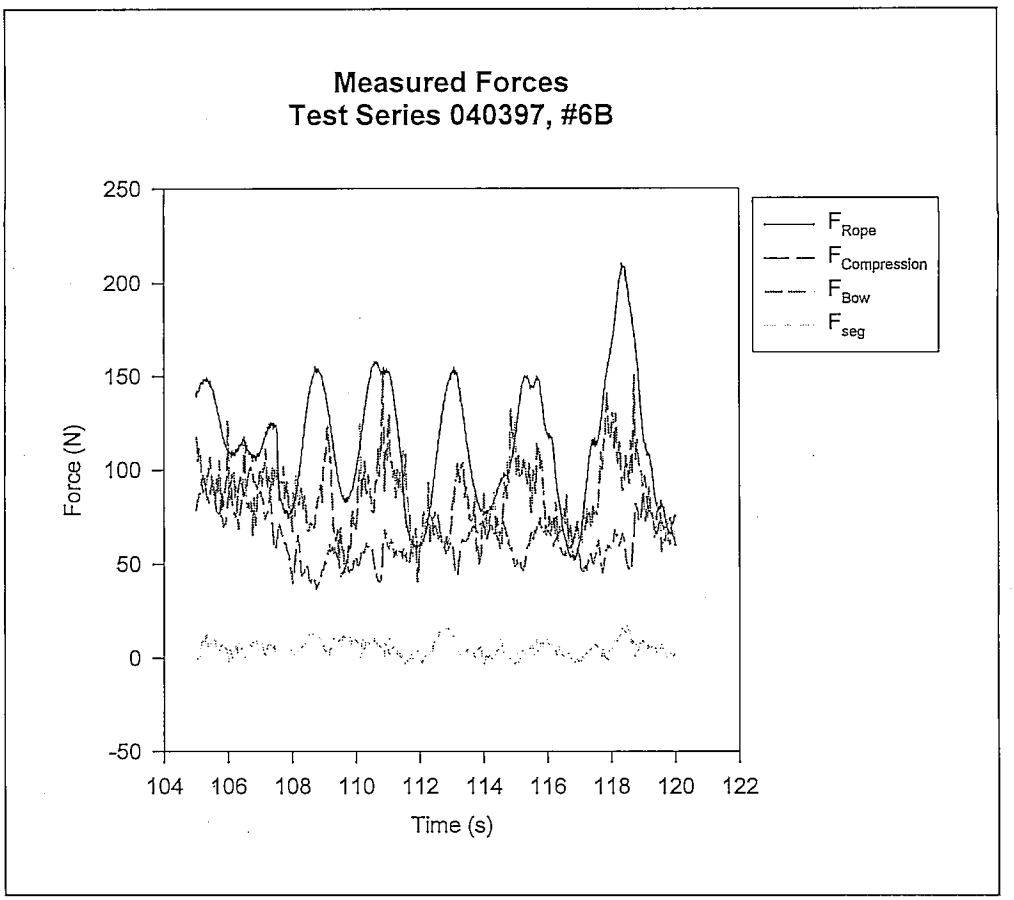
Measured Forces
Test Series 040397, #6B
Force (N)
Time (s)
250
200
150
100
50
0
-50
104
106
108
110
112
114
116
118
120
122
F Rope
F Compression
F Bow
F seg

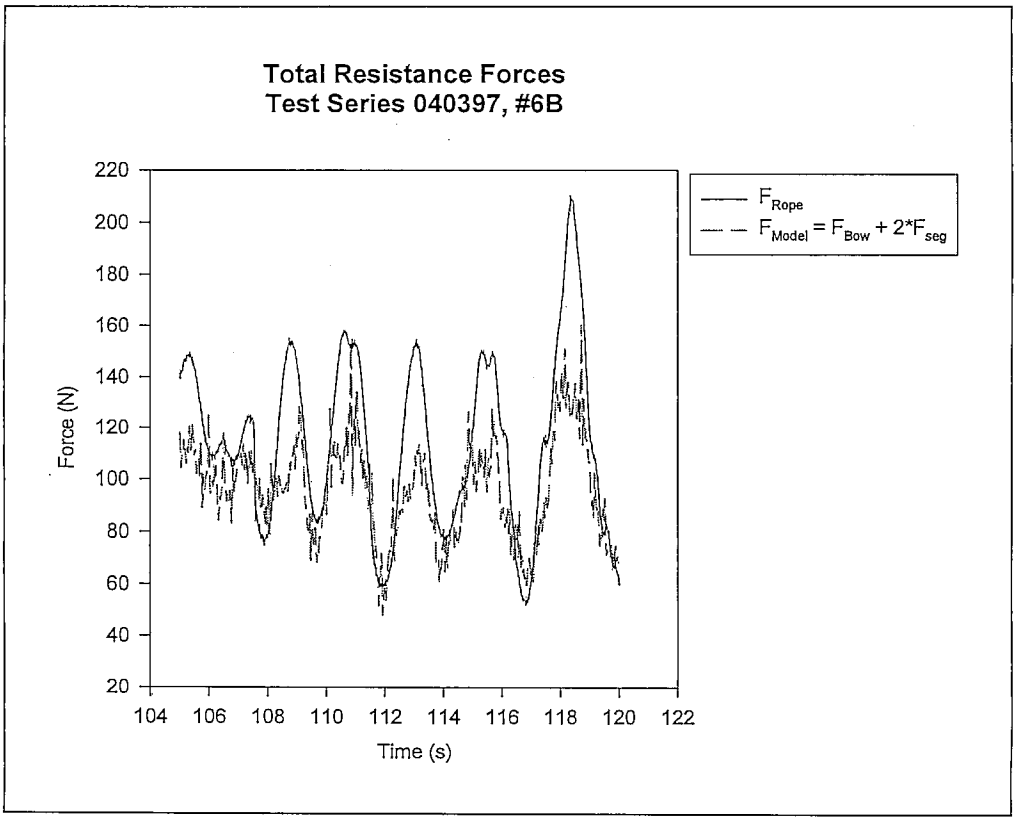
Total Resistance Forces
Test Series 040397, #6B
Force (N)
Time (s)
220
200
180
160
140
120
100
80
60
40
20
104
106
108
110
112
114
116
118
120
122
F Rope
F Model = F Bow + 2*F seg

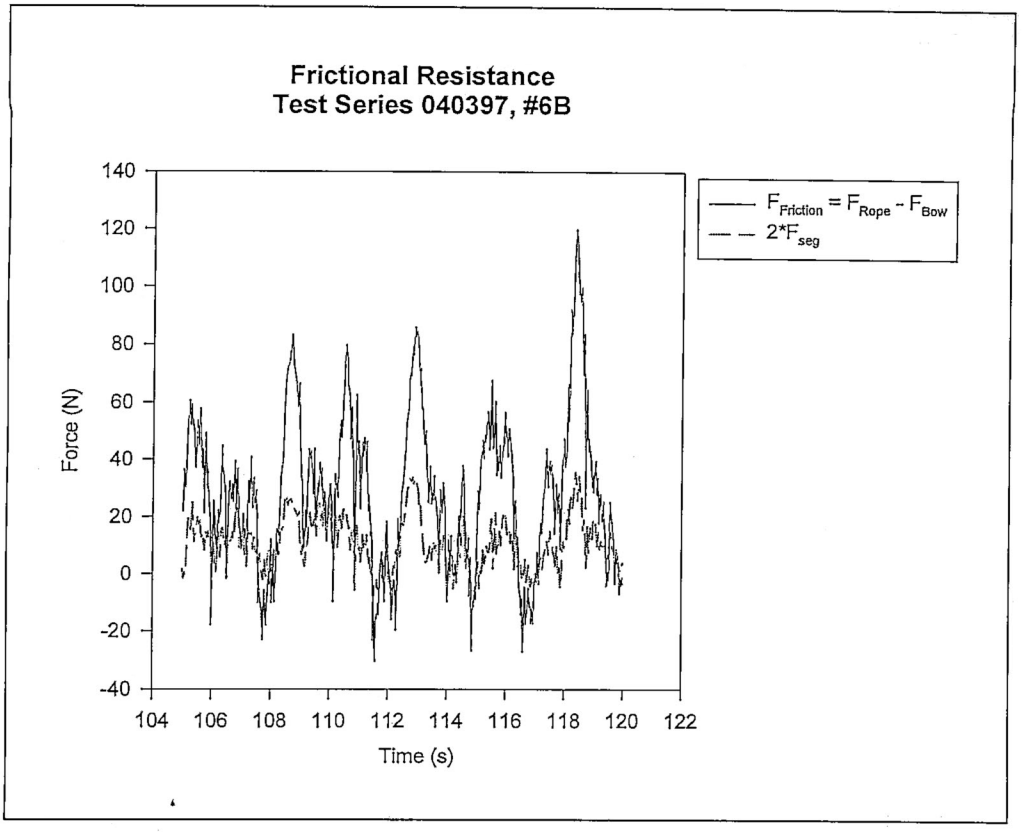
Frictional Resistance
Test Series 040397, #6B
Force (N)
Time (s)
$F_{Friction} = F_{Rope} - F_{Bow}$
$2*F_{seg}$

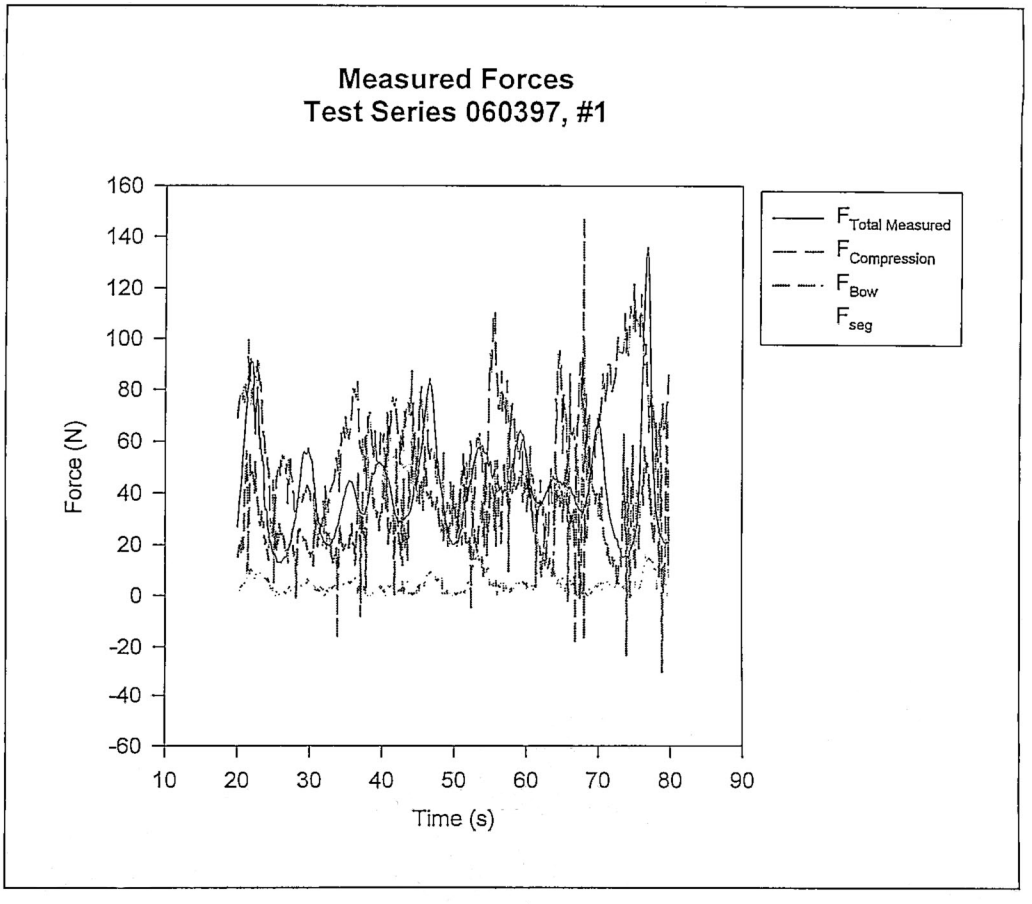
Measured Forces
Test Series 060397, #1
Force (N)
Time (s)
$F_{Total\ Measured}$
$F_{Compression}$
F_{Bow}
F_{seg}

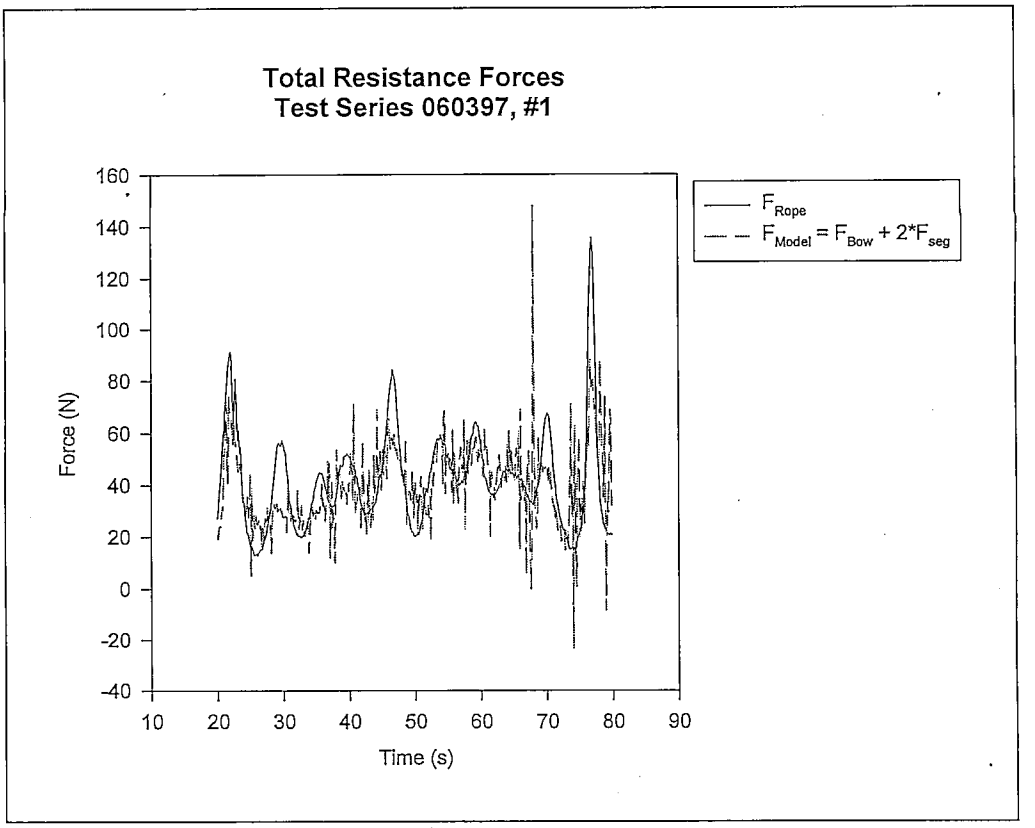
Total Resistance Forces
Test Series 060397, #1
Force (N)
Time (s)
160
140
120
100
80
60
40
20
0
-20
-40
10
20
30
40
50
60
70
80
90
F_Rope
F_Model = F_Bow + 2*F_seg

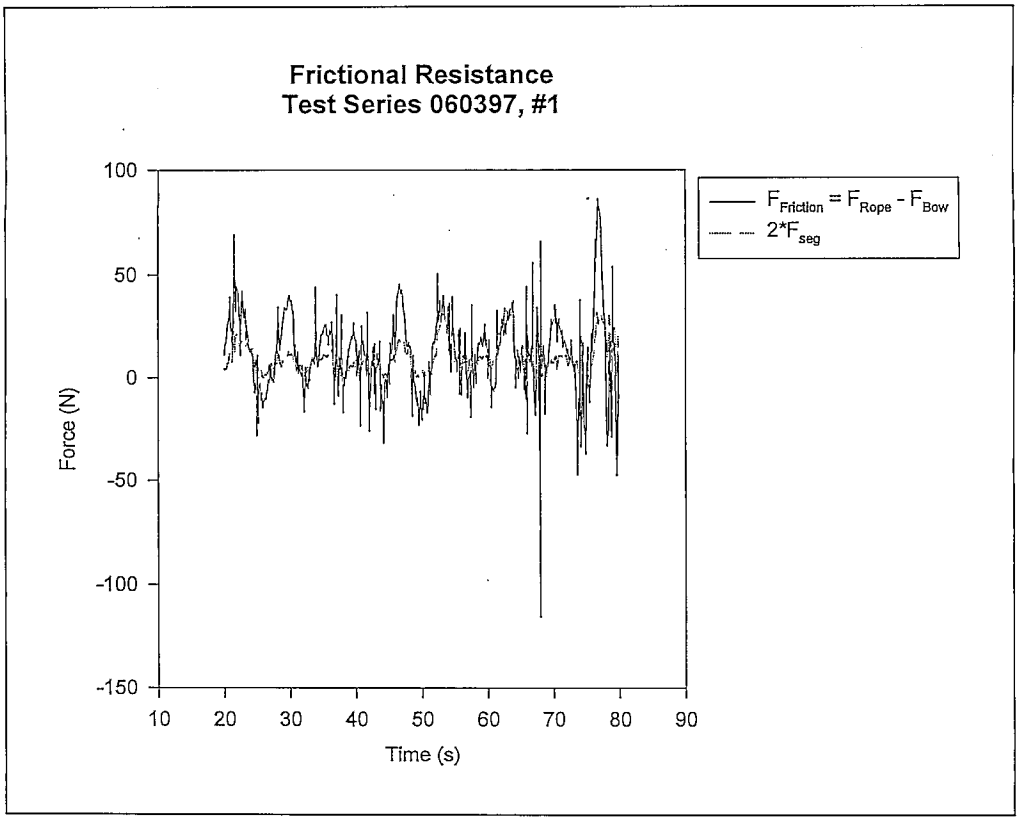
Frictional Resistance
Test Series 060397, #1
Force (N)
Time (s)
100
50
0
-50
-100
-150
10
20
30
40
50
60
70
80
90
F_Friction = F_Rope - F_Bow
2*F_seg

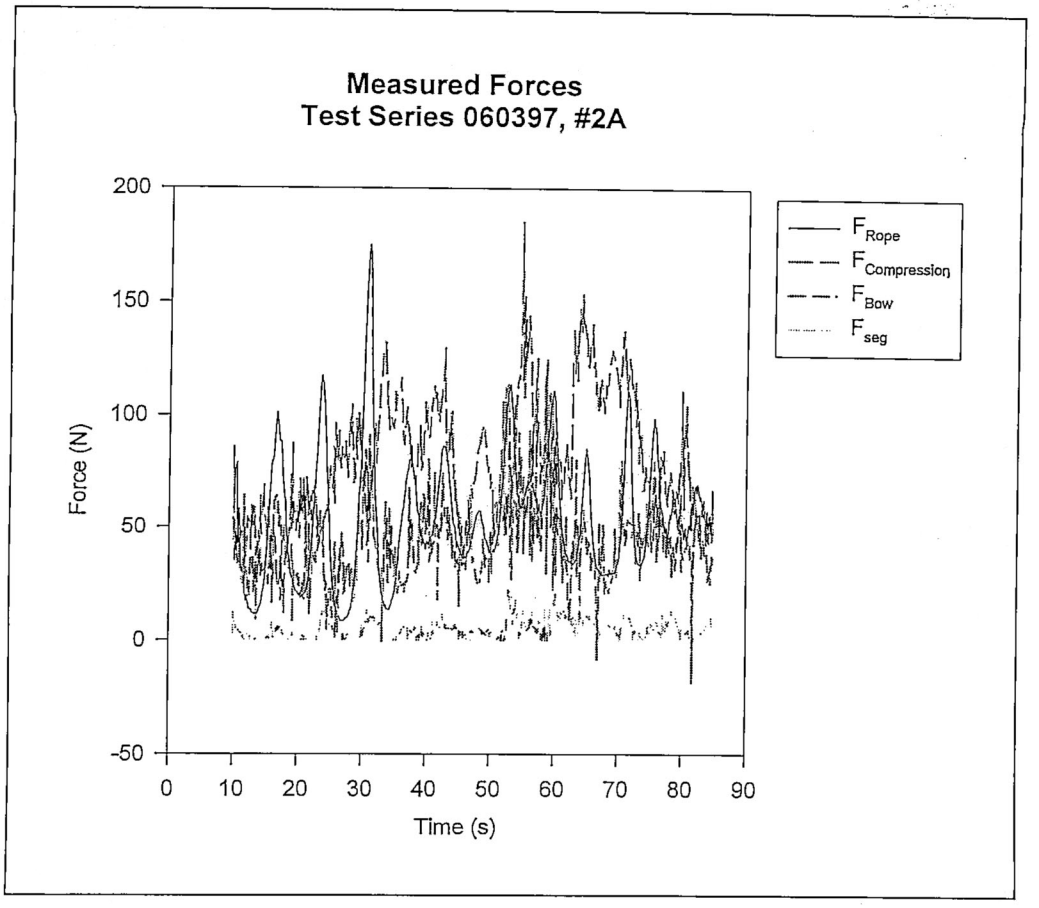
Measured Forces
Test Series 060397, #2A
Force (N)
Time (s)
200
150
100
50
0
-50
0
10
20
30
40
50
60
70
80
90
F Rope
F Compression
F Bow
F seg

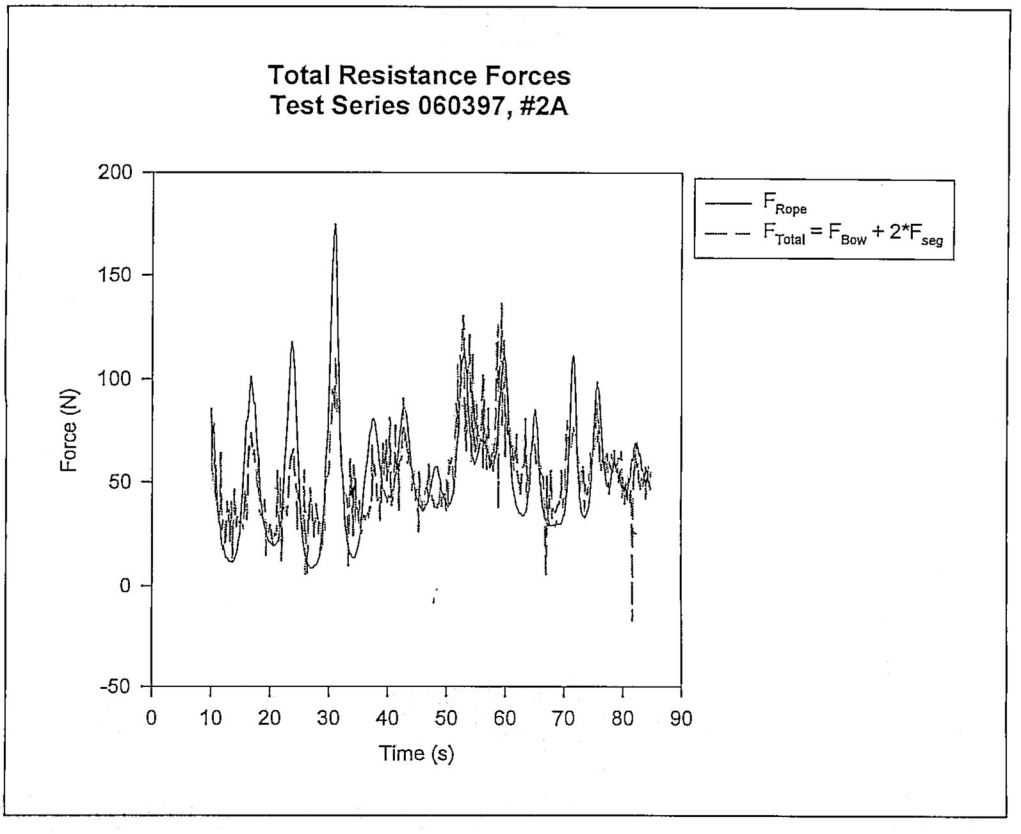
Total Resistance Forces
Test Series 060397, #2A
Force (N)
Time (s)
200
150
100
50
0
-50
0
10
20
30
40
50
60
70
80
90
F Rope
F Total = F Bow + 2*F seg

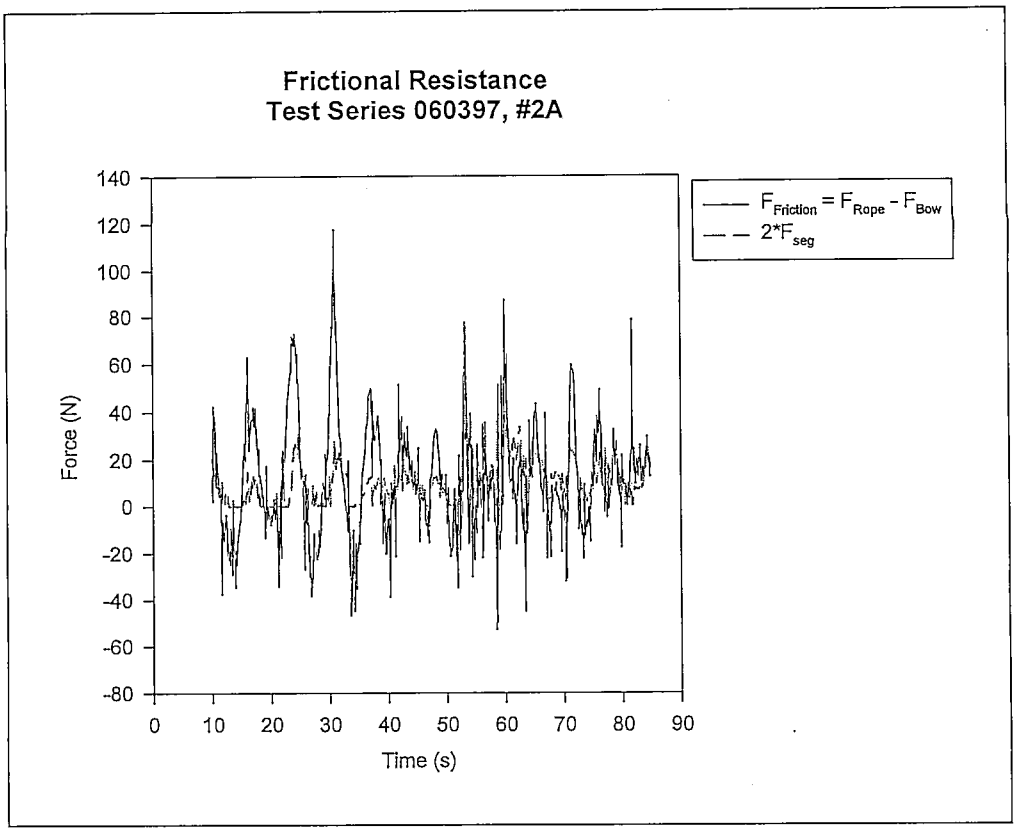
Frictional Resistance
Test Series 060397, #2A
Force (N)
Time (s)
$F_{Friction} = F_{Rope} - F_{Bow}$
$2*F_{seg}$

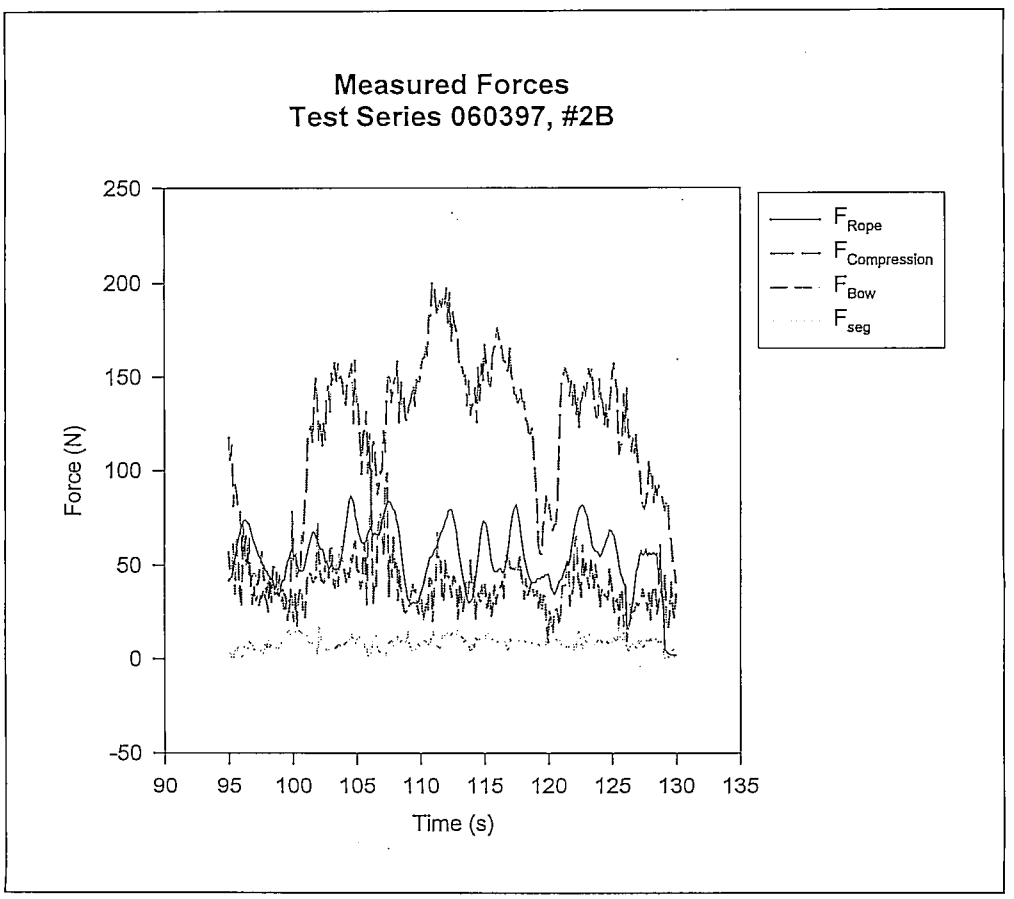
Measured Forces
Test Series 060397, #2B
Force (N)
Time (s)
F_{Rope}
$F_{Compression}$
F_{Bow}
F_{seg}

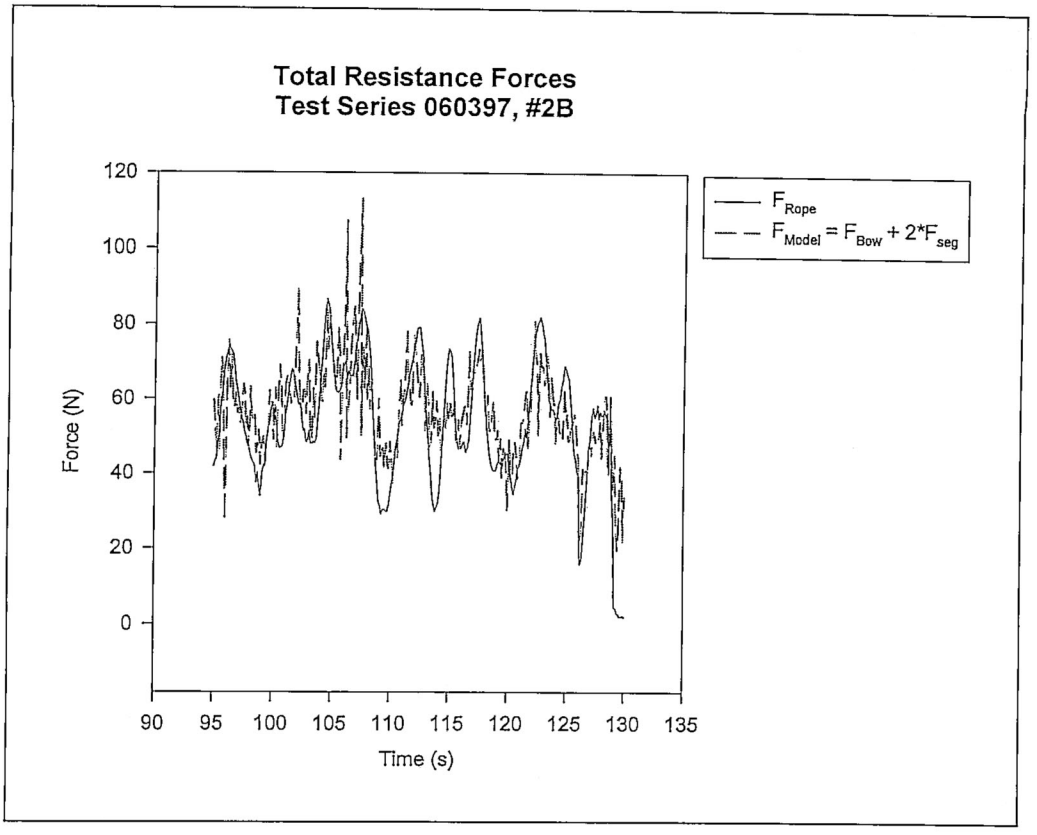
Total Resistance Forces
Test Series 060397, #2B
Force (N)
Time (s)
120
100
80
60
40
20
0
90
95
100
105
110
115
120
125
130
135
F_Rope
F_Model = F_Bow + 2*F_seg

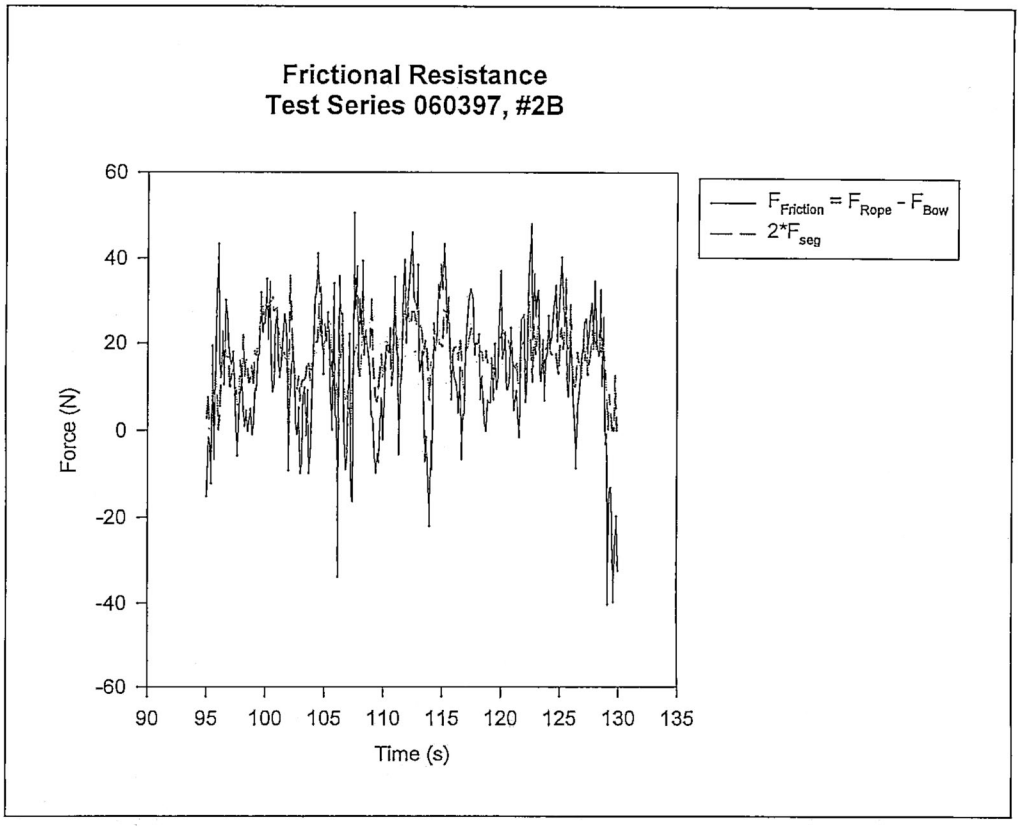
Frictional Resistance
Test Series 060397, #2B
Force (N)
Time (s)
60
40
20
0
-20
-40
-60
90
95
100
105
110
115
120
125
130
135
F_Friction = F_Rope - F_Bow
2*F_seg

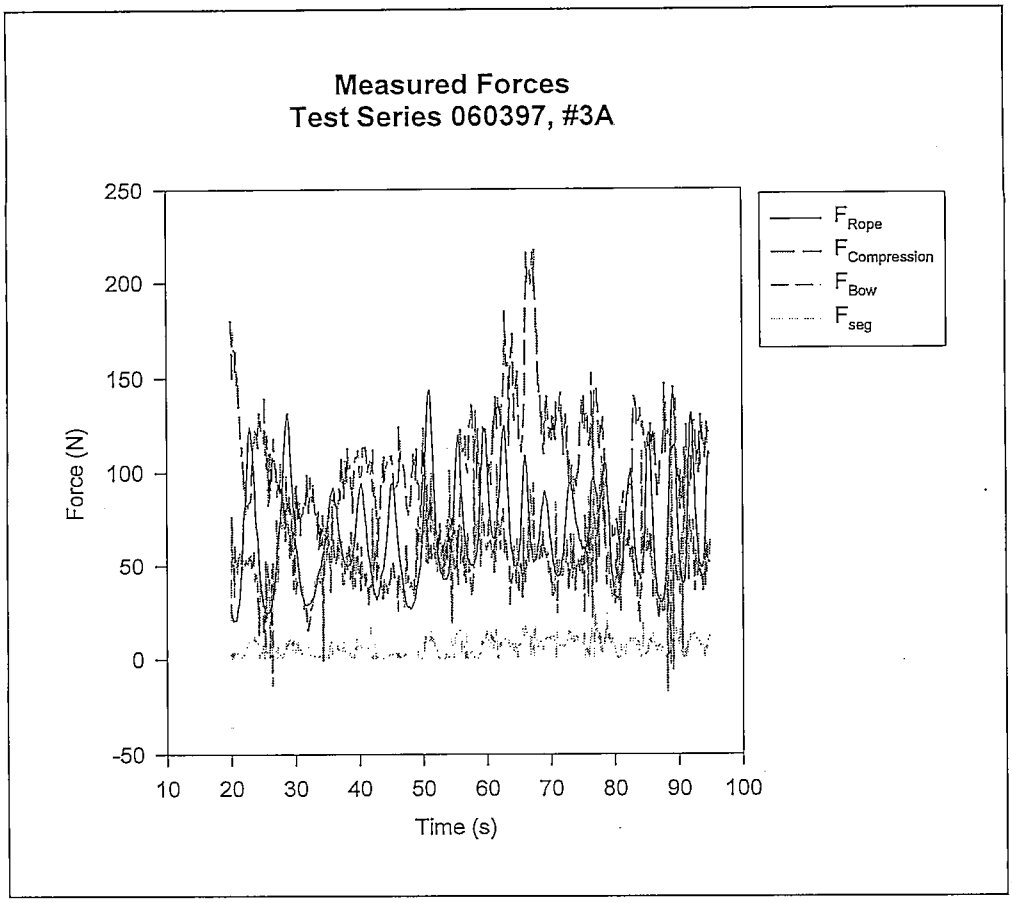
Measured Forces
Test Series 060397, #3A
Force (N)
Time (s)
250
200
150
100
50
0
-50
10
20
30
40
50
60
70
80
90
100
F_Rope
F_Compression
F_Bow
F_seg

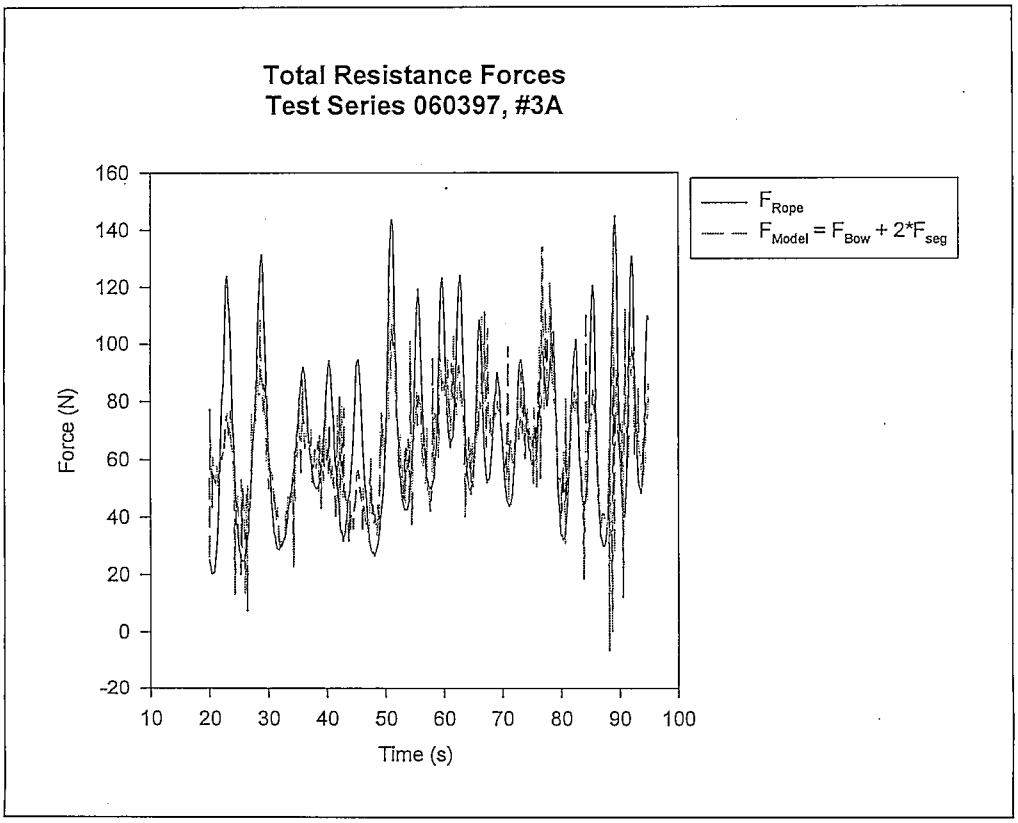
Total Resistance Forces
Test Series 060397, #3A
Force (N)
Time (s)
160
140
120
100
80
60
40
20
0
-20
10
20
30
40
50
60
70
80
90
100
F_Rope
F_Model = F_Bow + 2*F_seg

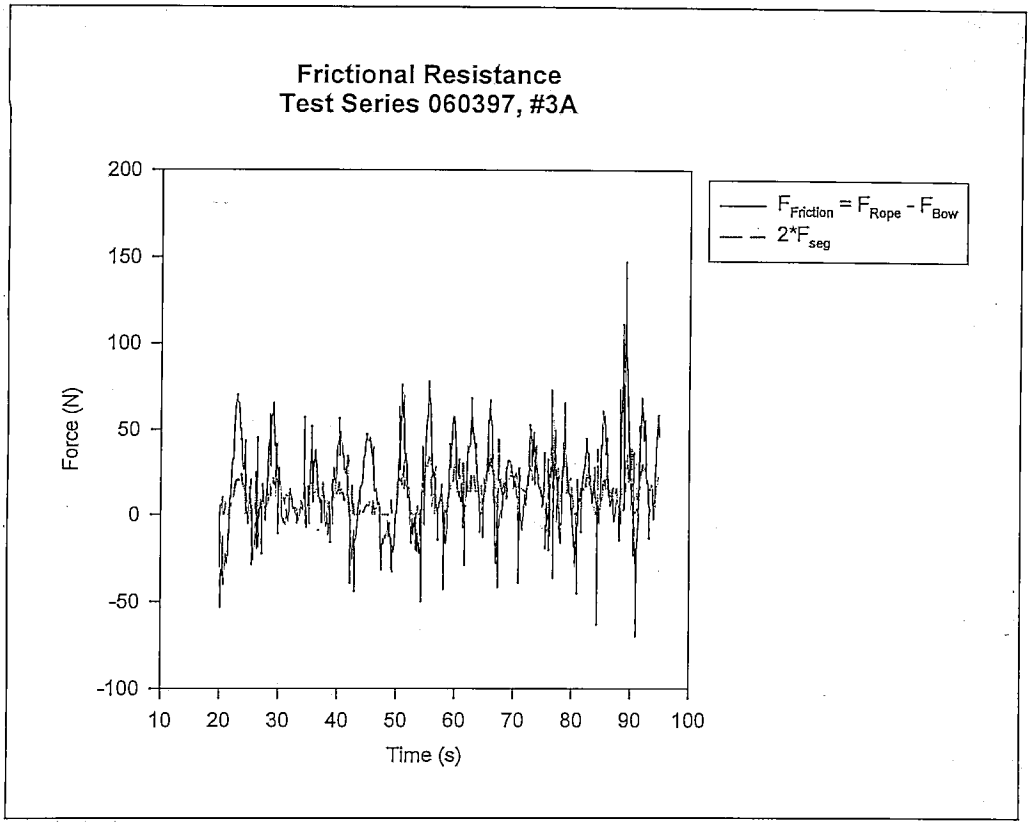
Frictional Resistance
Test Series 060397, #3A
Force (N)
Time (s)
200
150
100
50
0
-50
-100
10
20
30
40
50
60
70
80
90
100
F_Friction = F_Rope - F_Bow
2*F_seg

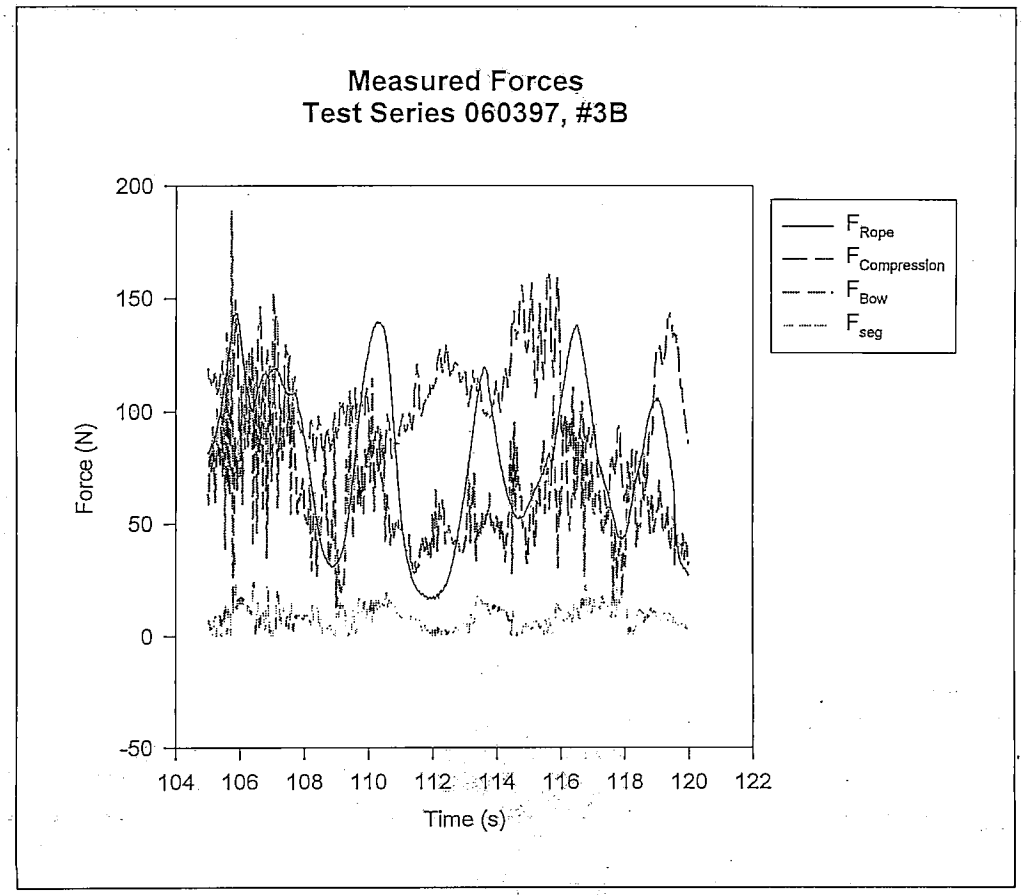
Measured Forces
Test Series 060397, #3B
Force (N)
Time (s)
200
150
100
50
0
-50
104
106
108
110
112
114
116
118
120
122
F_Rope
F_Compression
F_Bow
F_seg

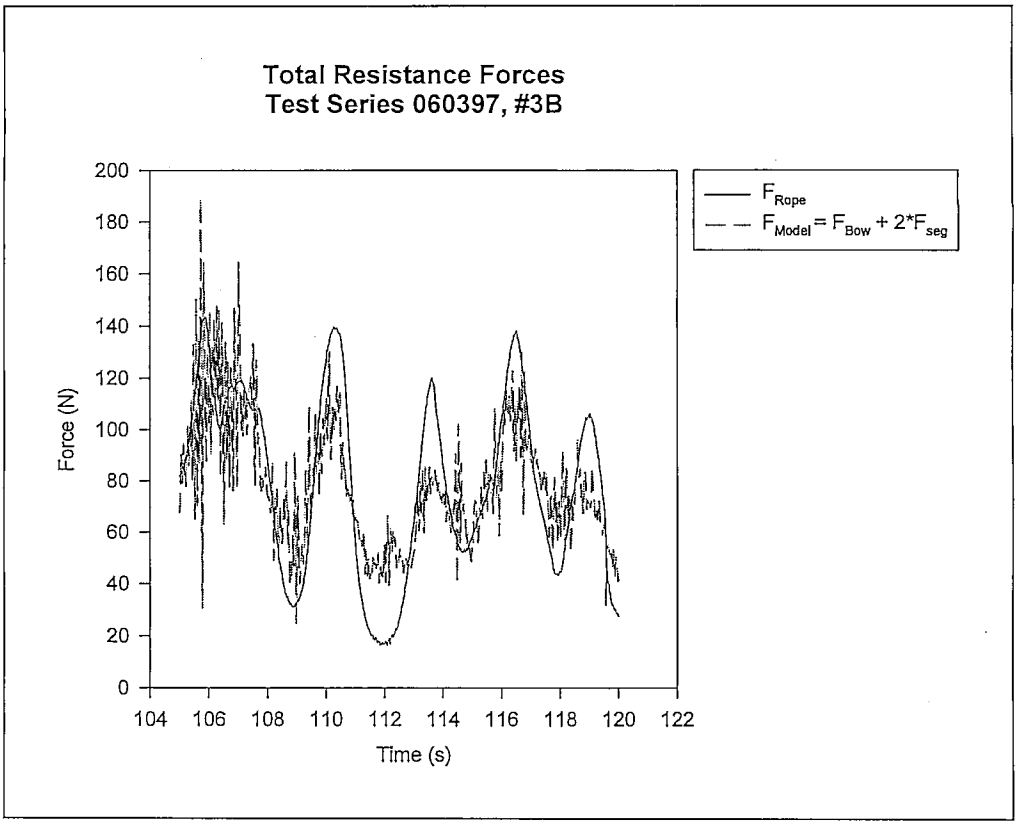
Total Resistance Forces
Test Series 060397, #3B
Force (N)
Time (s)
200
180
160
140
120
100
80
60
40
20
0
104
106
108
110
112
114
116
118
120
122
F_Rope
F_Model = F_Bow + 2*F_seg

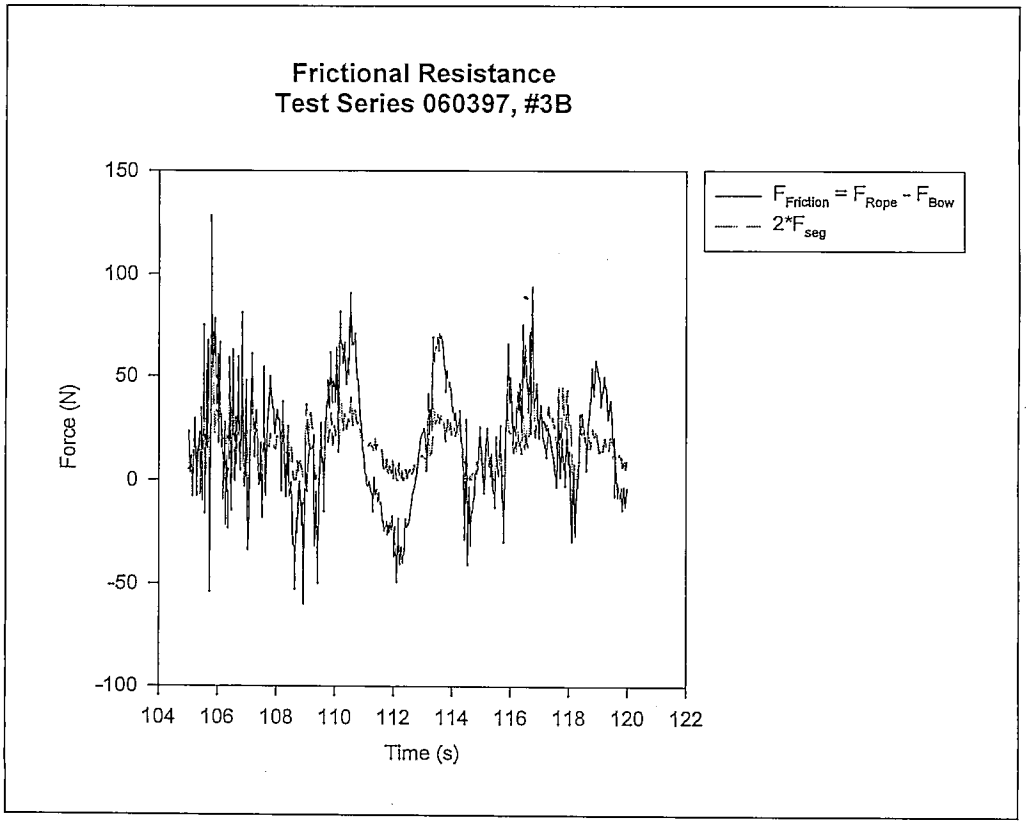
Frictional Resistance
Test Series 060397, #3B
Force (N)
Time (s)
150
100
50
0
-50
-100
104
106
108
110
112
114
116
118
120
122
F_Friction = F_Rope - F_Bow
2*F_seg

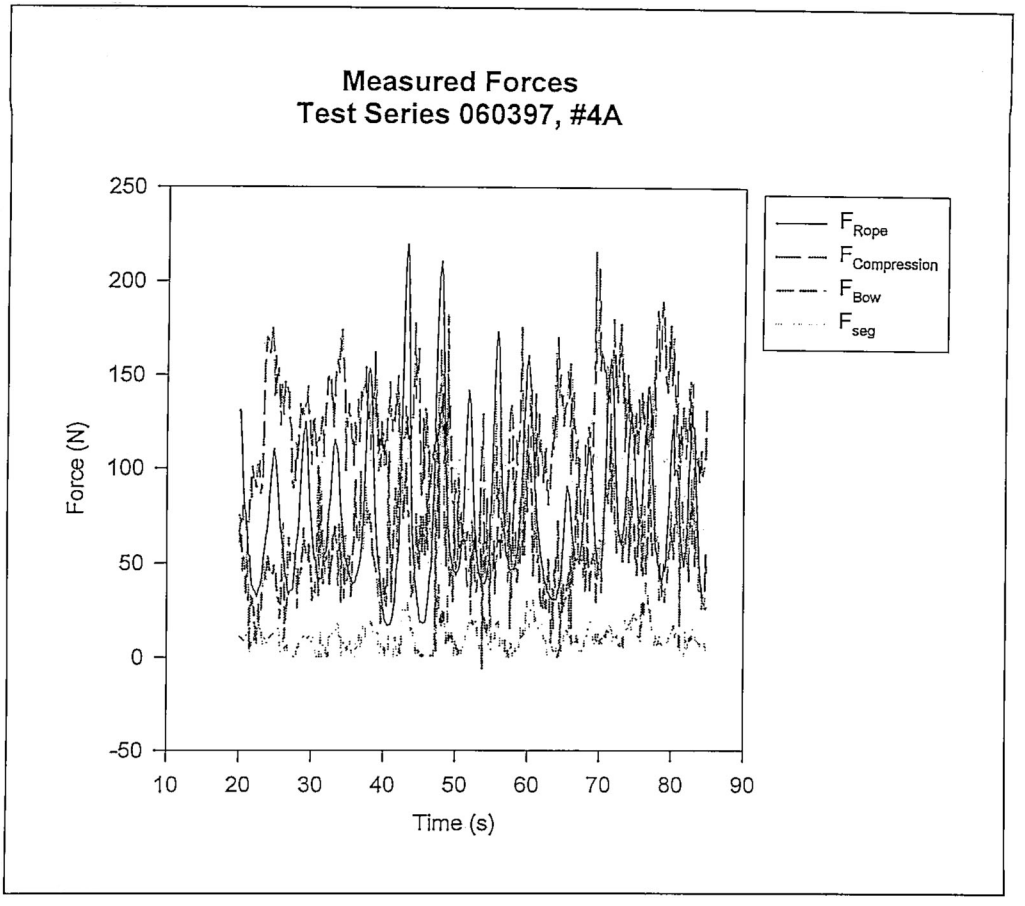
Measured Forces
Test Series 060397, #4A
Force (N)
Time (s)
250
200
150
100
50
0
-50
10
20
30
40
50
60
70
80
90
F Rope
F Compression
F Bow
F seg

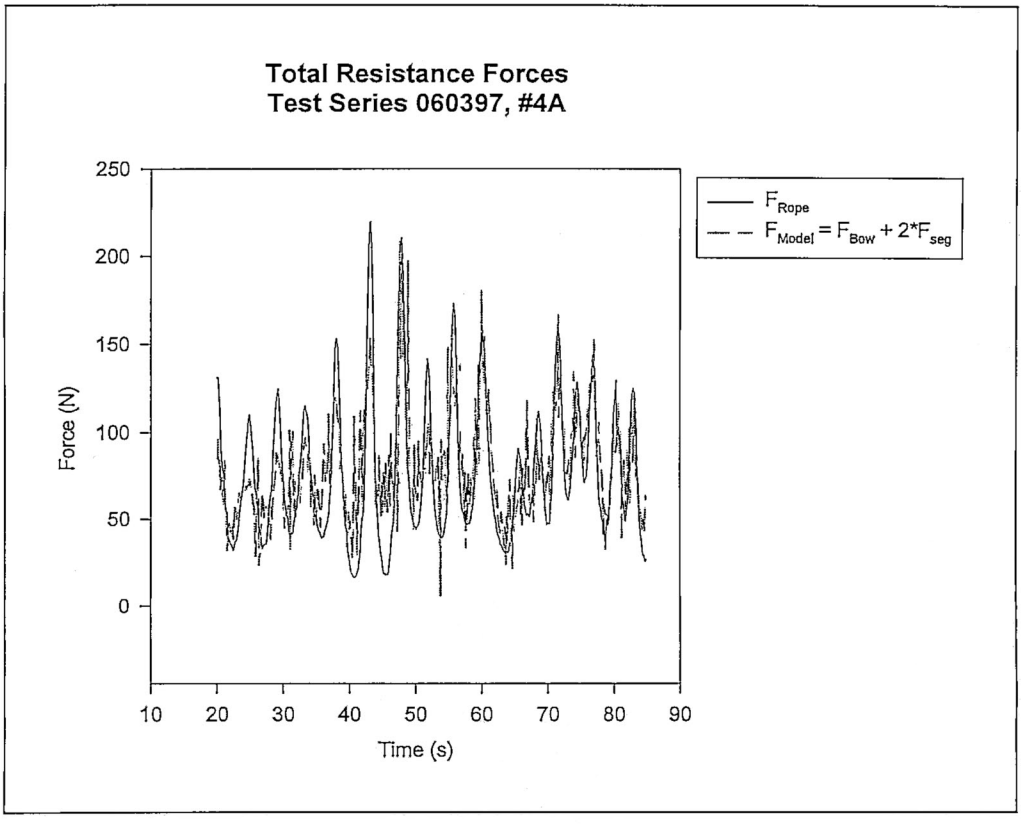
Total Resistance Forces
Test Series 060397, #4A
Force (N)
Time (s)
250
200
150
100
50
0
10
20
30
40
50
60
70
80
90
F Rope
F Model = F Bow + 2*F seg

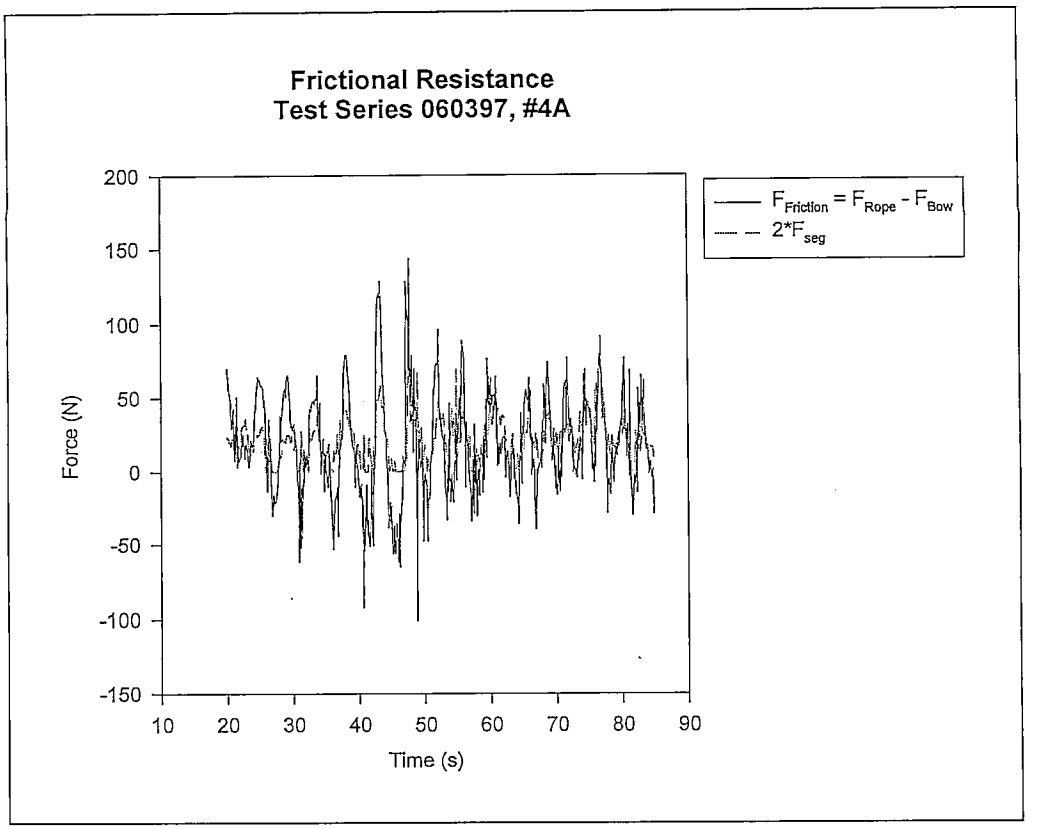
Frictional Resistance
Test Series 060397, #4A
Force (N)
Time (s)
200
150
100
50
0
-50
-100
-150
10
20
30
40
50
60
70
80
90
F_Friction = F_Rope - F_Bow
2*F_seg

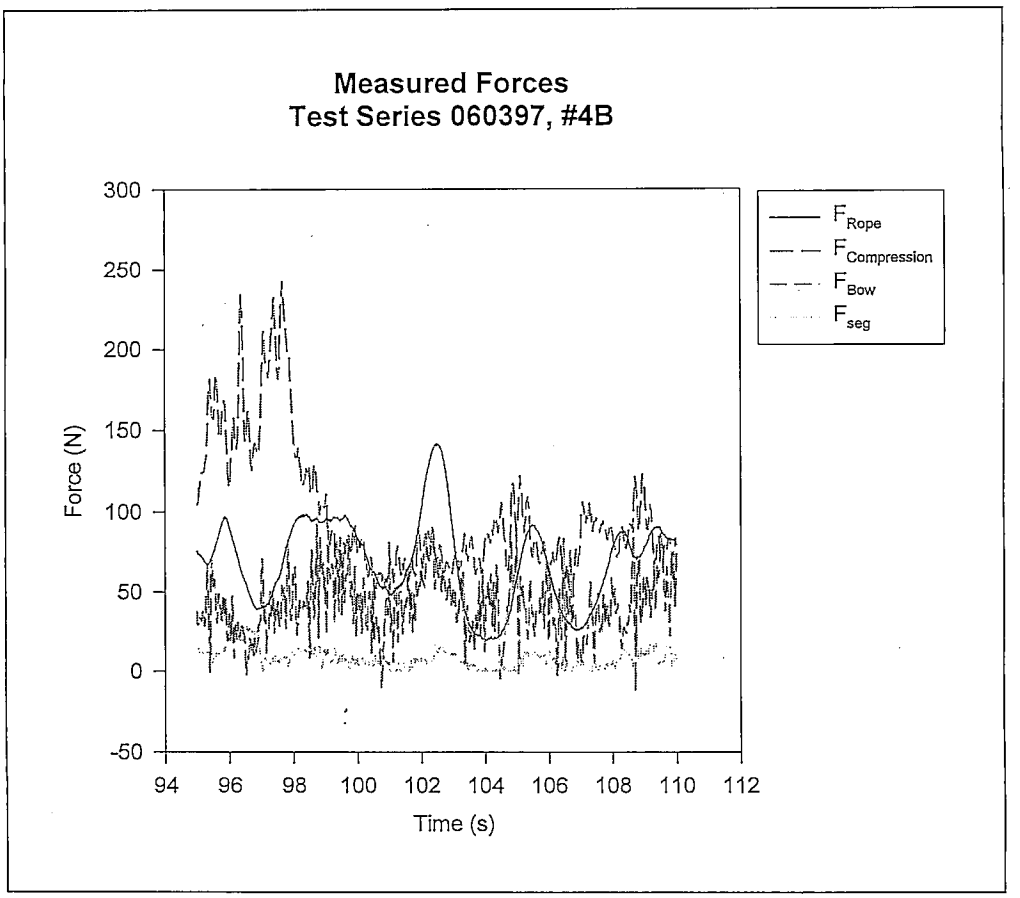
Measured Forces
Test Series 060397, #4B
Force (N)
Time (s)
300
250
200
150
100
50
0
-50
94
96
98
100
102
104
106
108
110
112
F_Rope
F_Compression
F_Bow
F_seg

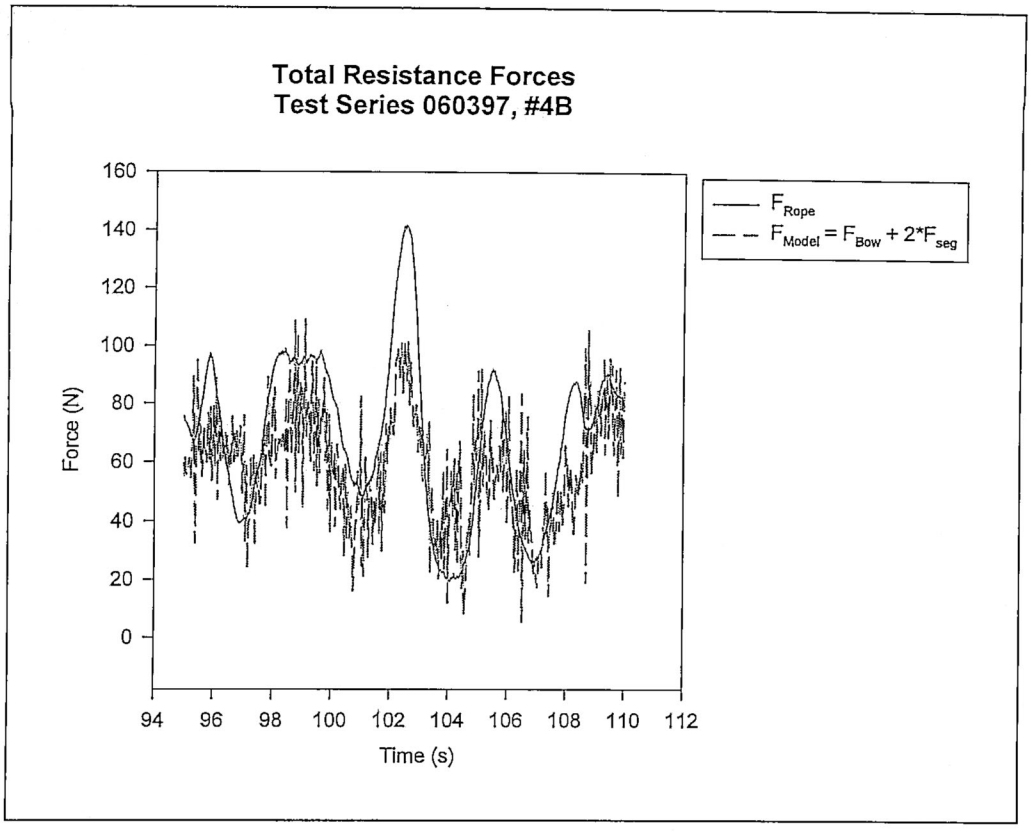
Total Resistance Forces
Test Series 060397, #4B
Force (N)
Time (s)
160
140
120
100
80
60
40
20
0
94
96
98
100
102
104
106
108
110
112
F_Rope
F_Model = F_Bow + 2*F_seg

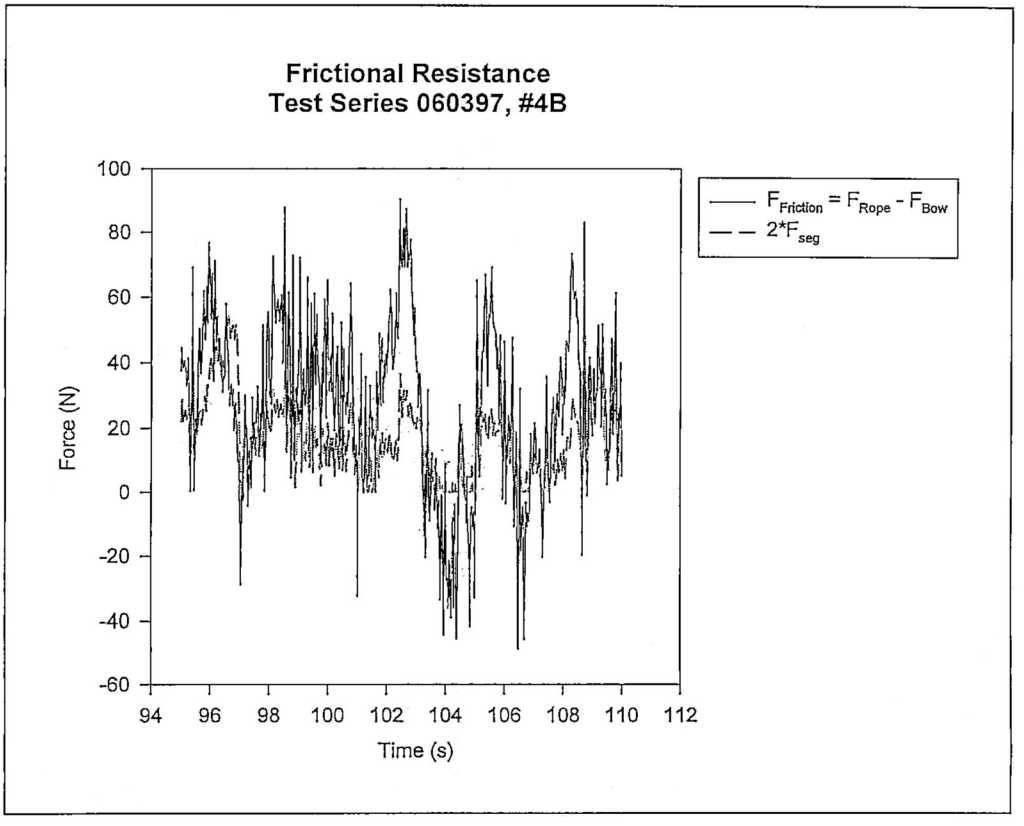
Frictional Resistance
Test Series 060397, #4B
Force (N)
Time (s)
100
80
60
40
20
0
-20
-40
-60
94
96
98
100
102
104
106
108
110
112
F_Friction = F_Rope - F_Bow
2*F_seg

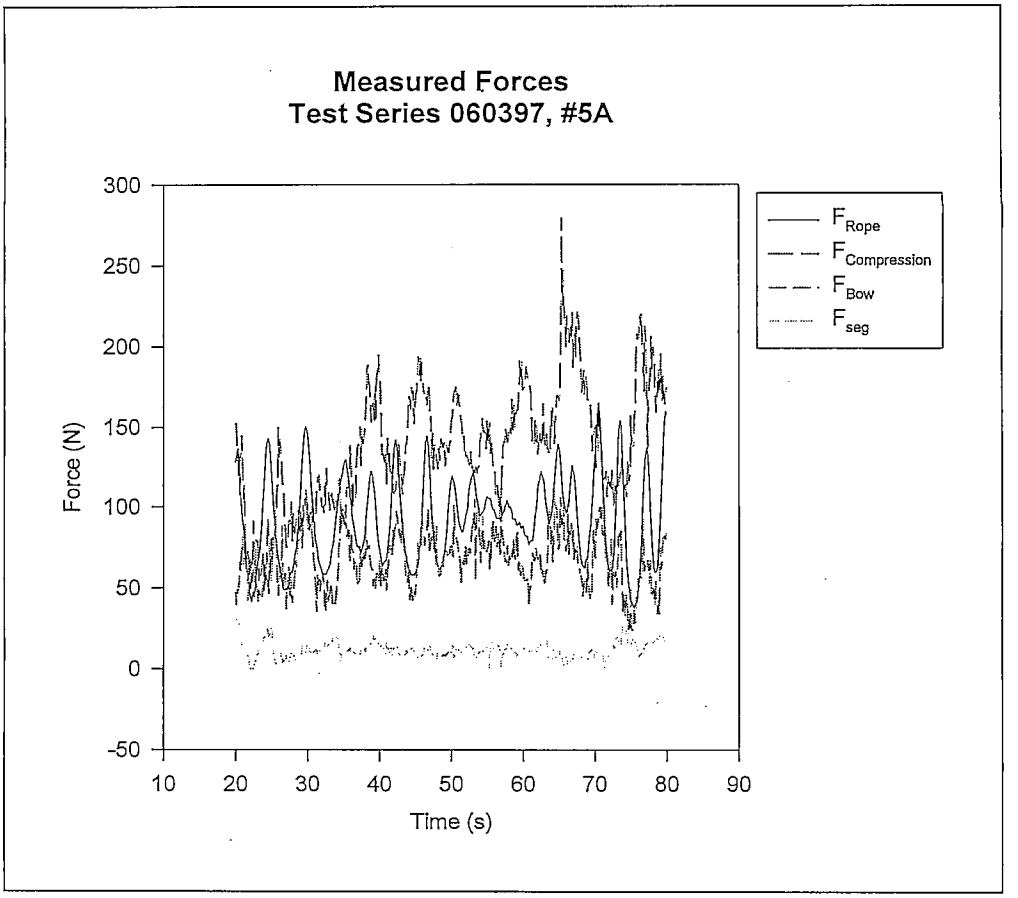
Measured Forces
Test Series 060397, #5A
Force (N)
Time (s)
300
250
200
150
100
50
0
-50
10
20
30
40
50
60
70
80
90
F Rope
F Compression
F Bow
F seg

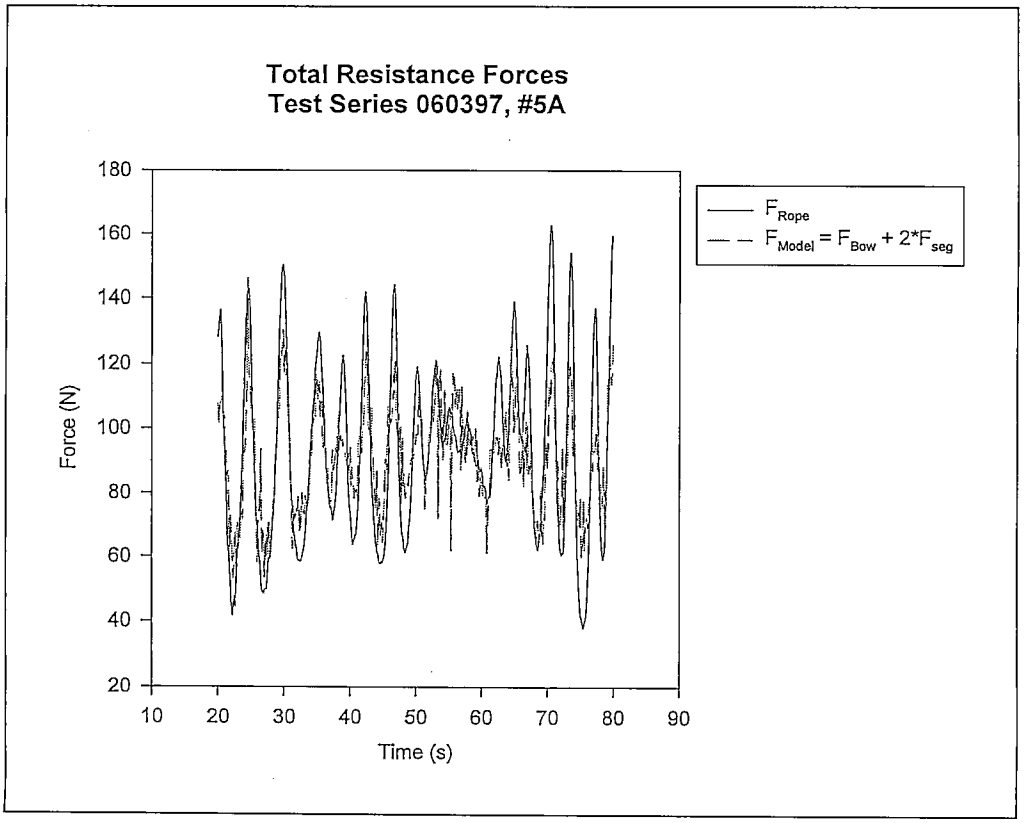
Total Resistance Forces
Test Series 060397, #5A
Force (N)
Time (s)
180
160
140
120
100
80
60
40
20
10
20
30
40
50
60
70
80
90
F Rope
F Model = F Bow + 2*F seg

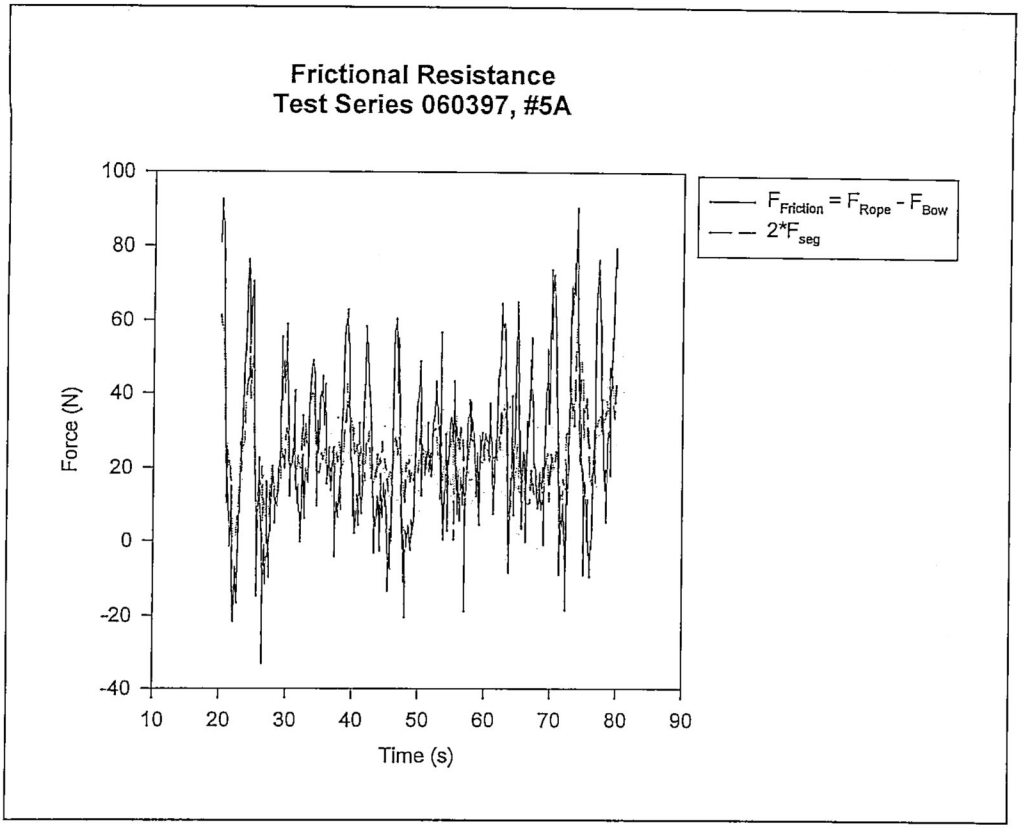
Frictional Resistance
Test Series 060397, #5A
Force (N)
Time (s)
100
80
60
40
20
0
-20
-40
10
20
30
40
50
60
70
80
90
F Friction = F Rope - F Bow
2*F seg

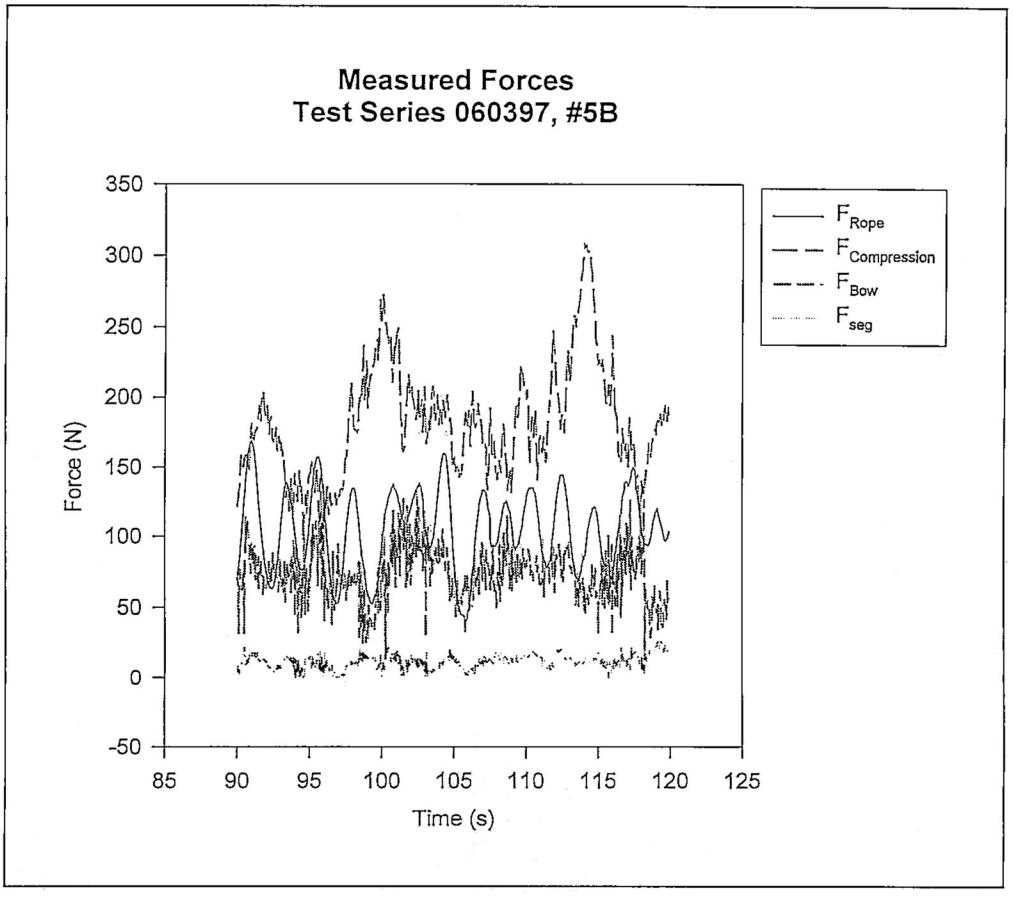
Measured Forces
Test Series 060397, #5B
Force (N)
Time (s)
350
300
250
200
150
100
50
0
-50
85
90
95
100
105
110
115
120
125
F Rope
F Compression
F Bow
F seg

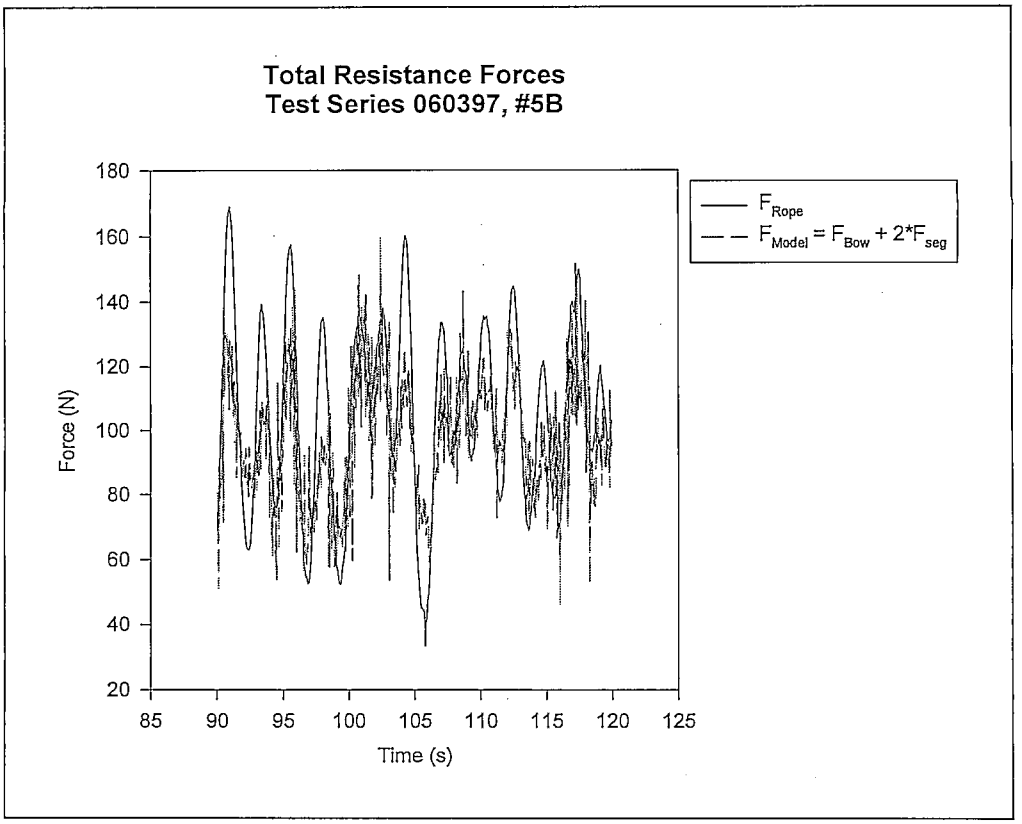
Total Resistance Forces
Test Series 060397, #5B
Force (N)
Time (s)
180
160
140
120
100
80
60
40
20
85
90
95
100
105
110
115
120
125
F_Rope
F_Model = F_Bow + 2*F_seg

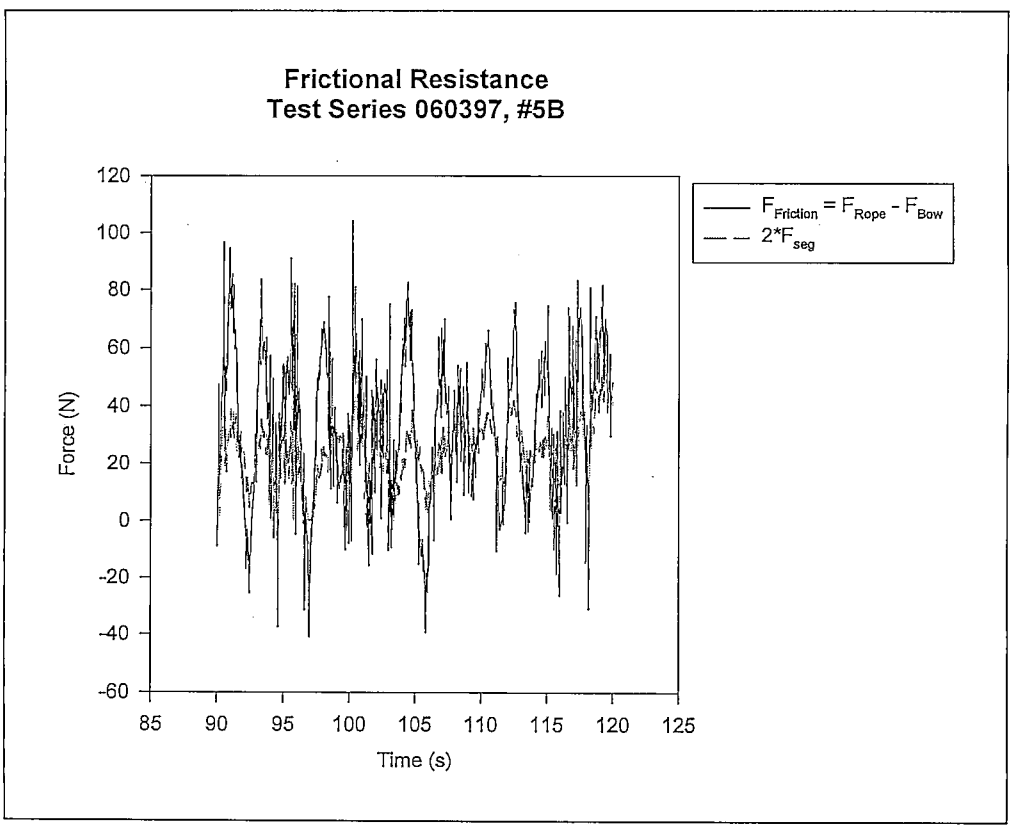
Frictional Resistance
Test Series 060397, #5B
Force (N)
Time (s)
120
100
80
60
40
20
0
-20
-40
-60
85
90
95
100
105
110
115
120
125
F_Friction = F_Rope - F_Bow
2*F_seg

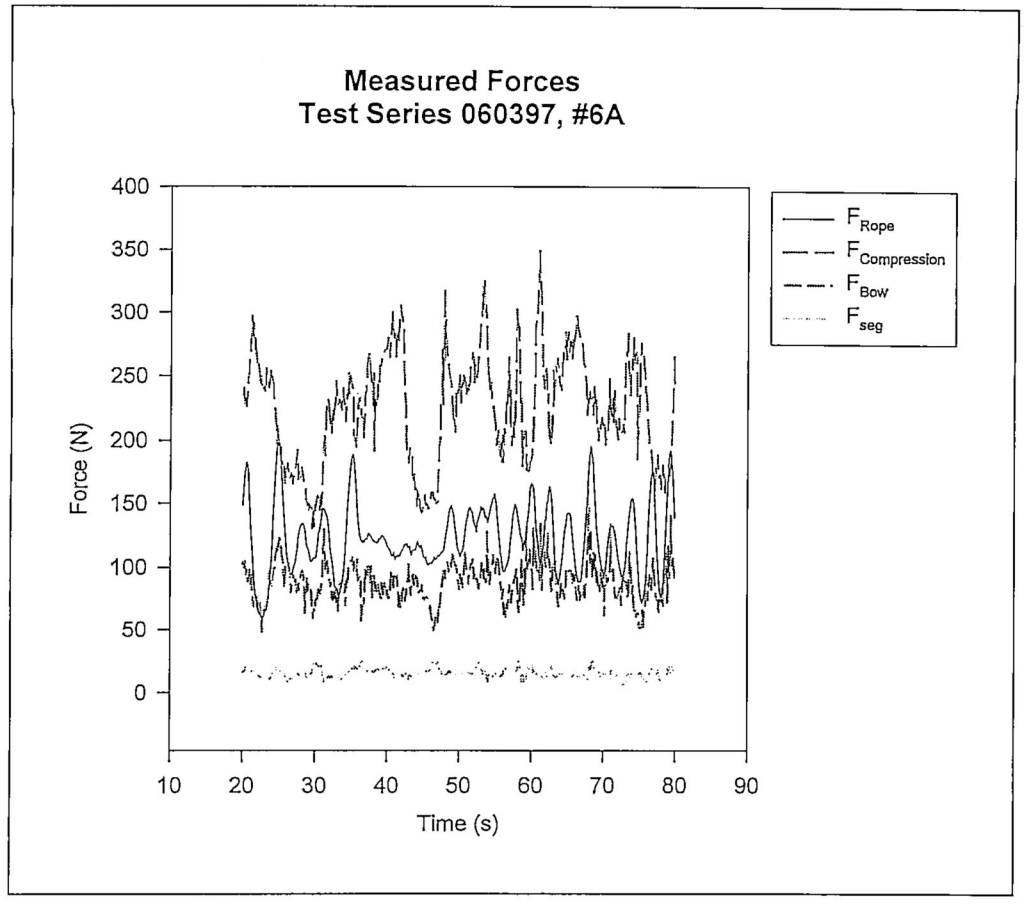
Measured Forces
Test Series 060397, #6A
Force (N)
Time (s)
400
350
300
250
200
150
100
50
0
10
20
30
40
50
60
70
80
90
F Rope
F Compression
F Bow
F seg

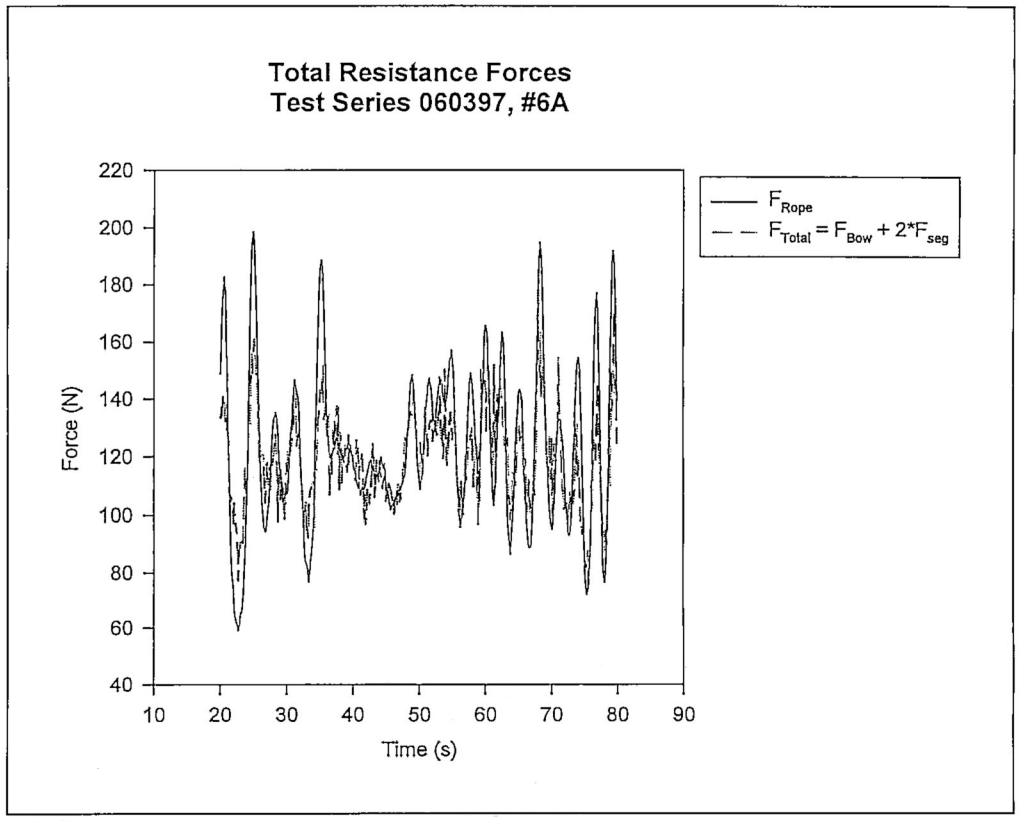
Total Resistance Forces
Test Series 060397, #6A
Force (N)
Time (s)
220
200
180
160
140
120
100
80
60
40
10
20
30
40
50
60
70
80
90
F Rope
F Total = F Bow + 2*F seg

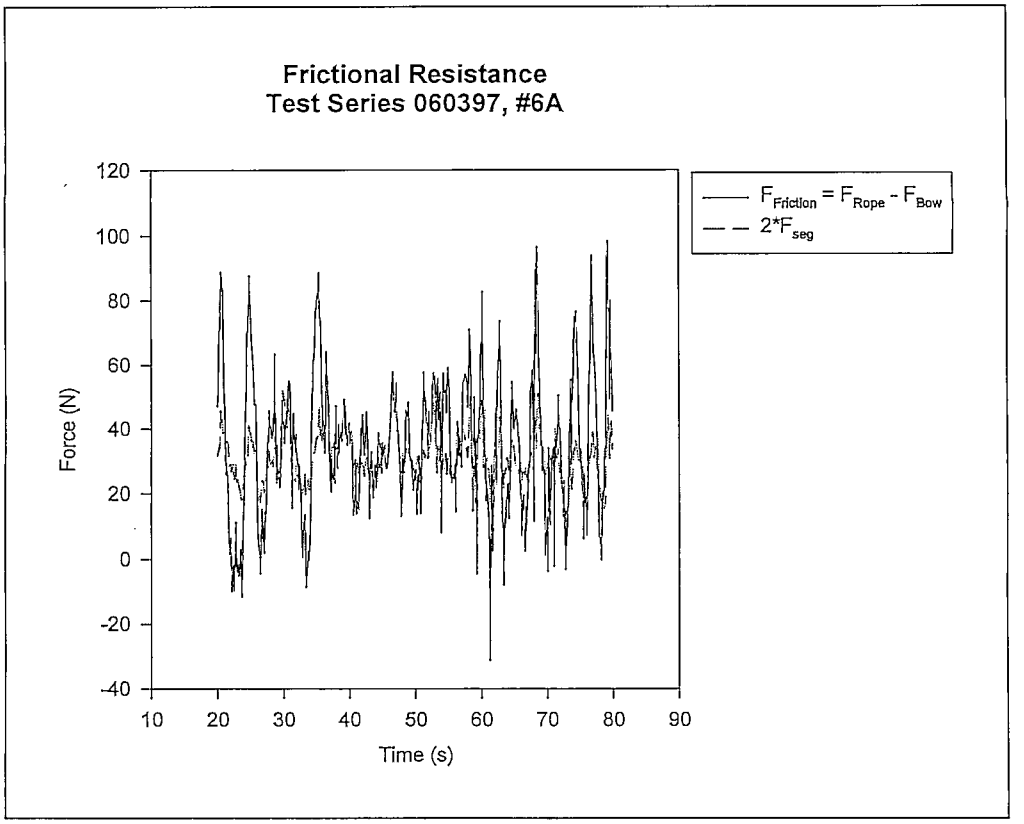
Frictional Resistance
Test Series 060397, #6A
Force (N)
Time (s)
120
100
80
60
40
20
0
-20
-40
10
20
30
40
50
60
70
80
90
F_Friction = F_Rope - F_Bow
2*F_seg

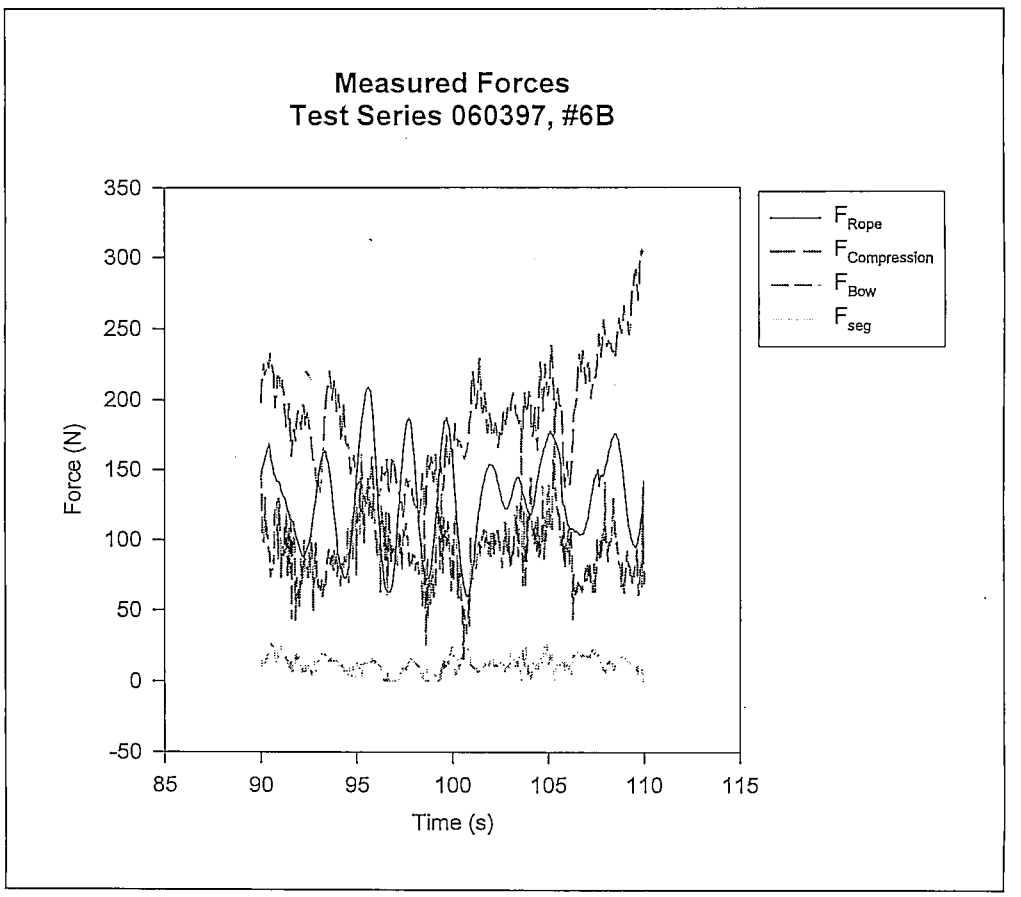
Measured Forces
Test Series 060397, #6B
Force (N)
Time (s)
350
300
250
200
150
100
50
0
-50
85
90
95
100
105
110
115
F_Rope
F_Compression
F_Bow
F_seg

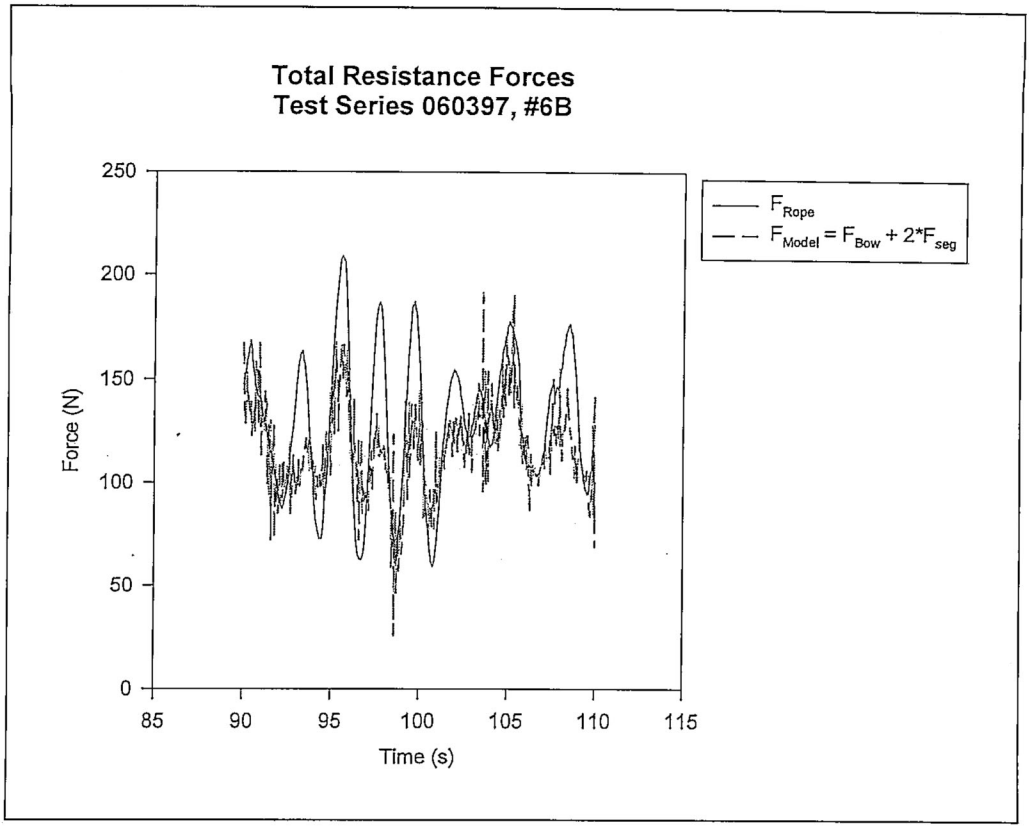
Total Resistance Forces
Test Series 060397, #6B
Force (N)
Time (s)
250
200
150
100
50
0
85
90
95
100
105
110
115
F_Rope
F_Model = F_Bow + 2*F_seg

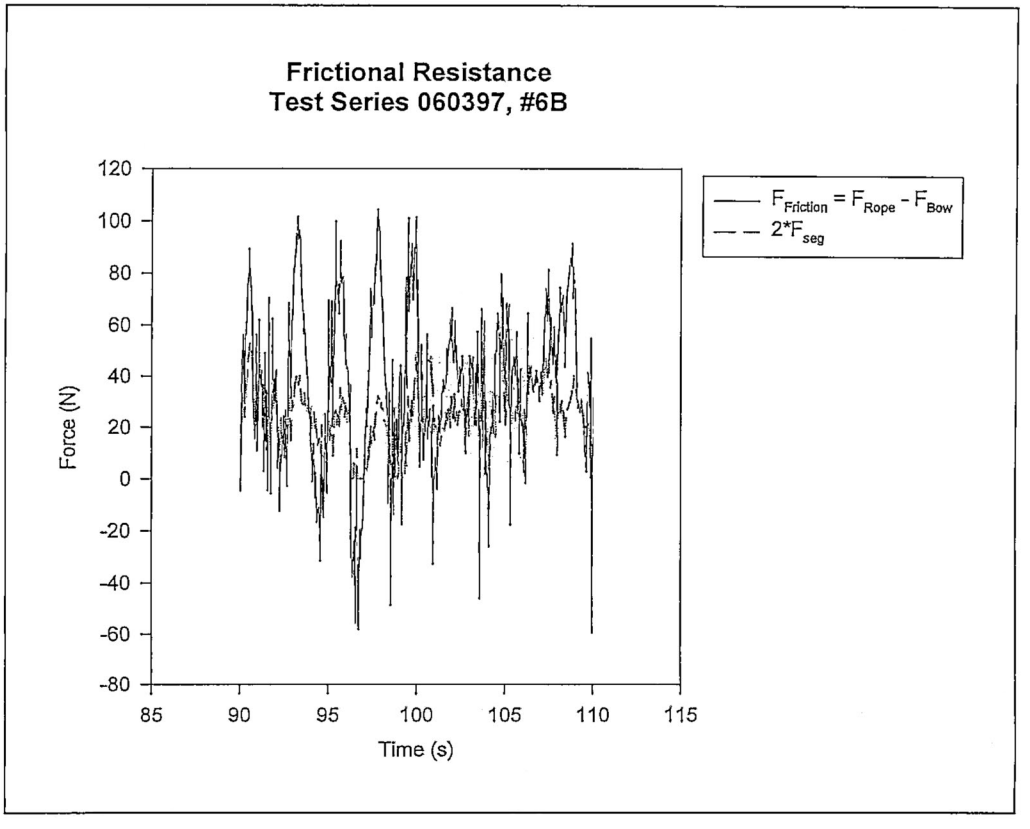
Frictional Resistance
Test Series 060397, #6B
Force (N)
Time (s)
120
100
80
60
40
20
0
-20
-40
-60
-80
85
90
95
100
105
110
115
F_Friction = F_Rope - F_Bow
2*F_seg

APPENDIX B.2

BAR CHARTS FOR SEGMENTED MODEL

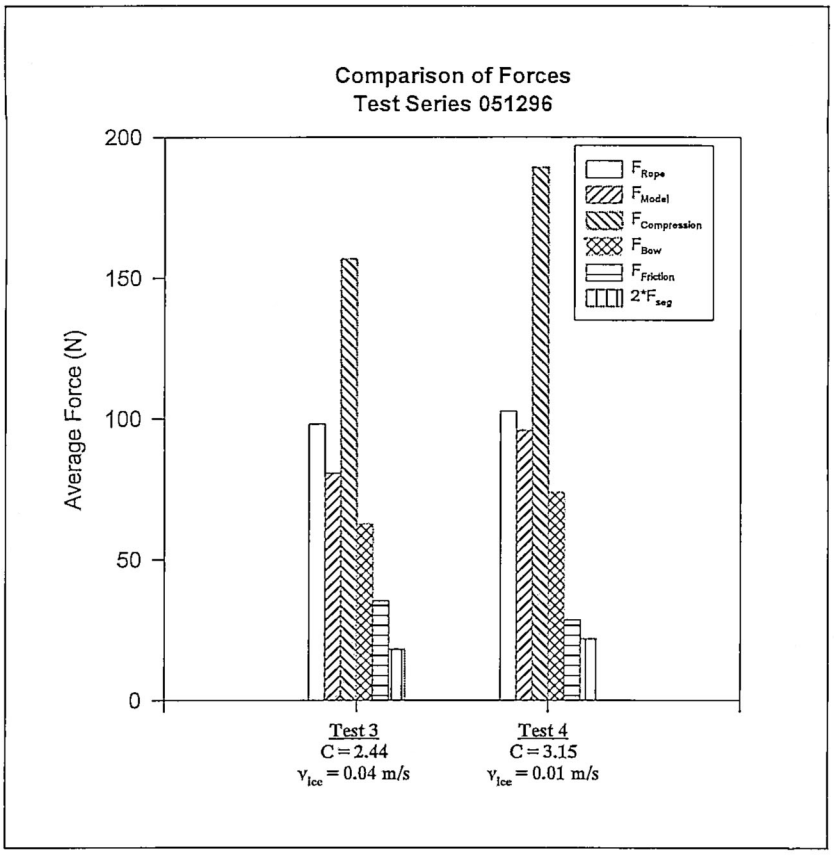
Comparison of Forces
Test Series 051296
Average Force (N)
200
150
100
50
0
F Rope
F Model
F Compression
F Bow
F Friction
2*F seg
Test 3
C = 2.44
v Ice = 0.04 m/s
Test 4
C = 3.15
v Ice = 0.01 m/s

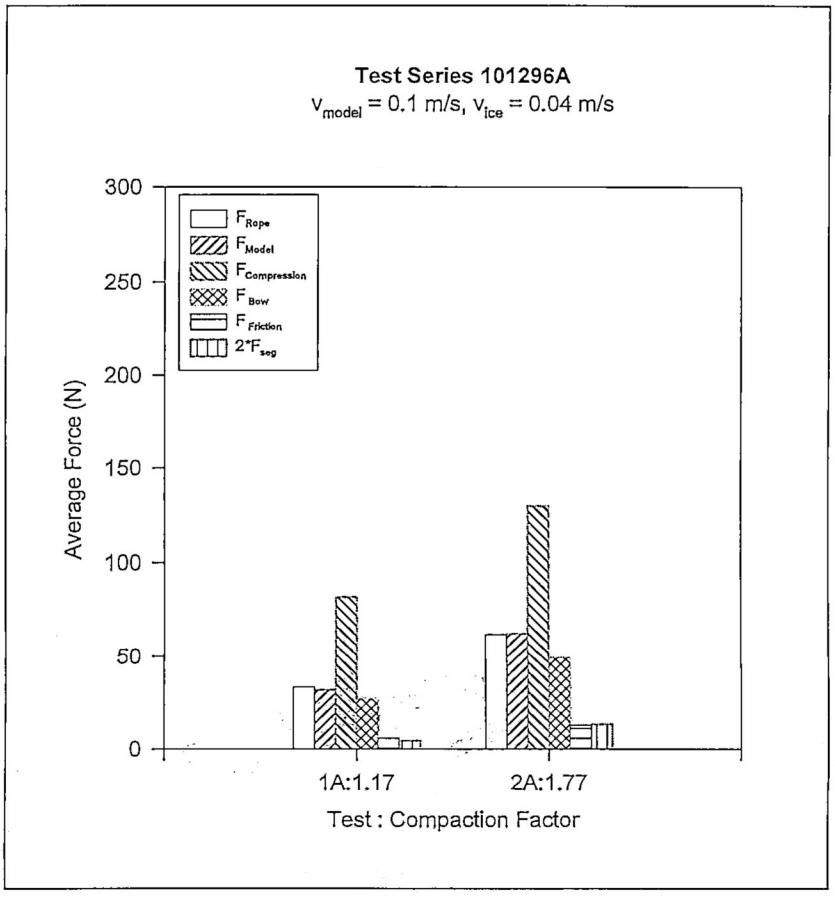
Test Series 101296A
v model = 0.1 m/s, v Ice = 0.04 m/s
Average Force (N)
300
250
200
150
100
50
0
F Rope
F Model
F Compression
F Bow
F Friction
2*F seg
1A:1.17
2A:1.77
Test : Compaction Factor

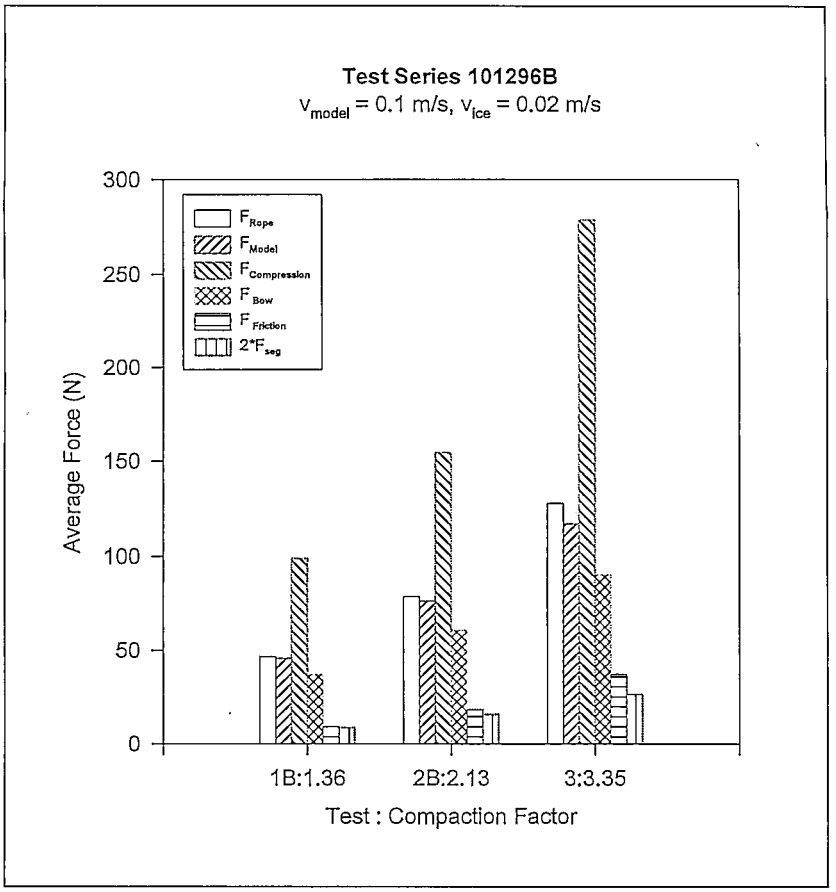
Test Series 101296B
v_{model} = 0.1 m/s, v_{ice} = 0.02 m/s
Average Force (N)
300
250
200
150
100
50
0
F_{Rope}
F_{Model}
$F_{Compression}$
F_{Bow}
$F_{Friction}$
$2*F_{seg}$
1B:1.36
2B:2.13
3:3.35
Test : Compaction Factor

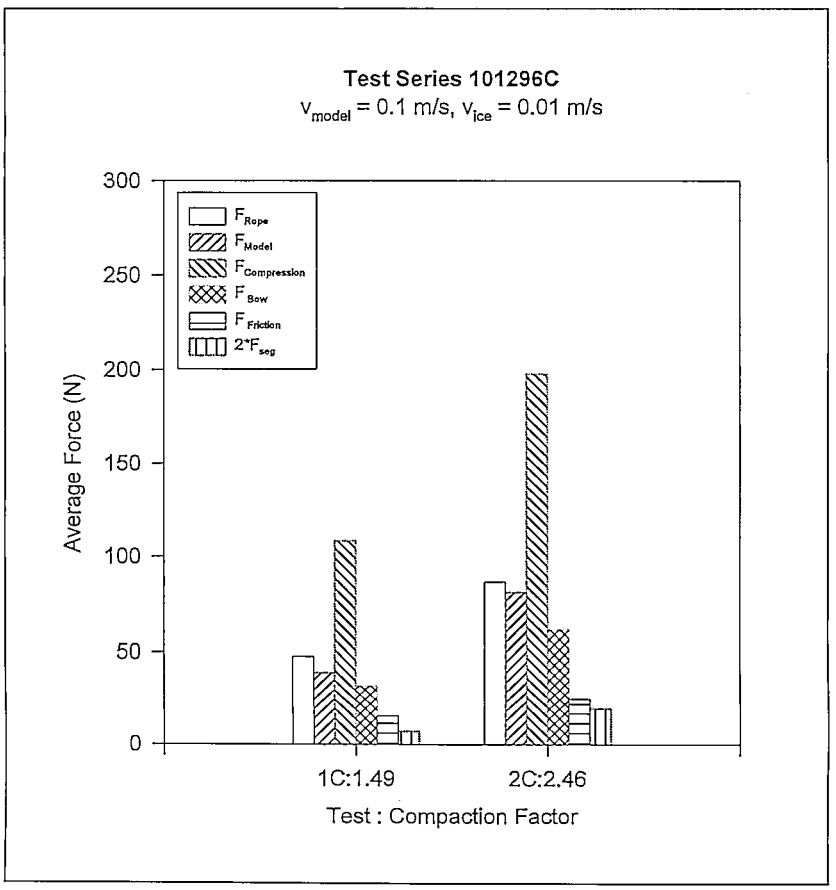
Test Series 101296C
v_{model} = 0.1 m/s, v_{ice} = 0.01 m/s
Average Force (N)
300
250
200
150
100
50
0
F_{Rope}
F_{Model}
$F_{Compression}$
F_{Bow}
$F_{Friction}$
$2*F_{seg}$
1C:1.49
2C:2.46
Test : Compaction Factor

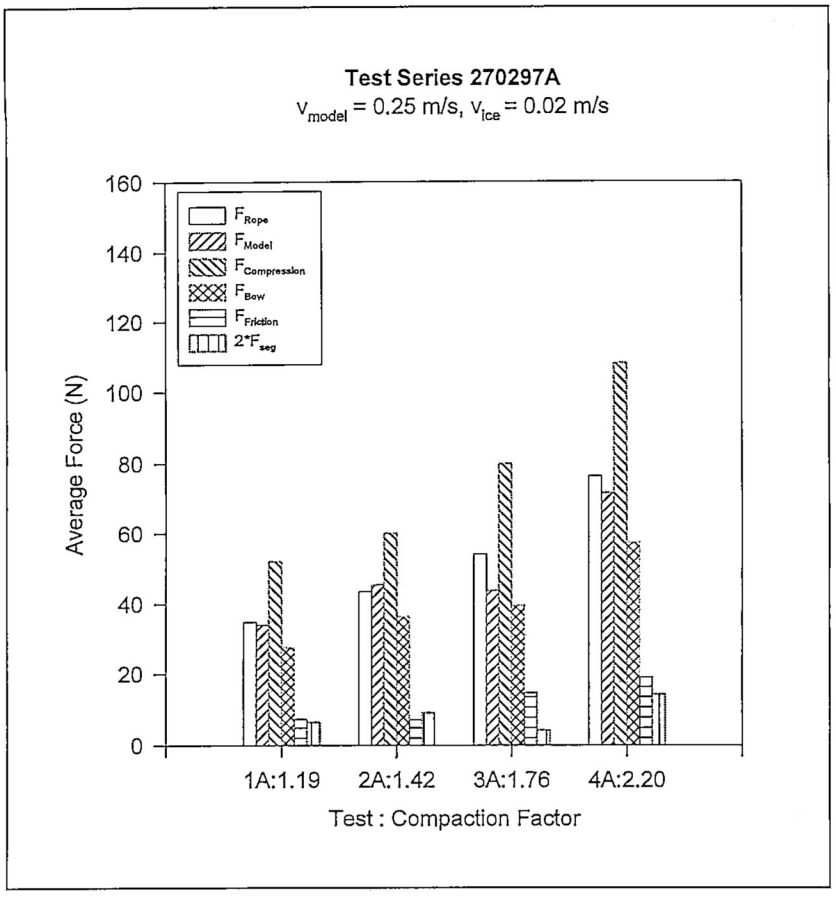
Test Series 270297A
v_{model} = 0.25 m/s, v_{ice} = 0.02 m/s
Average Force (N)
0
20
40
60
80
100
120
140
160
F_{Rope}
F_{Model}
$F_{Compression}$
F_{Bow}
$F_{Friction}$
$2*F_{seg}$
1A:1.19
2A:1.42
3A:1.76
4A:2.20
Test : Compaction Factor

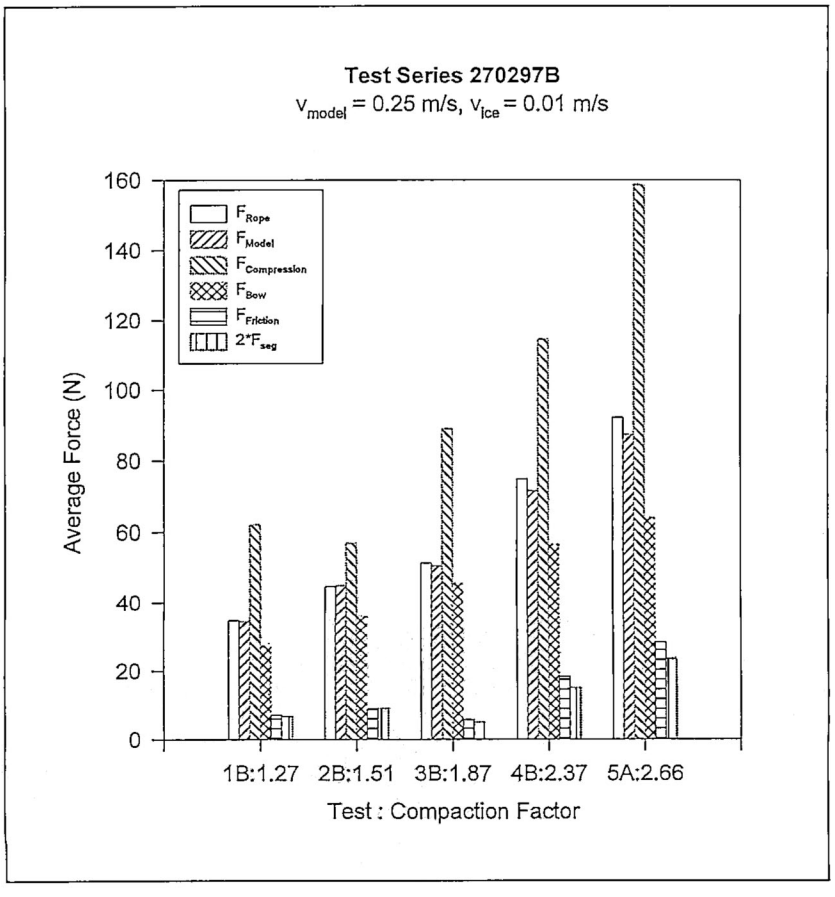
Test Series 270297B
v_{model} = 0.25 m/s, v_{ice} = 0.01 m/s
Average Force (N)
0
20
40
60
80
100
120
140
160
F_{Rope}
F_{Model}
$F_{Compression}$
F_{Bow}
$F_{Friction}$
$2*F_{seg}$
1B:1.27
2B:1.51
3B:1.87
4B:2.37
5A:2.66
Test : Compaction Factor

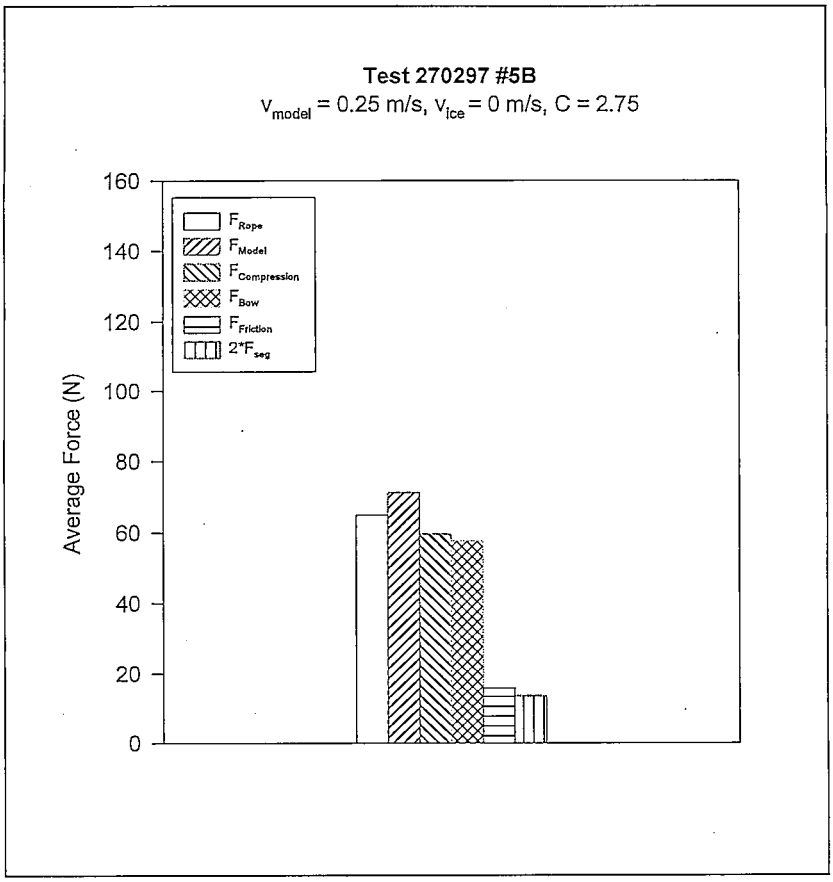
Test 270297 #5B
v_{model} = 0.25 m/s, v_{ice} = 0 m/s, C = 2.75
Average Force (N)
160
140
120
100
80
60
40
20
0
F_{Rope}
F_{Model}
$F_{Compression}$
F_{Bow}
$F_{Friction}$
$2*F_{seg}$

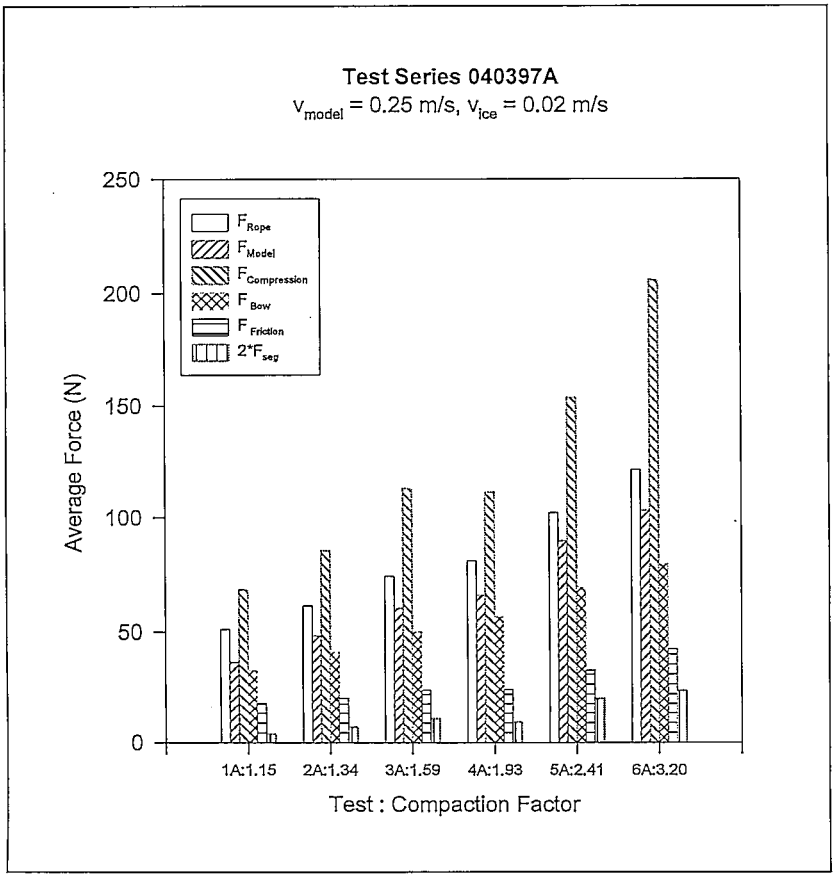
Test Series 040397A
v_{model} = 0.25 m/s, v_{ice} = 0.02 m/s
Average Force (N)
250
200
150
100
50
0
F_{Rope}
F_{Model}
$F_{Compression}$
F_{Bow}
$F_{Friction}$
$2*F_{seg}$
1A:1.15
2A:1.34
3A:1.59
4A:1.93
5A:2.41
6A:3.20
Test : Compaction Factor

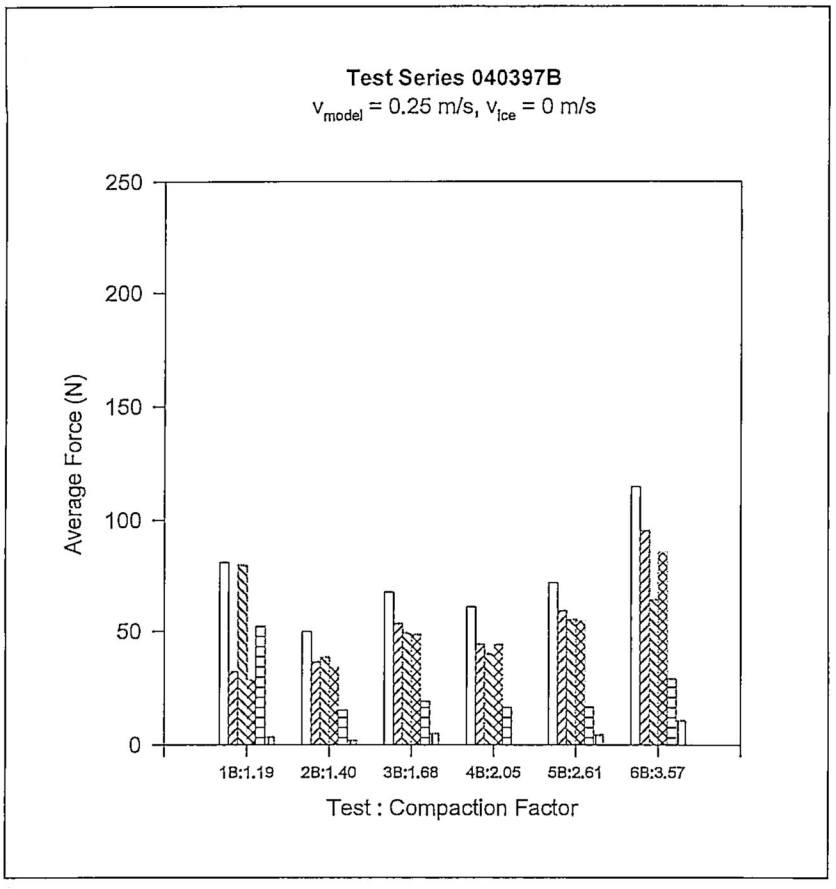
Test Series 040397B
v_{model} = 0.25 m/s, v_{ice} = 0 m/s
Average Force (N)
250
200
150
100
50
0
1B:1.19
2B:1.40
3B:1.68
4B:2.05
5B:2.61
6B:3.57
Test : Compaction Factor

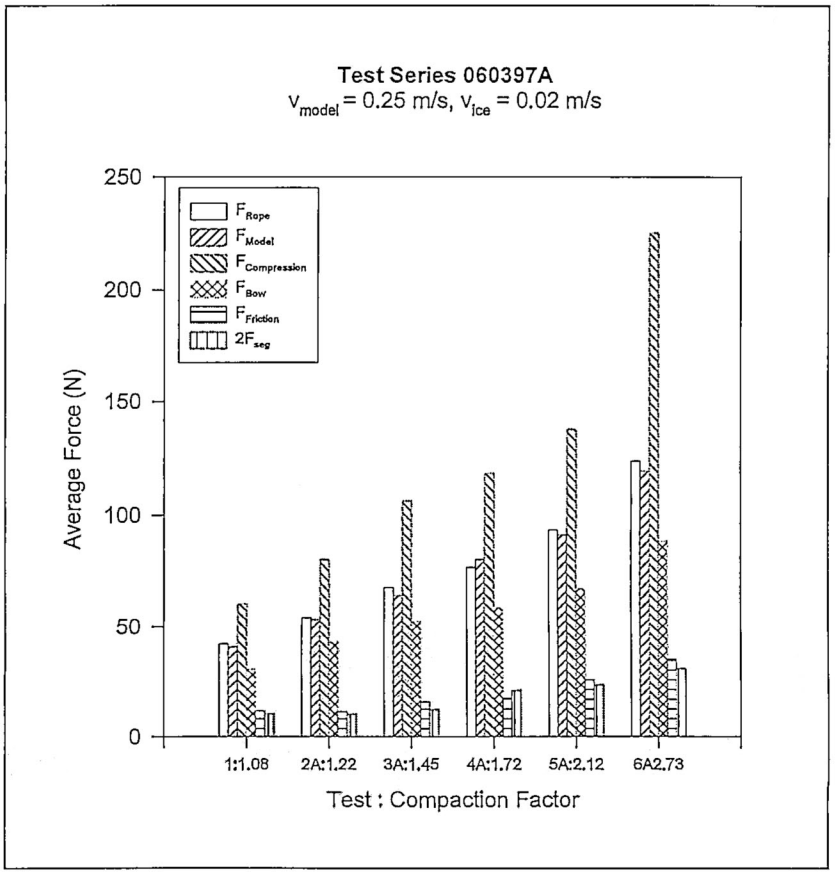
Test Series 060397A
v_{model} = 0.25 m/s, v_{ice} = 0.02 m/s
F_{Rope}
F_{Model}
$F_{Compression}$
F_{Bow}
$F_{Friction}$
$2F_{seg}$
Average Force (N)
250
200
150
100
50
0
1:1.08
2A:1.22
3A:1.45
4A:1.72
5A:2.12
6A2.73
Test : Compaction Factor

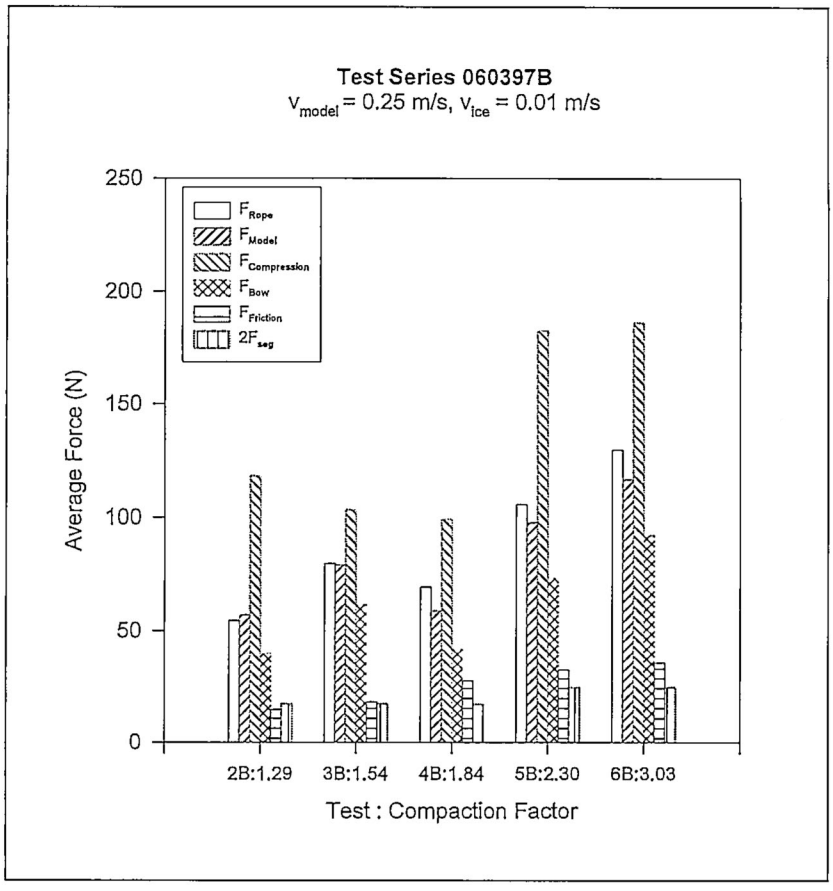
Test Series 060397B
V_{model} = 0.25 m/s, V_{ice} = 0.01 m/s
F_{Rope}
F_{Model}
$F_{Compression}$
F_{Bow}
$F_{Friction}$
$2F_{seg}$
Average Force (N)
250
200
150
100
50
0
2B:1.29
3B:1.54
4B:1.84
5B:2.30
6B:3.03
Test : Compaction Factor

APPENDIX B.3

VARIATIONS IN AVERAGE FORCES WITH ICE VELOCITY FOR SEGMENTED MODEL

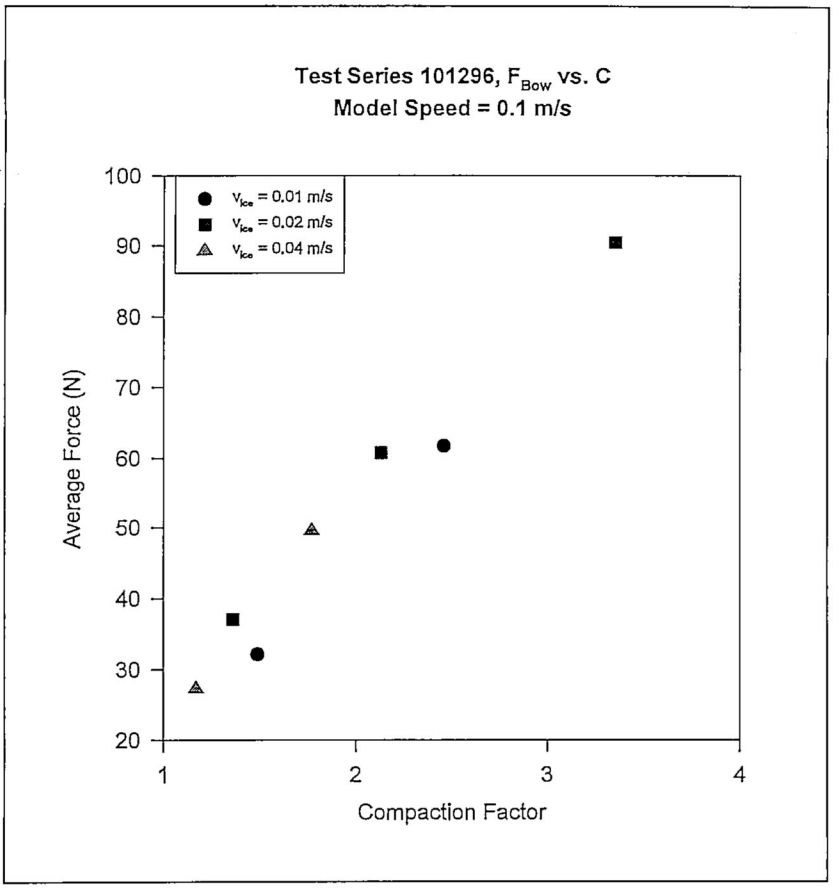
Test Series 101296, F_{Bow} vs. C
Model Speed = 0.1 m/s
v_{ice} = 0.01 m/s
v_{ice} = 0.02 m/s
v_{ice} = 0.04 m/s
Average Force (N)
100
90
80
70
60
50
40
30
20
1
2
3
4
Compaction Factor

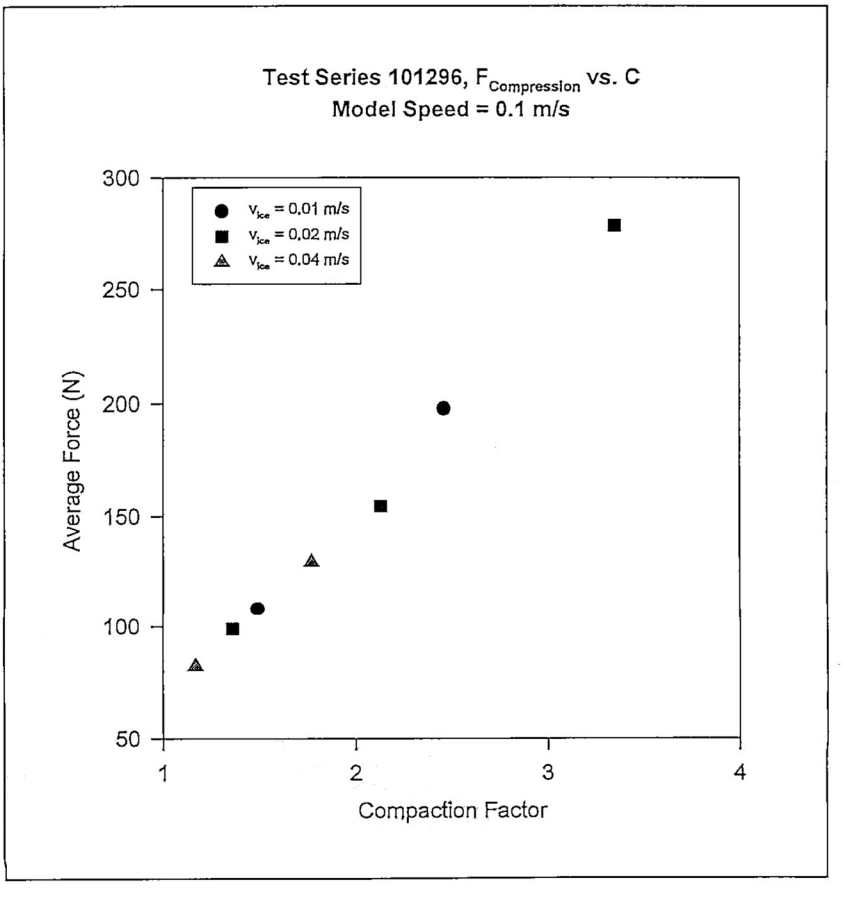
Test Series 101296, $F_{Compression}$ vs. C
Model Speed = 0.1 m/s
v_{ice} = 0.01 m/s
v_{ice} = 0.02 m/s
v_{ice} = 0.04 m/s
Average Force (N)
300
250
200
150
100
50
1
2
3
4
Compaction Factor

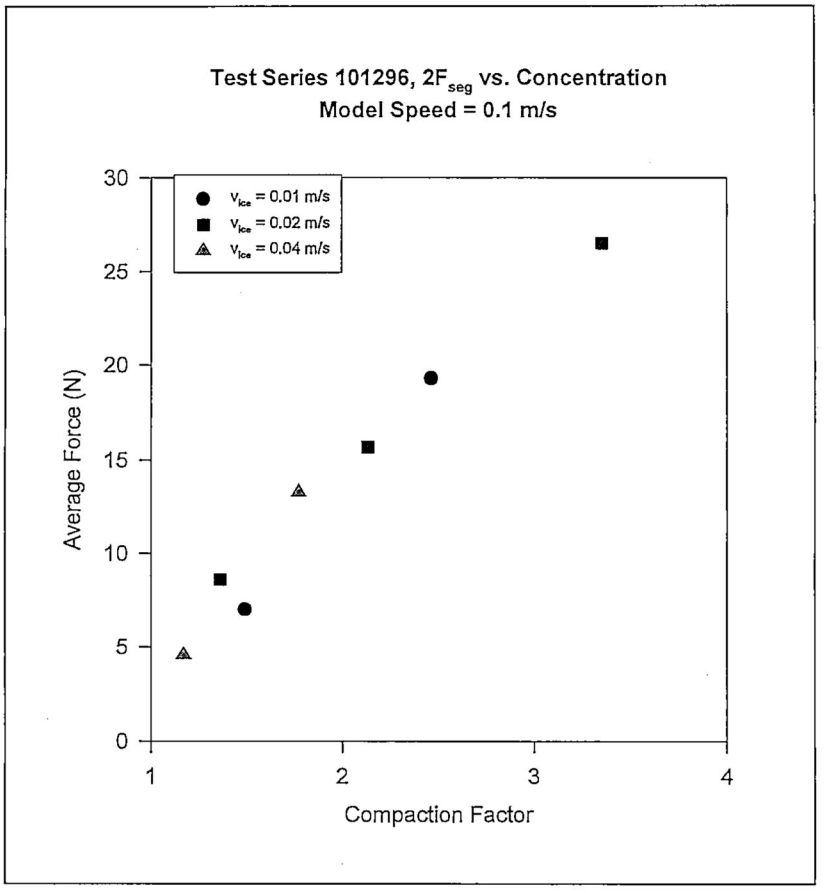
Test Series 101296, 2F$_{seg}$ vs. Concentration
Model Speed = 0.1 m/s
v_{ice} = 0.01 m/s
v_{ice} = 0.02 m/s
v_{ice} = 0.04 m/s
Average Force (N)
Compaction Factor
0
5
10
15
20
25
30
1
2
3
4

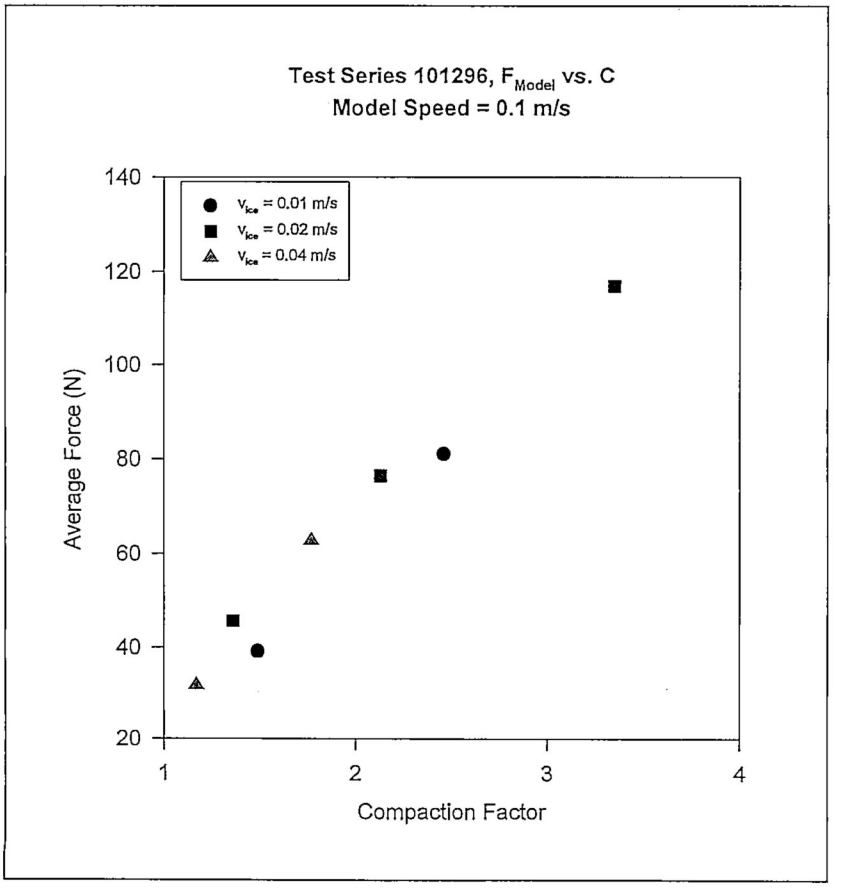
Test Series 101296, F$_{Model}$ vs. C
Model Speed = 0.1 m/s
v_{ice} = 0.01 m/s
v_{ice} = 0.02 m/s
v_{ice} = 0.04 m/s
Average Force (N)
Compaction Factor
20
40
60
80
100
120
140
1
2
3
4

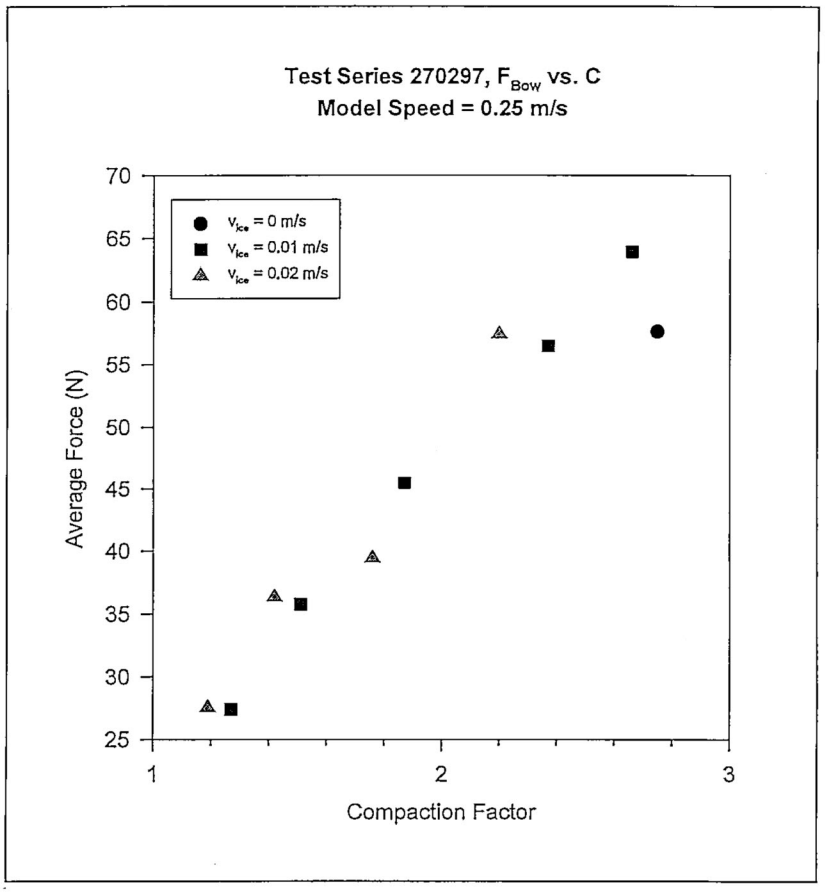
Test Series 270297, F_{Bow} vs. C
Model Speed = 0.25 m/s
v_{ice} = 0 m/s
v_{ice} = 0.01 m/s
v_{ice} = 0.02 m/s
Average Force (N)
70
65
60
55
50
45
40
35
30
25
1
2
3
Compaction Factor

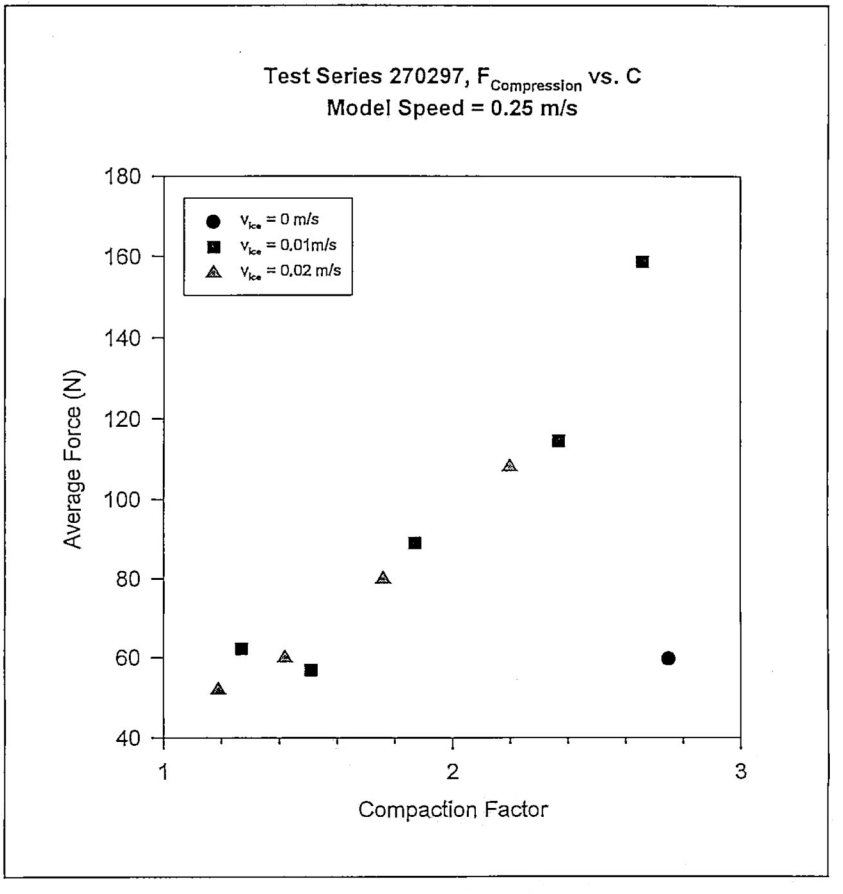
Test Series 270297, $F_{Compression}$ vs. C
Model Speed = 0.25 m/s
v_{ice} = 0 m/s
v_{ice} = 0.01m/s
v_{ice} = 0.02 m/s
Average Force (N)
180
160
140
120
100
80
60
40
1
2
3
Compaction Factor

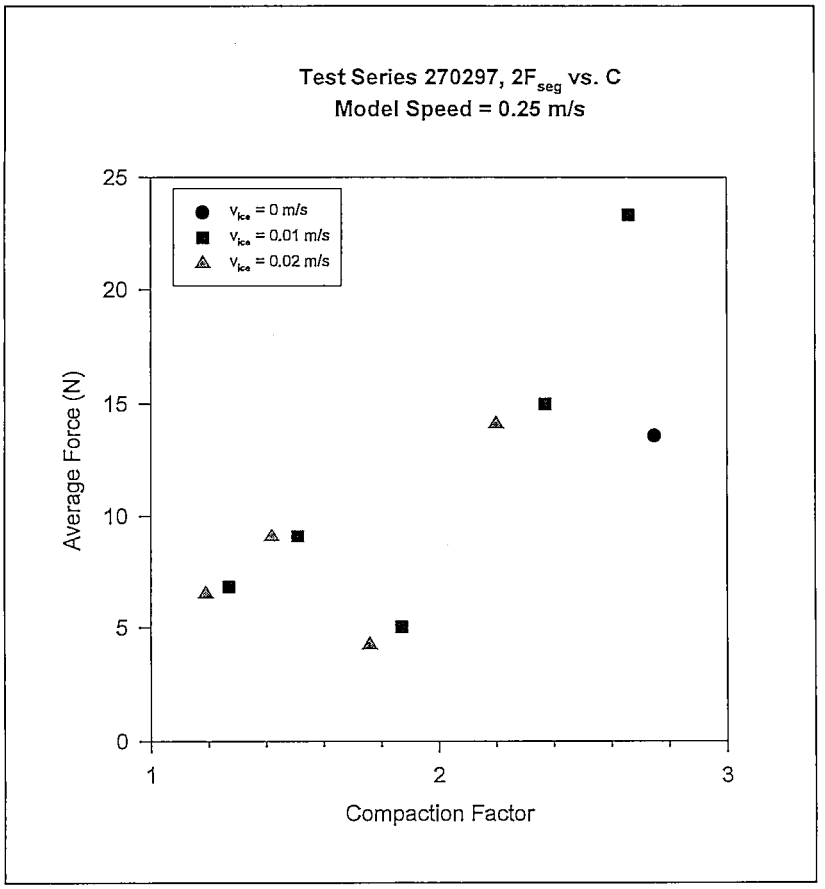
Test Series 270297, 2F$_{seg}$ vs. C
Model Speed = 0.25 m/s
v_{ice} = 0 m/s
v_{ice} = 0.01 m/s
v_{ice} = 0.02 m/s
Average Force (N)
Compaction Factor
0
5
10
15
20
25
1
2
3

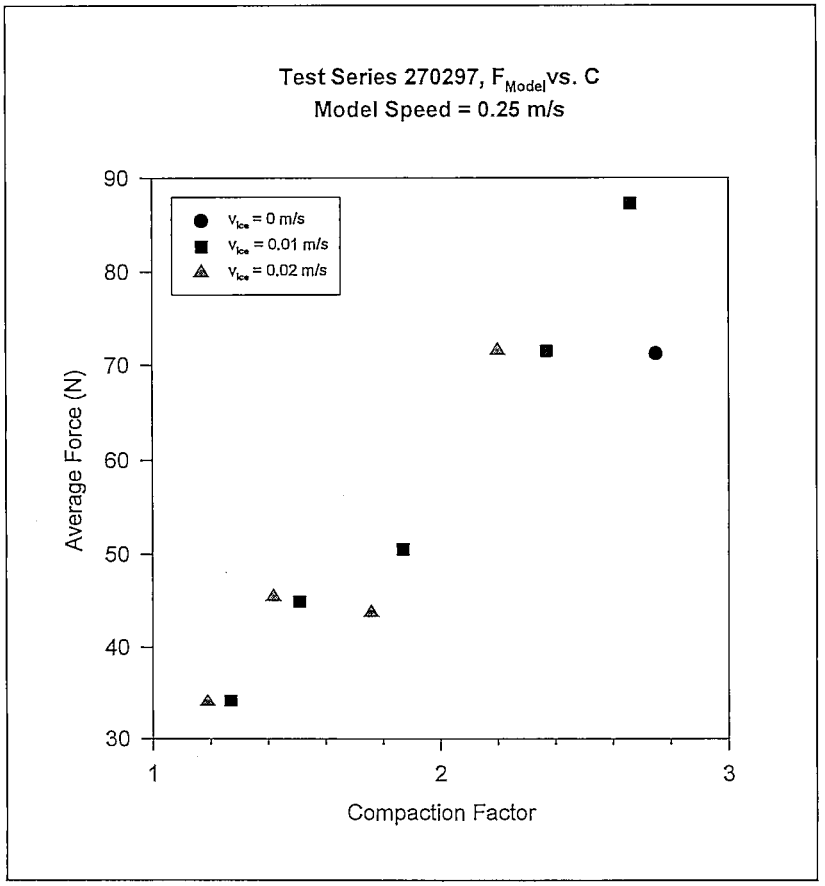
Test Series 270297, F$_{Model}$ vs. C
Model Speed = 0.25 m/s
v_{ice} = 0 m/s
v_{ice} = 0.01 m/s
v_{ice} = 0.02 m/s
Average Force (N)
Compaction Factor
30
40
50
60
70
80
90
1
2
3

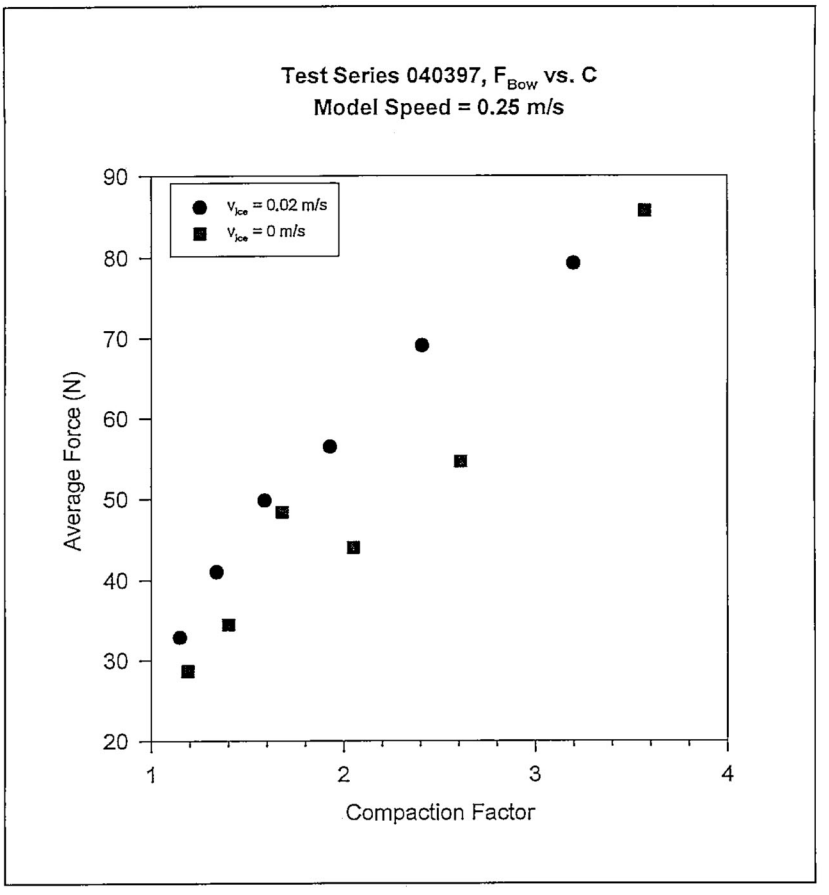
Test Series 040397, F_{Bow} vs. C
Model Speed = 0.25 m/s
v_{Ice} = 0.02 m/s
v_{Ice} = 0 m/s
Average Force (N)
Compaction Factor
90
80
70
60
50
40
30
20
1
2
3
4

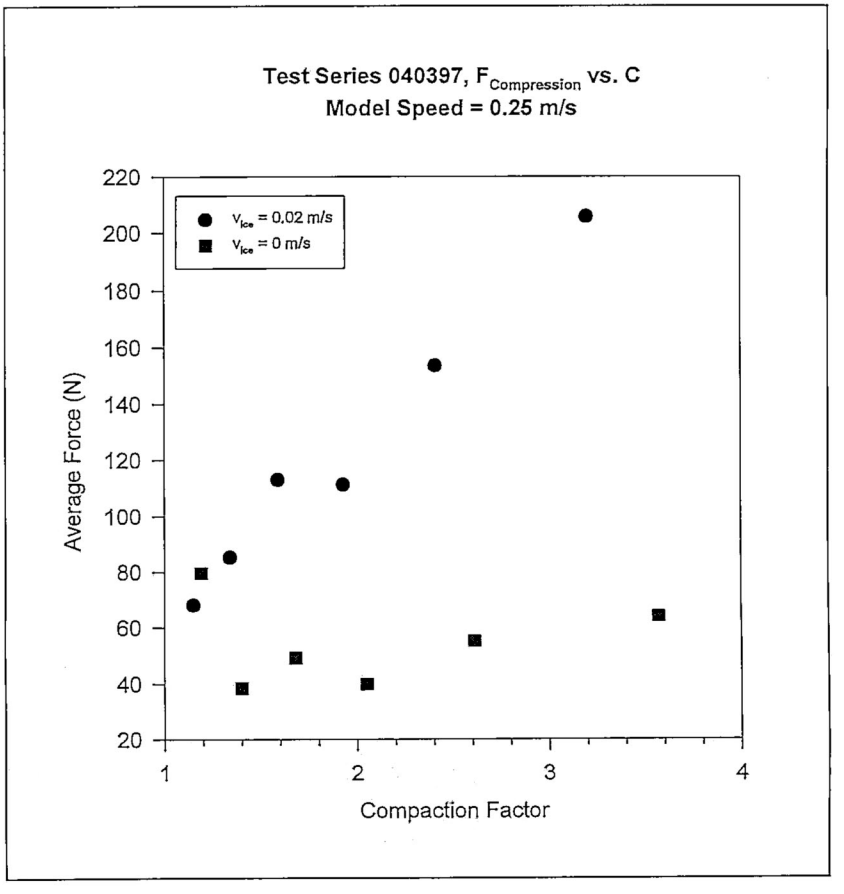
Test Series 040397, $F_{Compression}$ vs. C
Model Speed = 0.25 m/s
v_{Ice} = 0.02 m/s
v_{Ice} = 0 m/s
Average Force (N)
Compaction Factor
220
200
180
160
140
120
100
80
60
40
20
1
2
3
4

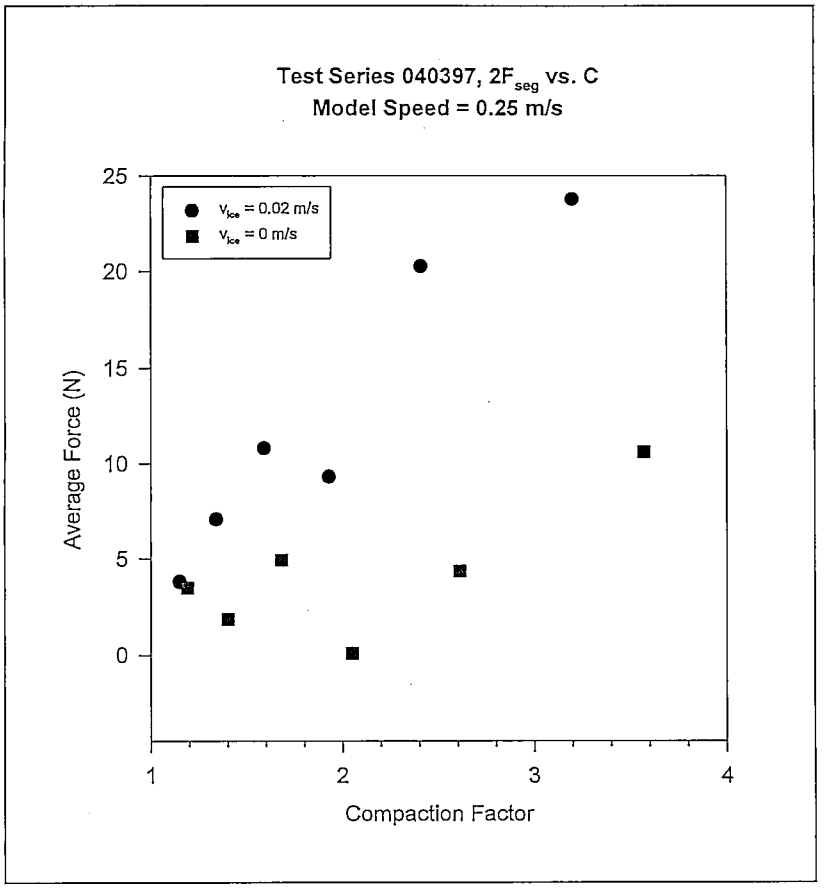
Test Series 040397, 2F$_{seg}$ vs. C
Model Speed = 0.25 m/s
v_{ice} = 0.02 m/s
v_{ice} = 0 m/s
Average Force (N)
Compaction Factor
25
20
15
10
5
0
1
2
3
4

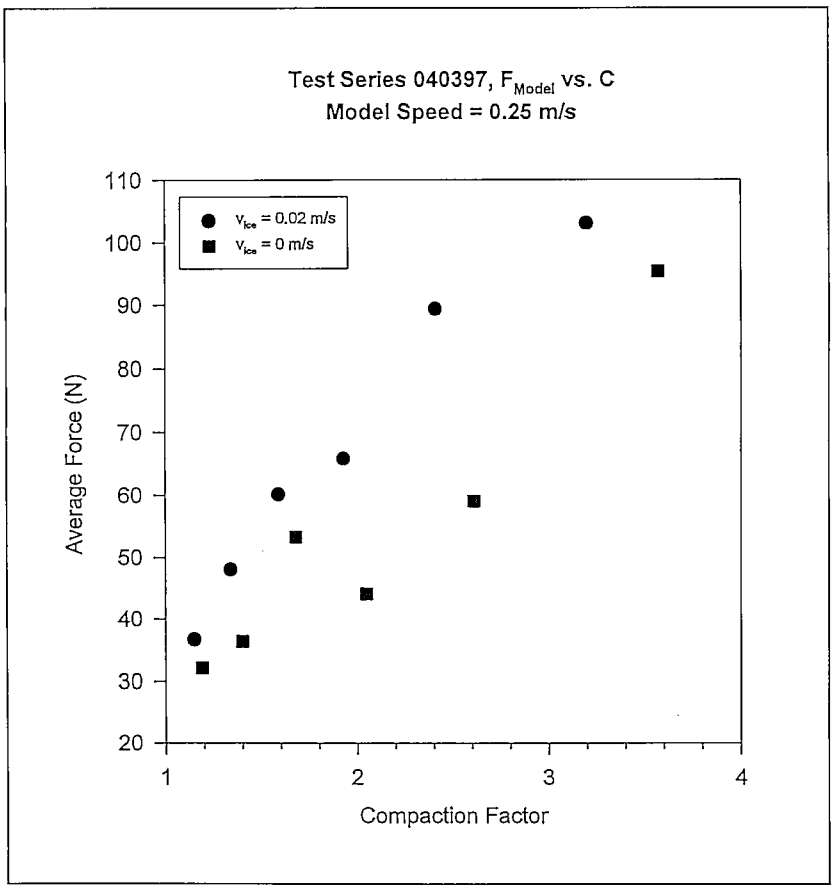
Test Series 040397, F$_{Model}$ vs. C
Model Speed = 0.25 m/s
v_{ice} = 0.02 m/s
v_{ice} = 0 m/s
Average Force (N)
Compaction Factor
110
100
90
80
70
60
50
40
30
20
1
2
3
4

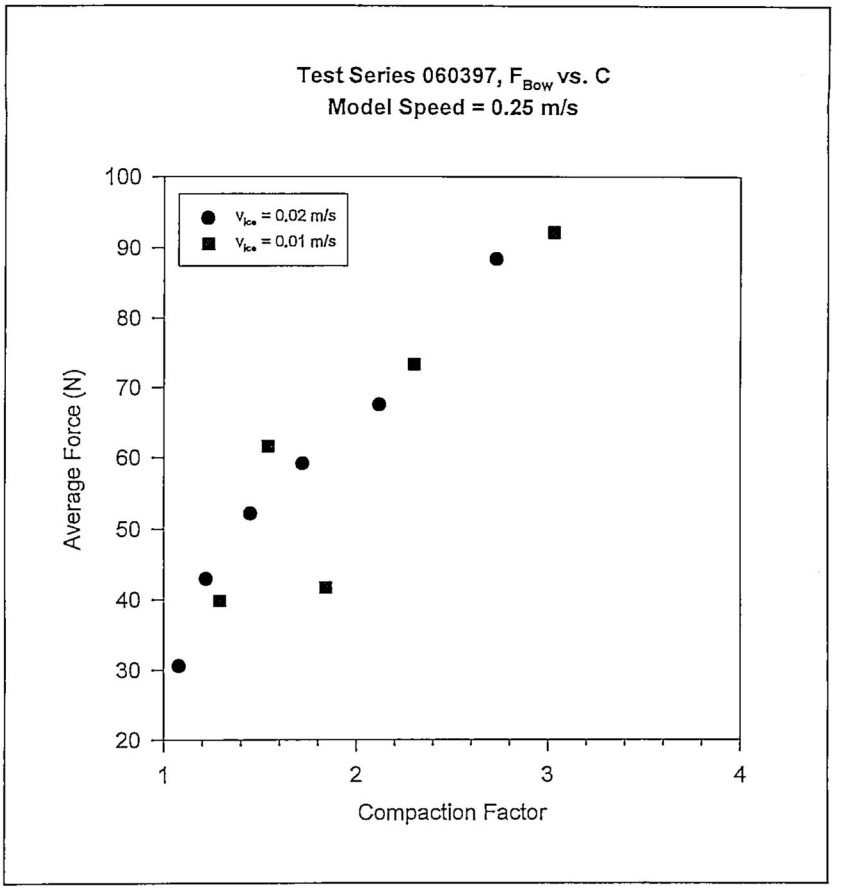
Test Series 060397, F_{Bow} vs. C
Model Speed = 0.25 m/s
v_{ice} = 0.02 m/s
v_{ice} = 0.01 m/s
Average Force (N)
Compaction Factor
100
90
80
70
60
50
40
30
20
1
2
3
4

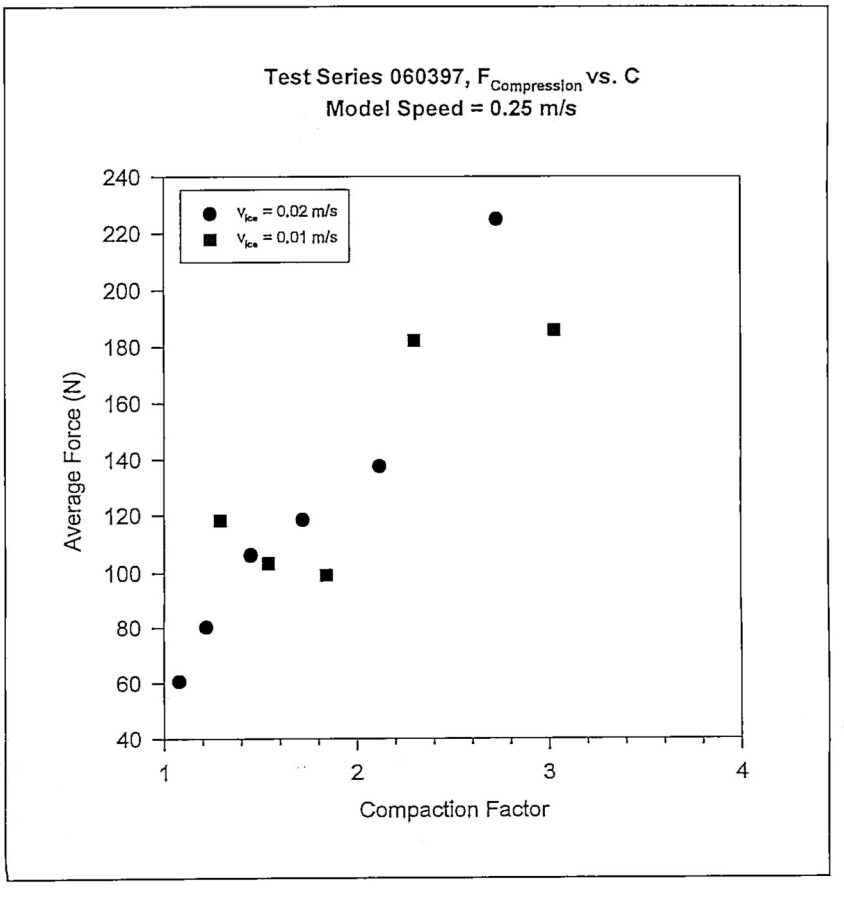
Test Series 060397, $F_{Compression}$ vs. C
Model Speed = 0.25 m/s
v_{ice} = 0.02 m/s
v_{ice} = 0.01 m/s
Average Force (N)
Compaction Factor
240
220
200
180
160
140
120
100
80
60
40
1
2
3
4

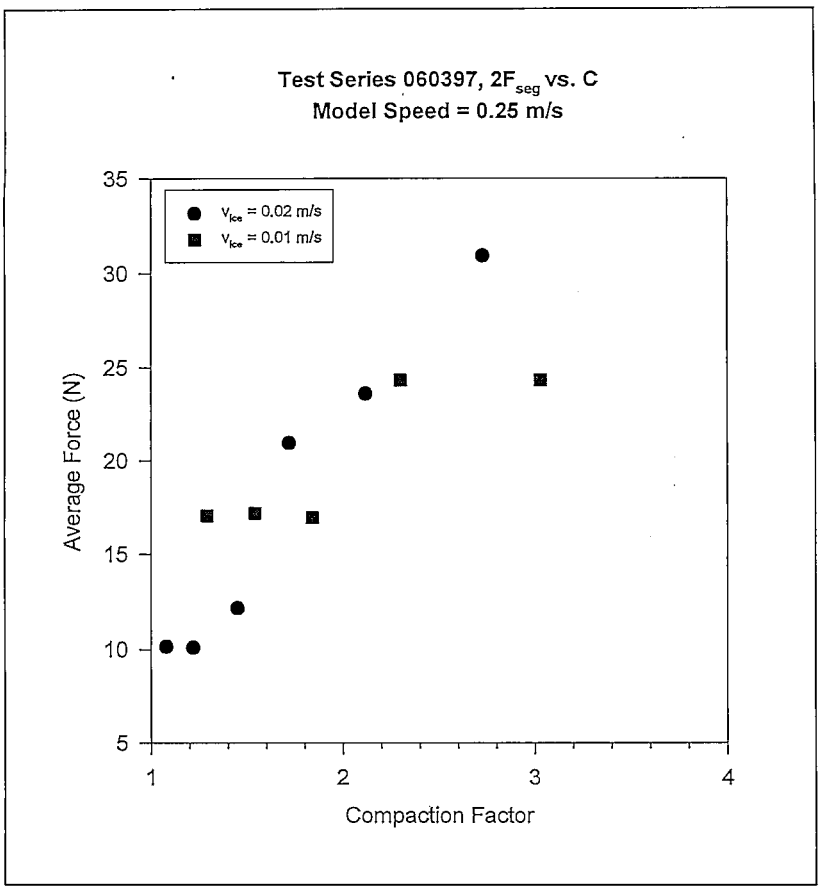
Test Series 060397, 2F$_{seg}$ vs. C
Model Speed = 0.25 m/s
v$_{ice}$ = 0.02 m/s
v$_{ice}$ = 0.01 m/s
Average Force (N)
Compaction Factor
35
30
25
20
15
10
5
1
2
3
4

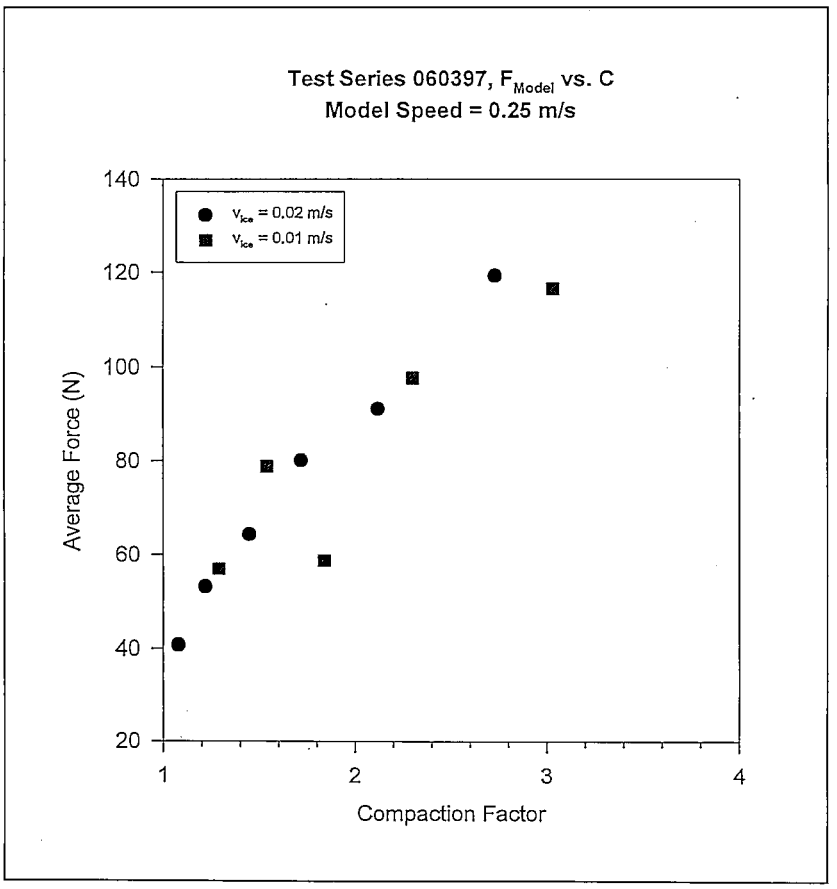
Test Series 060397, F$_{Model}$ vs. C
Model Speed = 0.25 m/s
v$_{ice}$ = 0.02 m/s
v$_{ice}$ = 0.01 m/s
Average Force (N)
Compaction Factor
140
120
100
80
60
40
20
1
2
3
4

APPENDIX B.4

COMPARISON OF BOW AND COMPRESSIVE FORCES FOR SEGMENTED MODEL

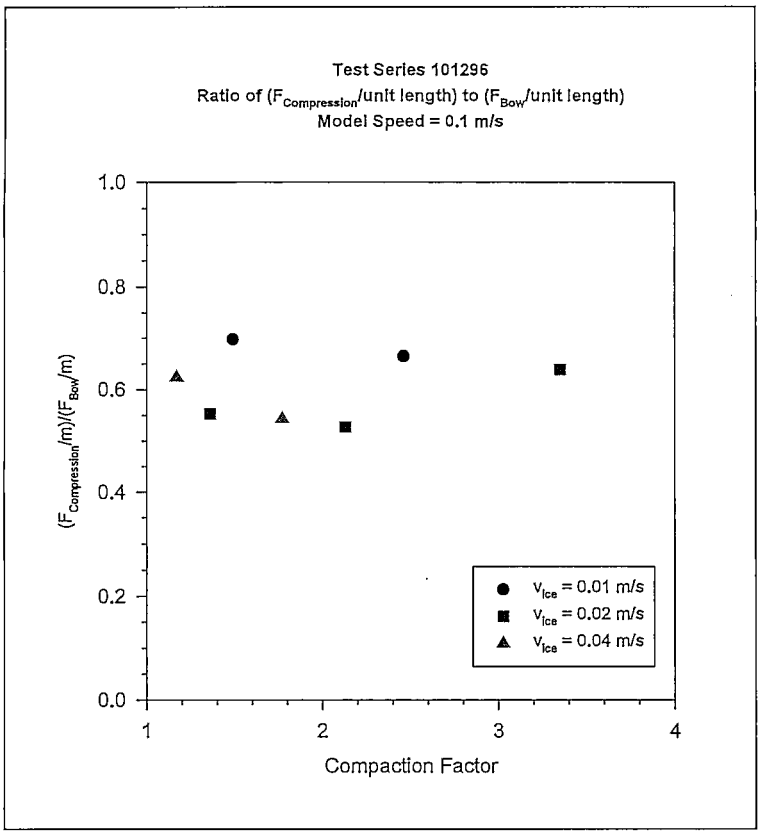
Test Series 101296
Ratio of ($F_{Compression}$/unit length) to (F_{Bow}/unit length)
Model Speed = 0.1 m/s
$(F_{Compression}/m)/(F_{Bow}/m)$
1.0
0.8
0.6
0.4
0.2
0.0
1
2
3
4
Compaction Factor
v_{Ice} = 0.01 m/s
v_{Ice} = 0.02 m/s
v_{Ice} = 0.04 m/s

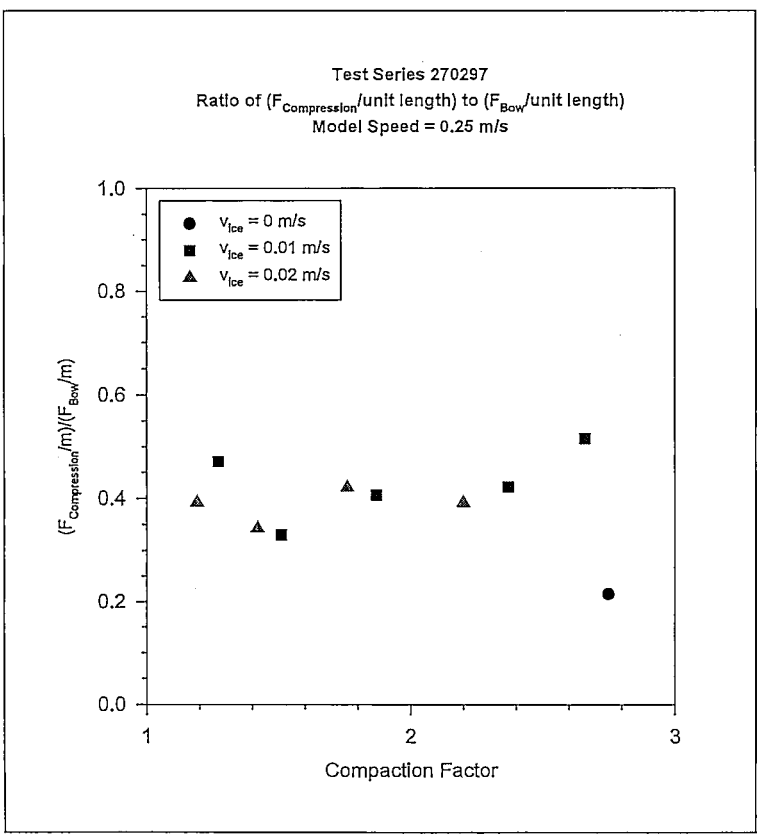
Test Series 270297
Ratio of ($F_{Compression}$/unit length) to (F_{Bow}/unit length)
Model Speed = 0.25 m/s
$(F_{Compression}/m)/(F_{Bow}/m)$
1.0
0.8
0.6
0.4
0.2
0.0
1
2
3
Compaction Factor
v_{Ice} = 0 m/s
v_{Ice} = 0.01 m/s
v_{Ice} = 0.02 m/s

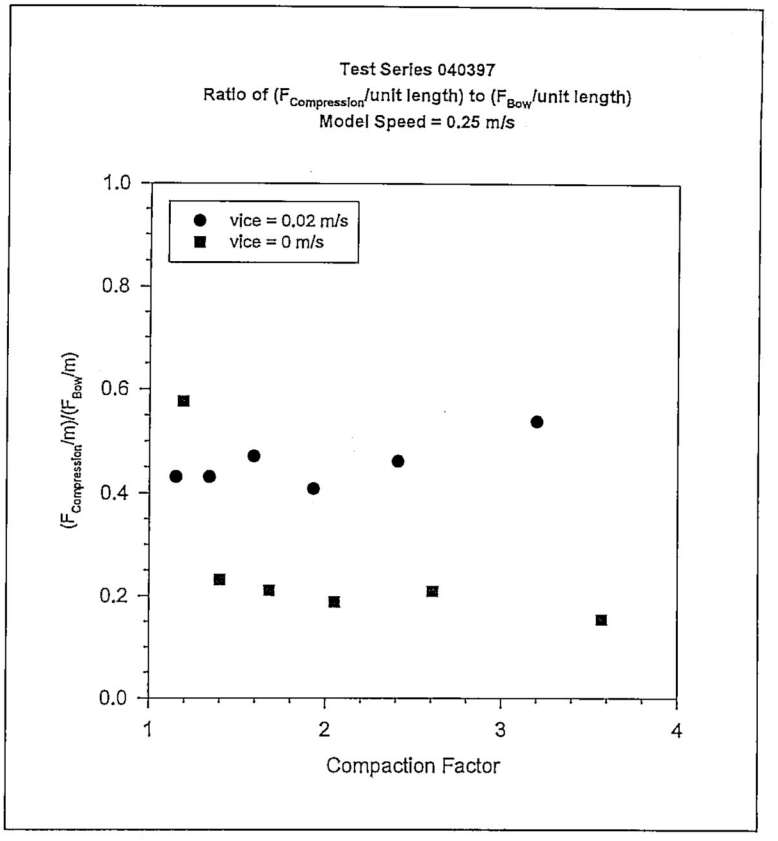
Test Series 040397
Ratio of ($F_{Compression}$/unit length) to (F_{Bow}/unit length)
Model Speed = 0.25 m/s
vice = 0.02 m/s
vice = 0 m/s
($F_{Compression}$/m)/(F_{Bow}/m)
1.0
0.8
0.6
0.4
0.2
0.0
1
2
3
4
Compaction Factor

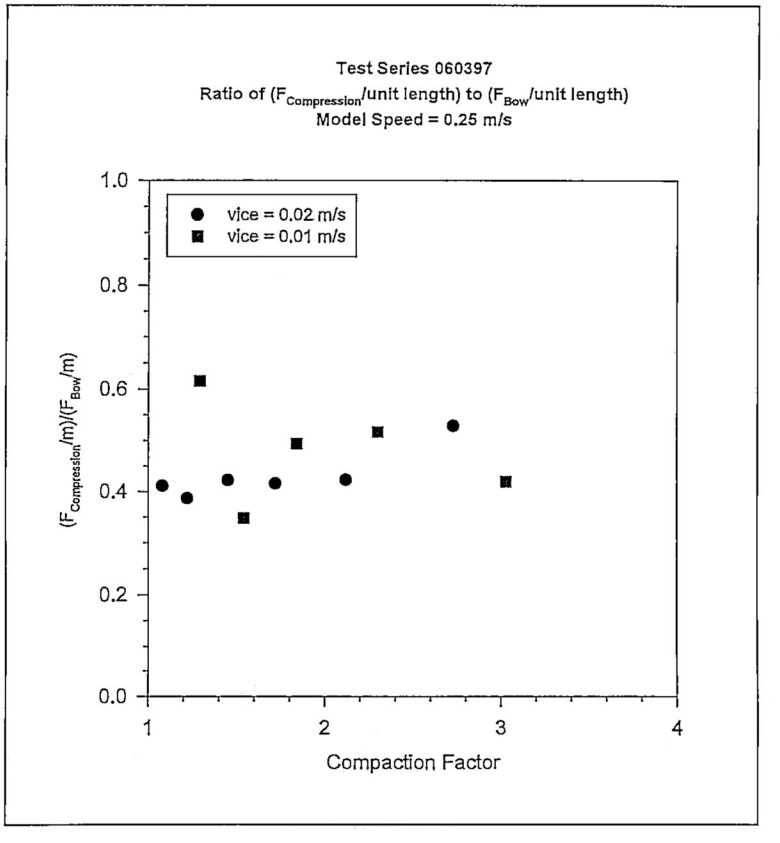
Test Series 060397
Ratio of ($F_{Compression}$/unit length) to (F_{Bow}/unit length)
Model Speed = 0.25 m/s
vice = 0.02 m/s
vice = 0.01 m/s
($F_{Compression}$/m)/(F_{Bow}/m)
1.0
0.8
0.6
0.4
0.2
0.0
1
2
3
4
Compaction Factor

APPENDIX B.5

BOW/FRICTION FORCE VARIATIONS FOR SEGMENTED MODEL

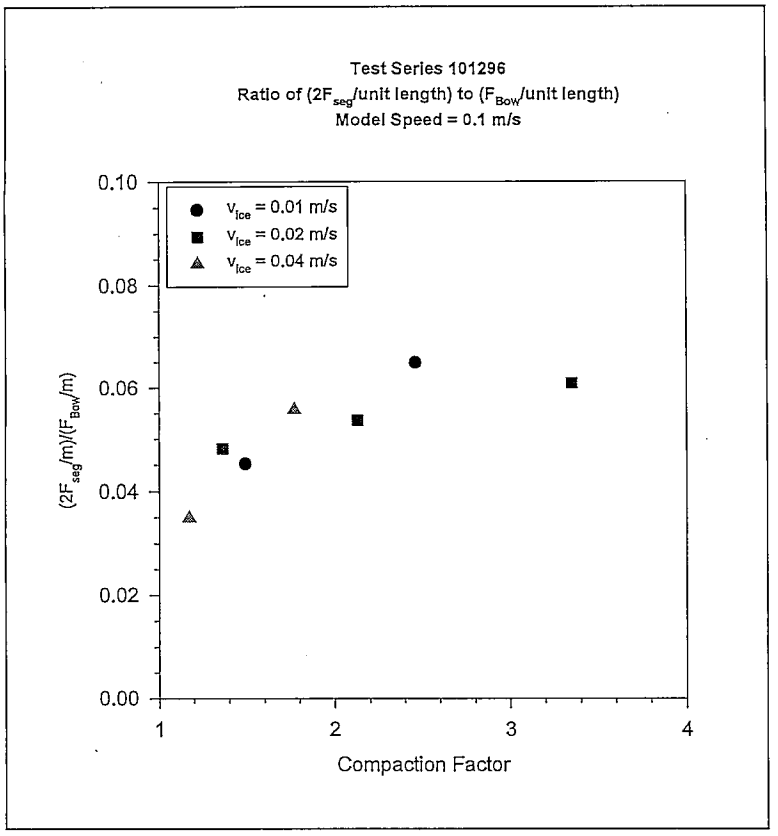
Test Series 101296
Ratio of (2F$_{seg}$/unit length) to (F$_{Bow}$/unit length)
Model Speed = 0.1 m/s
v$_{ice}$ = 0.01 m/s
v$_{ice}$ = 0.02 m/s
v$_{ice}$ = 0.04 m/s
(2F$_{seg}$/m)/(F$_{Bow}$/m)
0.10
0.08
0.06
0.04
0.02
0.00
1
2
3
4
Compaction Factor

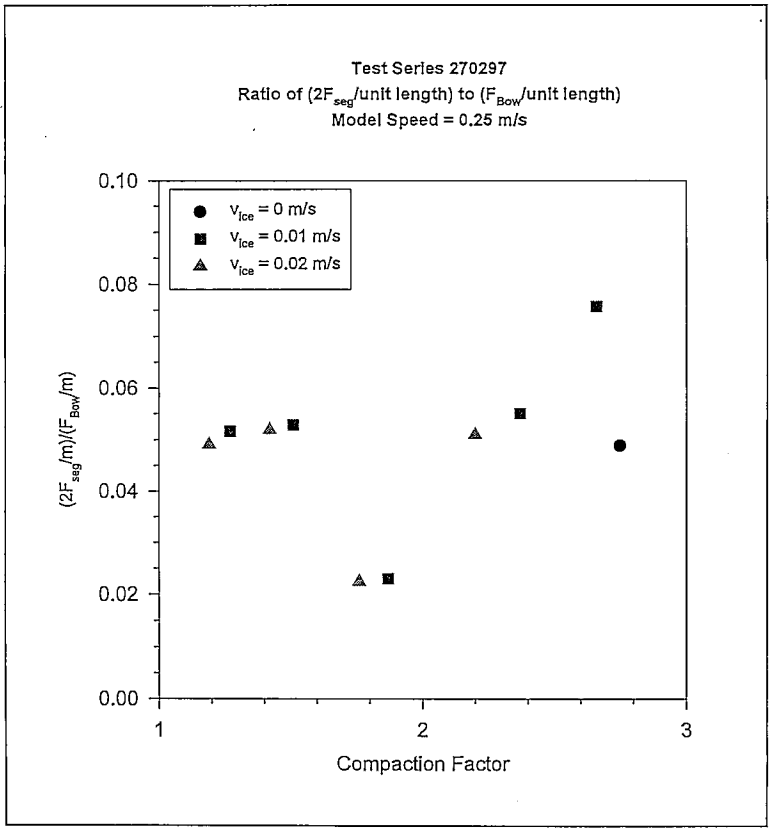
Test Series 270297
Ratio of (2F$_{seg}$/unit length) to (F$_{Bow}$/unit length)
Model Speed = 0.25 m/s
v$_{ice}$ = 0 m/s
v$_{ice}$ = 0.01 m/s
v$_{ice}$ = 0.02 m/s
(2F$_{seg}$/m)/(F$_{Bow}$/m)
0.10
0.08
0.06
0.04
0.02
0.00
1
2
3
Compaction Factor

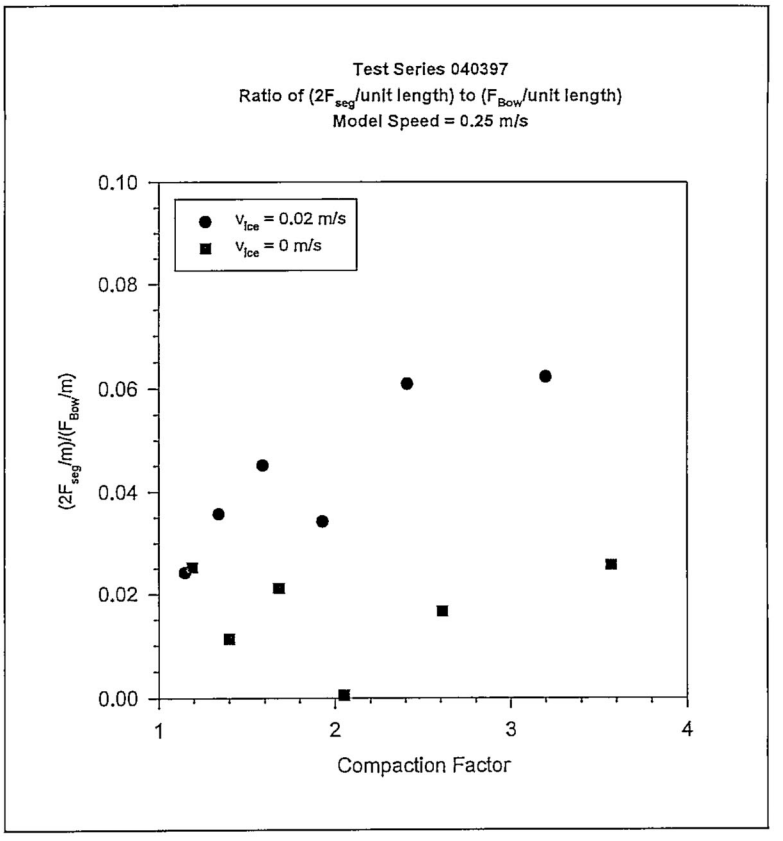
Test Series 040397
Ratio of (2F$_{seg}$/unit length) to (F$_{Bow}$/unit length)
Model Speed = 0.25 m/s
v_{Ice} = 0.02 m/s
v_{Ice} = 0 m/s
(2F$_{seg}$/m)/(F$_{Bow}$/m)
0.10
0.08
0.06
0.04
0.02
0.00
1
2
3
4
Compaction Factor

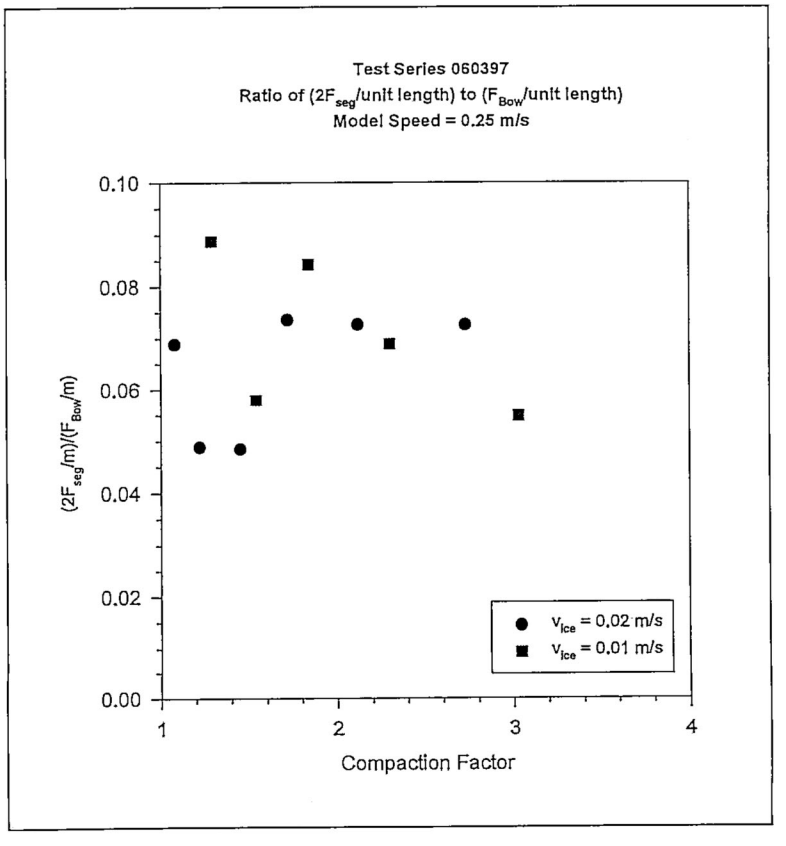
Test Series 060397
Ratio of (2F$_{seg}$/unit length) to (F$_{Bow}$/unit length)
Model Speed = 0.25 m/s
v_{Ice} = 0.02 m/s
v_{Ice} = 0.01 m/s
(2F$_{seg}$/m)/(F$_{Bow}$/m)
0.10
0.08
0.06
0.04
0.02
0.00
1
2
3
4
Compaction Factor

APPENDIX B.6

"FRICTION COEFFECIENT" VARIATIONS FOR SEGMENTED MODEL

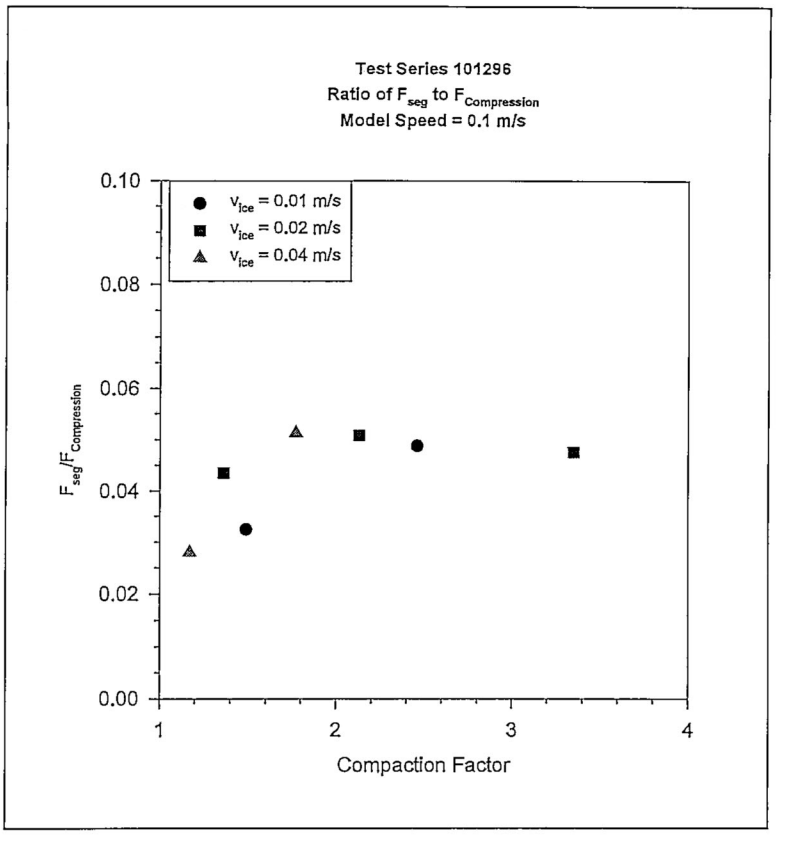
Test Series 101296
Ratio of F_{seg} to $F_{Compression}$
Model Speed = 0.1 m/s
v_{ice} = 0.01 m/s
v_{ice} = 0.02 m/s
v_{ice} = 0.04 m/s
$F_{seg}/F_{Compression}$
0.10
0.08
0.06
0.04
0.02
0.00
1
2
3
4
Compaction Factor

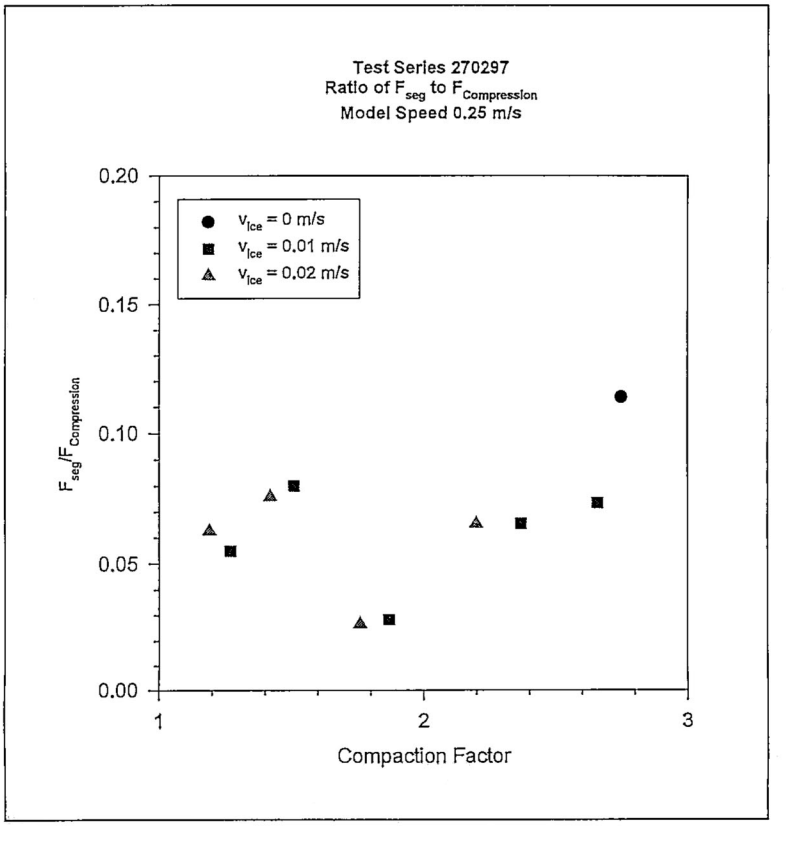
Test Series 270297
Ratio of F_{seg} to $F_{Compression}$
Model Speed 0.25 m/s
v_{ice} = 0 m/s
v_{ice} = 0.01 m/s
v_{ice} = 0.02 m/s
$F_{seg}/F_{Compression}$
0.20
0.15
0.10
0.05
0.00
1
2
3
Compaction Factor

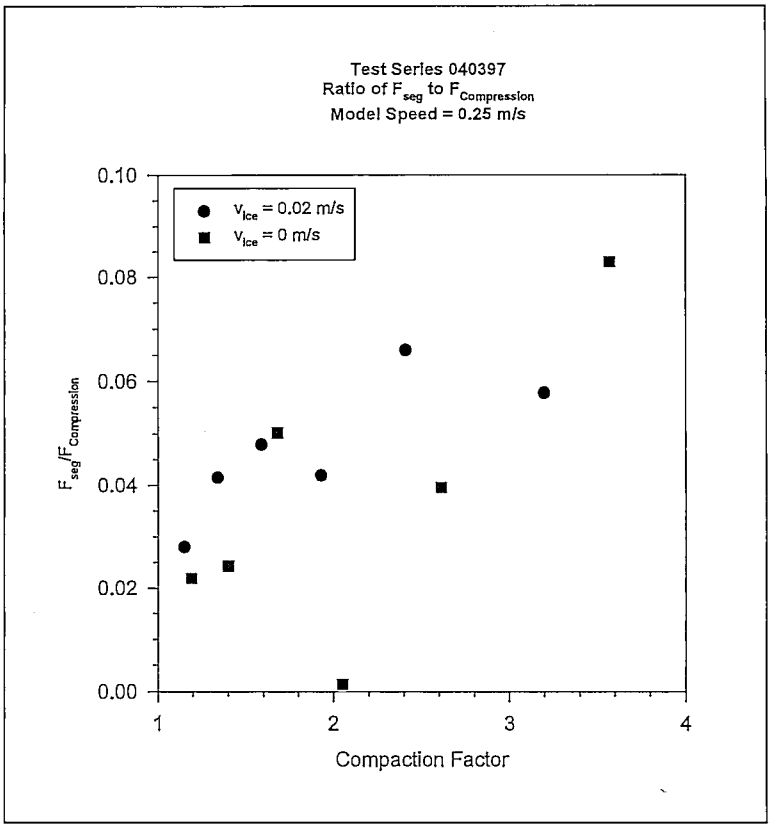
Test Series 040397
Ratio of F_{seg} to $F_{Compression}$
Model Speed = 0.25 m/s
v_{Ice} = 0.02 m/s
v_{Ice} = 0 m/s
$F_{seg}/F_{Compression}$
0.10
0.08
0.06
0.04
0.02
0.00
1
2
3
4
Compaction Factor

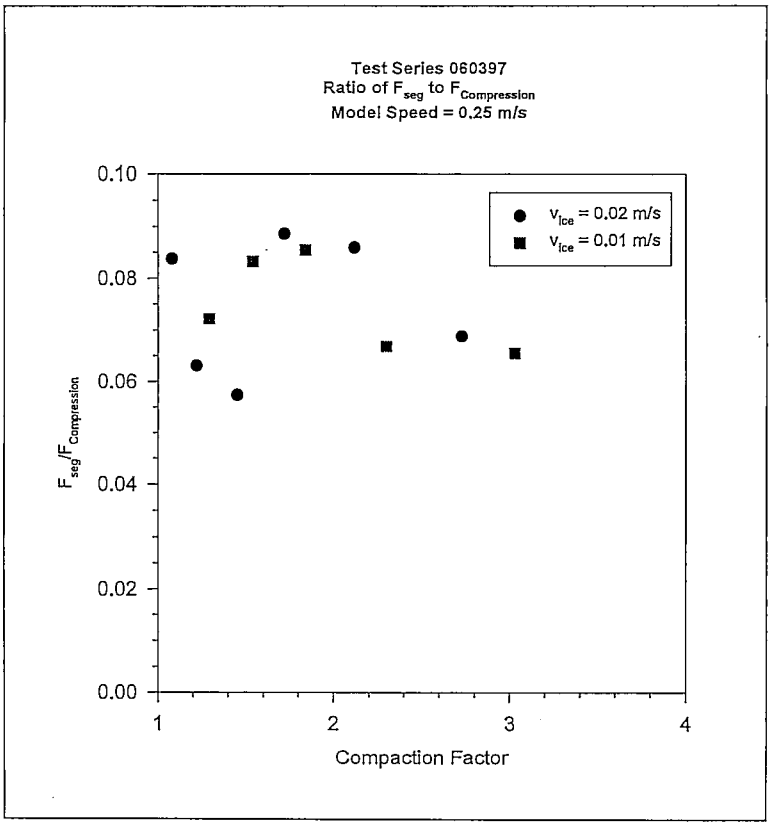
Test Series 060397
Ratio of F_{seg} to $F_{Compression}$
Model Speed = 0.25 m/s
v_{Ice} = 0.02 m/s
v_{Ice} = 0.01 m/s
$F_{seg}/F_{Compression}$
0.10
0.08
0.06
0.04
0.02
0.00
1
2
3
4
Compaction Factor

INSROP PROJECT 1.1.8 Part II
"Influence of Ice Compression on Feasible Navigation on the NSR

Discussion Paper by K. Juurmaa and others

Review by Ken Croasdale

This is an important topic as ice compression clearly has an influence on transit times and power requirements for ships and support vessels plying the Northern Sea Route (NSR) (and any ice region).

I agree with the overall goal of developing a procedure for the effects of ice compression on performance calculations. But this is a very difficult task to accomplish, not least because the processes in an ice field during ice compression are poorly understood, especially limits to compression as influenced by ridging and rafting.

The initial approach in Part 1 was a good one, in that it consisted of an examination of Russian data relating to the ball scale and ship performance. This Part 2 report starts with a review of the Part 1 results. The comment was made that the Russian data did not reveal any correlation between the ice compression in ball units and physically measurable units. This seems to be contradicted by the full scale test results examined in the bulk of the main report (pages 3 to 6).

This examination is very useful and it is a pity that more full scale trials in ice compression are not available.

The logic for conducting the model tests on the presumed "Lenin equivalent" is sound. In hindsight it would have been useful to have instrumented the pusher plate to measure lateral forces in the icefield and hence have direct assessment of the ice compression forces. This might have enabled some of the apparent inconsistent results between the two models to be understood and explained.

The use of the term compaction factor appears logical (at first thought), as it would appear to relate to the degree of compression in the ice. The factor also has ingredients which can be assessed from large scale strain patterns in the ice. However, there is a possible problem depending on how much of the compaction strain is recoverable or not. If none is recoverable when the forces causing compression are released, then the effects of the compaction are simply to increase the concentration and effective thickness of the icefield (due to ridging and rafting). That is why, in my opinion, it would be vital in any

further work to instrument the pusher bar in order to have the compression forces in the ice field prior to the ship passage.

The model tests performed in this study provide some interesting data and the general trends are expected. But, as the authors indicate, there are problems.

The fluctuating nature of the tow force is a concern and this has been noted by the authors.

There has to be a concern about the floe sizes used. It is not clear how they compare with the ship size. In my experience, in the Arctic, in the absence of wave swell, the floe sizes can be quite large in relation to the ship size. In these tests, the floe sizes appear to be too small to represent typical Arctic pack ice.

Can the equivalent of Figure 2 be constructed from the model tests of the "Lenin equivalent" for comparison ? If so, this would strengthen the report.

I am somewhat disappointed that the authors in their work have not reviewed ice compression measurements as indicated from in-situ pack ice stresses which have been measured over the last 15 years in various projects. A list of references of such work was provided after the review of Part 1 two and a half years ago (and is added again to this review). I believe that knowing typical limits to pack ice stress might be helpful in assessing limits to ship performance in ice compression.

Appendix 1, the experimental report is not marked as such.

On page 21 of Appendix 1, there is reference to Tables 3.1 and 3.2, where are these ?

On the figures depicting the effects of ice strength (e.g. 4.2.3.1), it be useful if actual key strengths could be indicated.

Overall, this is an interesting piece of work on a difficult issue. The authors are to be commended for these preliminary attempts.

It will be vital in any future model work to consider the effects of scaling on the internal ice stresses which can be generated in ice fields during ice compression. If these levels of ice compression cannot be properly understood and scaled, then the value of future model tests is in doubt.

INSROP
PROJECT I. 1. 8, Part II
Influence of Ice Compression on Feasible Navigation on the NSR

Reply to the Reviewer

We thank Mr. Ken Croasdale for the effort he put into reviewing our report. We have carefully studied his valuable comments and we will try to respond to them:

Comment on apparent contradiction
In the conclusions of Part I of the project it was stated that the Russian data did not have any conclusions about the correlation between the ice compression in ball units and physically measurable units and that there was data that connected the speed of a vessel to the compression in ball units.
One of the main objectives of Part II of the project was to convert and present that data in such a form that it can serve as a target for the model tests.

Comment on instrumentation of the pusher bar
As usual, model tests are a place for learning and we fully agree that in possible future tests the test arrangement should be developed so that the driving force not only can be measured but also controlled. This is, however, a quite expensive set-up and it was beyond the financial frames of this project.

Comment on floe size
In practise the ice compression may be present at smaller or larger ice floes. This test series concentrated only on smaller floe size. Because the tests were run with constant pusher plate speed, the increase of floe size would have resulted in large peak forces and comparatively low average forces. Test arrangement for large floes would require constant driving force at the pusher plate — not constant speed. This in turn would require feedback from the driving force to the pusher plate control system, which requires expensive equipment.

Comment on Figure 2 and creating equivalent figure from the MSC test results
The test results do not provide enough information to form similar curves as in Figure 2: *Ice resistance of NIB "Lenin"*. Single points of the tests could be plotted, but there is not enough information to form similar family of curves / lines. To be able to produce similar lines, the instrumentation and the general arrangement of the tests should be changed and the test series should be more comprehensive. E.g. the driving force should be measured and it should be kept as constant as possible. The budget of this project did not suffice the expenditure that would have been required for the instrumentation.

Comment on other ice compression measurements

This report mainly concentrates on practical ship performance in compressive ice, not on internal stresses within the ice field. The authors, however do fully agree that in order to eventually establish a theoretically correct solution to the problem of ice compression it is vital to know every aspect of the problem. Therefore the reference list from the reviewer is added to the end of the report under the title '**Further reading of pack ice compression**'.

Comment on figures depicting the effects of ice strength

Ice strength properties (compressive strength, bending up, bending down) for each day are presented in Table 3.2.2 and Table 3.2.4. This is now indicated in the figure texts. The ice strength information required too much space to fit into the figure.

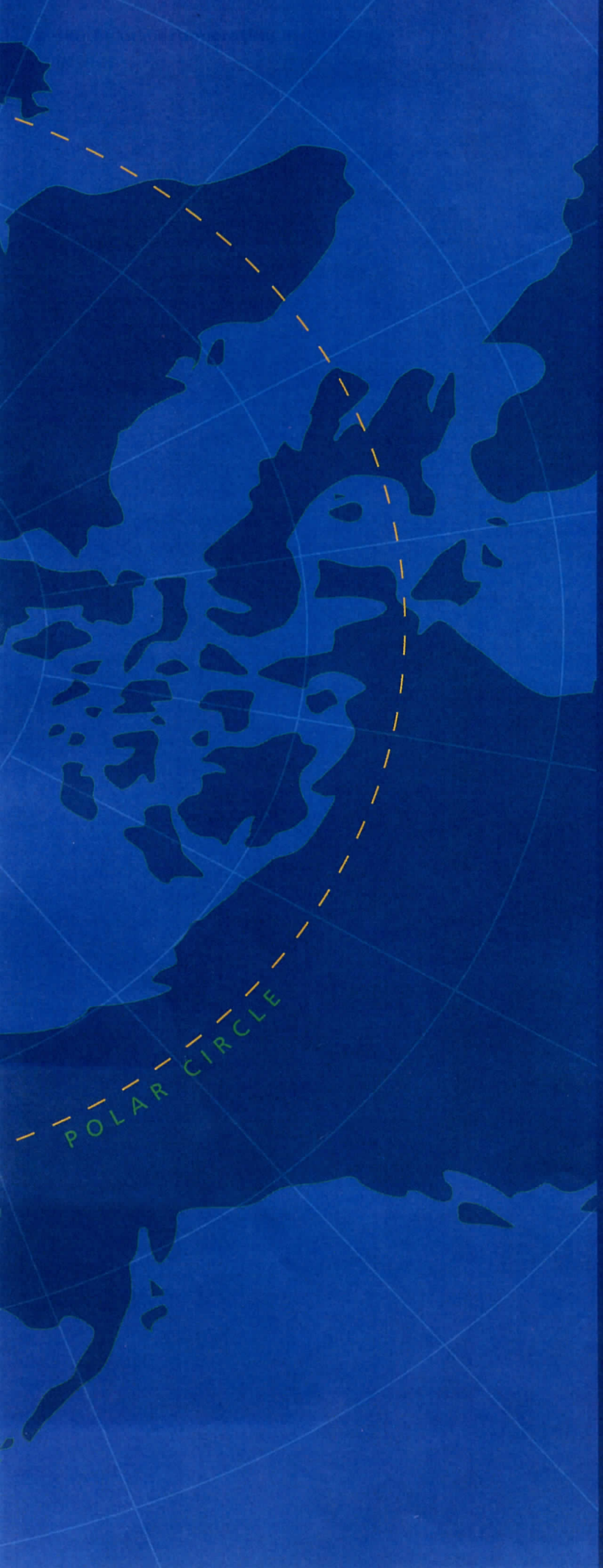

The three main cooperating institutions of INSROP

Ship & Ocean Foundation (SOF), Tokyo, Japan.

SOF was established in 1975 as a non-profit organization to advance modernization and rationalization of Japan's shipbuilding and related industries, and to give assistance to non-profit organizations associated with these industries. SOF is provided with operation funds by the Sasakawa Foundation, the world's largest foundation operated with revenue from motorboat racing. An integral part of SOF, the Tsukuba Institute, carries out experimental research into ocean environment protection and ocean development.

Central Marine Research & Design Institute (CNIIMF), St. Petersburg, Russia.

CNIIMF was founded in 1929. The institute's research focus is applied and technological with four main goals: the improvment of merchant fleet efficiency; shipping safety; technical development of the merchant fleet; and design support for future fleet development. CNIIMF was a Russian state institution up to 1993, when it was converted into a stock-holding company.

The Fridtjof Nansen Institute (FNI), Lysaker, Norway.

FNI was founded in 1958 and is based at Polhøgda, the home of Fridtjof Nansen, famous Norwegian polar explorer, scientist, humanist and statesman. The institute spesializes in applied social science research, with special focus on international resource and environmental management. In addition to INSROP, the research is organized in six integrated programmes. Typical of FNI research is a multi-disciplinary approach, entailing extensive cooperation with other research institutions both at home and abroad. The INSROP Secretariat is located at FNI.